Synthesis, Properties, and Morphology of Lignin Based Epoxy Resins

by

Klaus Hofmann

Dissertation submitted to the Faculty of the

Virginia Polytechnic Institute and State University

in partial fulfillment of the requirements for the degree of

PhD

in

Materials Engineering and Science

APPROVED:

Wolfgang G. Glasser, Chairman

Frederick A. Kamke

Alfred C. Loos

Thomas C. Ward

Garth L. Wilkes

May 1991

Blacksburg, Virginia

Synthesis, Properties, and Morphology of Lignin Based Epoxy Resins

by

Klaus Hofmann

Wolfgang G. Glasser, Chairman

Materials Engineering and Science

(ABSTRACT)

Star-like lignin-poly(propylene oxide) copolymers were prepared by chain-extending steam exploded lignins (*tulipifera liriodendron*) with propylene oxide and by subsequent endcapping with ethylene oxide. Epoxidation of these copolymers was carried out with epichlorohydrin at room temperature, using KOH as oxyanion forming reagent. The epoxidized compounds were fractionated by solvent precipitation to remove poly(alkylene oxide) homopolymers and to prepare fractions of narrow molecular weight distributions.

The epoxides were cross-linked with meta phenylene diamine yielding thermosets which were, depending on lignin content, either low modulus elastomers, or high modulus materials with considerable ductility. The modulus of elasticity was a strong and linear function of lignin content, whereby the highest value was $1100 MPa$ (57% lignin).

The curing reaction was of n^{th}-order type, whereby the reaction order changed from close to one at the beginning of the curing reaction to 2, once the reaction becomes diffusion controlled. Curing induced partial demixing of the lignin and poly(propylene oxide) phases which yielded a secondary structure where lignin rich domains in the order of $10 nm$ were interspersed in a matrix of lignin poor material. However, from TEM and ^{13}C solid state cross-polarized NMR analyses it was evident that the domain structure was not that of a classical micro-phase separated copolymer with well defined phase boundaries, but rather had broad interphases. Additionally, the results of multifrequency dynamic mechanical thermal analysis showed that the lignin containing thermosets have very broad

glass transition ranges which most likely were due to transitional phase inhomogeneities and provided these materials with good vibrational damping ability.

Table of Contents

List of Illustrations

List of Tables

Glossary of Symbols

A	pre-Arrhenius frequency factor	s^{-1}
a, a_1, a_2, a_0	amine concentration	
a_T	temperature shift factor	
B	magnetic field	*Tesla*
C_1, C_2	WLF constants of time-temperature-superposition-principle	
e, e_0	epoxide concentration	
e	base of natural logarithm	
E, E'	Youngs modulus,	*MPa*
	storage modulus	
E''	loss modulus	*MPa*
E_A	activation energy	*J/mol*
F	ratio of segmental mobilities,	
f	functionality	
f_g	fractional free volume at glass transition	
ΔH	enthalpy, heat of reaction	*Ws, J*
ΔH_{RXN}	total heat of exothermic reaction	*Ws/g, J/g*
k, k', K	reaction rate constant	s^{-1}

M	molecular weight	Dalton, g/mol
M_n, M_w	number, weight average molecular weight	Dalton, g/mol
m, n	order of reaction	
p	conversion	
p_c	critical conversion at gelation	
r	stoichiometric ratio	
R	absolute gas constant	$8.314\ Jmol^{-1}K^{-1}$
R^2	correlation coefficient	
T	temperature	$°C, K$
T_C	cure temperature	$°C, K$
T_g	glass transition temperature	$°C, K$
$T_{g,0}$	glass transition temperature of uncross-linked polymer	$°C, K$
$T_{g,x}$	glass transition temperature of cross-linked polymer	$°C, K$
$T_{g,\infty}$	maximum glass transition temperature of cross-linked polymer	$°C, K$
T_g^∞	maximum glass transition temperature of uncross-linked polymer as function of molecular weight	$°C, K$
T_1	spin-lattice relaxation time	ms
T_2	spin-spin relaxation time	ms
$T_{1,\rho}$	spin-lattice relaxation time in the rotating frame	ms
t	time	s
t_c	cross polarization contact time	ms
t_C	cure time	min

W	UV absorbing mass per *kg* HPL	*g/kg*
WPE	epoxy equivalent weight	*g/eq.*
x	consumption of epoxide groups	*mol*
$\bar{x}_n$, $\bar{x}_w$	number, weight average degree of polymerization	
α	conversion, extent of reaction	
γ	magnetogyrig ratio of nucleus	
ε, ε_{max}	strain, strain at break	%
ε	ratio of lattice energies,	
ε_{280}	UV absorption coeeficient at 280 *nm*	$lg^{-1}m^{-1}$
η	viscosity	$gm^{-1}s^{-1}$
ϕ	DSC heating rate	$^{\circ}\,min^{-1}$
σ, σ_{max}	stress, stress at break	*MPa*
ν	frequency	*Hz*
ν_g	frequency of E''_{max} at constant temperature	*Hz*
ω	Larmor frequency	s^{-1}

1.0 Introduction

The ever increasing awareness that the raw material base for most human made materials is finite has spurned an unprecedented effort to take a new look at renewable bio-based resources. Agricultural products including wood are now viewed not only as supply for food, paper and structural materials but also as feedstock for the chemical industry. But while drugs and other low molecular weight chemicals are made to a certain extent from plant and agricultural residues, the production of bio-based, high molecular weight structural polymers has not made significant inroads into the oil based field. But it is especially in the area of structural biopolymers where one can find many analogies and adaptation of "modern" polymer science principles. For instance, the two most abundant organic compounds in the biosphere, cellulose and lignin, are both part of the intricately designed biocomposite wood. Cellulose, as a semicrystalline rod like macromolecule acts as wood's reinforcing phase held together by a matrix of polysaccharide-lignin complexes. Although this is a very simplified view of the composite wood, it nevertheless suggests that these two compounds can be identified as potential candidates for similar use in human made materials and structures: cellulose as fibrous, high tensile strength and modulus-possessing, semicrystalline polymer and lignin as an amorphous network forming precursor. Although cellulose is used extensively for paper and paper products, it lost its "pioneer" position it held at the dawn of the polymer age to oil based polymers. The advent of new solvents and the prospect of controllable homogeneous phase re-

actions might reverse this trend. But it is lignin which, as a by-product of the pulping process, is severely underutilized albeit its potential as a polyphenolic macromer is great. Nevertheless, the fact that lignin is produced as a pulping waste product in huge quantities ($5*10^7$ tons/yr), its renewability, and the uncertainty of future availability and price of oil based chemicals has triggered numerous attempts in recent years to explore its potential as network polymer and its respective use [1,2,3]

1.1 Lignin as Part of Synthetic Chemical Networks

Although much research has been carried out to pin down the molecular structure of lignin, considerable uncertainty remains about its *in vivo* conformation. The early picture of a random polyphenolic network has been partially abandoned in favor of a polysaccharide-lignin copolymer structure abiding some degree of order [4,36]. The three dimensional random network is still considered a viable option for middle lamella lignin which accounts for about 20% of wood's lignin. By far the most lignin (70%) is found in the secondary wall [5] where it is partially distributed between the ordered arrays of cellulose microfibrillar structure. Its role there encompasses among others the protection of the fibrils and to act as stress transfer agent [6]. Goring's paradigm [4] of lignin's dual appearance as either order possessing structure in the secondary wall or as random three dimensional network in the middle lamella has been supported elegantly by Leclerc on the basis of percolation theory of lignin degradation [34].

Lignin as it is isolated during pulping processes is chemically altered and does not reflect its *in vivo* molecular weight and conformation characteristics. As a structure of inter linked phenylpropane units it has, depending on the pulping method, number molecular weight averages ranging from 1 000 to several ten thousands [7,8,9] and very broad molecular weight distributions. Figure 1 depicts an example of an *in vitro* lignin structure. Most of the phenyl propane (C9) units are con-

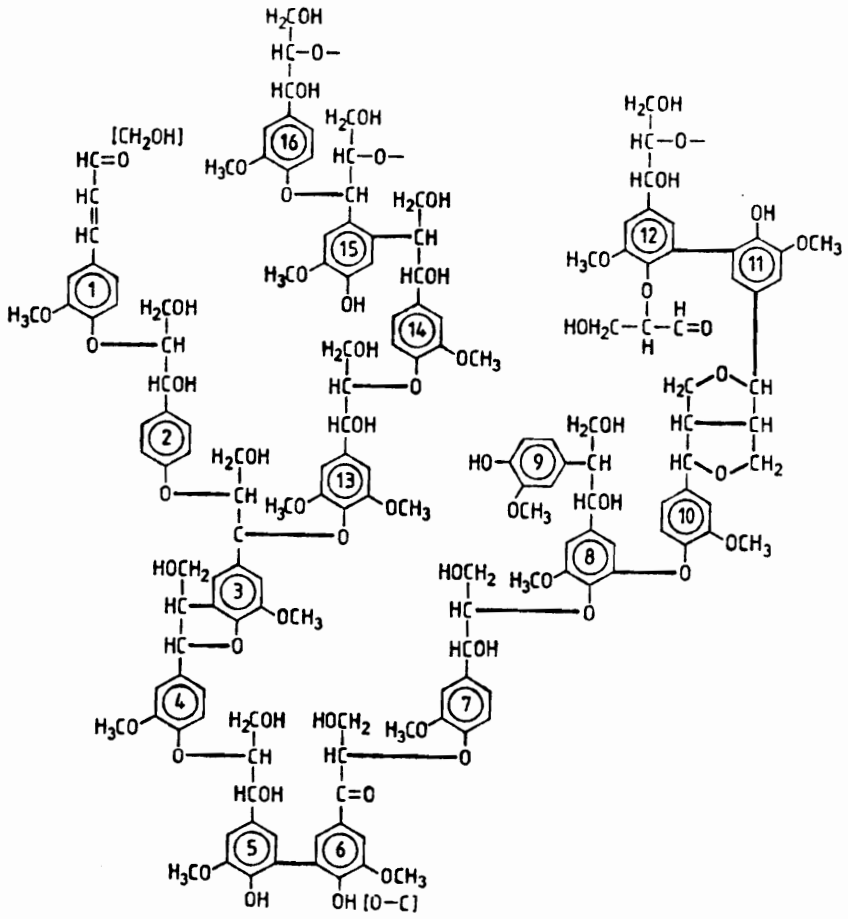

Figure 1. **Example of Isolated Lignin Fragment:** Spruce Lignin [36]

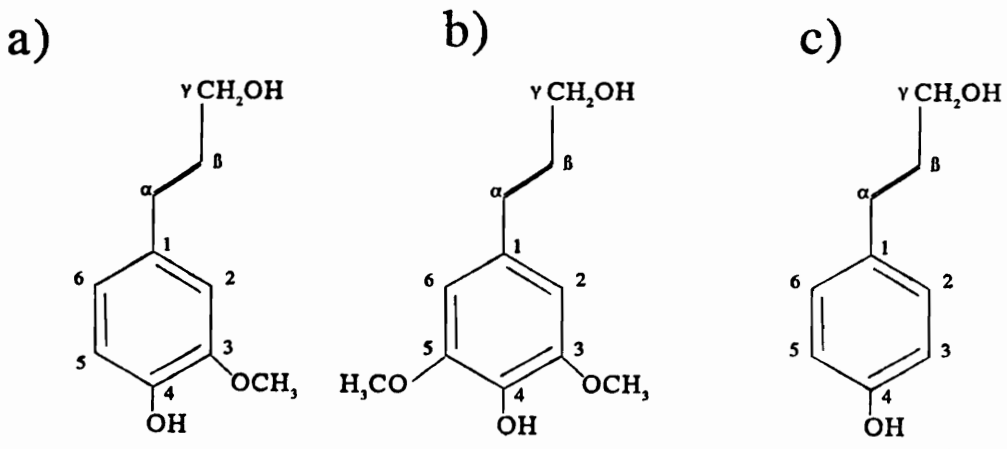

Figure 2. Lignin Precursor and Phenyl Propane Units

: a) coniferyl alcohol
b) sinapyl alcohol
c) *p*-coumaryl alcohol

nected by ether or carbon-carbon inter-unit bonds with a probability of occurrence depending on the π electron spin density of the biological lignin precursors coniferyl alcohol, sinapyl alcohol, and *p*-coumaryl alcohol (see. Figure 2). But although there exist plant specific differences among the lignins of which the most important is the differentiation between syringyl and guaiacyl lignin, these variations are of lesser importance than those resulting from the various isolation methods once lignin becomes incorporated into networks [10].

Except for lignosulfonates which are water soluble, lignins are insoluble in most organic solvents and are therefore difficult to react with functionalizing agents. Thus, in order for them to be reacted in homogeneous phase and to be made part of a covalent network, lignins must be physically or chemically modified.

Numerous attempts have been reported to change lignins from a rather inert and insoluble compound to a molecule which can be covalently incorporated into network structures. Some of them like alkoxylation [11], phenolation [12,13], enzymatic modification by phenoloxidases from white rot fungi [14], methylolation [15], ozonation [16], and the removal of low molecular weight species by ultrafiltration [17] gained limited importance.

Many potential routes to lignin based thermosetting resins have been discussed in a recent review [1]. By far the most important aspect of lignin concerning network formation is its phenolic character which permits crosslinking with formaldehyde or co-reacting with phenol-formaldehyde systems. Its use as replacement for traditional wood adhesives shows considerable promise [18]. Another very important class of polymeric networks where lignin has a potential role to play are polyurethanes. Especially when the phenolic hydroxyls are replaced by one or more units of alkylene oxide, lignin becomes a highly reactive polyol which can be crosslinked with di-isocyanates [19]. By adjusting the NCO : OH ratio to about 1:4, full crosslinking of the lignins takes place [20]. The polyols can be tailored to form flexible or rigid materials by adjusting the aliphatic ether chain length [21], or by co-reacting with glycols whereby the morphology can be controlled to range from totally phase separated, rubber toughened thermosets [22] to complete homogeneous systems [23].

Functionalization of lignins with vinyl groups by reacting them with isocyanatoethyl metacrylate or meta-TMI and subsequent co-polymerization with styrene or MMA yield chemical networks with a low sol fraction [24,37]. Epoxy functionalized compounds react with a variety of crosslinking agents such as amines and anhydrides, and show very good mechanical and chemical properties. Early reports of epoxidation of underivatized lignins appeared in the mid sixties [25,26]. These epoxies showed good gluability to wood but were difficult to use due to their relative insolubility. Epoxidation of lignin in DMSO was patented by d'Alelio [27]. Again, solubility is the problem and using a high boiling solvent like DMSO is not a particular practical solution. In order to be able to control the solubility of the epoxy functionalized lignins in low boiling solvents, Nieh et al. [28,31] and Glasser et al. [35] epoxidized hydroxypropyl and hydroxybutyl lignin with epichlorohydrin and crosslinked it successfully with ethylene diamine. Shiraishi [29] phenolated lignin with bisphenol A prior to epoxydation and was able to use it as plywood glue with satisfactory wet strength. It was also noted that purification of lignin did not have an effect on the mechanical properties of the resin; rather the unpurified lignin formulations exhibits better gluability.

This brief summary supports the notion that lignin could play a significant part in the future of thermosetting resins, especially wood adhesives, if properly modified, characterized, and standardized. Much work is still needed to show that well characterized and defined lignins can be practical and economical choices for thermosetting pre-polymers.

1.2 Aim and Scope of this Study

It has been established by now that lignin, especially if derivatized by converting the phenolic hydroxyls into mono or polyether side chains, behaves like any other complex star like macromer [30] and its properties and behavior can be predicted if one resorts to the tools of modern theoretical and applied polymer science. The recently developed procedure of epoxidation of hydroxy alkylated

lignin [28] opened the door to study the formation of thermosets containing lignin with methods developed for synthetic polymers. Furthermore, by comparing properties and characteristics in multiphase lignin epoxy networks with those found of lignin polyurethane systems, a more general picture of lignin in covalent networks can be drawn. It was therefore the goal of this study to modify lignins by controlled chain extension prior to epoxidation and to study the cure and the properties of the crosslinked material as a function of the degree of chain extension and lignin content. Lignin-poly(propylene oxide) has been shown to form homogenous polyurethane networks, and that it is possible to control the composition of the copolymer by adjusting the propylene oxide-lignin feed ratio during synthesis, which in turn allows to predict mechanical and viscoelastic properties of the networks [21]. It was also shown that fractionation of lignin has a significant influence on the glass transition temperature and mechanical performance of the network materials [32]. Also a clear trend of broadening the temperature range of energy dissipation with increasing lignin molecular weight was observed. It was expected that similar results will be obtained from the study of epoxy networks. Therefore, in order to study the dependance of mechanical and viscoelastic parameters on lignin content and molecular weight, lignin-poly(propylene oxide) copolymers with a range of lignin contents and molecular weights were prepared. These adjustments of compositional and size parameters were achieved by controlling the lignin-propylene oxide feed ratio during chain extension and by solvent precipitation fractionation of the chain extended lignin copolymers. Furthermore, it was expected that, as has been pointed out briefly by Kelley [32] for polyurethanes, epoxy networks show a lignin content and molecular weight dependent widening of the viscoelastic damping transition. Studies were carried out to investigate whether this is caused by an increase of undefined general molecular heterogeneity [32] or by micro-phase separation [33]. Additionally, since it is of considerable interest for the application of lignin containing epoxy thermosets to have knowledge about the cure reactions, the kinetics of the curing reaction at lower and higher extents of conversion were investigated.

Thus, to enhance the fundamental understanding of lignin's role in covalent networks and to investigate the potential of multifunctional lignin-poly ether epoxy copolymers for the use as structural materials, this study was carried out and is described in three sections which deal with

1. the derivatization, epoxidation, and fractionation of lignin, and the analysis with respect to molecular weights, lignin content, polyether chain length, and epoxy content;
2. the cure kinetics and the network formation of the lignin based epoxides during cure with an aromatic diamine; and
3. the properties and morphology of the lignin-poly(propylene oxide) copolymer networks, including their mechanical and viscoelastic characteristics.

1.3 References

1. W. G. Glasser, in R. W. Hemmingway and A. H. Conner, Eds., "Adhesives from Renewable Resources", ACS Symp. Ser. 385, Washington, DC, 1989
2. J. J. Lindberg, T. A. Kuusela, and K. Levon, in W. G. Glasser and S. Sarkanen, Eds., "Lignin, Properties and Materials", ACS Symp. Ser. 397, Washington, 1989
3. K. V. Sarkanen and C. H. Ludwig, "Lignins", Wiley-Interscience, New York, 1971
4. D. A. I. Goring, in W. G. Glasser and S. Sarkanen, Eds., "Lignin, Properties and Materials", ACS Symp. Ser. 397, Washington, 1989
5. W. G. Glasser and S . S. Kelley, "Lignin, Properties and Materials", in Mark, Bikales, Overberger, and Menges, Eds., Encyclopedia of Polymer Science, Vol. 8, 2nd Ed., John Wiley & Sons, Inc., 1987
6. R. E. Mark, "Cell Wall Mechanism of Tracheids", New Haven, 1967
7. F. E. Brauns and D. A. Brauns, "The Chemistry of Lignin", Academic Press, New York, 1960
8. M. E. Himmel, K. Tatsumoto, K. K. Oh, K. Grohmann, D. K. Johnson, and H. L. Chum, in W. G. Glasser and S. Sarkanen, Eds., "Lignin, Properties and Materials", ACS Symp. Ser. 397, Washington, 1989
9. K. Forss, R. Kokkonen, and P.-E. Sagfors, in W. G. Glasser and S. Sarkanen, Eds., "Lignin, Properties and Materials", ACS Symp. Ser. 397, Washington, 1989
10. T. G. Rials and W. G. Glasser, *Holzforschung*, 40, 1986, 353
11. L. C.-F. Wu and W. G. Glasser, *J. Appl. Pol. Sci.*, 29, 1984, 1111
12. P. C. Muller and W. G. Glasser, *J. Adhesion*, 17, 1984, 185
13. H.-K. Ono and K. Sudo, in W. G. Glasser and S. Sarkanen, Eds., "Lignin, Properties and Materials", ACS Symp. Ser. 397, Washington, 1989

14. A. Hüttermann, O. Milstein, B.Nicklas, J. Trojanowsky, A. Haars, and A. Kharazipour, in W. G. Glasser and S. Sarkanen, Eds., "Lignin, Properties and Materials", ACS Symp. Ser. 397, Washington, 1989
15. A. J. Dolenko and M. R. Clarke, *For. Prod. J.*,28(8), 1971,
16. B. Tomita, K. Kurozumi, A. Takemura, and S. Hosoya, in W. G. Glasser and S. Sarkanen, Eds., "Lignin, Properties and Materials", ACS Symp. Ser. 397, Washington, 1989
17. K. Forss and A. Fuhrmann, *For. Prod. J.*, 29, 1979, 39
18. H. H. Nimz, in A. Pizzi., Ed., "Wood Adhesives", Marcel Dekker, 1983
19. W. G. Glasser, O. H.-H. Hsu, D. L. Reed, R. C. Forte, and L. C.-F. Wu in K. N. Edwards, Ed., "Urethane Chemistry and Applications", ACS Symp. Ser. 172, Washington, DC, 1981
20. T. G. Rials and W. G. Glasser, *Holzforschung*, 38, 1984, 191
21. S. S. Kelley, "Lignin Copolymers in Polyurethane Materials", PhD Thesis, Virginia Tech, Blacksburg, 1987
22. V. P. Saraf, W. G. Glasser, and G. L. Wilkes, *J. Appl. Pol. Sci.*, 30, 1985, 3809
23. V. P. Saraf, W. G. Glasser, G. L. Wilkes, and J. E. McGrath, *J. Appl. Pol. Sci.*, 30, 1985, 2207
24. H.-X. Wang, "Lignin Acrylate Derivatives and their Behaviors in free Radical Copolymerizations", MS Thesis, Virginia Tech, Blacksburg, 1986
25. S. Tai, M. Nagata, J. Nakano, and N. Migita, *Nihon Mokuzai Gakkai*, 13, 1967, 102
26. S. Tai, J. Nakano, and N. Migita, *Nihon Mokuzai Gakkai*, 13, 1967, 257
27. G. F. D'Alelio, US-Pat.# 3,905,926, 1975
28. W. L.-S. Nieh, "Synthesis and Properties of Lignin Epoxide", MS Thesis, Virginia Tech, Blacksburg, 1986
29. N. Shiraishi, in W. G. Glasser and S. Sarkanen, Eds., "Lignin, Properties and Materials", ACS Symp. Ser. 397, Washington, 1989
30. W. de Oliveira and W. G. Glasser, *J. Appl. Pol. Sci.*, 37, 1989, 3135
31. W. L.-S. Nieh and W. G. Glasser, in W. G. Glasser and S. Sarkanen, Eds., "Lignin, Properties and Materials", ACS Symp. Ser. 397, Washington, 1989
32. S. S. Kelley and W. G. Glasser, *J. Wood Chem.*, 8, 1988, 341

33. L. H. Sperling, in R. D. Corsaro and L. H. Sperling, Eds., "Sound and Vibration Damping with Polymers", ACS Symp. Ser. 424, Whashington, DC, 1989
34. D. F. Leclerc, Abstract 24, "Proc. of ACS Cellulose Division Meeting", Atlanta, 1991
35. W. G. Glasser, W. L.-S. Nieh, W. de Oliveira, and S. S. Kelley, US-Pat.# 4,918,167, 1990
36. D. Fengel and G. Wegener, "Wood; Chemistry, Ultrastructure and Reactions", DeGruyter, Berlin, 1984
37. W. L.-S. Nieh and W. G. Glasser, in W. G. Glasser and S. Sarkanen, Eds., "Lignin, Properties and Materials", ACS Symp. Ser. 397, Washington, 1989

2.0 Synthesis of Epoxidized Lignin-Poly(propylene Oxide) Copolymers

2.1 Introduction

Epoxy compounds are molecules bearing a three membered heterocyclic, oxygen containing ring which is correctly classified as *oxirane*. Although such molecules have been synthesized and described as early as 1858 [1], it was not until 1947 that epoxy resins, as we know them today obtained commercial significance [2]. Since then consumption has steadily risen by 20%/yr. Despite their relative high price ($1.25-$1.50 [3]), epoxy resins were able to venture into diverse applications such as adhesives, coatings, structural materials, appliances, matrices of composites, etc., where the required performance justifies the higher material costs. The price of epoxy resins reflects the costs of the precursors such as bisphenols and the contribution of the epoxidation reaction. By using a cheaper but qualitatively satisfying alternative raw material base, such as natural prepolymers, it would be possible to arrive at a more cost effective, alternative source for epoxy resins. Indeed, early on plant oils were used and are still in use to formulate reactive diluents and additives [2].

However, other biobased materials, such as lignins show promise to be converted into epoxides for adhesive and structural applications [4].

Epoxidation methods are as numerous as there are commercial epoxy resins. Many functional groups can be converted as has been reviewed by, among others, Rosowsky [5], Pruckmayr [6], and Tanaka [7]. The conversion of unsaturated hydrocarbons with peroxy acids, and of substituted hydroxyl groups with halohydrins are the two most commonly performed epoxidation reactions. The latter is predominately employed to prepare phenolic type epoxy resins such as the many members of the bisphenol A family. The most useful halohydrin is 1-chloro-2,3 epoxy propane or epichlorohydrin (I), which reacts with oxyanions (II) to forms, upon dechlorination with a suitable base, an epoxy functionalized compound (III):

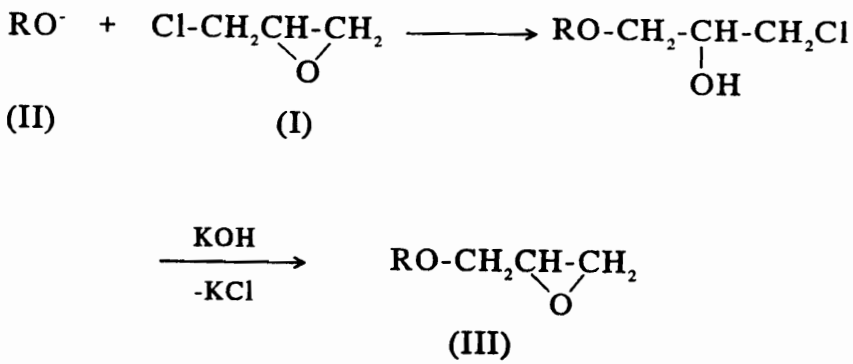

Attempts to epoxidize natural monomers or polymers which bear hydroxyl groups were reported several times. Hollinger et al. [8], and Lelievre [9] epoxidized potato starch with epichlorohydrin to study its swelling mechanism. Epoxidations of other carbohydrate derivatives were carried out by Lee and Perlin [10], Wing et al. [11], and McKelvey et al. [12]. Lindström et al. [32] reacted Kraft lignin (Indulin) with epichlorohydrin to form gelled beads suitable for gel permeation chromatography. But none of the above were geared towards the production of epoxy resins for structural or adhesive end use nor were the epoxides characterized with this aim in mind. On the

other hand, a few scattered reports can be found since the mid 1950's where lignin epoxidations were described with the eyes on the prize of lignin epoxy resins as potential alternative for commercial engineering thermosets.

When epoxidizing lignin, one has to overcome problems intrinsic to most lignins. Not only are many lignins insoluble in most organic solvents, they also bear a range of hydroxyls with an uneven reactivity distribution. Thus suitable pretreatment or modification becomes a necessity. In 1955, Förster [13] obtained a patent claiming that it is possible to epoxidize a polynuclear phenol (lignin) with epichlorohydrin which was previously etherified with haloacetic acid. Mikhailov and Budevska [14] were able to epoxidize sulfate lignin with epichlorohydrin in NaOH solution but could not avoid cross-linking upon distilling off the reagent. By mixing the lignin with phenol, the same authors [15] obtained liquids with high epoxy content which upon curing with diethylamine could be used as adhesives or coatings. In 1966, Tai et al. [16,17] reported the successful epoxidation of thiolignin with epichlorohydrin yielding a maximum epoxy content of 0.19 *eq.*(epoxy group)/100*g*(material) (526*g*/*eq.*). This was achieved by carrying out the reaction at 97°C and 117°C with 40% (of lignin) sodium hydroxide. Prior phenolation of lignin led to an increase to 0.28*eq.*/100*g* (357*eq.*/100*g*). Also, phenolated lignin epoxy was soluble in a series of solvents such as DMF, DMSO, acetone, and others, while their unmodified counterparts were not or only slightly soluble in these solvents. Cured with phthalic anhydride, the phenolated lignins showed good adhesive strength performance. In 1975, D'Alelio [18] patented the epoxidation of alkali lignin with epichlorohydrin whereby the aliphatic hydroxyl groups were esterified with carboxylic acid to improve solubility and reactivity. Although reactive solvents such as phenol and cresol were named as possible reaction media, the solvents of choice were DMSO and dioxane. 5-9 moles of NaOH per one mol of lignin was used and the reaction was carried out at 90-100°C, for 14*hrs.* Epichlorohydrin was distilled off and the resin was recovered by precipitation in water. The yield was 0.26*eq.*/100*g* (385*g*/*eq.*). The epoxide was cross-linked with various amines and anhydrides. Holsopple et al. [19] filed a patent in 1981 for making epoxidized lignin from soluble black liquor extracts. These very low molecular weight lignins were further reacted with mesityl oxide and

formaldehyde to form a reactive carbonyl intermediate which was epoxidized with peroxides. Nieh et al. [20,21,33] were able to epoxidize hydroxy alkylated lignin model compounds and hydroxyalkyl lignin with excess epichlorohydrin at room temperature in methylene chloride. Potassium hydroxide was added stepwise in $1.25 mol/(eq.\mathrm{OH})$ quantities over a period of several days without experiencing premature cross-linking reactions, whereby a yield $0.15 eq./100 g$ ($667 g/eq.$) was achieved. Elevated temperatures, however, decreased the maximum yield due to internal side reactions. A phase transfer agent (Aliquat™) was used as additional catalyst. Five fold excess of epichlorohydrin was necessary to keep inter and intra molecular side reactions at a minimum.

2.2 Materials and Methods

2.2.1 Outline

This chapter deals with the synthetic aspects of lignin-poly(alkylene oxide) epoxy preparation and their characterization. The lignins used throughout this study were, with one exception, extracted from steam-exploded yellow poplar (*liriodendron tulipifera*) wood with alkali [22]. One lignin was a low molecular commercial organosolv product (Allcell™) used as received. All lignins were insufficiently soluble in organic solvents and were modified prior to epoxidation by replacing the phenolic hydroxyls with poly(propylene-oxide) (PPO) segments (Figure 3, 1), and by subsequent capping of the secondary hydroxyls with ethylene oxide (EO) (Figure 3, 2) (Ch. 2.2.1.1). This procedure not only had the effect of making the lignins soluble and provide them with evenly reactive primary hydroxyls, it also yielded products with a range of viscoelastic properties depending on the amount of propylene oxide (PO) used. The next step was the epoxidation of the copolymer with epichlorohydrin (Figure 4, 3) (Ch. 2.2.1.2). The lignin polyols were thereby converted into an oxirane bearing star-like copolymer with a rigid polyphenolic core and flexible polyether arms

1.) Propoxylation and Chainextension:

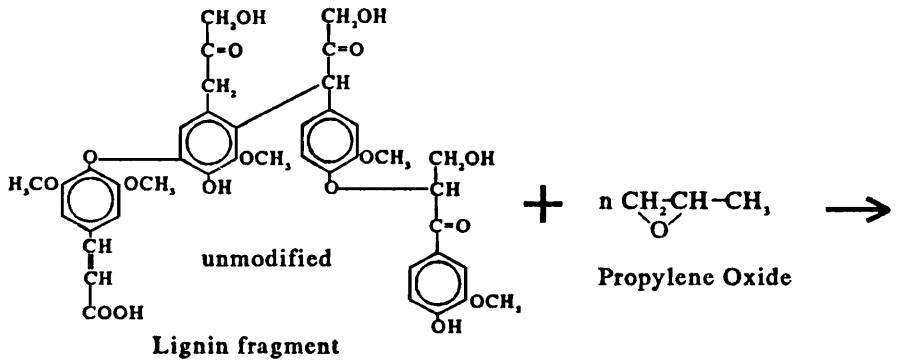

2.) Ethoxylation:

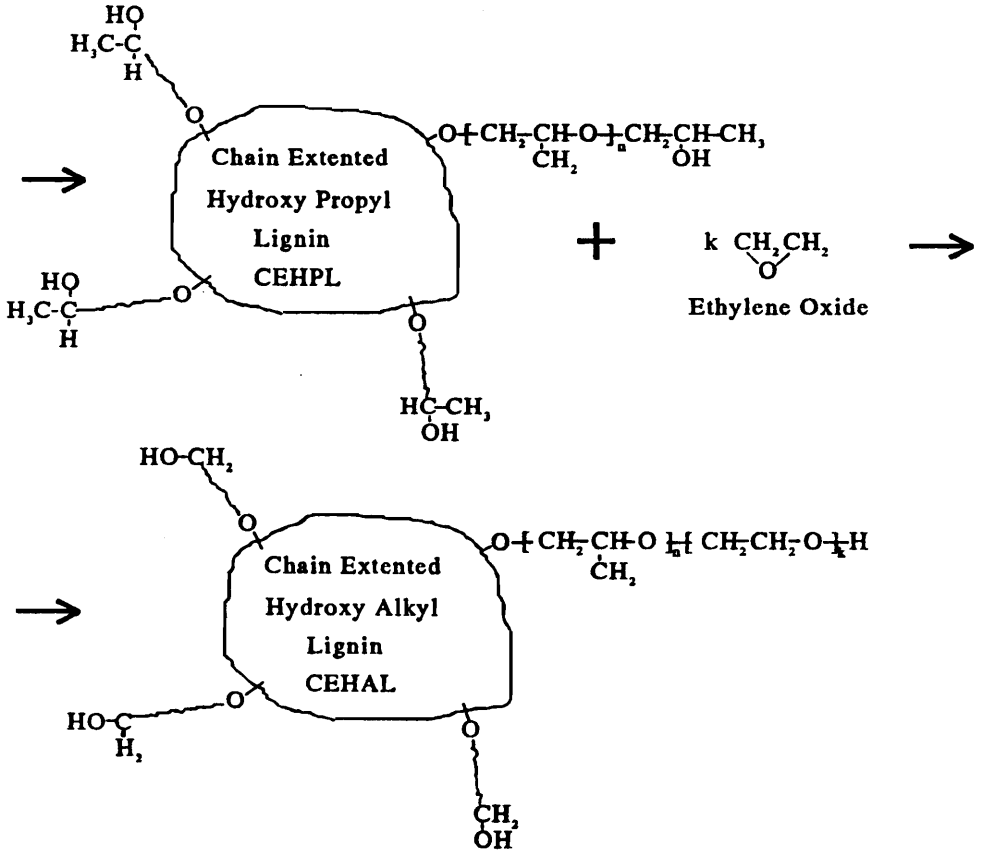

Figure 3. Modification of Lignin with Propylene Oxide and Ethylene Oxide

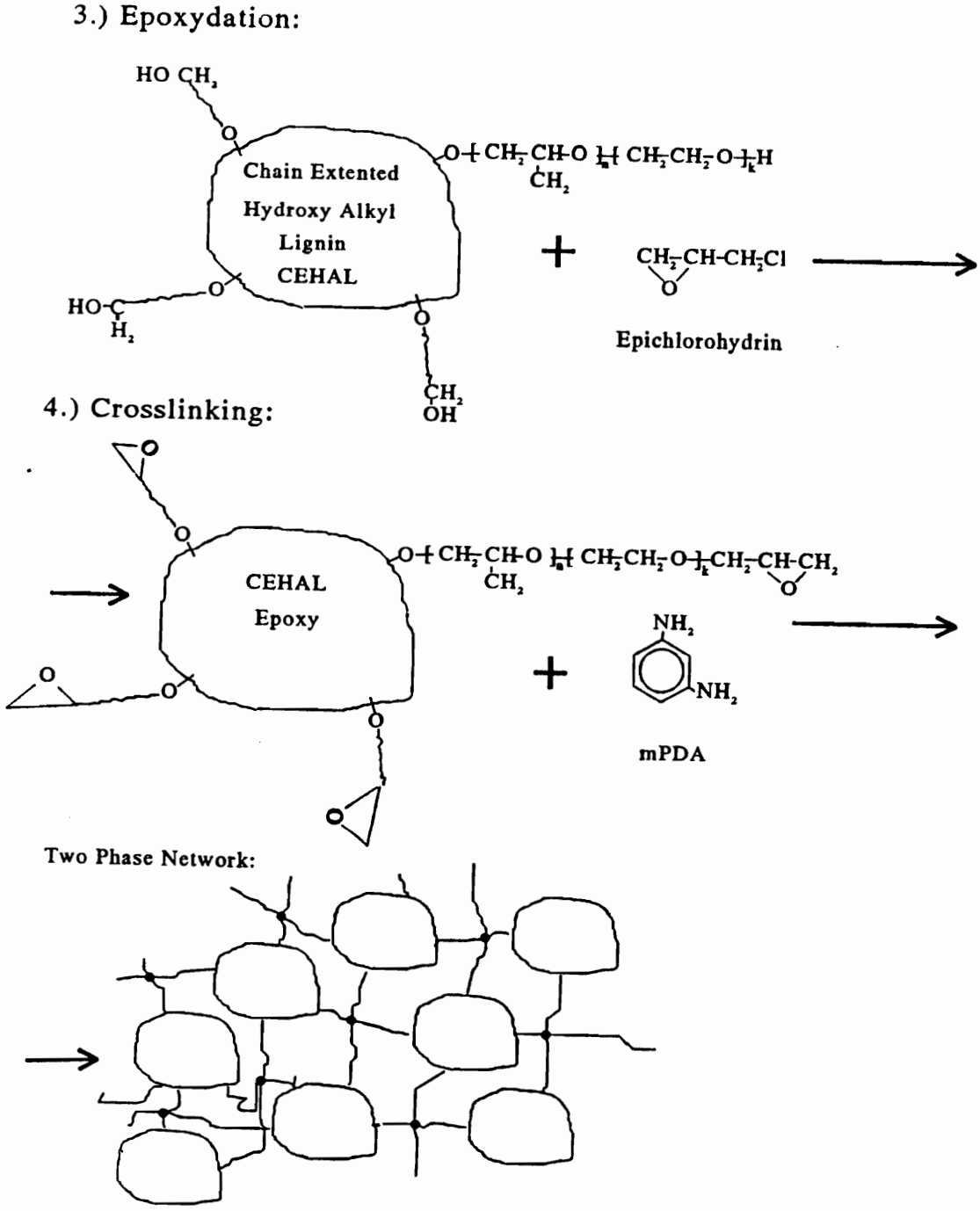

Figure 4. Epoxidation of Lignin-Polyether Copolymer and Network Formation

which carry the epoxy functional group. Before curing the epoxides with an aromatic diamine which will be described in Ch. 3, the resins were fractionated by solvent precipitation. This not only removed most of the poly(alkylene oxide) homopolymers formed during the propoxylation reaction, but also yielded lignin epoxides with a narrower molecular weight distribution. Thus, by adjusting the feed ratio during chain extension and by precipitation fractionation, specimens with widely differing compositional parameters were obtained.

The analytical procedures are described in Ch. 2.2.2 which consist mainly of measuring the oxirane concentration (2.2.2.1) by HBr titration, determining the molecular weight distributions of the fractions by GPC (2.2.2.2), and of the calculation of copolymer composition from UV and ^1H NMR data (2.2.2.3).

2.2.1.1 Chain Extension of Lignin with Propylene and Ethylene Oxide

Chain extension by hydroxyalkylation has been carried out routinely more than 100 times in an one gallon Parr pressure reactor in this laboratory. Synthesis and characterization of these star-like polymers have been described in detail by Kelley et al. [23,24] and de Oliveira and Glasser [25]. Lignin with a moisture content of 6% was dried in toluene by azeotropic distillation. The toluene was previously mixed with distilled water containing potassium hydroxid. 550*g* of the dry potassium lignate in toluene suspension were added to the reactor which was sealed subsequently. The temperature was raised to 140°C while the content was stirred mechanically. Propylene (PO) and ethylene oxide (EO) had previously been loaded into pressurized storage cylinders which were connected to the pressure reactor via a pressure regulated solenoid valve. After an initial injection of PO, the temperature was lowered to 110°C and the remaining propylene oxide was added stepwise whereby the amount was controlled by upper and lower pressure set limits. This procedure has been found to minimize the formation of poly(alkylene oxide) homopolymer which preferentially forms when most of lignin's phenolic hydroxyl groups have been converted [26]. After depletion of the propylene oxide reservoir, ethylene oxide was injected in order to cap the chains

with primary hydroxyls. The entire reaction was controlled by a pressure sensor which triggers the solenoid valve and the temperature was kept constant within ± 1°C. Depending on the amount of chain extension the reactions lasted 24 to >100*hrs*. After completion of the reaction and cooling, the reactor was opened and the product collected. Depending on the extent of the modification the reaction products were either in solution (medium to highly modified) or precipitated (short chain extension). Toluene was distilled off under vacuum.

Seven samples have been prepared by this method, whereby the highly chain extended lignins appeared as liquids at room temperature, and the medium to lower modified products were tars or powders. However, factors such as homopolymer content and lignin molecular weight also influenced the texture of the chain extended product. All products were soluble in many organic solvents such as acetone, methylene chloride, chloroform, and acetonitrile. Table 1lists all lignin-poly(alkylene oxide) copolymers produced for this study. All sample designations contain the prefix LX which is followed by for digits, whereby the first two reflect the number of *mol* PO and the second pair the number of *mol* EO per *kg* dry lignin.

2.2.1.2 Epoxidation of Lignin-Polypropylene Oxide Copolymers

Epoxidations of lignin-poly(alkylene oxide) star-like copolymers bearing primary hydroxyl groups were carried out either prior to (LX1204, LX2404) or after homopolymer extraction and fractionation (LX1512, LX4003). The epoxidation procedure was similar to the one described by Nieh [21], however, no phase transfer agent was used. As reaction solvents toluene was used for highly extended lignins and methylene chloride for the toluene insoluble samples. Although minor variations and modifications occurred in the eleven epoxidation reactions which were carried out for this study, most preparations were performed according to the following scheme:

A 25% solution of the chain extended lignin was prepared by slowly adding the lignin copolymer into a six liter reaction flask. The solution was stirred magnetically with a teflon coated two inch

Table 1. Listing of Lignin-Poly(propylen Oxide) Copolymers

LX0013[1]	LX0513[2]	LX1204[3]	LX1512[3]
LX2404[3]	LX3010[2]	LX4003[3]	

[1]Organosolv lignin, not fractionated
[2]Steam-exploded lignin, not fractionated
[3]Steam-exploded lignin, fractionated

stir bar at ambient temperature. Ten mols of epichlorohydrin per equivalent hydroxyl group were added at the start of the reaction. Ground KOH was added in four steps of one equivalent each (based on copolymer hydroxyl content), every 24*hrs*. After 120*hrs* the reaction was quenched by addition of solid carbon dioxide to neutralize the excess KOH. The solution was centrifuged twice at 5000 *rpm* for 20 minutes to remove KCl and KOH. Solvent and epichlorohydrin was distilled off by rotoevaporation. The solvent free product was filled into polyethylene jars and stored at -20°C.

2.2.1.3 Homopolymer Extraction and Fractionation

During the propoxylation reaction a considerable amount of poly(propylene oxide) homopolymer was produced and subsequently epoxidized. Although, a controlled addition of a polyether {_}i}iz3E !S}iKo ¬ %UxDyesopolymer epoxide could be beneficial as reactive diluent, it was chosen to remove the homopolymer. Wu and Glasser [26] described a solvent-solvent extraction procedure where hexane was used to extract homopolymer from an acetonitrile solution of the copolymer-homopolymer mixture. However, this procedure has the disadvantage of being very time consuming. In addition, it prooved to be incapable of removing all of the homopolymer in cases of chain extension. Knowing that both homopolymer and copolymer are soluble in acetone but only the homopolymer remains in solution in hexane, a 60% solution of the copolymer-homopolymer blend was prepared in acetone and subsequently added to 10 times the volume of hexane. The mixture was stirred for five minutes before it was allowed to settle for two hours. The clearly separated faint yellowish homopolymer solution was decanted, rotoevaporated, and collected as pale yellow oily liquid.

The resulting homopolymer free lignin-poly(alkylene oxide) copolymers have a high degree of polydispersity. Their molecular weight distributions usually range from 500 to 500 000 Daltons with polydispersity indices in the order of 10 to 15 (see Figure 8 and Figure 9). To obtain lignin containing epoxy resins with narrower molecular weight distributions precipitation fractionations were

a)

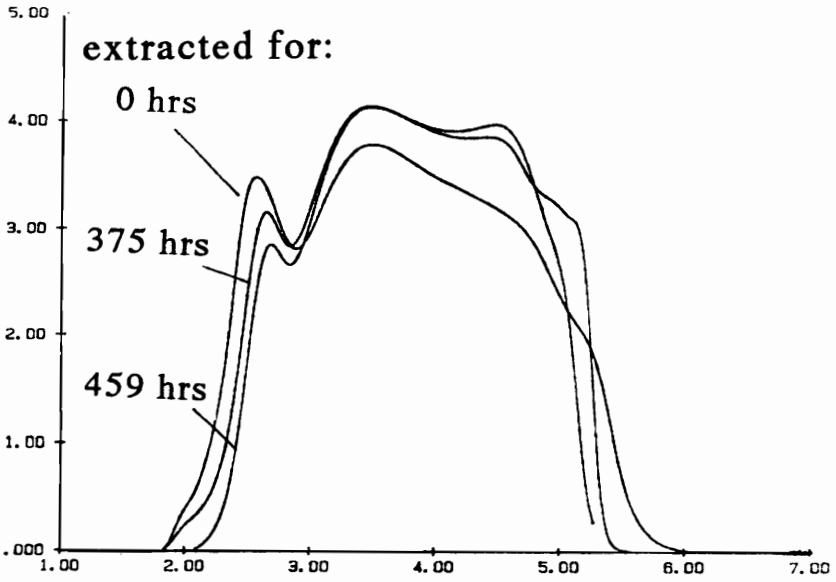

b)

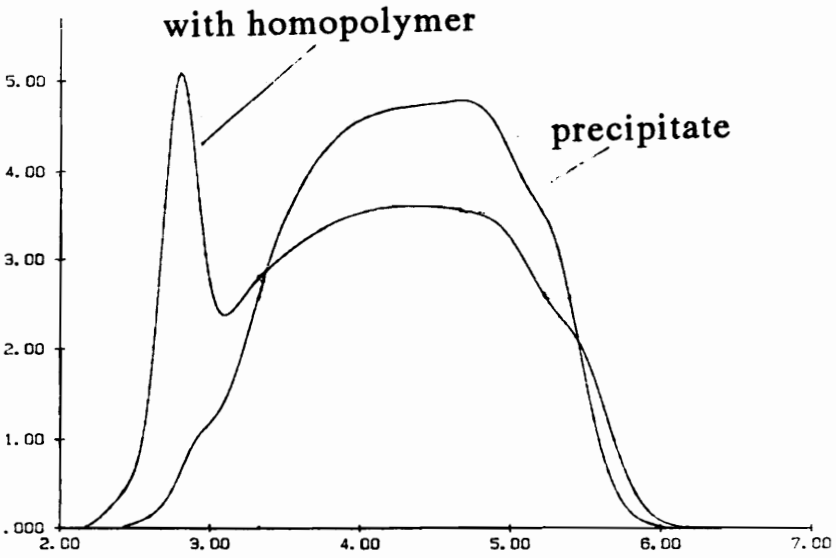

Figure 5. Comparison of Methods for Homopolymer Extraction
: a) Solvent-solvent extraction
b) Precipitation in hexane

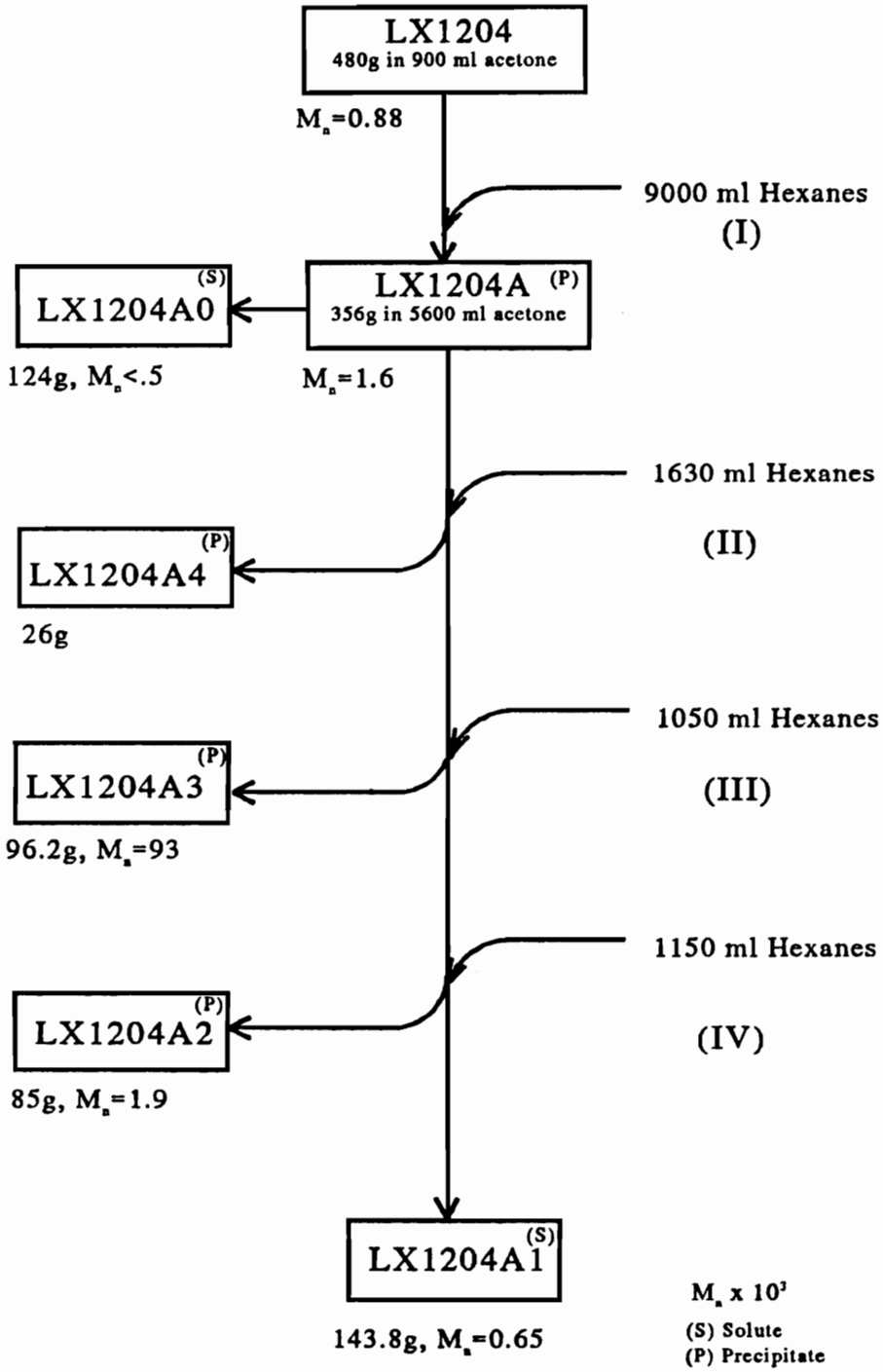

Figure 6. Fractionation Scheme of LX1204

carried out. Efficient fractionation requires the preparation of very dilute mother solutions [27]. While this is feasible for analytical amounts, the quantities of solvent necessary to fractionate 100 to 200 grams of lignin copolymers are prohibitive. However, it was found that the preparation of 10% starting solutions, by stepwise adding nonsolvent, yielded satisfactory results. Thus, by successive precipitation in acetone : hexane solvent mixtures, it was possible to collect three to four fractions which differed not only in molecular weight, but also in copolymer composition. By increasing the hexane content, larger star-like copolymer molecules having a higher lignin content will precipitate first.

Since the solubility profiles of the four samples varied, the fractionation schedule was devised individually for each copolymer by test tube precipitation. It was thereby attempted to obtain three fractions with different molecular weight distributions of approximately the same amount. The following example of the fractionation of LX1204 is representative for the other fractionations (see Figure 6); however, the actual solvent ratios may vary.

The first step (I) is the removal of homopolymer by adding a ten fold amount of hexane to the 60% acetone solution whereby the precipitate, LX1204A, is redissolved in a 6.4% acetone solution. Steps II, III, and IV involve stepwise addition of hexane to this solution and the precipitation of LX1204A4, LX1204A3, and LX1204A2 (see Figure 6). The lowest molecular weight fraction, LX1204A1 remained in solution. All fractions were dried in a rotoevaporator and stored at -20°C. Figure 6 includes also the number molecular weights of the fractions and their actual amount in gram. The data for all fractionated samples including copolymer compositions are compiled in Table 2 on page 32. In most cases the highest molecular weight fractions were not used because of solubility problems. It took for instance more than one week to redissolve LX1204A4 or LX2404A3 once they have been dried thoroughly.

2.2.2 Analysis of Lignin-Poly(propylene Oxide) Copolymers

2.2.2.1 Epoxy Content

The determination of the epoxy equivalent weight was carried out by potentiometric titration of the dissolved epoxide with hydrogen bromide [28]. A 0.05N solution of HBr in acetic acid was prepared and routinely checked by titration of a known quantity of hydrogen potassium phthalate. Weighed lignin epoxide (ca. 0.4*g*) was dissolved in about 10 *ml* chloroform and stirred magnetically. The change in resistivity of the solution during titration was recorded by a Brinkmann E576 Potentiograph. The rate of addition was 2*ml*/ min. Upon consumption of all epoxide groups the recorded resistivity usually undergoes a sharp transition whereby the midpoint is taken as volume of consumed titrant. However, in the case of unfractionated samples the transition was rather gradual in which case the intersection of the transition tangent with the final baseline tangent has been taken as the endpoint. From the consumed titrant volume the epoxy equivalent weight (WPE) in *g/eq*.. was calculated.

Besides the quantitative epoxide determination by HBr titration a quick test of epoxidation by ^{1}H NMR was performed. Unlike FTIR, proton NMR spectra unambiguously show the presence of oxirane groups in lignin whereby the three epoxide protons can be found at 2.6, 2.8, and 3.2 ppm [21] (see. Figure 7).

2.2.2.2 Molecular Weight Distribution

Molecular weight distributions were recorded by gel permeation chromatography with a refractive index recorder (Waters 410) and a differential viscometer (Viscotek Model 100) connected in series after three Ultra Styrogel™ Waters columns of size: 10^3Å, 10^4Å, and 10^6Å, thereby allowing for the separation of molecular weights from 500 to 4 000 000 Daltons. Both, injection port (UK6)

Figure 7. Proton NMR Spectra of LX1204 Fractions

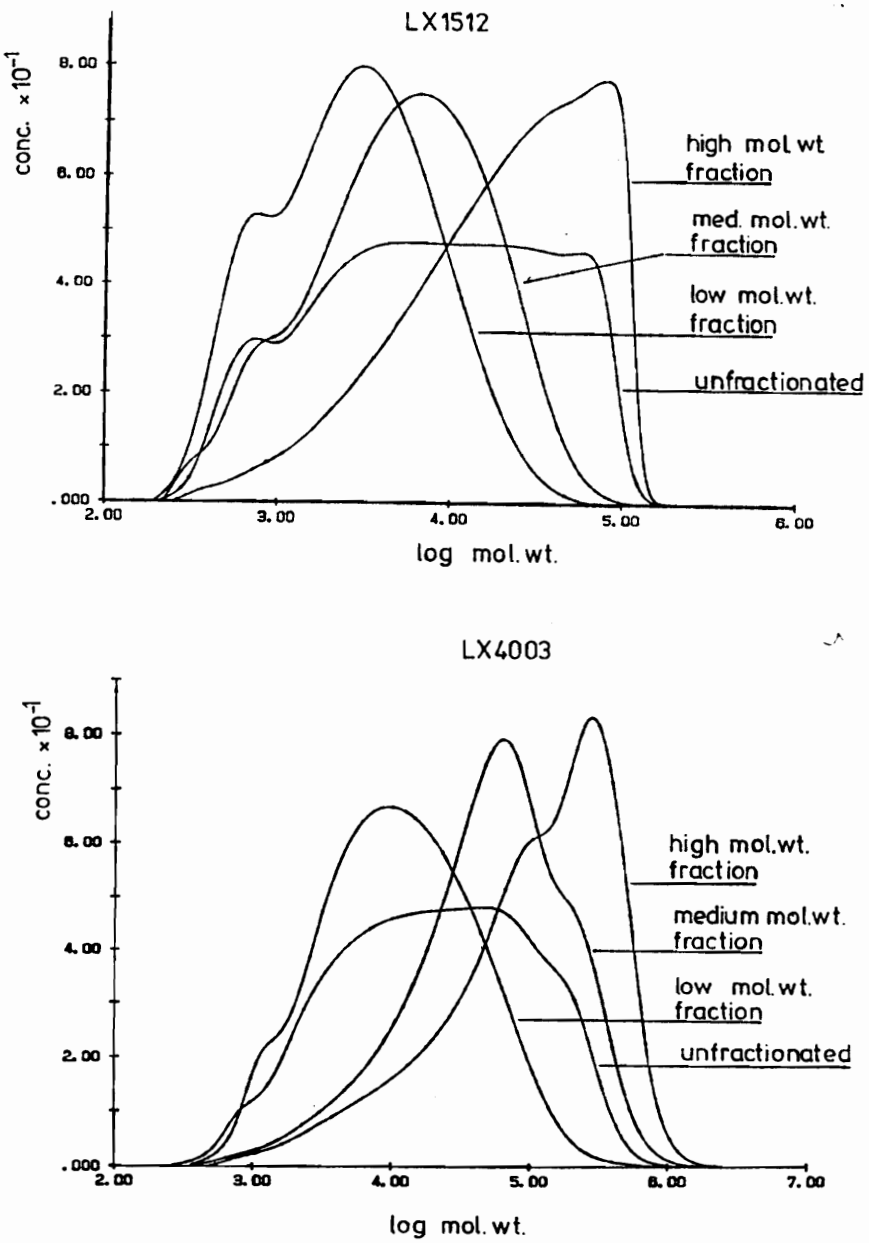

Figure 8. Molecular Weight Distributions of LX1512 and LX4003 Fractions

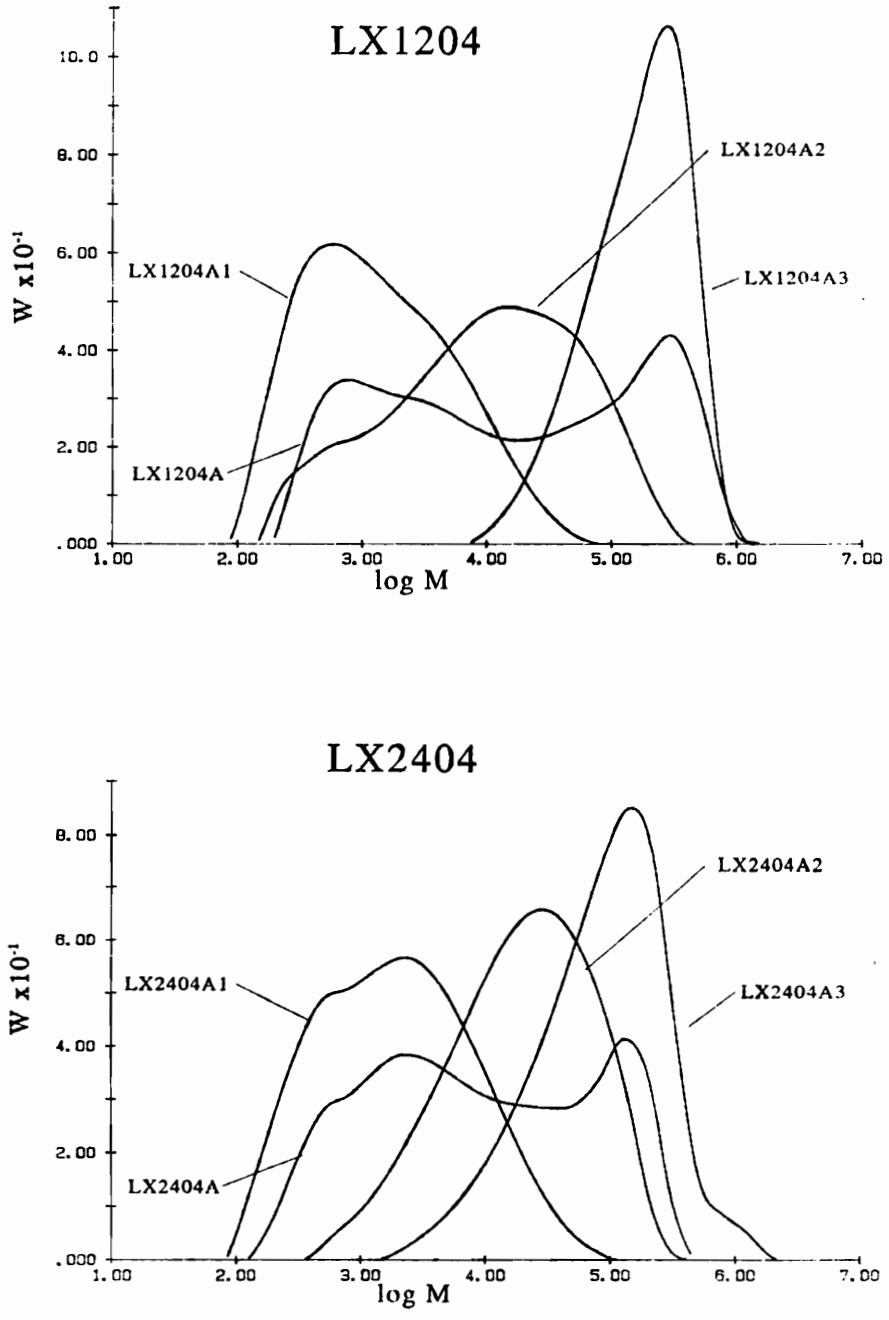

Figure 9. Molecular Weight Distributions of LX1204 and LX2404 Fractions

and HPLC pump (510) were manufactured by Waters. The mobile phase was THF. Molecular weight calculations were performed by UNICAL™ software on an IBM compatible computer. By simultaneously recording concentration and intrinsic viscosity it is possible to calculate an absolute calibration curve of hydrodynamic volume $[\eta]M$ versus elution volume. Hence, this method has the advantage vis á vis conventional GPC methods that universal calibration curves could be devised with high precision linear polystyrene standards instead of using lignin standards. This method applied to the measurement of molecular weights of hydroxypropyl lignins (HPL) has been shown by Siochi et al. [29] to yield reliable results. The molecular weight distributions of most of the samples are compiled in Figure 8 and Figure 9.

2.2.2.3 Lignin Content and Arm Length

Lignin has a strong UV absorbance at 280*nm* [30] which can be used to quantitatively asses the lignin content of the chain extended lignin copolymers. De Oliveira [25] developed an algorithm to calculate the amount of non UV absorbing mass, W per kg hydroxypropyl lignin from the absorptivity constant ε_{280}

$$W = \frac{22100}{\varepsilon_{280}} - 1000 \qquad [2.1]$$

By assuming an average hydroxyl content of the unmodified lignin of 5% [31] which means that onekg of HPL contains 162g of non UV absorbing propylene oxide it is possible to calculate the percentage of unmodified lignin in the copolymers as

$$\text{Lignin content } (\%) = 100 - 100\frac{W + 162}{W + 1000} \qquad [2.2]$$

Knowing the molecular weight and the epoxy equivalent weight, one can calculate the average number of arms per mole. Subsequently, the average arm length can be derived from the lignin content. However, the average arm length also can be determined by proton NMR. As pointed out

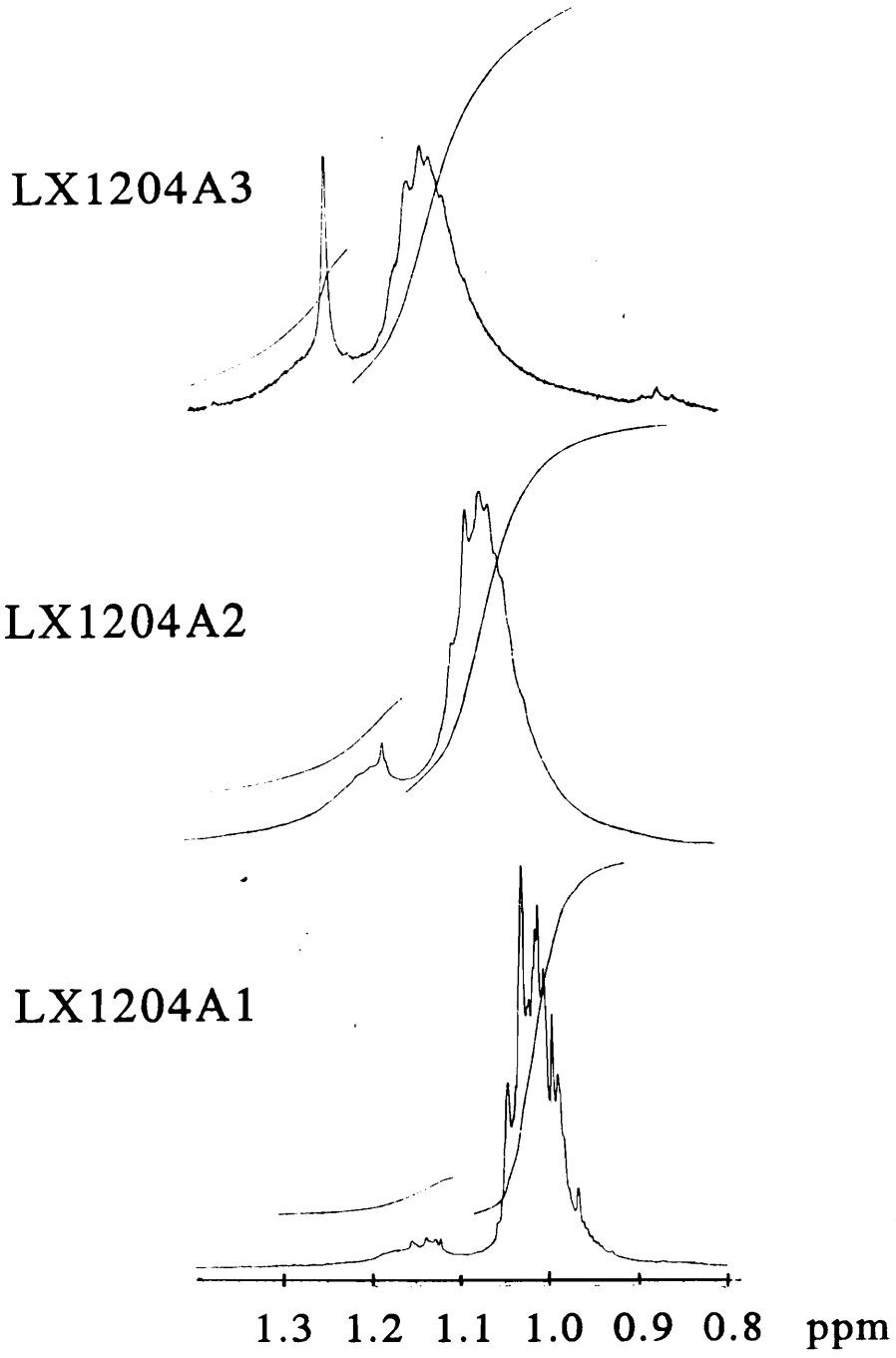

Figure 10. Proton-NMR Spectra of LX1204 Fractions; Expanded Methyl Region

by Kelley and Glasser [23], the methyl protons in the spectra of chain extended hydroxypropyl lignins appear at two positions: the majority at 1.0 ppm and a smaller peak at 1.12 ppm. The authors could show that this "split" reflects the different environment where methyls can be found in chain extended hydroxypropyl lignin. All methyls are attached to the poly(propylene oxide) chain but those connected to the first propylene oxide unit, i.e., closest to lignin, appear as more down field peak while the rest of the methyls are represented by the larger upfield peak. Employing a VARIAN 400MHz NMR spectrometer, it was possible to baseline separate the two methyl peaks (see Figure 10) and to calculate the ratio of the two areas which yield an average chain length in PO units ($M = 58g/mol$). The results of both methods of determining the average arm lengths are contrasted in Table 2.

2.3 *Results and Discussion*

All relevant results of the lignin modification, epoxidation, and fraction are compiled in Table 2. Epoxidation of the lignin-poly(alkylene oxide) copolymers by excess addition of epichlorohydrin and stepwise addition of potassium hydroxide without the use of further catalysts is an efficient procedure of preparing lignin containing epoxy resins. Due to the fact that epoxidation was primarily carried out prior to homopolymer extraction and fractionation, it is difficult to gauge the extent of conversion of the various fractions. Nevertheless, compared with the work of Nieh et al. [20,21,33] who epoxidized unfractionated hydroxypropyl lignin (HPL), where secondary hydroxyls were converted and equivalent weights (WPE) of $670g/eq.$ were achieved, the conversion of primary hydroxyls by this procedure is more efficient. Those fractions having comparable molecular weights have epoxy equivalent weights of 300 to $400g/eq.$, and even the high molecular weight fractions have WPE values of not less than 600 to $700g/eq.$. Although no detailed kinetic and yield investigations were conducted, it is evident that the majority of hydroxyls have been converted into epoxy groups.

Table 2. Compilation of Molecular Weights, Copolymer Compositions, and Epoxy Contents

Sample[1]	Homopol.[2] Content	Fraction #	%	M_n[3]	M_w[3] x10³	Lignin[4] Content %	Epoxy Eq.[5] Weight g/eq.	Funct.[6]	Arm Length calc.[7]	Arm Length ^{1}H NMR[8]
LX0013[9]	n/a	n/a		1.2	9.9	57.0	670	1.8	288	
LX0513	n/a	n/a		11.3	129.0	55.0[10]	532	21.2	239	
LX1204	25.8	A1	40.9	0.63	3.0	16.0	231	3.6	195	563
		A2	24.3	1.9	28.0	36.7	399	4.8	252	220
		A3	27.4	93.8	213.7	42.1	439	211.0	254	162
		A4	7.4							
LX1512	17.0	A1	30.0	1.4	4.2	34.0	390	3.6	257	
		A2	10.0	2.1	9.0	44.0	550	3.8	308	
		A3	58.0	6.4	33.4	48.0	430	14.9	224	
LX2404	38.2	A1	43.6	0.79	4.3	21.4	360	3.6	283	557
		A2	28.4	3.02	36.0	38.7	507	20.9	311	267
		A3	28.0	30.2	132.8	33.6	602	94.7	400	
LX3010	n/a	n/a		3.6	32.3	25.0[10]	413	8.7	310	
LX4003	25.8	A1	47.5	5.2	24.0	34.9	385	13.4	251	
		A2	20.6	15.3	96.0	43.2	518	29.5	295	
		A3	31.9	22.7	190.0	41.7	714	31.8	416	

1 all lignins from steam - exploded yellow poplar wood, excpt. LX0013
2 by acetone - hexane precipitation, excpt. LX1512
3 by GPC, universal calibration
4 by UV_{280}, excpt. LX0513 and LX3010
5 by HBr titration
6 Functionality, M_n/WPE
7 $M_n(1 -$ Lignin Content)/Funct.
8 ratio of upfield (1.0 ppm) to downfield (1.15 ppm) CH_3 signal area
9 Organosolv Lignin
10 from lignin propylene oxide feed ratio
11 by solvent-solvent extraction

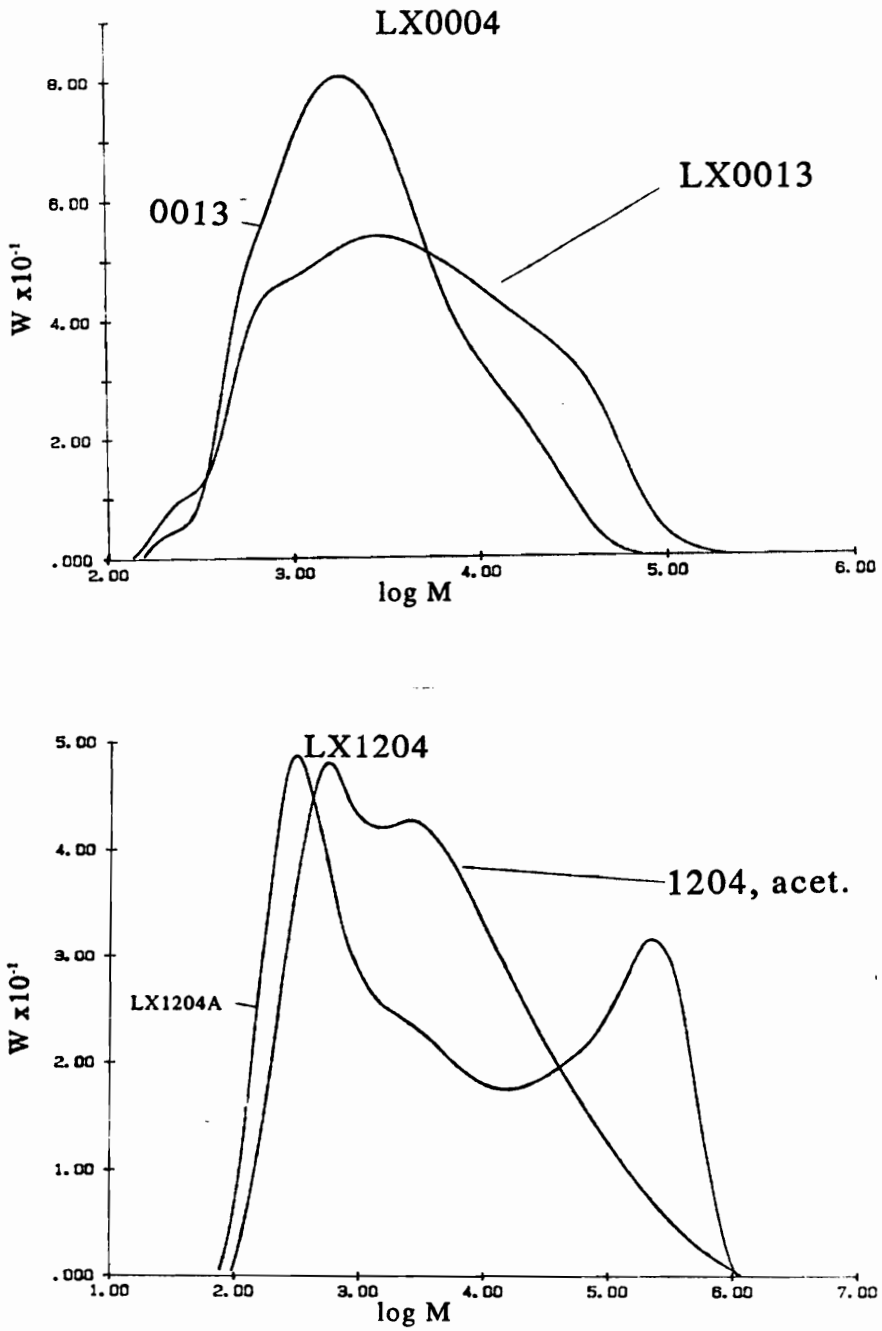

Figure 11. Molecular Weight Increase During Epoxidation

: a) 0013: ethoxylated organosolv lignin
LX0013: epoxidized 0013
b) 1204, acet: acetylated lignin copolymer containing homopolymer
LX1204A: Epoxidized 1204

However, intermolecular side reactions during the epoxidation reaction could not have been avoided completely. Though no gel formation was observed, the number of species with molecular weights of about 10^5 increased considerably at the expense of smaller molecules (Figure 11 b). The most obvious path for this side reaction is the reaction of an oxyanion with a newly formed epoxy group. Nieh et al. [20,21,33] reported that epoxidation reactions carried out for more more than nine days exhibit formation of insoluble material. Although, no insoluble material was found, a continuation of the epoxidations of chain extended lignins beyond 120*hrs* would have led to gel formation. Indeed, those copolymers which precipitated first during fractionation were very difficult to redissolve and they were not used for further experiments. It might be advisable for further epoxidation work on lignin derivatives to increase the number of KOH addition steps and reduce the amount of base added during each step. This would decrease the number of available oxyanions at any given time and thereby diminish the possibility of side reactions. Although, the number of larger molecules have increased also during the epoxidation of the ethoxylated organosolv lignin (LX0013) (Figure 11 a), it seems that it happened to a lesser degree even though the reaction conditions were identical to those of other samples.

In spite of the goal to minimize homopolymer formation during propoxylation, a substantial amount of poly(propylene oxide) was produced. Homopolymer content was in general above 20% with an extreme value of 38.2% for LX2404. However, extraction with a 1:10 acetone : hexane solvent mixture was possible. The efficiency of this procedure is demonstrated by the molecular weight distributions (Figure 5). While it took 668*hrs* to remove most of the lower molecular weight peak representing the homopolymer of LX1512 by liquid-liquid extraction (Figure 5, a) the same task was achieved more efficiently within two hours by hexane precipitation (Figure 5, b). The further fractionation of the homopolymer free copolymer in acetone-hexane systems of increasing hexane content had a two fold effect. Firstly, reducing the "goodness" of the solvent (acetone) by addition of a nonsolvent (hexane) decreases the radius of gyration of the star-like copolymers and results in the eventual precipitation of the largest species, thereby separating the highly polydisperse lignin epoxides into fractions of narrower molecular weight distributions. Following the diagram

of Figure 5, and the molecular weight values compiled in Table 2, as well as the graphs of the molecular weight distributions (Figure 8 and Figure 9), it is evident that the employed fractionation method efficiently separates the epoxides by molecular weight. Secondly, fractionation in acetone-hexane has also a separation effect in terms of lignin content. Since hexane is a good solvent for poly(propylene oxide) but a non solvent for lignin and the copolymer, those species with relatively higher aliphatic polyether content should remain longer in solution once the hexane content is increased. Indeed, as can be seen from Table 2, the lignin content is lowest for the samples remaining longest in solution. The fractions precipitating at a lower hexane content have a higher lignin content. However, only for the short chain modified lignins, i.e., LX1204 and LX1512, this trend is continuous while the higher extended samples LX2404 and LX4003 exhibit a lignin content maximum for the medium fraction and a slight decrease for the first precipitate. Although, the primary reason for carrying out the fractionation routine was to obtain fractions with narrower molecular weight distributions and not to systematically study the solution properties of the copolymers, it can nevertheless be concluded that

a. fractionation in acetone-hexane solvents with increasing hexane content yields copolymer fractions which are clearly separated by molecular weight;
b. the fact that the aliphatic polyether arm of the star-like copolymer has a higher affinity for hexane than the lignin core results in additional separation by lignin content, which is more pronounced for the lesser propoxylated lignins; and
c. homopolymer content can be effectively reduced by precipitation of the acetone dissolved homopolymer-copolymer blend in a ten fold volume of hexane.

It is conceivable that the fractionation by lignin content has an influence on the length of the poly(propylene oxide) arms. Their size can be calculated from the lignin content and the epoxy functionality by assuming that all arms are capped by epoxy groups.[1] However, such calculations overestimate to a certain degree the length of the arms, especially for the high molecular fractions,

[1] Only those arms carrying epoxides will become effective network chains upon cross-linking. However, epoxy free poly(alkylene oxide) chains still will have a plasticizing effect on the thermoset

because those chains having participated in the premature inter-lignin reactions during epoxidations are not accounted for in the calculation of functionality. Nevertheless, the calculated sizes of the poly(propylene oxide) side chains permit the estimation of the overall length of the flexible connections in the cross-linked copolymers. As it can be seen from Table 2, the so calculated arm lengths are remarkably constant between 200 and 300 Daltons, about 5-7 propylene oxide units. A slight increase with lignin content is observed for some samples. This result could be seen as an indication that during the propoxylation reaction all hydroxyl groups were extended to the same extent regardless of the size of the lignin molecules. Contrasted with these data are the results of the arm length determination by ^1H NMR area ratio of the two methyl proton signals (see. Figure 10). The so derived arm sizes do not match the calculated results and suggest a trend to shorter chains with higher molecular weight. This would imply that propoxylation results in longer arms on smaller lignin molecules. In fact the difference between the calculated and NMR based arm length is only significant for the lowest lignin content samples, where the method of rationing the methyl signal areas is most prone to errors since the downfield peak is relatively small.

2.4 Conclusion

Epoxidation of lignin-poly(alkylene oxide) copolymers which contain primary hydroxyls by a method of adding 10 fold excess epichlorohydrin to a 25% toluene or methylene chloride solution and the stepwise addition of KOH has been carried out on eleven fractionated and unfractionated samples with good yield of conversion. The epoxide copolymers contain up to 57% lignin and are soluble in many organic solvents. Fractionation in acetone-hexane solutions has been shown to be an efficient method to extract poly(propylene oxide) homopolymer and to yield fractions clearly separated by molecular weight, and to a lesser extent by lignin content. The length of the epoxy group carrying chain was nearly constant throughout the samples if calculated from lignin content and epoxy functionality.

2.5 *References*

1. A. Wurtz, *Compt. Rend.*, 48, 1859, 101
2. C. A. May, in C. A. May, Ed., "Epoxy Resins, Chemistry and Technology", Marcel Dekker, Inc., New York, 1988
3. *Modern Plastics*, Jan., 1990
4. W. G. Glasser, in R. W. Hemingway and A. H. Conner, Eds., "Adhesives from Renewable Resources", ACS Symp. Ser. 385, Washington, DC, 1989
5. A. Rosowsky, in A. Weissberger, Ed., "Heterocyclic Compounds with Three- and Four-Membered Rings, Part 1", Interscience Publ., New York, 1964
6. G. Pruckmayr, in K. C. Frisch, Ed., "Cyclic Monomers", Wiley- Interscience, New York, 1972
7. Y. Tanaka, in in C. A. May, Ed., "Epoxy Resins, Chemistry and Technology", Marcel Dekker, Inc., New York, 1988
8. G. Hollinger, L. Kuniak, and R. H. Marchessault, *Biopol.*, 13, 1974, 879
9. J. Lelievre, *J. Coll. Interf. Sci.*, 101, 1984, 225
10. D.-S. Lee and A. S. Perlin, *Carbohyd. Res.*, 106, 1982,
11. R. E. Wing, W. M. Doane, and C. E. Rist, *Carbohyd. Res.*, 106, 1982,
12. J. B. McKelvey, B. G. Webre, and E. Klein, *Text. Res. J.*, 29, 1959, 918
13. W. Förster, US Pat. # 2,868,768, 1955
14. M. Mikhailov and K. Budevska *Compt. Rend. Acad. Bulg. Sci.*, 15, 1962, 155, Abstr. #402 in F. Boye, "Utilization of Lignins and Lignin Derivatives", The Institute of Paper Chemistry, Appleton, 1985
15. M. Mikhailov and S. Gerdzhikova *Compt. Rend. Acad. Bulg. Sci.*, 18, 1965, 829, Abstr. #403 in F. Boye, "Utilization of Lignins and Lignin Derivatives", The Institute of Paper Chemistry, Appleton, 1985
16. S. Tai, M. Nagata, J. Nakano, and N. Migita, *Nihon Mokuzai Gakkai*,13, 1967, 102

17. S. Tai, J. Nakano, and M. Nagata, *Nihon Mokuzai Gakkai*, 13, 1967, 257
18. G. F. D'Alelio, US Pat. # 3,905,962, 1975
19. D. B. Holsopple, W. W. Kurple, W. M. Kurple, K. R. Kurple, US Pat., 4,265,809, 1981
20. W. Nieh, "Synthesis and Properties of Lignin Epoxides", MS Thesis, Virginia Tech, Blacksburg, 1986
21. W. Nieh and W. G. Glasser, in W. G. Glasser and S. Sarkanen, Eds., "Lignin, Properties and Materials", ACS Symp. Ser., Washington, DC, 1988
22. W. G. Glasser, "Proc. Int. Symp. Wood Pulp. Chem.", Melbourne, May 1991
23. S. S. Kelley and W. G. Glasser, *J. Wood Chem. Techn.*, 8, 1988, 341
24. S. S. Kelley, "Lignin Copolymers in Polyurethane Materials", PhD Thesis, Virginia Tech, Blacksburg, 1987
25. W. De Oliveira and W. G. Glasser, *J. Appl. Pol. Sci.*, 37, 1989, 3119
26. L. C.-F. Wu and W. G. Glasser, *J. Appl. Pol. Sci.*, 29, 1984, 1111
27. S. S. Kelley, T. C. Ward, T. G. Rials, and W. G. Glasser, *J. Appl. Pol. Sci.*, 37, 1989, 2961
28. ASTM D1652-73 (reaproved 1980)
29. E. J. Siochi, T. C. Ward, M. A. Haney, and B. Mahn, *Macromolecules*, 23, 1990, 1420
30. D. Fengel and G. Wegener, "Wood; Chemistry, Ultrastructure, and Reactions", DeGruyter, Berlin, 1984
31. F. E. Brauns and D. A. Brauns, "The Chemistry of Lignin", Academic Press, New York, 1960
32. T. Lindström, C. Söremark, and L. Westman, *J. Appl. Pol. Sci.*, 21, 1977, 2873
33. W. G. Glasser, W. de Oliveira, and W. L.-S. Nieh, US-Pat. # 4,918,167, 1990

3.0 Cure of Lignin Based Epoxy Resins

3.1 Introduction

In the forgoing chapter the epoxidation and fractionation of lignin-poly(alkylene oxide) copolymers were discussed. These materials are characterized by a varying lignin content and molecular weight, and were intended to be incorporated into multicomponent lignin containing networks. Properties of these networks were to be studied as function of compositional parameters. However, preceding to the formation of thermosetting networks it was necessary to investigate the influence of lignin content and/or molecular weight on the curing kinetics and on network formation. As described, the epoxy groups are not attached directly to the polyphenolic lignin molecule but separated from it by a poly(propylene / ethylene oxide) chain (see Figure 4). The kinetics of reaction of a thermosetting system at the early stage is only a function of chemistry of the reactants, but at later stages becomes also controlled by the morphology of the forming network, i.e., the ever tightening network structure increasingly curtails the mobility of the reactants [25]. Expecting that lignin is a decisive factor determining the diffusivity of the reactants beyond the gel point, it is certainly possible that a variation in lignin content influences the rate, and maybe the order of reaction once the

reaction is in a more advanced state. It has been shown for instance that commercial DGEBA-*m*PDA systems change the order and type of reaction after the gel point [25,42].

Specifically, the aim of the work described in this chapter was to probe the influence of composition on such kinetic parameter as rate and order of reaction. Although, epoxidized lignins have been described previously [45,46,47,48], no systematic investigations of lignin epoxide curing reactions have been reported. The kinetics of the reactions were investigated by dynamic differential scanning calorimetry (DSC) with multiple heating rates. Network formation and vitrification were studied by measuring the glass transition temperatures of the partially cured epoxides as function of cure time and cure temperature by dynamic mechanical thermal analysis (DMTA). The rise of the glass transition temperature, ΔT_g, during cross-linking was thereby monitored as a function of conversion. Other aspects of the cross-linking process which influence ΔT_g, such as reduction of the free volume, increase in cross-link density and simultaneous reduction of segmental mobility, and phases separation, will be discussed in Ch. 4.3.

3.1.1 Epoxy - Amine Reaction

Epoxides are very versatile and can be tailored to fit a wide variety of applications. Many combinations of epoxy - hardener systems are on the market yielding materials ranging from flexible adhesives to high temperature matrices for fiber reinforced composites [1]. Epoxides are a class of chemicals containing the oxirane ring

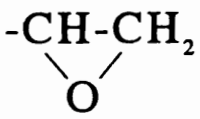

as reactive functional group. In order for an epoxidized compound to be fully incorporated into a chemical network, it should be a telechelic polymer with at least two oxirane functionalities or a multifunctional, branched molecule. The oldest and most widely used group of epoxy monomers

or prepolymers are based on diglycidyl ether of bisphenol A (DGEBA) of varying molecular weight [1]. For applications where high cross-link density and high performance at elevated temperatures are desired multifunctional epoxy novolac resins are employed [1,20]. The majority of cross linking agents or hardeners are amines, and to a lesser extent anhydrides. Amines can be roughly grouped into aromatic and aliphatic ones, whereby the latter are used to preferentially produce low T_g, flexible resins which can be cured at room temperature [3]. Aromatic amines are in general used for high T_g materials of considerable rigidity. Most epoxy - hardener systems are two component resins mixed in the appropriate stoichiometric amount prior to use. However, some systems are one component types with long shelf life at room temperature, based one dicyanoamide (DICY) which must be heat activated before becoming reactive [3].

3.1.1.1 Reaction Kinetics

Although several mechanisms have been suggested for the reaction between oxirane rings and amines [2], the one described in Figure 12 is considered the most likely option [2,9,43]. The rate determining step of the reaction is the bimolecular oxirane ring opening via a transition state (Figure 12, b), which succeeds a fast activation step of the ring by a hydrogen bond donating catalyst [HX] (Figure 12, a) [9,10]. The final step of the reaction is a proton abstraction and the recovery of [HX]. The overall reaction of a primary amine with an epoxy is a combination of two successive steps (Figure 13) which are the formation of a secondary amine with a pending hydroxyl group (a), and a tertiary amine acting as cross-link center (b). Both steps are catalyzed by hydrogen bond donors, like the pending hydroxyls formed during the reaction. However, they also may be present initially as impurities, added catalyst, or as part of the reacting system. It has been shown that phenolic hydroxyl groups are very good catalysts for this reaction, even at low temperature [2]. Depending on the initial concentration of [HX], epoxy - amine reactions can follow autocatalytic or *n*-th order type (Figure 14).

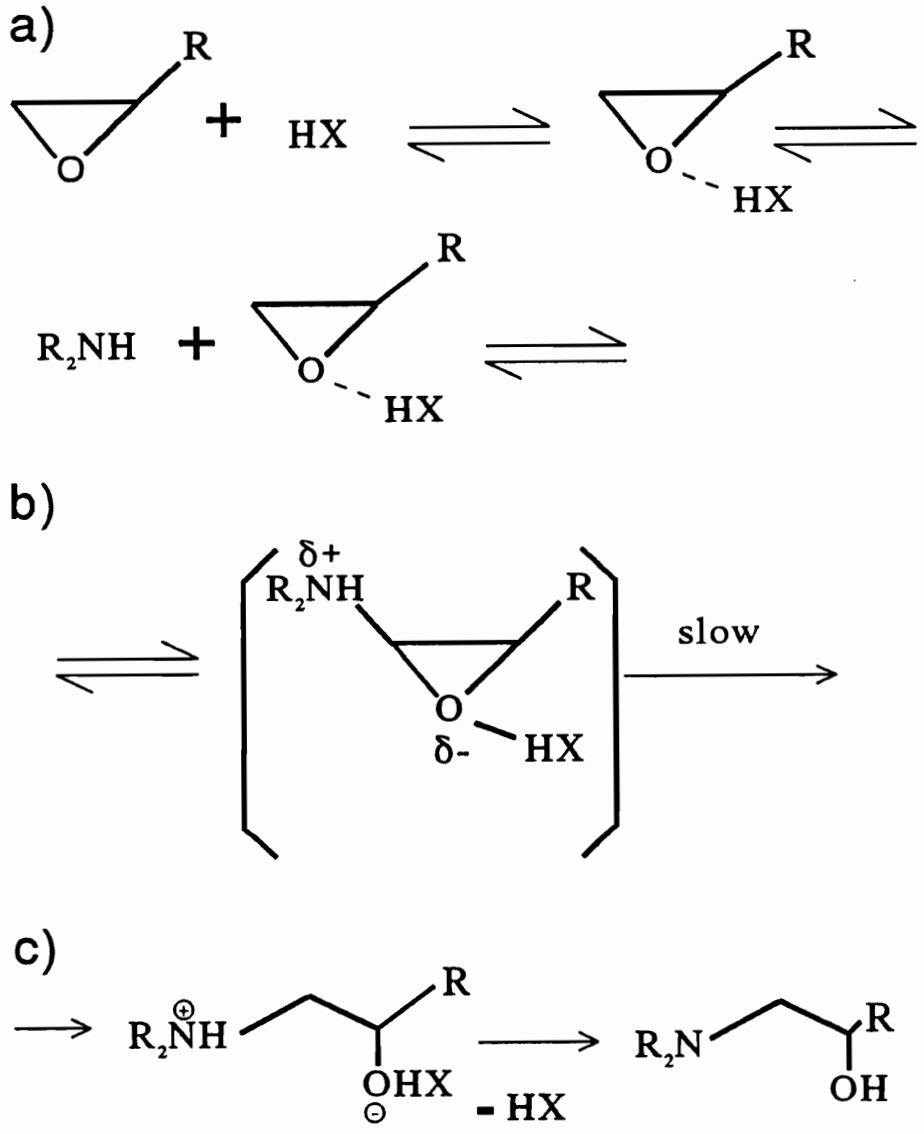

Figure 12. Mechanism of Epoxy-Amine Reaction
: a) Formation of activated oxirane ring, hydrogen bonding between [HX] and oxygen of ring
b) Formation of transition stage ring opening,
c) Proton abstraction and recovery of [HX] (rate determining step) [9]

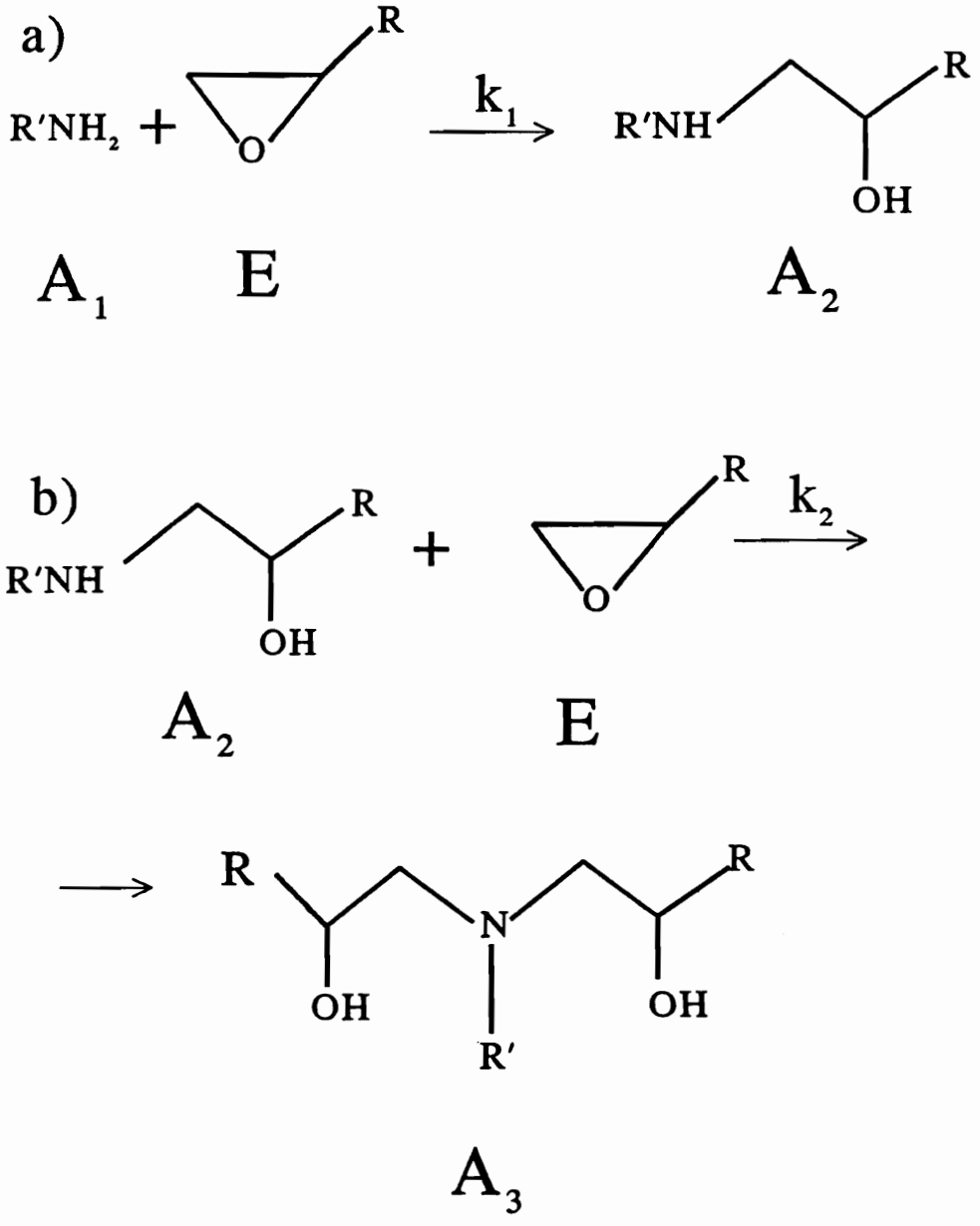

Figure 13. Generalized Epoxy-Amine Reaction
: a) Primary amine-epoxy reaction
b) secondary amine-epoxy reaction

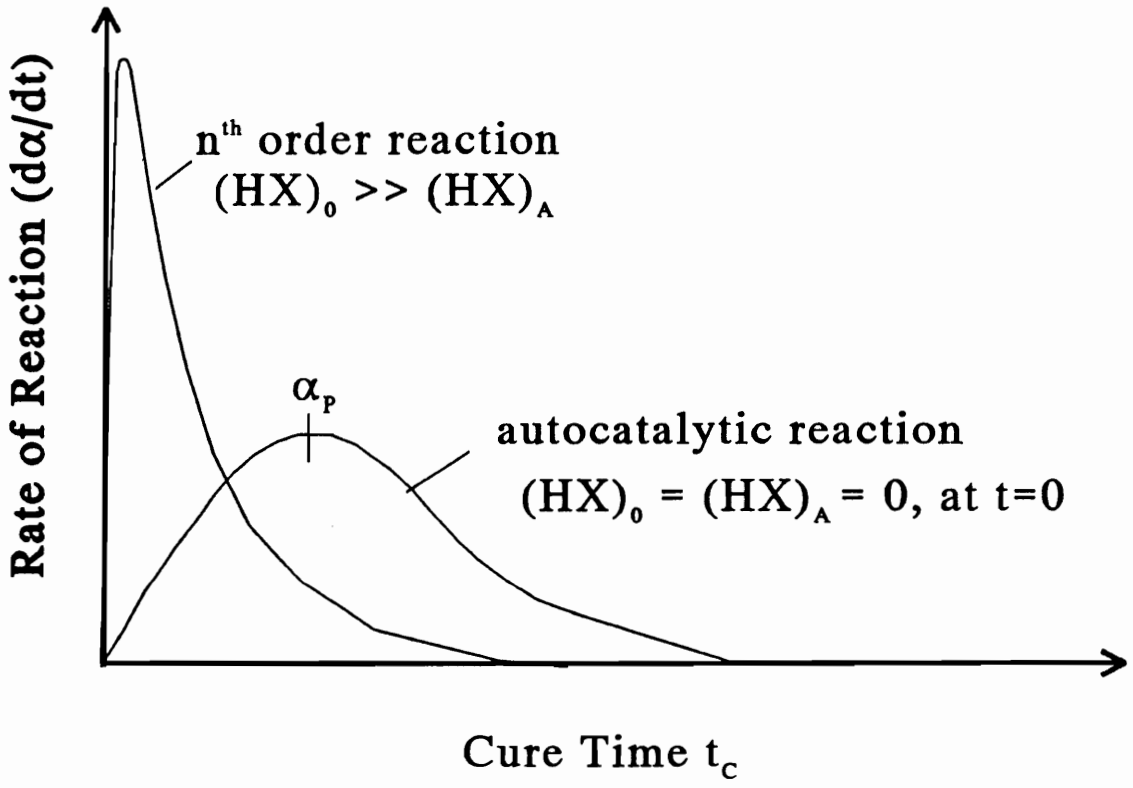

Figure 14. Types of Epoxy-Amine Cure Reactions
: a) Autocatalytic
b) n-th order

The basic kinetic rate equation of the curing reaction, based on the disappearance of the functional epoxide group is

$$\frac{d\alpha}{dt} = kf(\alpha) \qquad [3.1]$$

where α is the fractional conversion or extent of reaction defined as $(e_0 - e)/e_0$, and e_0 and e are the concentration of epoxide groups at 0 and t, respectively. k is the rate constant and $f(\alpha)$ is a function of the concentration of the reactant. If the reaction follows n^{th} order kinetics, $f(\alpha)$ is usually $(1 - \alpha)^n$, where n is the reaction order. On the other hand, autocatalytic reactions are characterized by $f(\alpha) = \alpha^m(1 - \alpha)^n$, where m is also an order of reaction. The kinetics of the bimolecular epoxy-amine reaction (step b in Figure 12) is complex and has been focus of numerous investigations and reviews [2,5,6,7,8,9] of which Horie et al. [6] presented a widely accepted kinetic model. Based on the reaction scheme of Figure 13, the individual rate equations can be written as:

$$\begin{aligned}
A_1 + E + (HX)_A &\xrightarrow{k_1} A_2 + (HX)_A \\
A_1 + E + (HX)_0 &\xrightarrow{k_1'} A_2 + (HX)_0 \\
A_2 + E + (HX)_A &\xrightarrow{k_2} A_3 + (HX)_A \\
A_2 + E + (HX)_0 &\xrightarrow{k_2'} A_3 + (HX)_0
\end{aligned} \qquad [3.2]$$

where A_1, A_2, and A_3 are the respective amines, and E represents the epoxide. $(HX)_0$ and $(HX)_A$ are the initially present, and the formed catalytic hydrogen bond donating group, respectively. Most often, these groups are hydroxyls which are also formed during the reaction (see Figure 13). k_1 and k_2 are the rate constants of the primary and secondary amine reaction, catalyzed by $(HX)_A$, and \f. <k sub 1> prime ' and ' <k sub 2> prime are the respective rate constants of the $(HX)_0$ catalyzed reactions. The reaction set forth above assumes that the catalytic group is not consumed in side reactions, and that for each epoxy group consumed there is one $(HX)_A$ formed. The concentration of A_1, A_2, and E at time t are denoted as a_1, a_2, and e. The initial concentration of

E and A_1 is e_0 and a_0, and c_0 is the concentration of $(HX)_0$. The amount of epoxy groups consumed, $x = e_0 - e$, whereby x is also the concentration of $(HX)_A$, is converted into the fractional conversion α by $\alpha = x/e_0$. Applying these definitions the following rate equations can be deduced from eq. 3.2:

$$\begin{aligned} \frac{dx}{dt} &= k_1 a_1 ex + k_1' a_1 ec_0 + k_2 a_2 ex + k_2' a_2 ec_0 \\ \frac{d\alpha}{dt} &= k_1 a_1 ee_0\alpha + k_1' a_1 ec_0 + k_2 a_2 ee_0\alpha + k_2' a_2 ec_0 \end{aligned} \qquad [3.3]$$

Both, the primary and the secondary amines are approximately equally reactive [2,6] which allows one to write

$$\frac{k_2}{k_1} = \frac{k_2'}{k_1'} = \frac{1}{2} \qquad [3.4]$$

since a primary amine bears two and a secondary one hydrogen. Inserting this and using the relation $e = e_0 - x$, eq. 3.3 simplifies to

$$\begin{aligned} \frac{dx}{dt} &= (e_0 - x)\left(a_1 + \frac{a_2}{2}\right)(k_1 x + k_1' c_0) \\ \frac{d\alpha}{dt} &= (1 - \alpha)\left(a_1 + \frac{a_2}{2}\right)(k_1 e_0 \alpha + k_1 c_0) \end{aligned} \qquad [3.5]$$

At any time t during the course of the reaction an amine balance can be written as $a_1 + \frac{a_2}{2} = a_0 - \frac{\alpha e_0}{2}$ which upon substituting into eq. 3.5 yields

$$\frac{d\alpha}{dt} = (1 - \alpha)\left(\frac{2a_0}{e_0} - \alpha\right)\left(\alpha + \frac{k_1' c_0}{k_1 e_0}\right)\left(\frac{k_1 e_0^2}{2}\right) \qquad [3.6]$$

Further simplification involves substituting the stoichiometric ratio $r = \frac{2a_0}{e_0}$, the rate constant $K = \frac{k_1 e_0^2}{2}$, and the parameter $B = \frac{k_1' c_0}{k_1 e_0}$, which for $r = 1$ leads to

$$\frac{d\alpha}{dt} = K(1 - \alpha)^2(\alpha + B) \qquad [3.7]$$

The parameter B is a function of c_0, the initial concentration of hydroxyl species. In the extreme case of $c_0 = 0$, eq. 3.7 reduces to

$$\frac{d\alpha}{dt} = K\alpha(1-\alpha)^2 \qquad [3.8]$$

which is the rate equation of a second order autocatalytic reaction. At $\alpha = 0$, also $\frac{d\alpha}{dt}$ is zero, meaning that without some traces of $(HX)_A$ impurities, an autocatalytic epoxy amine reaction would not commence. However, for all practical purposes this is not a problem since even minute amounts of impurities are sufficient to start the reaction [43]. Autocatalytic reactions typically exhibit an initial delay time, since the necessary catalytic hydroxyl groups are themselves a product of the reaction. The course of an autocatalytic reaction is exemplified in Figure 14 (a). The conversion at the exotherm peak, α_P, can be calculated by taking the derivative of eq. 3.7 and setting it zero. Thereby, it was shown that α_P is a constant independent of isothermal cure temperature [11]. The other extreme of this reaction is encountered when $c_0 >> e_0$, i.e., $(\alpha + B)$ becomes a constant, and eq. 3.7 reduces to the rate equation of a n^{th} order equation

$$\frac{d\alpha}{dt} = K(1-\alpha)^2 \qquad [3.9]$$

Such a reaction is characterized by a very high initial rate ($\alpha = 0$), and therefore a large percentage of conversion takes place in the first minutes of the reaction (Figure 14, b).

3.1.1.2 Kinetic Analysis by Differential Scanning Calorimetry (DSC)

Differential scanning calorimetry has become the method of choice to study the cure kinetics of epoxy amine systems. Two recent reviews by Prime [2] and Barton [43] deal extensively with this subject. DSC is defined by ICTA[2] as a technique which measures the differences in energy consumption of a sample and a reference material, both held at the same temperature as a function of

[2] International Confederation for Thermal Analysis

temperature [43,44]. The underlying assumption of kinetic studies by DSC is that the rate of exothermic heat, as it is recorded as a function of time (or temperature), is proportional to the rate of conversion, and that the thermal gradients within the sample or reference materials are negligible. The first assumption

$$\frac{d\alpha}{dt} \sim \frac{d\Delta H}{dt} \qquad [3.10]$$

is valid as long as no other thermal events such as melting, crystallization or volatilizing happen at the same time. The second assumption can be achieved by using small sample sizes in the order of 5-25mg. The integral of the entire exotherm peak from a dynamic cure experiment is the total heat evolved, ΔH_{RXN}, and is used to normalize the isothermal rates of heat production, $(d\Delta H/dt)_t$ and the partial areas, $(\Delta H)_t$, which yield the rates of conversion $(d\alpha/dt)_t$ and the partial conversions α_t, respectively, as a function of reaction time t:

$$\left(\frac{d\alpha}{dt}\right)_t = \frac{\left(\frac{d\Delta H}{dt}\right)_t}{\Delta H_{RXN}} \qquad [3.11]$$

$$\alpha_t = \frac{(\Delta H)_t}{\Delta H_{RXN}}$$

$\frac{d\Delta H}{dt}$ is usually expressed in W/g and ΔH_{RXN} in J/g; hence, the rate of conversion has the units of s^{-1}, and α is dimensionless.

3.1.1.3 Kinetic Analysis by Multi-heating Rate Dynamic DSC

Principally, DSC can be carried out in isothermal and scanning mode, and kinetic data can be obtained from both techniques. Nevertheless, the isothermal method is more straight forward, since rate and extent of conversion are recorded only as function of time while in the dynamic mode these parameters are simultaneously determined as a function of time and temperature. Isothermal experiments also provide the maximum extent of conversion which can be achieved at a particular

cure temperature, and can therefore be used to measure vitrification[3] [8,12,25]. From these data kinetic parameters such as the rate constants, activation energies, the reaction order, pre-Arrhenius factors, as well as the factor B (eq. 3.7) can be determined [6,8,11,12,13]. The disadvantage of isothermal DSC is that the recorded traces show an initial data uncertainty due to the necessary heating of the sample to the desired cure temperature. As long as the reaction is "sluggish" or of autocatalytic nature, this gap does not pose a problem. However, n^{th}-order reactions do exhibit their maximum rate of conversion at the very beginning of the reaction, which makes the isothermal method very inaccurate in these cases (Figure 14). As an alternative technique, it is possible to employ DSC in scanning method with multiple heating rates as alternative technique. The extraction of kinetic data from this method was pioneered by Ozawa [15,16] based on the work of Doyle [17] and verified by Prime [18] and Duswald [19].

The key to this method lies in the separation of temperature and time influences on the rate of released enthalpy $\left(\frac{d\Delta H}{dt}\right)_{t,T}$. Substituting T/ϕ for t, where ϕ is the heating rate, into the basic rate equation (eq. 3.1), where the rate constant is replaced by $Ae^{-(E_A/RT)}$, and integrating both sides yields

$$\begin{aligned}\int_0^{\alpha_t}\frac{d\alpha}{f(\alpha)} &= \frac{A}{\phi}\int_0^{T} e^{-(E_A/RT)}dT = \\ &= \frac{AE_A}{\phi R}\left(\frac{e^{-(E_A/RT)}}{E_A/RT} - \int_0^{T}\frac{e^{-(E_A/RT)}}{E_A/RT}dT\right) = \\ &= \frac{AE_A}{\phi R}g(E_A/RT)\end{aligned} \qquad [3.12]$$

The integral of the type $\int e^{1/x}xdx$ can not be solved analytically. However, Doyle [17] approximated $g(E_A/RT)$ as

[3] Vitrification is the cessation of reaction due to diffusion limitations of reactant mobility

$$\log g(E_A/RT) = -2.315 - 0.4567\frac{E_A}{RT} \qquad [3.13]$$

which is very accurate for $15 < E_A/R < 60$. Under the assumption that α_P, the conversion at the peak temperature T_P, is constant and independent of the heating rate (i.e. $\int_0^{\alpha_P} d\alpha/f(\alpha) = const.$) which has been experimentally confirmed [20, 18, 2], it is possible to determine E_A, the activation energy by plotting $\log(\phi)$ vs. T_P^{-1}, where the slope is $0.4567E_A/R$. This plot is sometimes referred to as Ozawa plot [15]. The so-obtained activation energies are comparable within 3% with the respective values obtained from isothermal studies [18,19]. Also, expressions for the pre-Arrhenius factor A can be calculated for n^{th} order (eq. 3.14) and autocatalytic (eq. 3.15) reaction [19,21] from dynamic DSC data which has been verified by isothermal experiments to be accurate within 2 - 4% [2].

$$A = \frac{\phi E_A e^{(E_A/RT_P)}}{RT_P^2} \qquad [3.14]$$

$$A = \frac{\phi E_A e^{(E_A/RT_P)}}{RT_P^2[3\alpha_P^2 + 4\alpha_P]} \qquad [3.15]$$

Although not as straightforward as by the isothermal method, it is also possible to determine $f(\alpha)$, including the reaction order, and the rate constant k from scanning experiments. From isothermal DSC data, k and n are usually found by plotting $\ln(d\alpha/dt)$ vs. $\ln(1-\alpha)$, whereby the slope equals n and the intercept $\ln k$. Also the factor B of the autocatalytic rate equation can be evaluated by plotting $\frac{d\alpha/dt}{(1-\alpha)^2}$ vs. α, where the slope gives K and the intercept equals KB [12]. Similar procedures can be carried out with data from dynamic experiments. However, it is necessary to correct the rate of conversion, $\frac{d\alpha}{dt}$, for the change of temperature during the experiment. Since the activation energy is assumed to be temperature independent, it is possible to recast eq. 3.1 as

$$\ln[Af(\alpha)] = \ln\left(\frac{d\alpha}{dt}\right)_T + \frac{E_A}{RT} \qquad [3.16]$$

where $(d\alpha/dt)_T$ is the rate of conversion at temperature T. Assuming that the reaction is of n^{th} order type (i.e. $f(\alpha) = (1 - \alpha)^n$), one can find $\ln(A)$ as the intercept and n as the slope of $\ln[Af(\alpha)]$ vs. $\ln(1 - \alpha_T)$ plots. Deviation from straight lines suggests partial autocatalytic character of the reaction [20].

3.1.2 Thermosetting Cure and Network Formation

Epoxy resins owe their widespread use and practicality not only to their versatility but to a large extent to the fact that most of them form chemical networks. Such cross-linked materials have superior mechanical properties and are widely used for appliances, matrices of fiber reinforced composites, adhesives, automotive applications, etc [1,22]. The effect of cross-linking has important implications on the polymer properties [24], and knowledge of network formation is of foremost importance. But although cross-linked systems are among the oldest synthetic polymers, their very nature defies ease of analysis, because insolubility and infusibility do not permit the employment of most of the analysis techniques developed for thermoplastic polymers.

The formation of chemical networks typically passes through distinct stages. After the reaction is initiated molecular weight is building up and viscosity increases. This process culminates in the formation of a gel fraction having infinite molecular weight. At this point, commonly termed gelation, also viscosity becomes singular and the material stops to flow. Beyond gelation, the cure reaction continues until it stops due to diffusion limitations. This cessation of cure is called vitrification and may happen before the chemical conversion is complete, in some cases even before the onset of gelation. Both, gelation and vitrification, are the main features of the time-temperature-transformation (TTT) diagram of thermosetting cure [Gillham, 12,25,38,61] which is described in Ch. 3.1.3.

3.1.2.1 Gelation

The forming of a gel fraction with infinite network during the curing reaction depends largely on reaction statistics. Flory and Stockmayer [26] defined a critical branching coefficient, α_c, and a critical conversion, p_c, as condition for the occurrence of gelation [4]. α, the branching coefficient is defined as the probability that a chain segment connected to one branching point is also connected to a second branching point. If this probability is larger than the probability that the chain segment will terminate as a loose end, the system is a gel. However, the branching coefficient does not account for cyclization effects which has been addressed recently by Stanford et al. [27], Gordon and Murphy [28], Steppto [29], Dusek and MacKnight [30], and Dusek [31]. The critical branching coefficient is a function of the functionality f of the branch point as

$$\alpha_c = \frac{1}{f-1} \qquad [3.17]$$

For the simple case of a stoichiometric reaction of a multifunctional cross-linker, A_f, with a bifunctional telechelic chain segment, $B-B$, the branching coefficient α equals p^2, and the critical conversion at gelation is

$$p_c = \frac{1}{(f-1)^{1/2}} \qquad [3.18]$$

For example, the theoretical critical conversion for a tetra-functional diamine reacting with a diepoxy chain assumes the value of 0.577. In most cases, the theoretical value is smaller than the measured value due to the failure to account for intra chain looping effects. Also based on the Flory - Stockmayer approach, the average molecular weights and their distribution can be calculated. The number and weight average degree of polymerization is given as

[4] For the sake of consistency with the original papers, p, rather than α is used as symbol of conversion

$$\bar{x}_n = \frac{1}{1-\alpha f/2}$$
$$\bar{x}_w = \frac{1+\alpha}{1-(f-1)\alpha} \qquad [3.19]$$

where α is the branching coefficient. At gelation, $\bar{x}_n$ will assume a finite value while $\bar{x}_w$ will become infinite. Macosco and Miller [32,33,34] used a recursive approach based on the law of conditional expectations to calculate the weight average molecular weight, $\overline{M}_w$, of a non-linear step growth polymerization as a function of p and M_{A_f} and M_B, the initial molecular weight of the reaction partners,

$$\overline{M}_w = \frac{(2r/f)(1+rp^2)M_{A_f}^2 + (1+(f-1)rp^2)M_B^2 + 4rpM_{A_f}M_B}{(2rM_{A_f}/f + M_B)(1-r(f-1)p^2)} \qquad [3.20]$$

where r is the stoichiometric ratio. This equation proves very useful for application in computer models, and has been applied several times [35,36,37]. It can be expanded to accommodate reactants with polydisperse molecular weight distributions. As can be shown easily, M_w approaches infinity when $(1-r(f-1)p^2) = 0$, which for $r = 1$ yields eq. 3.18 for the critical conversion.

3.1.2.2 Vitrification

As long as chain mobility is high enough to allow for unrestricted contact between the reactants during cure, the reaction is not controlled by diffusion[5]. The onset of gelation does not impair chemical kinetics which makes this event undetectable by thermal methods such as DSC. However, at some point during the course of the reaction, the network structure becomes tight enough so that the reaction changes to diffusion control, and eventually, it comes to a halt [25]. This point, usually termed vitrification, is, unlike gelation, not a fixed conversion event but a function of the cure

[5] to distinguish a non-diffusion controlled reaction from one where mobility control by network diffusion is important, it is sometimes described as "kinetically controlled", as opposed to "diffusion controlled" [25]

temperature, T_C. During network-building, the glass transition temperature, T_g, rises as a function of conversion. A very useful expression to relate these two variables is the DiBenedetto equation [24,40,54]

$$\frac{T_g - T_{g,0}}{T_{g,0}} = \frac{\varepsilon - F\alpha}{1 - (1 - F)\alpha} \qquad [3.21]$$

where $T_{g,0}$ is the glass transition temperature of the uncross-linked resin system. F is the ratio of the segmental mobilities of the cross-linked and uncross-linked polymer, and ε is the ratio of the respective lattice energies. Both parameters are interrelated as

$$\frac{\varepsilon}{F} = \frac{T_{g,\infty}}{T_{g,0}} \qquad [3.22]$$

where $T_{g,\infty}$ is the maximum glass transition of the fully reacted system. No clear opinion exists of the values ε and F can assume. While Enns and Gillham [25] found that both ratios can vary between 0 and 1, Addabo and Williams [55] suggested that $\varepsilon = 1$ and F varies. On the contrary, Nielsen [24] estimated that F should be essentially 0 and ε roughly 1. From the analysis of a DGEBA-*m*PDA system by DMTA [42], F and ε were estimated to be 0.198 and 0.34, respectively.

Theoretically, as long as T_g is below T_C, the chain mobility is sufficient for the reaction to continue. However, once T_g becomes equal to T_C or surpasses it the reaction will stop. Raising the cure temperature will again provide the necessary mobility for the reaction to restart. Only if T_C is higher than the glass transition of the fully cured thermoset, $T_{g,\infty}$, the reaction will proceed to completion. The time to reach $T_g = T_C$ in isothermal cure is defined as vitrification time, t_{vit}. Unlike gelation, vitrification is not an iso-conversion event but depends on cure temperature as

$$t_{vit} = A^{-1} e^{(E_A/RT)} \int_0^{\alpha_g} \frac{d\alpha}{f(\alpha)} \qquad [3.23]$$

where α_g is the conversion at $T_g = T_C$ and can be calculated from eq. 3.21 by setting $T_g = T_C$. Vitrification times can be determined experimentally by TBA [25], DMTA [42], DMA [56], other dynamic mechanical methods [57], or even DSC. Eq. 3.23 can be fitted by to experimentally determined t_{vit} data by adjusting F, and/or E_A and A. Additionally, the type of $f(\alpha)$, either autocatalytic or n^{th} order can be estimated by this method [25,42]. Numerous publications by Gillham and his co-workers [12,25,38,39] have elucidated vitrification and the relationship between glass transition and conversion, based on theoretical work by DiBennedetto [40,24]. By using torsional braid analysis (TBA) [41] as an isothermal dynamic technique to monitor the curing reaction from the liquid, through gelation, to the solid state of the resin mixture he was able to condense gelation and vitrification into the "Time-Temperature-Transformation (TTT)" cure diagram (see Figure 15). The typical sigmoidal shape of the vitrification curve reflects the temperature-dependent interplay of rheology and kinetics [25]. Just above $T_{g,0}$, vitrification is reached at very short times since only a very low extent of conversion is necessary to lift the T_g of the system above the cure temperature T_C. At slightly higher T_C's the times to vitrify, t_{vit}, pass through a maximum since the rate of conversion is low and the viscosity of the resin is high. Raising T_C shortens t_{vit}, since a higher rate of conversion helps to faster attain the necessary extent of conversion to elevate the glass transition temperature above T_C. However, at cure temperatures considerably closer to $T_{g,\infty}$, the times to solidify again increase as the result of the long conversion times necessary to reach the high extent of reaction which is needed to elevate T_g above T_C.

3.1.3 Time - Temperature - Transformation (TTT) Diagram and Cure Monitoring by Dynamic Mechanical Methods

Referred to it in the preceding chapters, the TTT- diagram has been shown to be an efficient form of describing the temperature dependent thermosetting network formation on the basis of the macroscopic observable parameters, gelation and vitrification. A very important role in determining

these is played by dynamic mechanical analysis methods. Work was carried out to elucidate the possibility of using a Dynamic Mechanical Thermal Analyzer (DMTA) as designed by Polymer Laboratories, Laughborough, UK, [62] to monitor the cure of a DGEBA - amine system. This work was summarized in a published paper [42] and will be reprinted hereunder and made part of the dissertation, since it contains description of the TTT-diagram and of experimental methods developed during this study and used later on for evaluating lignin based epoxides.

Cure Monitoring of an Epoxy-Amine System by Dynamic Mechanical Thermal Analysis (DMTA)[6]

Klaus Hofmann and Wolfgang G. Glasser

Dept. of Wood Science and Forest Products

Virginia Polytechnic Institute & State University

Blacksburg, Virginia 24061

Abstract

A method has been devised to study the cure of epoxy resins by using a Dynamic Mechanical Thermal Analyzer (DMTA) in combination with differential scanning calorimetry (DSC). Special glass fiber braids (25 x 13 x 0.15 mm) were impregnated with the liquid epoxy/amine (DGEBA/m-PDA) mixture at room temperature and subjected to forced oscillations at elevated cure temperatures. The modulus and the tanδ undergo transitions typical of gelation and vitrification. The times to gelation and vitrification were used to generate the well known Time-Temperature-Transformation (TTT) diagram proposed by J. Gillham on the basis of Torsional Braid Analysis (TBA) data. DMTA also provides information about the rate of modulus increase during cure which was compared with theoretical calculations of the rise in crosslink density.

---

[6] *Thermochimica Acta*, 166 (1990), 169; Presented at the 18th Annual NATAS Conference, San Diego, Sept. 24-27, 1989

3.1.3.1 INTRODUCTION

Thermosetting epoxy resins possess thermal and mechanical properties which make them the preferred choice for polymer composites, aerospace applications, coatings, appliances, adhesives, etc. For optimum performance of the finished product it is of foremost importance to know and monitor the curing reaction. Unfortunately, thermosets are by their very nature difficult to study because of their insolubility and infusibility. The widely used Differential Scanning Calorimetry (DSC) technique provides considerable insight into the reaction mechanism. However, events like gelation and vitrification are not observable by this method. Lately, dynamic mechanical methods have been employed to investigate these features which are not accessible by DSC. Gillham's very extensive work [1,2,3] with the Torsional Braid Analyzer (TBA) lead to the introduction of the Time-Temperature-Transformation (TTT) diagram for thermosetting resins. Gill [4] used a Dynamic Mechanical Analyzer (DMA) to study matrix epoxies in a cone and plate arrangement while Zukas et al. [5] employed Dynamic Spring Analysis (DSA) to probe the cure of an epoxy resin coated onto a spring. So far, Dynamic Thermal Mechanical Analysis (DMTA) has rarely been used for this task and only one entry in the literature has been found to date [6]. The purpose of this study was to investigate the potential of this method of monitoring the viscoelastic aspects of thermoset cure from the liquid phase through B- and C-stage.

3.1.3.2 TTT-Diagram of Thermosetting Resins

The cure of thermosetting resins typically passes through two crucial events: gelation and vitrification. Gelation marks the onset of forming an insoluble gel-fraction, a molecular arrangement of infinite molecular weight, whereas vitrification is understood as solidification of the reaction mixture due to the rise of the glass transition temperature upon tightening the thermoset network. On a molecular level gelation as a distinct event is defined as the incipient occurrence of one mol-

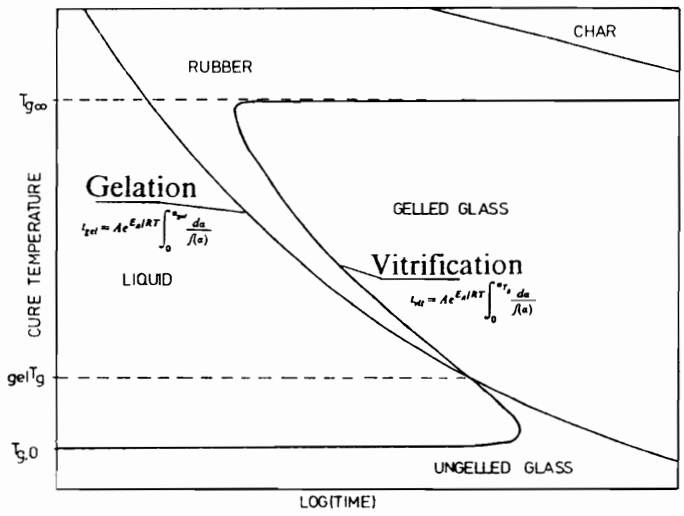

Figure 15. Schematic time–temperature–transformation diagram [1].

ecule of infinite molecular weight. Gelation occurs at a defined extent of reaction and does not change the kinetics of the reaction. Thus it can not be observed by DSC and related methods. However, gelation does change mechanical and electrical properties of the reaction mixture which makes it detectable by methods based on changes of mechanical, electrical and viscoelastic properties. Vitrification or solidification of a thermosetting resin can occur at any stage of reaction when the rising glass transition temperature of the reacting gel approaches the cure temperature.

Gelation and vitrification can be combined to form part of the TTT-diagram of thermoset cure (see Figure 15). The times to gelation, t_{gel}, and to vitrification, t_{vit}, are plotted as function of the normalized glass transition temperature of the system. In the case of the generalized TTT-diagram, the T_g of the cured resin is identical to the cure temperature. $T_{g,0}$ is the glass transition temperature of the unreacted resin mixture; ${}_{gel}T_g$ is the minimum cure temperature to form a gel; and $T_{g,\infty}$ is the maximum possible glass transition temperature or the minimum cure temperature to achieve full cure. For real systems however, the assumption of $T_g = T_c$ where T_c is the actual cure temperature does not hold so that T_c rather than the glass transition temperature is used as independent variable. The times to gelation and vitrification as a function of cure temperature can be calculated based on the relationship between reaction kinetics and glass transition temperature, as will be shown in the following.

The overall reaction rate $d\alpha/dt$ can be written as an Arrhenius type function of the extent of reaction, α, as long as the reaction is not diffusion controlled. Thus the times to gelation and vitrification can be written as

$$t_{gel} = Ae^{E_A/RT}\int_0^{\alpha_{gel}} \frac{d\alpha}{f(\alpha)} \qquad [1a]$$

and

$$t_{vit} = Ae^{E_A/RT}\int_0^{\alpha_{T_g}} \frac{d\alpha}{f(\alpha)} \qquad [1b]$$

where A is a pre-Arrhenius factor, E_A the activation energy. $f(\alpha)$ is a function of α, reflecting the type and order of the reaction. α_{gel} is the conversion at gelation and α_{T_g} is a function of $(T_g - T_{g,0})$ where T_g is the system's rising glass transition temperature and T_c the cure temperature. α_{T_g} can be calculated by means of the rearranged DiBenedetto equation [7,8] which relates the T_g of the thermoset to the extent of conversion:

$$\alpha_{T_g} = \frac{T_g - T_{g,0}}{T_{g,0}(\varepsilon - F) + (T_g - T_{g,0})(1 - F)} \qquad [2]$$

Eq.2 inserted into a cure kinetic equation like eq.6, yields the time to vitrify at isothermal conditions. The parameters ε and F are material constants of the polymer and are determined empirically. The typical sigmoidal shape of the vitrification curve reflects the temperature-dependant interplay of rheology and kinetics [1]. Just above $T_{g,0}$ vitrification is reached a very short times since only a very low extent of conversion is necessary to lift the T_g of the system above the cure temperature T_c. At slightly higher T_c's the times to vitrify, t_{vit}, pass through a maximum since the rate of conversion is low and the viscosity of the resin is high. Raising T_c shortens t_{vit} since a higher rate of conversion helps to faster attain the necessary extent of conversion to elevate the glass transition temperature above T_c. However, at cure temperatures considerably close to $T_{g,\infty}$ the times to solidify again increase as the result of the long conversion times necessary to reach the high extent of reaction which is needed to elevate T_g above T_c.

3.1.3.3 Modulus Increase During Cure

Ideally, the equilibrium modulus of a thermoset can be calculated following classical rubber elasticity theory as

$$E = 3\frac{\rho RT}{M_c} \qquad [3]$$

where ρ is the density of the material and M_c the number average molecular weight between crosslinks. ρ/M_c can be substituted by ν, the concentration of effectively anchored network chains. In general, eq.3 can not be applied to very dense networks close to full cure since the assumptions regarding random coil state or equilibrium modulus can not be met. This relationship nevertheless describes fairly well the modulus changes taking place during formation of the gel at moderate extents of conversion, as will be demonstrated in the following.

It is of interest to see whether the modulus gain data obtained from dynamic experiments reflect theoretical predictions. Although numerous models describe the effects of crosslinking reactions on the change of molecular weight of the sol and the gel, the recursive approach of Miller and Macosco [11] to step growth type crosslinking reaction has been chosen because of its clarity and elegance. The density of network chains, ν, is the weighed sum of the crosslink densities, $[X_m]$

$$\nu = \sum_{m=3}^{f} \frac{m-2}{m}[X_m] \qquad [4]$$

where m is a chain's degree of anchoring in the gel. This must be larger than three to be effective, and f is the functionality of the one reaction partner whose functionality is larger than two. The following equation is the application of Miller and Macosko's [11] general procedure to a binary reaction system having functionalities of two (DGEBA) and four (m-PDA), assuming equal reactivity:

$$v = [A_4]_0 \left\{ \frac{4}{3} \left[\left(\frac{1}{\alpha^2} - \frac{3}{4} \right)^{0.5} - \frac{1}{2} \right] \times \left[\frac{1}{2} - \left(\frac{1}{\alpha^2} - \frac{3}{4} \right)^{0.5} \right]^3 + \right.$$
$$\left. + \frac{1}{2} \left[\frac{1}{2} - \left(\frac{1}{\alpha^2} - \frac{3}{4} \right)^{0.5} \right]^4 \right\} \qquad [5]$$

where $[A_4]_0$ is the initial concentration of the four functional species. By calculating α, the extent of conversion as a function of time and temperature one can construct theoretical plots of E *vs.* time or log E *vs.* time and compare them with the respective DMTA results.

3.1.3.4 Dynamic Mechanical Thermal Analysis

Measurements of the times to gelation and vitrification were carried out by Gillham [1] by means of a Torsional Braid Analyzer (TBA). A resin-impregnated glass fiber braid is subjected to dampened torsional oscillations whereby the logarithmic increment of successive amplitudes, $\Delta = \log[A_i/A_{i+1}]$, is a measure of energy dissipation or damping of the material, and the relative rigidity $1/P^2$ (P is the period $2\pi/\omega$) is a measure of the sample's stiffness. Gillham could show that several damping maxima occur over time when an epoxy resin is isothermally cured. The two most prominent peaks have been assigned to gelation and vitrification of the resin.

In contrast to Torsional Braid Analysis, using a Dynamic Mechanical Thermal Analyzer (DMTA) a sample is subjected to forced oscillations of constant frequency in bending, shear or tension. Loss and storage moduli are recorded and tanδ is obtained as the ratio of E''/E'. DMTA is primarily a tool for studying the thermo-mechanical response of solid samples. Hence, a composite sample consisting of an inert fibrous support for the liquid resin must be prepared in order to monitor the full range of cure from liquid to solid.

In analogy to the results of the TBA-studies one should expect the same damping maxima as tanδ peaks. When the resin approaches gelation its viscosity increases to eventually become infinite. This

results in increased energy dissipation of the network forming liquid. Further crosslinking of the gel and tightening of the network, however, decreases the network's ability to dissipate energy, and hence, tanδ passes through a local maximum at the point of gelation.

Vitrification of a curing resin is caused by quenching of the reaction due to the rise of the glass transition temperature of the system to and above the cure temperature. Since a polymer has a local damping maximum at its glass transition temperature it is logical that tanδ passes through another local maximum at the time of vitrification.

3.1.3.5 MATERIALS AND METHODS

The epoxy resin used for this study was a commercially available diglycidyl ether of bisphenol A (DGEBA, Epon 826) cured with an aromatic diamine (m-PDA), both used as received. Resin and hardener were mixed at a stoichiometric ratio of 1:1, which in this case amounts to four epoxy equivalents for each m-PDA equivalent. The epoxy equivalent weight was determined by titration with HBr according to ASTM D 1652. Mixing was carried out by melting the crosslinking agent at 79°C and dissolving it in the epoxy resin by stirring for 10 minutes. The system was degased and stored at -70°C until use. This system follows autocatalytic cure kinetics [10] of the type

$$f(\alpha) = \alpha(1-\alpha)^2 \qquad [6]$$

which, substituted into eq.1b, yields

$$t_{vit} = Ae^{E_A/RT}\left\{\left(\frac{1}{1-\alpha_{T_g}}\right) - \ln\left[\frac{1-\alpha_{T_g}}{\alpha_{T_g}}\right]\right\} \qquad [7]$$

3.1.3.6 Differential Scanning Calorimetry

A Perkin Elmer DSC-4 controlled by a System-4 microprocessor were used to provide conversion data. Total heat of reaction, ΔH was determined by integrating of the area under a ΔC_P vs. T curve, obtained from a temperature scan of the system. The scan rate was 4°C per min. Isothermal conversion data were obtained by integrating the areas under the individual ΔC_P traces and relating it to total ΔH. Isothermal experiments were carried out for T = 30°C to T = 150°C in 10°C intervals.

3.1.3.7 Dynamic Mechanical Thermal Analysis

The Dynamic Mechanical Thermal Analyzer (DMTA) equipped with a bending head and a Universal Temperature Programmer (UTP) were manufactured by Polymer Laboratories. They are interfaced to an Hewlett-Packard 9816 microcomputer. Samples were prepared by submerging a woven glass fiber braid (DuPont #980228-901) of 25 mm length and 13 mm width in the liquid resin mixture at room temperature. The soaking time was one minute. The excess resin was blotted off, and the ends were covered with aluminum foil to protect the DMTA clamps from the resin. The samples were stored in polyethylene bags at -70°C. Prior to testing the samples were allowed to equilibrate for ten minutes before opening the bag to avoid condensation. Bending of the sample was carried out in cantilever mode at a frequency of one hertz. The free length was 1 mm. Isothermal runs were carried out from 30 to 190°C. The heating rate during heat up was 60°C/min initially until 20°C below the desired cure temperature, followed by 20°C/min up to 8°C below. The final heating rate was 8°C. After closing the assembly it took typically 2 to 2.5 minutes to reach equilibrium. Although reaction takes place during the initial heat up period the authors are confident that gelation does not occur during this period except for temperatures above 170°C. At these temperatures the experiment only yielded the times to vitrify (see Figure 18). The times to gelation for high T_c's were obtained by extrapolation. The temperature was stable within $\pm$1°C. Immediately after the isothermal run the sample was cooled to room temperature and subsequently

probed in scanning mode to determine the T_g. The conditions were the same as for the isothermal mode; the scan rate was 4°/min. The DMTA experiments were carried out under static air.

3.1.3.8 RESULTS AND DISCUSSION

3.1.3.9 Temperature Scan

The temperature scan (Figure 16) of the uncured epoxy resin shows softening of the reaction mixture at -12°C. This corresponds to $T_{g,0}$ in the TTT-diagram. The mixture remains a low viscosity liquid until 20°C beyond which the modulus rises to an intermediate modulus plateau. Reaction as it is recorded by DSC (Figure 16) starts at 75°C, has its maximum at 133°C and ends at 180°C. During the first half of the reaction the modulus attains a plateau value which has been reached at the onset of the reaction (70°C). Considerable rise of the modulus takes place after 130°C, whereby the tanδ peak of 150°C appears to mark the onset of gelation. Since the cure temperature is at any point higher than the T_g of the system, quenching by vitrification does not take place, and the modulus is that of a rubbery material.

3.1.3.10 Isothermal Cure

Examples for isothermal cure monitoring by DMTA are given in Figure 17. This represents modulus and tanδ traces for $T_c = 130°$ and 140°C. The superimposed DSC trace is drawn as a dashed line. The absolute value of the modulus is not representative of the true modulus of the resin since it is that of the composite sample. Nevertheless, assuming that classical rubber elasticity theory holds, the slope dE/dt is proportional to the rise in crosslink density and the decrease of M_c. Two linear portions of the log modulus slope can be identified which coincide with the two tanδ maxima,

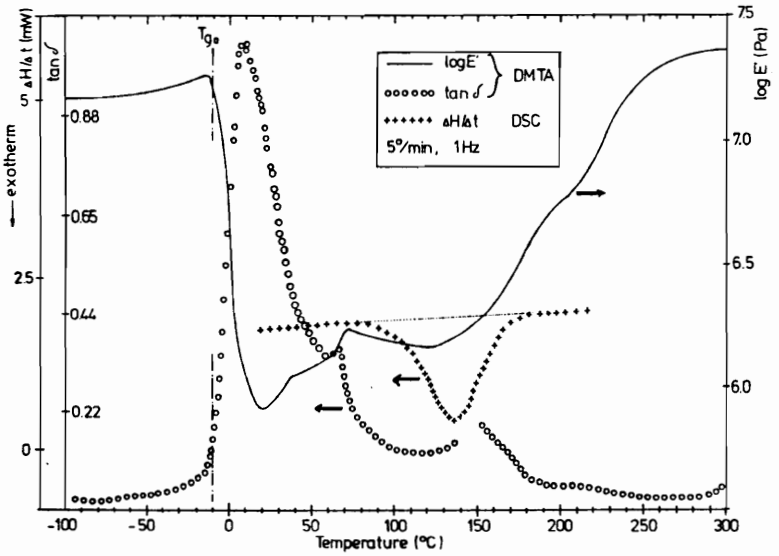

Figure 16. Temperature Scan of DGEBA/mPDA

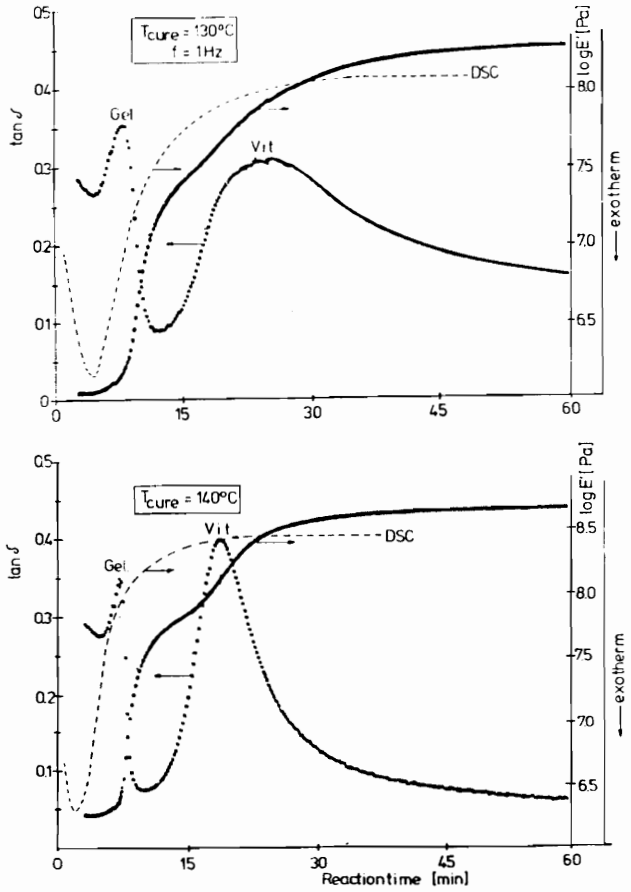

Figure 17. Isothermal Traces of DGEBA/mPDA

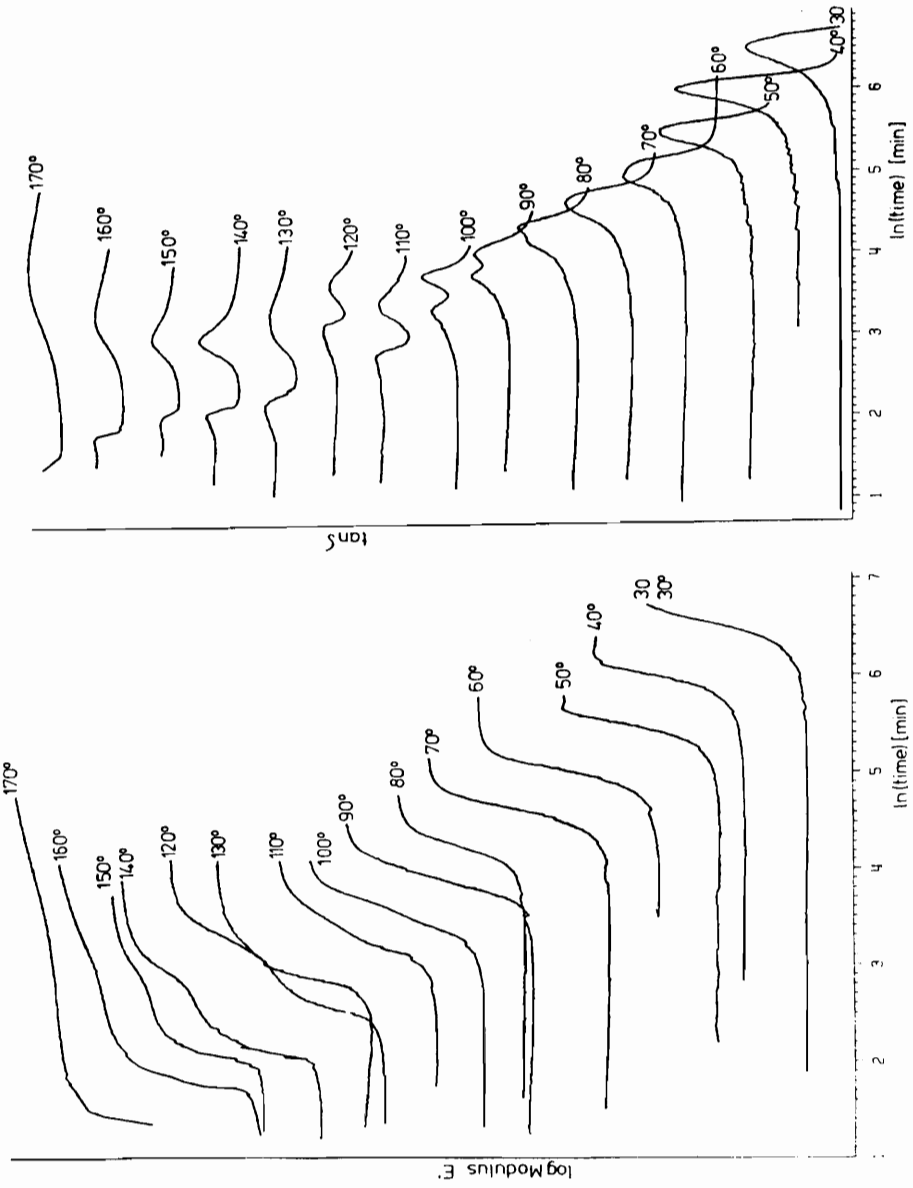

Figure 18. Summary of Isothermal Traces (DGEBA/mPDA)

gelation and vitrification which means that the crosslink density rises logarithmically with cure time. Gelation is an iso-conversion event and occurs in this case at 52% extent of reaction measured from DSC. The theoretical conversion at gelation for this system is 58% [11]. This is in contrast to observations by Enns and Gillham [1] who reported that the gelation peak measured by TBA for a similar system occurs above 70%. The second peak, although labeled as vitrification, does not mark the end of network formation; rather it indicates that the system's glass temperature has reached the cure temperature. Hence, the T_g of the isothermally cured resin is higher than the cure temperature.

This procedure has been carried out for temperatures ranging from 30° to 190°, and results are summarized in Figure 18. Typically the single tanδ peak of the low temperature cured samples tells that solidification takes place before the necessary conversion into a gel has been reached. A splitting of the peak can be observed at approximately 60°C. The gap between the peaks widens with increasing T_c. The higher the cure temperature, the earlier both gelation and vitrification occur. Above 150°C, however, the vitrification peak moves to the right and disappears at high temperatures, indicating that the cure-temperature approaches the glass transition temperature of the fully cured resin, $T_{g,\infty}$, which is about 180°C for this system. At low cure temperature (< 60°C) the modulus rises linearly in a one step fashion which is followed by a splitting of the slope into two linear portions above 60°C. At high temperatures the approach of $T_{g,\infty}$ is marked by the disappearance of the second part of the slope.

Although the second tanδ peak is taken as indication for vitrification conversion continues sometimes past this point. Hence, the final T_g of a isothermally cured sample below $T_{g,\infty}$ should be higher than the cure temperature. In order to show this phenomenon the glass transition temperatures that were taken immediately following the isothermal cure experiments are plotted plotted against isothermal cure temperature (Figure 19). The dashed line represents $T_g = T_c$. below $T_c = 150$°C, the glass transition temperature is considerably higher than the cure temperature. The gap closes at about 180°C which can be regarded as the glass transition temperature of the fully cured resin, $T_{g,\infty}$.

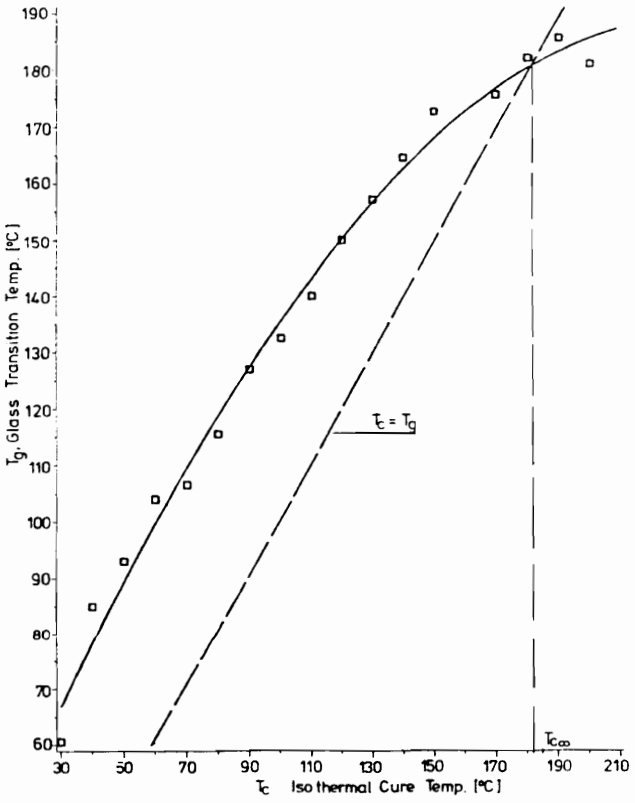

Figure 19. Glass Transition Temperature vs. Cure Temperature of Isothermally Cured DGEBA/mPDA

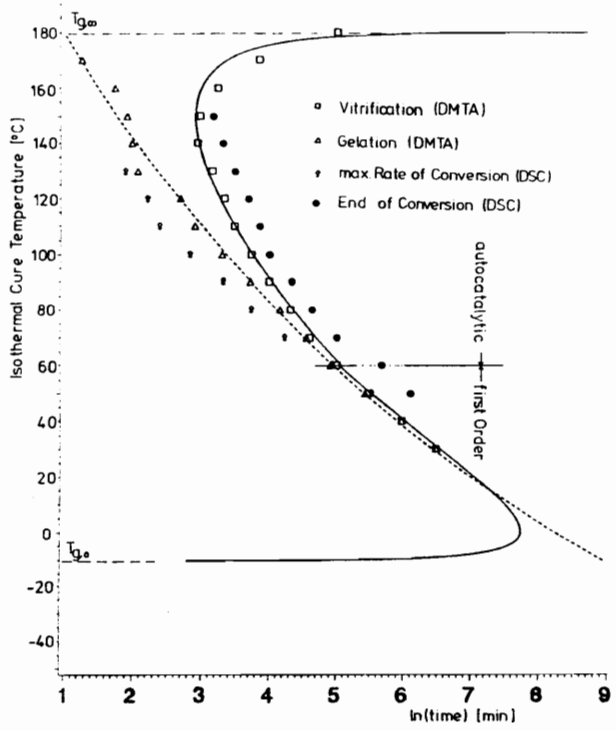

Figure 20. TTT-Diagram of DGEBA/mPDA

DMTA and DSC data are combined to form the TTT-diagram of this system (Figure 20). The triangular data points represent the time to gel formation, and the squares reveal the time to vitrification. Both are taken from the tanδ peaks of the DMTA measurements. Additionally, the maximum and end of conversion as obtained from DSC are included. The lines for gelation and vitrification have been calculated using eqs.1a and 7. Above ca. 60°C an autocatalyzed approach (see eq.6) has been found to best represent the experimental data. Below this point, however, first order kinetics fit the data better. This transition has been observed by Gillham as well [1], although a first to second order kinetics transition rather than a first order to an autocatalytic approach has been used. The minimum cure temperature to reach full conversion or $T_{g,\infty}$, as it is asymptotically approached by the vitrification line, is 180°C; the other extreme, the maximum storage temperature without cure taking place or $T_{g,0}$ is -10°C. From these calculations the values of ε and F (see eq.2) have been calculated to be 0.34 and 0.198, respectively. From the Arrhenius type TTT-diagram (Figure 21), the activation energy of gelation, E_A has been calculated to be 40.6 kJ/mol.This is somewhat lower than reported elsewhere for the same system [9].

The slopes of log E *vs.* time (Figure 18) reveal two distinct linear portions, one at about gelation and the other towards the end of cure (or vitrification). The slope data have been summarized in Figure 22 in Arrhenius form. Typically, the logarithmic values of the slopes of log E *vs.* time during gelation lie on a straight with an activation energy of 39.6 kJ/mol ($R^2 = 0.995$). The respective data for vitrification lie on a semicircle, and this reflects the fact that at higher cure temperature the rate of modulus rise is small. This can be explained with the fact that at higher cure temperatures, most of the system's final modulus is gained during and after gelation, and, on the other hand, the vitrification time is considerably longer.

Theoretical values of increases in log modulus over time have been calculated using eq. 4. A conversion range of between 0.58 and 0.74 has been chosen for the modulus rise during which the system passes through gelation. The initial concentration of $[A_4]_0$ of m-PDA is 1430 mol/m^3. The theoretical data are in good agreement with the experimental DMTA data (Figure 23). Although the theoretical values are slightly higher than the corresponding experimental data, the two curves

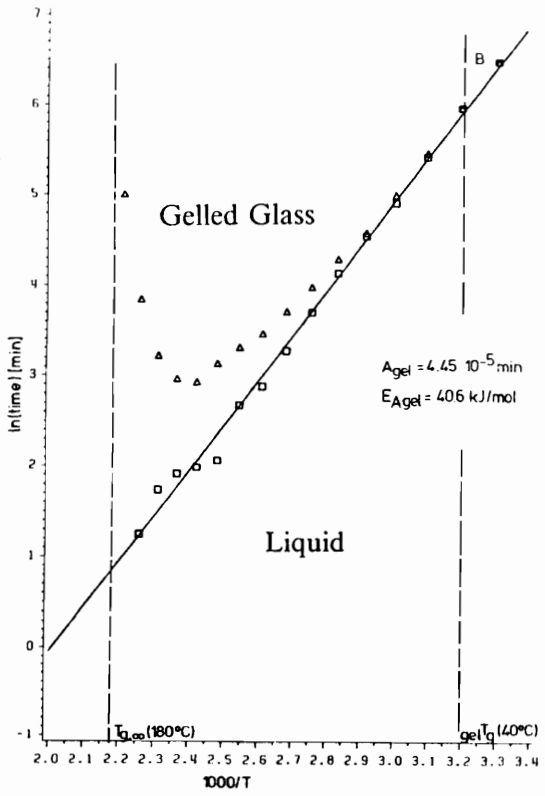

Figure 21. Arrhenius Type TTT-Diagram of DGEBA/mPDA

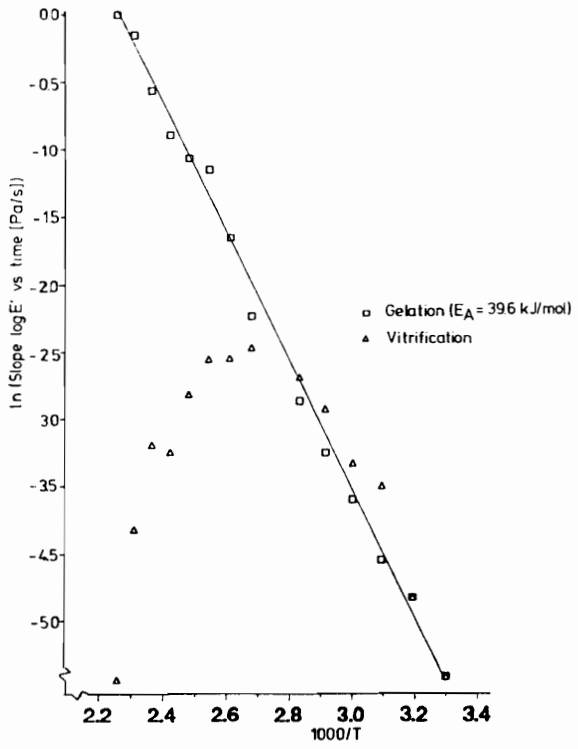

Figure 22. Arrhenius Plot of Slopes of log E vs. time (DGEBA/mPDA)

follow very closely the same trend, which indicates that the gain in modulus at moderate extents of conversion as it is measured with this method is in close agreement with the one predicted by rubber elasticity and the Miller-Macosco theory. The same procedure has been applied to the second linear portion of the modulus rise taking place during vitrification (Figure 24) with the notable difference that these events do not happen at fixed conversions but rather at temperature dependent conversions and cure times. Hence, the actual beginning and termination points on the time scale of the linear portion of the DMTA signals have been taken to calculate the extents of conversions using eqs. 1b and 7. The results are summarized in Fig. 10. Clearly, the agreement is by far not as good as in the case of gelation. Although the theoretical data mirror somewhat the trend that the fastest rise in modulus occurs at around 100°C, the absolute values are too small. The failure of the theory to represent the DMTA results can be attributed primarily to the fact that very dense networks are too far from ideality to be represented by classical rubber elasticity. the discrepancy between the DMTA data and theory at this level of conversion is not caused by the influence of diffusion control on the reaction kinetics since only the linear portions of the log E′ slopes have been included in the calculations of the concentration of active network chains. The onset of diffusion control takes place after vitrification which is also characterized by a change in the respective log E′ slope. Corrections of eq.4 to account for entanglement effects lead only to a slight increase in the respective slopes.

3.1.4 Conclusion

The cure of an epoxy system (DGEBA/mPDA) has been monitored isothermally by Dynamic Mechanical Thermal Analysis (DMTA) in bending mode at a fixed frequency (1 Hz). The resin was supported by an inert glass fiber braid. It could be shown that a dynamic mechanical system utilizing forced oscillation such as DMTA is a fast and reliable tool to monitor the cure of an epoxy-amine system and the results are comparable to a free oscillation methods such as TBA.

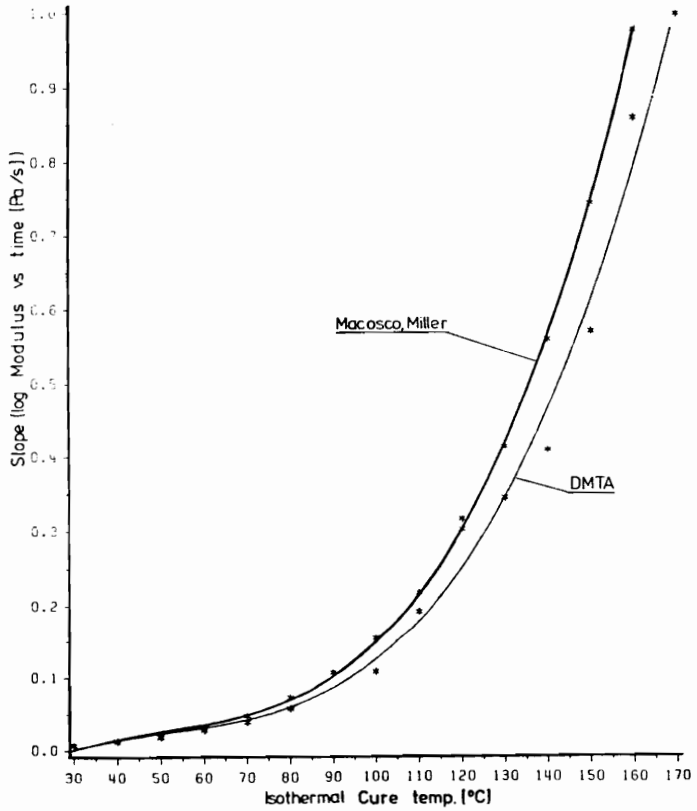

Figure 23. Slope of Log Modulus vs. Time During Gelation: Theoretical data are calculated following Macosko and Miller [11]

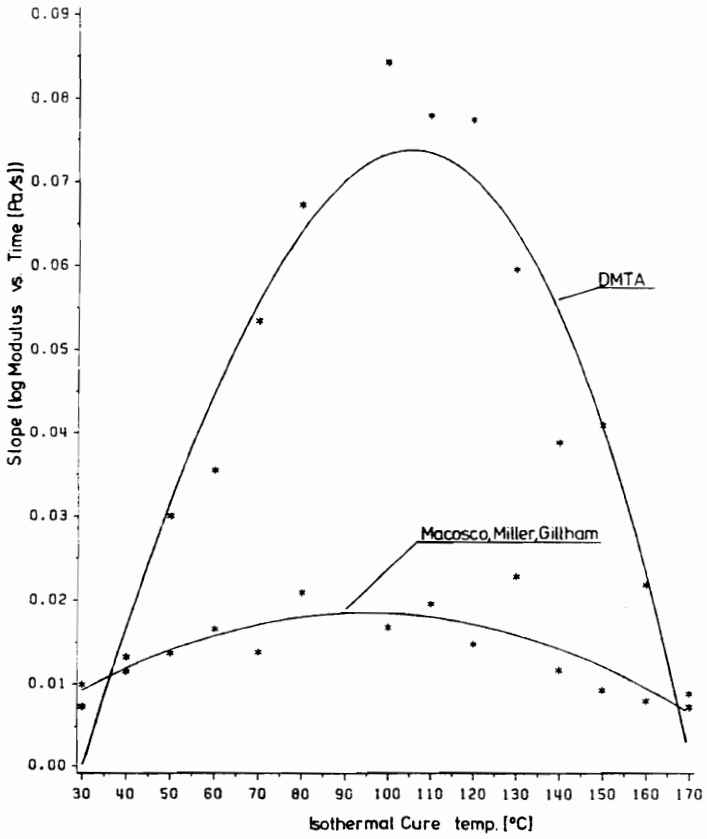

Figure 24. Slope of Log Modulus vs. Time During Vitrification: Theoretical data are calculated following Macosko, Miller and Gillham [11,1]

Typically, the damping (tanδ) passes through two maxima, designated as gelation and vitrification. From the tanδ data a Time-Temperature-Transformation (TTT) diagram was developed and the times to gelation and vitrification have been calculated. The activation energy of gelation was 40.6 kJ/mol. The increase of log E is linear for both, gelation and vitrification; however, the slopes are different. From this the activation energy of gelation has been calculated to be 39.6 kJ/mol. Comparison of theoretical slope data of log E *vs.* time based on rubber elasticity theory with actual DMTA values of modulus rise during cure yielded very good agreement for the range of $\alpha = 0.58 - 0.74$ however; they failed for the high conversion portions of the diagram. This can be explained with the fact that classical rubber elasticity can not be applied to very dense networks. This study has shown that DMTA is a useful and reliable method for monitoring the cure of an epoxy thermoset throughout all stages.

This study was supported by a grant from th US Department of Agriculture (contract #: 87-FSTY-9-0250); and by funds from the center for Adhesion and Sealant Science of Virginia Tech.

3.1.5 Literature Cited

1. J. B. Enns and J.K. Gillham, *J. Appl. Pol. Sci.* 28, 1983, 2567
2. X. Peng and J. K. Gillham *J. Appl. Pol. Sci.* 30, 1985, 4685
3. M. T. Aronhime and J. K. Gillham, in K. Dusek, Ed., "Advances in Polymer Sciences", Vol. 78, Springer Verlag, Berlin, 1986
4. P. S. Gill and R. L. Blaine, in B. Miller, Ed., "Proc. 7th Int. Conf. on Thermal Analysis", Vol. 2, Wiley, Chichester, 1982
5. W. X. Zukas, J. MacKnight, and N. S. Schneider, in C. A. May, Ed., "Chemorheology of Thermosetting Polymers", ACS Symp. Ser. 227, Washington, 1983
6. D. Wingard, W. Williams, K. Wolking, and C.L. Beatty, in "Cross-Linked Polymers: Chemistry, Properties, and Applicatio", ACS Symposium Series 367, 1988

7. A. T. DiBenedetto, *J. Pol. Sci., B*, 25, 1987, 69

8. L. E. Nielsen *Macromol.Sci.- Revs.Macromol.Chem.* C3(1), 1969, 69

9. R. D. Miller and C.W.Macosco, *Macromolecules* 9(2), 1976, 206

10. S. Sourour and M.R.Kamal, *Thermochimica Acta*, 14, 1976, 41

11. 4.Gill P.S.

12. R. B. Prime R.B. in E. Turri, Ed., "Thermal Characteization of Polymeric Materials", Academic Press, New York 1981

3.2 Materials and Methods

3.2.1 Materials

In order to investigate the cure reaction of lignin based epoxies as a function of lignin content, molecular weight, and poly(alkylene oxide) chain length, two fractionated epoxies (LX1204 and LX2404) based on steam explosion lignin from yellow poplar wood (*liriodendron tulipifera*) and one unfractionated resin (LX0013) based on a commercial organosolv lignin were studied. The epoxidation, fractionation, isolation and analysis of these resins are described in Ch. 2.2 and their characteristic parameters are summarized in Table 2 on page 32, and in Table 3. As cross-linking agent, meta-phenylene diamine (*m*PDA) was chosen, primarily for the reason that it has become a model curing agent for epoxy resins [2], and no catalyst is needed. It has been purchased from Aldrich Chemicals, and was used as received. The opened bottle was stored under nitrogen at -20°C.

3.2.1.1 Preparation of Resin Mixture.

The low molecular weight fractions LX1204A1 and LX2404A1, and LX0013 were sufficiently liquid at room temperature to be mixed with the cross-linking agent *m*PDA in neat form. The procedure involved weighing the resin into a wide mouth amber storage bottle and heating it in an oil bath to 80°C while stirring. The stoichiometric amount of *m*PDA (WPE = $27 g/eq.$) was weighed into a small open glass dish and brought to a melt (~ 70°C). The low viscosity melt was added to the epoxy and stirring continued for five minutes. While reaction during mixing never can be completely avoided, the conversion during the mixing procedure is small since from this and earlier studies it was known that reaction does not significantly start before the temperature surpasses 100°C. The bottle was flushed with argon, sealed, and stored at -70°C.

Table 3. Compilation of Molecular Weight, Epoxy Equivalent Weight, and Lignin Content of LX1204, LX2404, and LX0013

Sample Designation[1]	M_n [2] ($x10^3$)	M_w [2] ($x10^3$)	WPE[3] (*g/eq.*)	Lignin Content[4] (%)
LX1204A1	0.63	3.0	231	16
LX1204A2	1.9	28.0	399	37
LX1204A3	93.8	214.0	439	42
LX2404A1	0.8	4.4	360	21
LX2404A2	5.5	36.0	507	39
LX0013[5]	1.2	9.9	670	57

1) Sample designation reflects feed of propylene oxide (PO) and Ethylene oxide (EO) in mole/kg dry lignin
2) by GPC (see Ch. 2.2.2.2)
3) by HBr titration (see Ch. 2.2.2.1)
4) by UV (see Ch. 2.2.2.3)
5) Hydroxy ethyl lignin PO = 0, EO = 13

The other fractions LX1204A2, LX1204A3, and LX2404A2 were not suited for this method since they were either highly viscous tars, or, in the case of LX24042 and LX1204A3 glassy solids. To ensure intimate mixing of epoxy and hardener, it was necessary to blend them in solution and recover the solid or tary blend by vacuum evaporation of the solvent at ambient temperature.

3.2.1.2 Preparation of DMTA Samples

For the conducting of dynamic mechanical cure studies of the epoxy resins, fiber braid-based composite samples were produced following the description in Ch. 3.1.3. However, those specimens which were solids (LX1204A2, LX1204A3, LX2404A2) had to be prepared by solution impregnating of the braids (25*mm* x 13*mm*). Concentrated methylene chloride solutions were prepared in which the fiber braids were dipped and subsequently air dried for 3 minutes. This cycle was repeated 3 times upon which the specimens were dried for 12 hrs under vacuum in a desiccator. All samples were wrapped in aluminum foil, leaving a 2 *mm* center gap, packed individually in small plastic bags, and stored at -20°C.

3.2.2 Experimental Methods

3.2.2.1 Differential Scanning Calorimetry (DSC)

Throughout this study, a DSC-4 instrument by Perkin Elmer connected to a temperature controller and interfaced to a Perkin Elmer computer (TADS) was used for differential scanning calorimetry experiments. The DSC head as a heat sink can be cooled by a Perkin Elmer refrigerator to -70°C. The software used throughout was the manufacturer-provided "DSC-Standard" package which allows for total, but not for partial peak integration. In order to integrate partial peak areas, which

was necessary to calculate α_T, traces were digitized on a HP 7470A plotter connected to a personal computer using the UNPLOTIT™ software package.

All DSC experiments were carried out with the head cooled to -70°C since it was found that this yields more reliable results than operating the head at ambient, especially if the rate of exothermal heat evolved, $d\Delta H/dt$, is small. The disadvantage of this method is that the very narrow gas lines within the head leading to the sample and reference pans holders were blocked by frozen condensate. Thus all experiments were performed under static air. The entire ensemble was covered by a transparent enclosure and flushed with dry nitrogen to keep condensation at a minimum.

Dynamic experiments were carried out at four heating rates ranging from 10 to 40° min^{-1}. All scans were done under simultaneously correcting the signals with a prerecorded baseline. Temperature calibration based on the melting endotherm of indium was carried out periodically according to the user manual. Isothermal experiments were conducted by programming the temperature controller to initially raise the temperature to the desired level with 200°min^{-1}. Subsequently, the temperature was kept at this level for the pre-determined time, while simultaneously, the computer was manipulated to record a "scanning experiment" with a virtual heating rate of 1°min^{-1}, which allowed for direct reading of the temperature axis as time axis in minutes. This procedure was preferred over the isothermal software supplied by Perkin Elmer, since it was more versatile and data manipulation was easier. Two types of sample and reference pans were used: sealed steel pans for the liquid resins and crimped aluminum pans for the solid film samples.

3.2.2.2 Dynamic Mechanical Thermal Analysis (DMTA)

A DMTA bending configuration head by Polymer Laboratories, controlled by an Universal Temperature Controller (UTP), and interfaced to an HP personal computer, was used throughout the project. The data acquisition procedure is described in detail in Ch. 3.1.3.

As has been discussed, the glass transition temperature of a chemical network is an indication of the advancement of the curing reaction. If the reaction is halted before it reaches completion, the glass transition temperature is a function of the extent of conversion, $T_g(\alpha)$, and thus, a function of cure time, t_C, and cure temperature, T_C. On the other hand the rising glass transition of the forming network by itself is the cause of the cessation of reaction once it reaches the level of T_C. These arguments can be formulated by rewriting and integrating the basic reaction equation 3.1, where $k = Ae^{-(E_A/RT)}$, for $T = T_C$ and $t = t_C$ [12]

$$\ln\left(\int_0^{\alpha} \frac{d\alpha}{f(\alpha)}\right) = \ln(A) - \frac{E_A}{RT_C} + \ln(t_C) = \ln[k(T_C)] + \ln(t_C) = g(T_g(\alpha)) \qquad [3.24]$$

The implication of this relationship is that as long as the reaction is kinetically controlled and follows an Arrhenius type mechanism one can write

$$\ln[k(T_{C,1})] + \ln(t_{C,1}) = \ln[k(T_{C,2})] + \ln(t_{C,2})$$

$$\ln\left(\frac{t_{C,1}}{t_{C,2}}\right) = \ln\left(\frac{k(T_{C,2})}{k(T_{C,1})}\right) = a_T \qquad [3.25]$$

where $t_{C,1}$ and $t_{C,2}$ are the cure times necessary to reach the same glass transition temperature at different cure temperatures $T_{C,1}$ and $T_{C,2}$. Thus, $\ln[k(T_2)/k(T_1)]$ is the time independent shift factor a_T. By subjecting specimens of the same system to isothermal cure cycles of increasing lengths at a range of temperatures, it is possible to determine this shift factor.

Respective studies were carried out for the six lignin based epoxy samples listed in Table 3. The principle instrument for this investigation was a dynamic mechanical thermal analyzer as described in Ch. 3.1.3. Individual specimens were cured in the DMTA furnace at a fixed temperature for selected times, ranging from 75°C to 200°C, and from 5 minutes to 14*hrs*. Prior to inserting the specimens into the heating chamber, it was preheated to the specified cure temperature. The impregnated and aluminum covered specimens were mounted onto the heated bending ensemble

(single cantilever mode) and the isothermal experiment was started simultaneously. The temperature initially dropped about 20 to 30° during the clamping procedure, but rose immediately after closing the assembly. Total equilibrium was established about 1.5 minutes after the experiment commenced. This initial temperature fluctuation is of little importance for the long time experiments, but might have influenced the very short runs. However, care was taken to standardize the clamping procedure for all specimens and temperatures. And since most of the initial drop in temperature was recovered within 30 seconds, no further actions were undertaken regarding the initial heat up time. The sample temperature was measured with a platinum resistor located about $1mm$ behind the specimen and was stable within $\pm 1°$.

To preclude possible post cure aging effects [63], the specimens were cooled with liquid nitrogen upon elapsing of the cure time. After the furnace was at a temperature 100° below the expected glass transition temperature, or at room temperature, whichever was lower, the dynamic experiment was started in order to determined the glass transition temperature. The frequency was $10Hz$ and the heating rate $10°min^{-1}$. The glass transition temperature was taken as the peak temperature of the main damping transition. The results were compiled and plotted as function of $\ln(t_C)$, and the respective T_g vs. $\ln(t_C)$ traces where shifted to a reference temperature of 150°C and the shift factor was determined. Since the shift factor a_T is a function of the rates of reactions it can be expressed as function of the activation energies [12] as

$$a_T = \frac{E_A}{R}\left(\frac{1}{T_{ref}} - \frac{1}{T}\right) \qquad [3.26]$$

which allows to determine the activation energy from a plot of a_T vs. T^{-1} where the slope equals E_A/R and the intercept E_A/RT_{ref}.

3.3 *Results and Discussion*

3.3.1 Differential Scanning Calorimetry of LX1204 Fractions

The following discussion is sectioned into two parts of which the first one involves the extraction of kinetic information from dynamic DSC experiment of the three fraction of LX1204, while dynamic mechanical thermal analysis of glass braid supported resins will be discussed in the second section.

3.3.1.1 Multi-heating Rate Dynamic DSC

As discussed in section 3.2.1, the three fractions of the lignin based epoxy resin LX1204 were cured with *m*PDA whereby the epoxy equivalent weight of the fractions was determined by HBr titration. LX1204A1 was mixed in neat form and LX1204A2 and LX1204A3 were mixed in solution and vacuum dried in a rotation evaporator at room temperature. Sealed steel pans were used for the liquid LX1204A1 system, while for LX1204A2 (highly viscous tar) and LX1204A3 (powder) aluminum pans were sufficient. The heating rates were 10, 20, 30, and 40°min^{-1}. Starting temperature was 10°C and most samples were taken to 300°C under simultaneous baseline correction. The exotherms of all samples for the four heating rates are compiled in Figure 25, Figure 26, and Figure 27. Total heat of reaction, ΔH_{RXN}, was calculated individually for each experiment by drawing a straight baseline from the beginning to the end of the exotherm and integrating the peak area. The peak temperature, T_P, was chosen as the point of maximum $(d\Delta H/dt)_T$. The rate of conversions were calculated according to eq. 3.11 using the exothermic heat of the individual scan rather than the average. The values of ΔH_{RXN} (see Table 4) are very consistent for the lower lignin

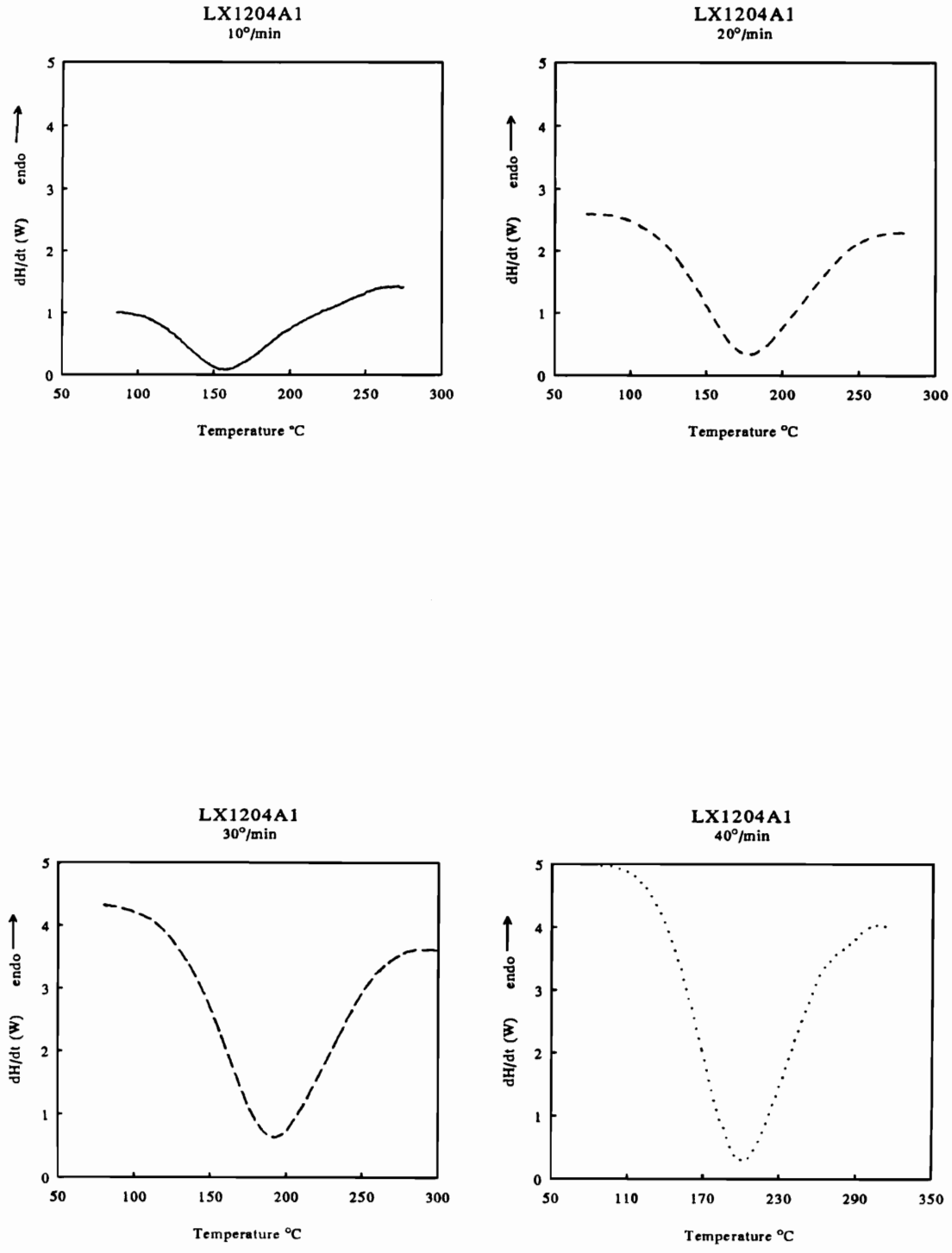

Figure 25. Dynamic DSC Traces of the System LX1204A1-mPDA

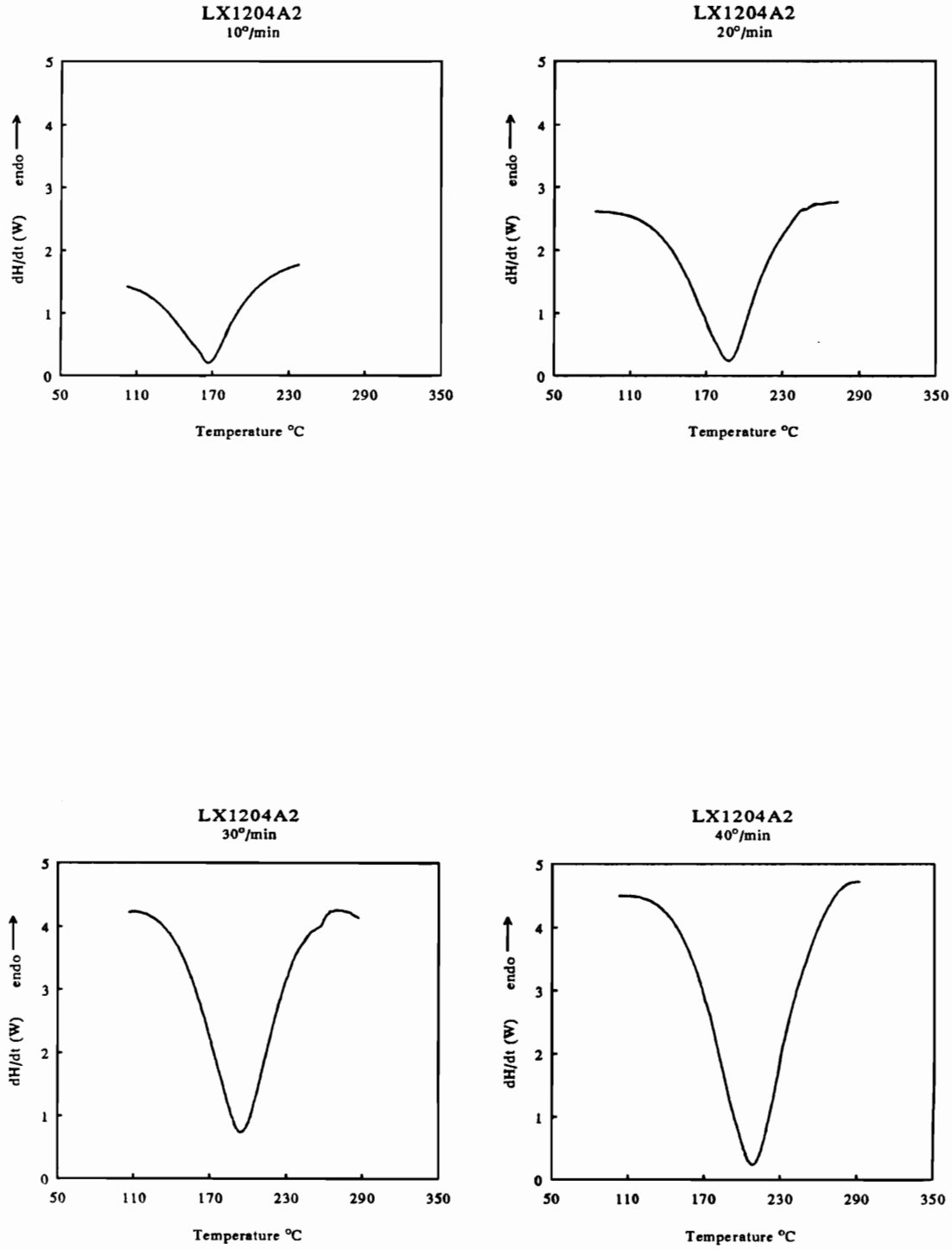

Figure 26. Dynamic DSC Traces of the System LX1204A2-mPDA

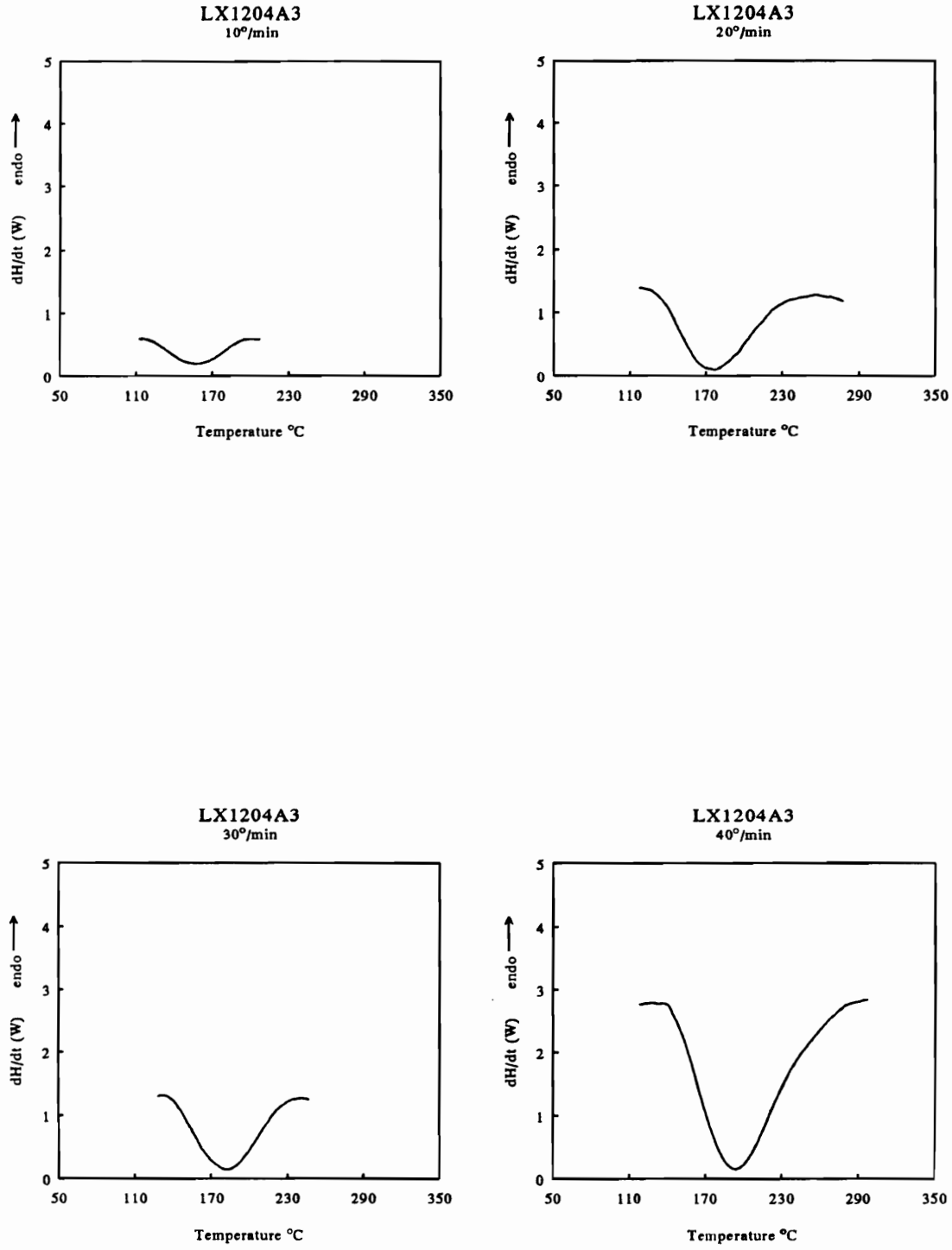

Figure 27. Dynamic DSC Traces of the System LX1204A3-mPDA

content fractions LX1204A1 and LX1204A2. The variation is less than 10% among the four heating rates and it can be safely concluded that between 10 and 40°min^{-1} the total exotherm is independent of heating rate which is consistent with observations originally reported by Fava [60]. However, the high lignin, high molecular weight sample LX1204A3 does not exhibit the same level of consistency, but rather shows considerable variation. Especially, the total heat value of the 10° min^{-1} and 30°min^{-1} scans are too low and most likely artefacts. Examining the respective traces (Figure 27) it can be seen that these exotherms end prematurely. In light of this problem only the 20 and 40°min^{-1} scans were used for the calculation of kinetic parameters of the fraction LX1204A3. Nevertheless, the peak temperatures were used from all four experiments to determine the activation energy.

In order to assess the validity of the obtained data, ΔH_{RXN} values which were averaged over the heating rates were compared on a per mol epoxy basis. The heat of reaction released by one mole of epoxide undergoing an epoxy - amine reaction is 110.7 kJ/mol [2]. From this value it is possible to estimate an expected value of ΔH_{RXN} for each fraction by dividing it by the epoxy equivalent weight (WPE), which yields

	ΔH_{RXN} (J/g)	
	expected	measured
LX1204A1	479	522
LX1204A2	277	431
LX1204A3	252	253[7]

Although the measured values do not match the expected ΔH_{RXN} exactly, the overall magnitude and the trend are consistent, especially considered that both, the expected and the experimental values are fraught by independent experimental errors.

[7] only for 20 and 40 ° min^{-1}

Table 4. Total Exothermic Heat and Peak Temperature of LX1204 Fractions

	Heating Rate (°min^{-1})							
	10		20		30		40	
	T_P[1)]	ΔH_{RXN}[2)]	T_P	H_{RXN}	T_P	H_{RXN}	T_P	H_{RXN}
LX1204A1	157.8	500	176.8	503	190.2	547	200.3	537
LX1204A2	166.6	434	187.7	448	193.7	416	206.8	428
LX1204A3	158.3	120[3)]	172.2	228	181.7	121[3)]	192.7	278

[1)] Temperature of $(d\Delta H/dt)_{max}$ (°C)
[2)] Total Heat of Reaction (J/g)
[3)] not used for further calculations

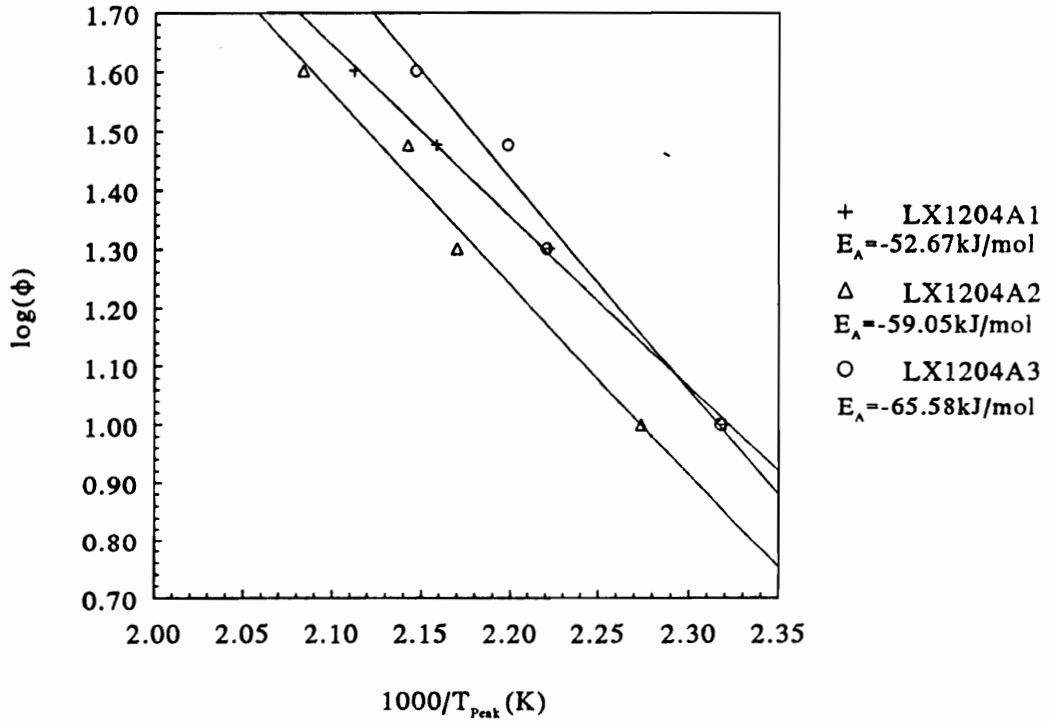

Figure 28. Ozawa Plot of LX1204 Fractions

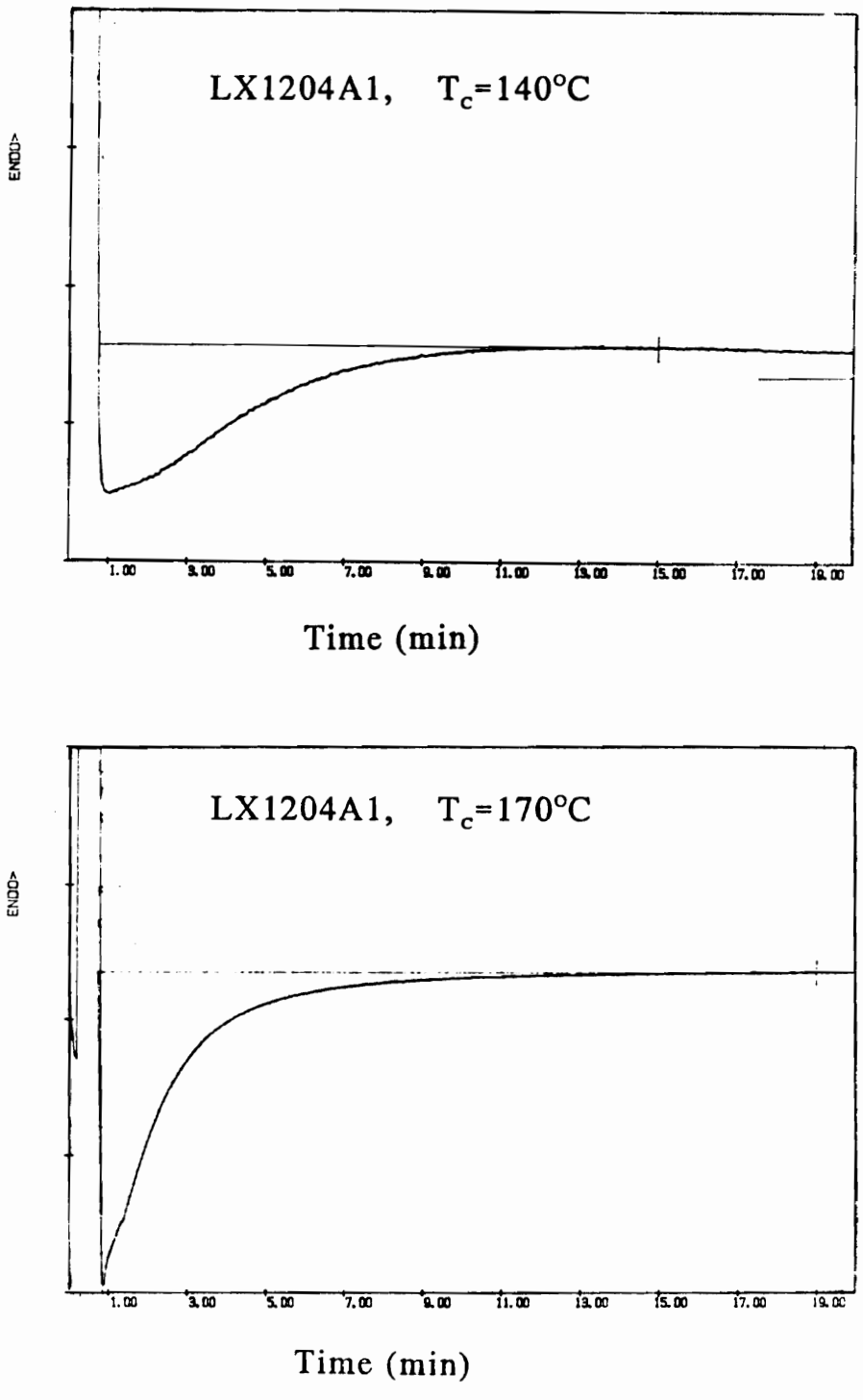

Figure 29. Selected Isothermal DSC Traces of Cure Exotherms

The cure activation energies, E_A, of the three systems were obtained from the slopes of Ozawa plots ($\log \phi$ vs $1000/T_P$, Figure 28) utilizing the approximate relationship outlined in eq. 3.13. From the linear least square fits the activation energies in kJ/mol were calculated:

	E_A (kJ/mol)	R^2
LX1204A1	52.67	0.999
LX1204A2	59.05	0.980
LX1204A3	65.58	0.977

The fitting procedure yielded best results for the low lignin fraction LX1204A1, but also the two other systems showed good correlation (R^2 = 0.980 and 0.977, respectively). The values are in good agreement with the overall range of activation energies reported for epoxy - aromatic amine reactions (46 - 59kJ/mol) [49]. The activation energies show a consistent positive correlation with lignin content and/or molecular weight of the copolymer (see Table 3). Aside from the nature of E_A as a measure of energy barrier of the reactions, it also can be considered a time-temperature shift factor in Arrhenius type processes giving information about the magnitudes of the temperature dependent rate constant. This allows to make predictions about the relative speed of reactions as a function of isothermal process temperature. However, to make absolute assessments about the time needed to reach a fixed extent of conversion, it is also necessary to have knowledge about the type, the reaction order, and the pre-Arrhenius frequency factor of the reactions. Considering the examples of isothermal cure exotherms in Figure 29, it is obvious that the reaction is closer to an n^{th} order than an autocatalytic type, usually encountered in epoxy - amine reactions (see Figure 14). It is also clear that it is not feasible to extract meaningful conversion and rate data from these graphs since the maximum rate of reaction happens very close to the start and goes unrecorded by DSC. Rather, the dynamic results (Figure 25, Figure 26, and Figure 27) were partially integrated in 30° intervals which yielded ΔH_T, the heat evolved up to the respective temperature, while the ordinate at this point gave $(d\Delta H/dt)_T$. Additionally, the peak exothermic heat, ΔH_P, and rate, $(d\Delta H/dt)_P$,

were determined. To convert these values into the respective extent, α_T, and the rate of conversion, $(d\alpha/dt)_T$, the individual total heat values, ΔH_{RXN}, rather than averages was used as normalization constant (eq. 3.11). Compilation of these data for the three systems as function of temperature and heating rate can be found in Table 5.

The method of utilizing dynamic DSC experiments with multiple heating rates is based, among others, on the assumption that α_P, the conversion at the peak temperature is a constant independent of ϕ, the heating rate. This assumption seemingly is not met since values of α_P exhibit considerable scatter. However, it has to be taken into account that these values are highly affected by slight errors in determining T_P, since $(d\Delta H/dt)_T$ is a maximum at this point. A likely cause for errors of the temperature values lies in the change of instrument characteristics at different heating rates. Although, the calibration of the calorimeter has been carried out only for $10° \, min^{-1}$ it might be advisable to calibrate the DSC for each heating rate. Nevertheless, the good fits of the "Ozawa" - plot (Figure 28) gave enough confidence in the validity of this technique for the systems under observation. Values of $\ln[Af(\alpha)]$ were calculated by adding $\ln(d\alpha/dt)_T$ and E_A/RT, and by plotting them for each temperature slice of the DSC scan as a function of $\ln(1-\alpha)_T$ (see eq. 3.16). Yielding a linear correlation between these variables over a wide range of conversion would be an additional indication of n^{th} order kinetics. Additionally, the slope is the reaction order n, and the intercept equals $\ln(A)$, the natural logarithm of the pre-Arrhenius frequency factor. Indeed, examining Figure 30, the results of this treatment are strikingly good. Not only do all three reactions follow the straight line relations indicative of n^{th} order reactions for $\alpha>10\%$, but also the data for the different heating rates closely overlap. This consistency between the heating rates is for example much better as similar results reported for an epoxy-novolac - amine system [20]. At low conversion ($\alpha<10\%$), the data do deviate from the straight line relationship which is an indication of an initial autocatalytic character. Slope and intercept yielded the following values for n and A for the three systems, determined by excluding values at conversions less than 10%:

Table 5. Extent of Conversion and Rate of Conversion of LX1204 - Amine Reactions from Dynamic DSC Experiments

T (°C)	α_T	$(d\alpha/dt)_T$ ($\times 10^{-3}$)	T (°C)	α_T	$(d\alpha/dt)_T$ ($\times 10^{-3}$)
LX1204A1					
	10° min^{-1}			**30° min^{-1}**	
157.8[1]	0.3575	1.94	190.2[1]	0.4688	6.05
120	0.055	0.707	110	0.003	0.199
150	0.303	2.053	140	0.239	1.747
180	0.677	1.693	170	0.239	4.79
210	0.889	0.827	200	0.585	5.735
240	0.981	0.26	230	0.861	2.356
			260	0.982	0.886
	20° min^{-1}			**40° min^{-1}**	
176.8[1]	0.451		200.2[1]	0.455	7.75
100	0.003	0.153	140	0.015	1.272
130	0.059	1.27	170	0.219	4.916
160	0.256	3.45	200	0.455	7.75
190	0.616	3.86	230	0.764	5.45
220	0.884	2.00	260	0.937	2.13
250	0.988	0.397	290	0.986	0.574
LX1204A2					
	10° min^{-1}			**30° min^{-1}**	
166.8[1]	0.5106	3.35	193.8[1]	0.4977	8.44
130	0.062	0.875	140	0.017	0.926
160	0.391	2.762	170	0.176	4.803
190	0.855	1.469	200	0.600	8.032
220	0.976	0.228	230	0.918	2.532
			260	0.995	2.972
	20° min^{-1}			**40° min^{-1}**	
187.9	[1]0.558	5.504	206.8[1]	0.521	10.22
110	0.008	0.241	140	0.012	0.753
140	0.063	1.312	170	0.108	4.129
170	0.297	4.096	200	0.407	9.484
230	0.964	1.081	230	0.814	6.596
250	0.997	.195	260	0.973	1.445
LX1204A3					
	20° min^{-1}			**40° min^{-1}**	
177.2[1]	0.474	5.486	192.7[1]	0.412	9.519
130	0.004	0.343	150	0.013	1.632
160	0.208	1.88	180	0.235	8.317
190	0.668	4.649	210	0.648	8.139
210	0.975	0.748	230	0.833	4.86
240	0.989	0.341	250	0.945	2.433
			270	0.986	0.812
			280	0.999	0.256

[1]) Peak temperature

a)

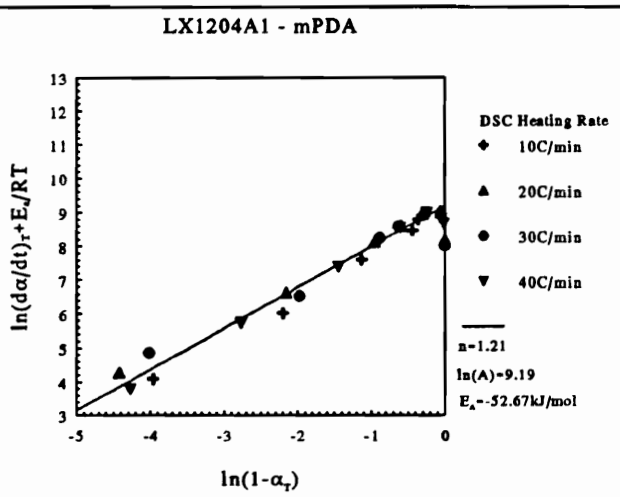

b)

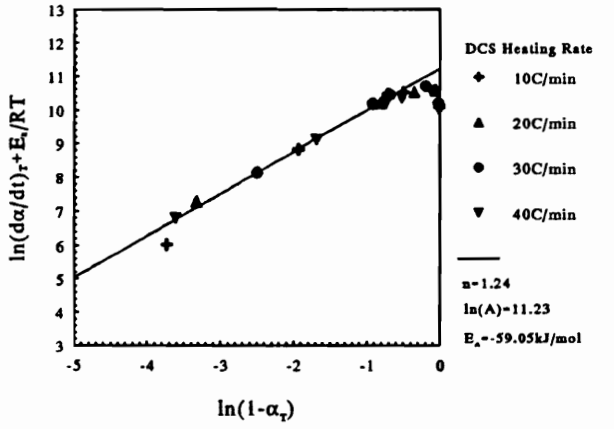

c)

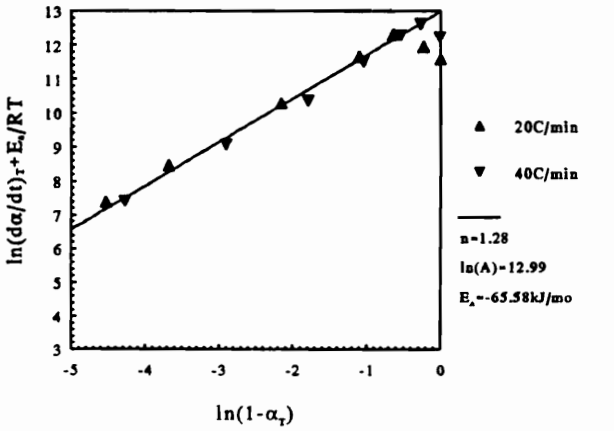

Figure 30. Determination of Kinetic Parameters from Dynamic DSC Experiments

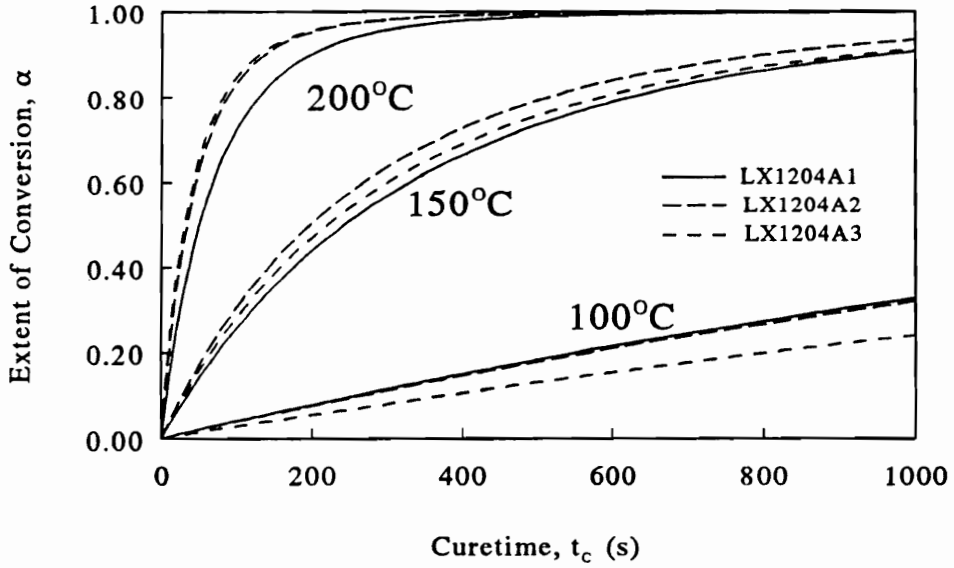

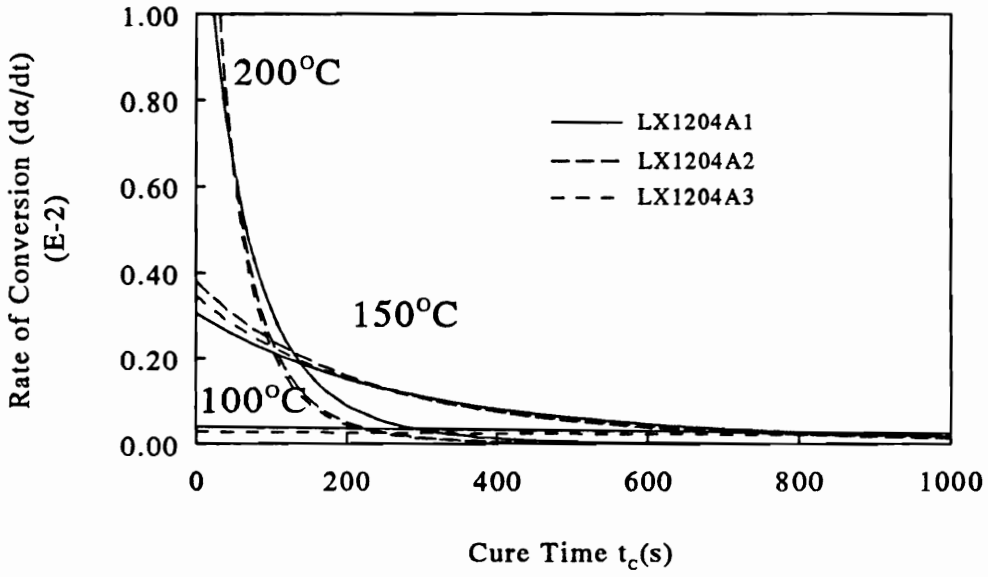

Figure 31. Theoretical Isothermal Cure of LX1204 Epoxy Fractions for 100°C, 150°C, and 200°C
: a) extent of conversion
b) rate of conversion

	n	$\ln(A)$ (s^{-1}) experimental	R^2	$\ln(A)$ (s^{-1}) from eq. 3.14
LX1204A1	1.21	9.19	0.993	9.49
LX1204A2	1.24	11.23	0.996	11.00
LX1204A3	1.28	12.99	0.998	13.24

The reaction orders slightly increase with lignin content while the pre-Arrhenius constants increases. The frequency factor A is a function of the collisions probability of the reactants [53,58] and, thus, related to the mobility of the species. It is interesting to note that contrary what one would assume $\ln(A)$ increases with lignin content and molecular weight. It is not clear whether this is rooted in distinct physical differences among the fractions, or whether it is an artifact, compensating for errors in the determination of the activation energy. In any event, it is difficult to assign a specific molecular meaning to those trends, since the determination of the activation energy from the slope of $\log \phi$ vs. T_P^{-1} is very susceptible to errors. By adding E_A/RT to $\ln(d\alpha/dt)$, $\ln(A)$ is found as the intercept at $\alpha = 0$ (Figure 30). Thus, the frequency factor determined by this method is a strong function of the activation energy (see also eq. 3.14), and errors in the determination of E_A are partially compensated for by $\ln(A)$. Nevertheless, the calculation of $\ln(A)$ with equation 3.14 yielded the same trend and values.

The reaction orders of the three reactions vary between 1.21 and 1.28. Although not an integer number, the order is close to one. n^{th} order epoxy - amine reactions where $n = 1$ have been reported [2,18], but this would be in conflict with the basic mechanism given in Figure 12. The rate equation of the rate determining step b) is $-de/dt = kea$, where e and a are the concentrations of the epoxy and amine at time t. Substituting α for $1 - e/e_0$ and assuming stoichiometric conditions and the absence of side reactions one can write

$$\frac{d\alpha}{dt} = k(1-\alpha)^2 \qquad [3.27]$$

which would be the rate equation of a second order reaction. The fact that the reaction orders for the lignin epoxy - amine systems are fractional numbers closer to one than to two suggests that in these cases the rate determining step is not the bimolecular ring opening, but rather that both, the activation (Figure 12, a) and the ring opening step (b) have comparable rate constants [53].

3.3.1.2 Calculation of Isothermal Kinetic Parameters

Notwithstanding the uncertainty about A and E_A, it is possible to write overall rate equations for the three lignin epoxy-amine systems:

$$\begin{aligned}
&\text{LX1204A1:} \quad \frac{d\alpha}{dt} = \ln(9.2)e^{-(52670/RT)}(1-\alpha)^{1.21} \\
&\text{LX1204A2:} \quad \frac{d\alpha}{dt} = \ln(11.2)e^{-(59050/RT)}(1-\alpha)^{1.24} \\
&\text{LX1204A3:} \quad \frac{d\alpha}{dt} = \ln(13.0)e^{-(65580/RT)}(1-\alpha)^{1.28}
\end{aligned} \qquad [3.28]$$

From these rate equations it is possible to calculate the isothermal time dependance of α and $d\alpha/dt$. The extent of reaction, α, as a function of $d\alpha/dt$ can be determined by integrating eq. 3.1 where $f(\alpha) = (1-\alpha)^n$ yields

$$\alpha = 1 - [(n-1)kt + 1]^{1/(1-n)} \qquad [3.29]$$

where $k = Ae^{-E_A/RT}$. Inserting eq. 3.29 back into eq. 3.1 gives

$$\frac{d\alpha}{dt} = k[kt(1-n) + 1]^{n/(1-n)} \qquad [3.30]$$

Eqs. 3.29 and 3.30 were evaluated with the kinetic parameter obtained for the three fractions at three cure temperature levels: 100, 150, and 200°C (Figure 31 a, b). It immediately becomes clear

that there are no significant differences in the cure time dependency of the three fractional lignin systems. The rates of conversion as a function of extent of conversion and cure time (Figure 31 a and b) are almost identical for the three fractions. Very often it is convenient to relate reactions by comparing the half time, $t_{1/2}$, the time when 50% of the epoxy groups are depleted. The respective half times for the three fractions at 100, 150, and 200°C are compiled in Table 6. Although most likely not significant, a slight influence of lignin content is detectable since the reaction is relatively faster for the low lignin material at low temperatures, but the trend is reversed at high temperature.

Most epoxies react with aromatic amines in an autocatalytic mechanism and it is therefor not easy to compare literature values with those obtained in this study. Nevertheless, reported activation energies and frequency factors of commercial epoxy-amine systems are in very good agreement with the lignin epoxy-*m*PDA values. Some of these results are shown in Table 7.

3.3.1.3 Summary of DSC Cure Kinetic Investigations

Concluding, it can be said about the cure reactions of the three lignin epoxy fractions with meta phenylene diamine that

- it is possible to extract isothermal kinetic parameter from dynamic DSC experiments with multiple heating rates;
- poly(propylene oxide) extended lignin based epoxies react with *m*PDA following n^{th} order kinetics;
- the reaction order of the epoxy consumption ranges from 1.21 to 1.28, which indicates that the rate determining step is not the bimolecular ring opening, but that the reaction is complex with the unimolecular activation and the bimolecular ring opening steps having comparable rate constants;
- the activation energy increases with increasing lignin content and increasing molecular weight, but so does also the pre-Arrhenius frequency factor;

Table 6. Cure Reaction Half Times of LX1204 Fraction with Meta Phenylene Diamine

	Cure Temperature (°C)			Lignin	M_n of
	100	150	200 (%)	Content ($\times 10^3$)	Copolymer
LX1204A1	1 810	243	50	16	0.63
LX1204A2	1 872	197	33	37	1.9
LX1204A3	2 680	220	31	42	93.8

Table 7. Kinetic Parameter of Selected Epoxy Amine Reactions

System	Reaction Type[1]	E_A (*kJ/mol*)	ln(A) (s^{-1})	Ref.
LX1204A1 - *m*PDA	n	52.67	9.2	this work
LX1204A2 - *m*PDA	n	59.05	11.2	this work
LX1204A3 - *m*PDA	n	65.58	13.0	this work
DGEBA[2] - *m*PDA	a	47.9	11.3	11
DGEBA - *m*PDA	n,a[3]	40.6	15.3	42
DGEBA - *m*PDA	a	62	10.6	43,50
DGEBA - *m*PDA	a	64	11.7	43,51
DGEBA - PACM-20	n	53	11.2	25
DGEBA - Versamid™	a	60.9	8.7	2

[1]) a..autocat., n..n^{th} order
[2]) diglycidyl ether of bisphenol A
[3]) see Ch. 3.1.3 for details

- the overall rate of the kinetically controlled reaction is only moderately influenced by compositional parameters;
- the values of activation energies and frequency factors are in the same range as those reported for other aromatic amine cured systems.

3.3.2 Network Formation by Dynamic Mechanical Thermal Analysis (DMTA)

3.3.2.1 Glass Transition Temperature of Partially Cured Lignin Epoxides

While the last section discussed the kinetic aspects of the curing reaction, it is the focus of the following to report results which correlate the course of reaction to network formation. Beyond gelation, thermosetting systems are characterized by a rise of glass transition due to the formation of an ever tightening network which has increasingly severe repercussions on the rate of reaction due to growing diffusion control. Since it is expected that lignin, as the rigid center of the star-like copolymer, plays a decisive role in determining diffusivity within the network, it is of interest to study the contributions of lignin and its concentration on the course of reaction at the later stages of the cure. Because the relative magnitude of the glass transition temperature is a function of conversion, it was therefore the aim of this study to measure the glass transitions of partially cured systems, and relate it to the advancement of cure as function of T_C and t_C, and of compositional parameters.

The recording of the modulus and damping during the isothermal experiments unfortunately does not yield the same information as they were observed for DGEBA based systems [25,42], (Figure 18). Not only are the modulus traces flat, only slightly increasing during the course of the reaction, there is also no sign of a gelation damping transition. Furthermore, the event of

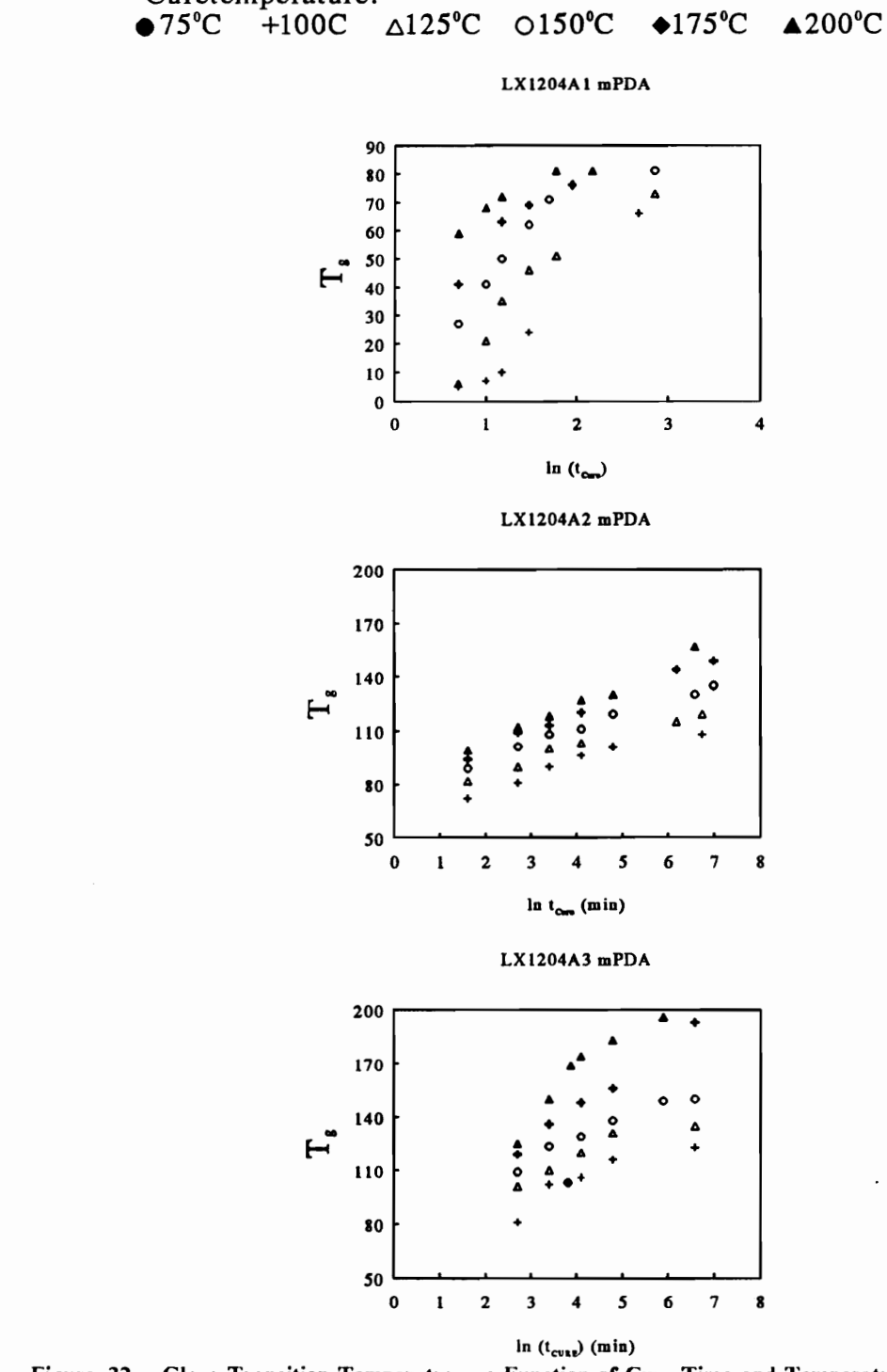

Figure 32. Glass Transition Temperature as Function of Cure Time and Temperature (LX1204 Fractions)

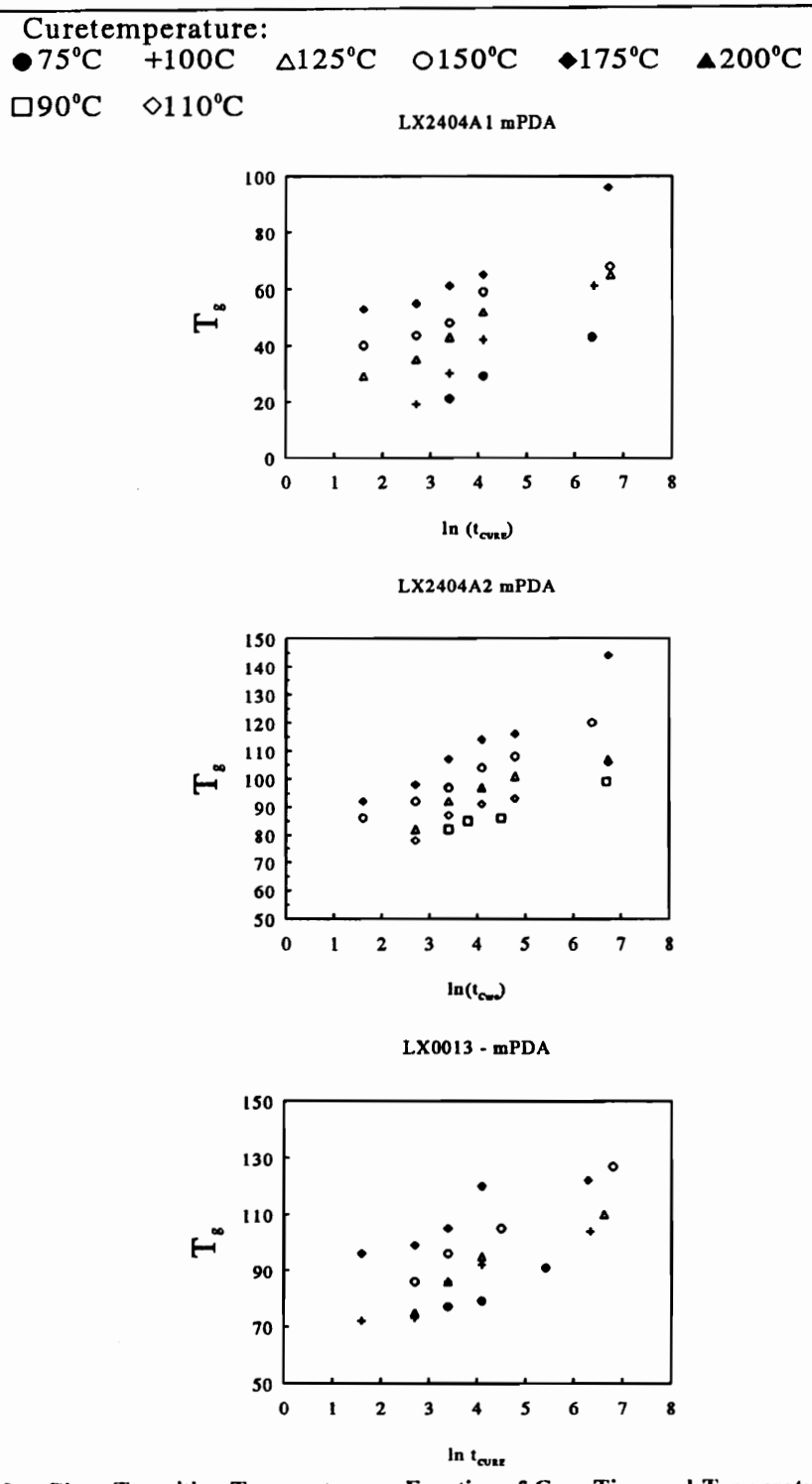

Figure 33. Glass Transition Temperature as Function of Cure Time and Temperature (LX2404 Fractions and LX0013)

vitrification is not marked by a dramatic incline of the log E' data and the occurrence of a second damping maximum as it was observed for the DGEBA based resin cure. Obviously, the vitrification, or the halting of the reaction by diffusion limitations within the forming network is a markedly more gradual process and more complex in the case of a polydisperse two component system (lignin-polyether) than in the well defined commercial resins with a very narrow low molecular weight distribution.

The glass transition temperatures of the lignin containing epoxides in the form of impregnated glass braid composites have been recorded as function of the cure time and cure temperature. The respective data were compiled in Figure 32 and Figure 33. It is evident that the T_g vs. $\ln(t_C)$ traces at the individual cure temperatures can be shifted to a reference temperature. Viewing the shifted graphs of T_g vs. $\ln(a_T t_C)$ (Figure 34 and Figure 35) it can be observed that up to a certain point the traces are superimposable, but that thereafter the individual lines diverge. This is especially the case for the high lignin fractions. At this point the reaction does not obey anymore the Arrhenius relationship of a kinetically controlled mechanism, but it becomes diffusion controlled. The activation energies were calculated from the inserted shift plots (eq. 3.27) and compiled in Table 8.

From the master curves of Figure 34 and Figure 35, it can be seen that those resins with low lignin content (LX1204A1, LX2404A1) have superimposed traces leading to the same maximum T_g, and there is little divergence from the master plot. On the other hand, the higher lignin content systems show divergence of the T_g vs. $\ln(t)$ data; i. e., the maximum glass transition is different for different cure temperatures. But while at the lower cure temperatures the resulting T_g's surpass the T_C's, it is interesting to observe that at higher T_C's the respective traces level off at or slightly below the T_C. As discussed, the slowing and halting of the reaction and the subsequent limits imposed on the glass transition temperature are a function of the fact that the glass transition temperature bypasses the cure temperature and thereby reduces the mobility of the reactants. As shown in Ch. 3.1.3 [42] for a commercial DGEBA - *m*PDA system this implies that the maximum glass transition attainable at any cure temperature below $T_{g,\infty}$ is about 10 to 20° higher than the cure temperature. It is assumed that the main cause of the premature slowing of the reaction is due to diffusion limitations

Table 8. Cure Reaction Activation Energies of LX1204 and LX2404 Fractions and LX0013

Sample	E_A (*kJ/mol*)	M_n ($\times 10^3$)	Lignin Content (%)
LX1204A1	48.3	0.63	16
LX1204A2	39.1	1.9	37
LX1204A3	35.2	93.8	42
LX2404A1	39.2	0.8	21
LX2404A2	49.5	5.5	39
LX0013	39.2	1.2	57

LX1204A1 - mPDA

a)

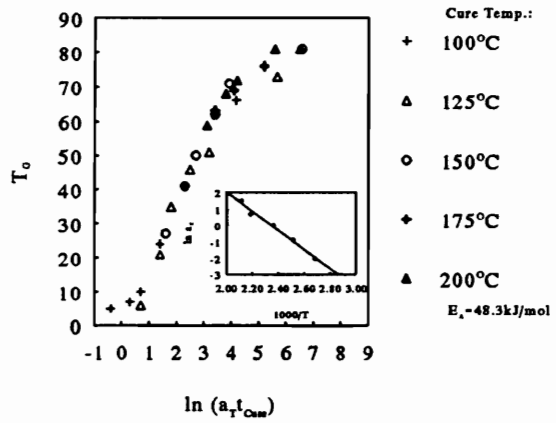

LX1204A2 mPDA

b)

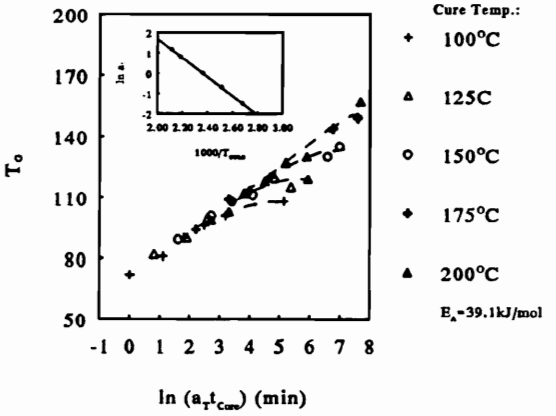

LX1204A3 mPDA

c)

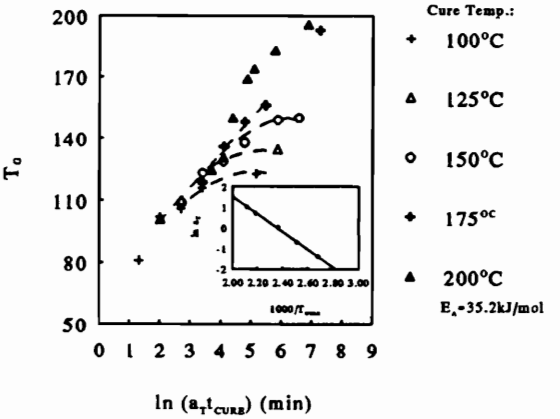

Figure 34. Curetime - temperature Shifts, Shift Plots of LX1204 Epoxy - Amine Resins

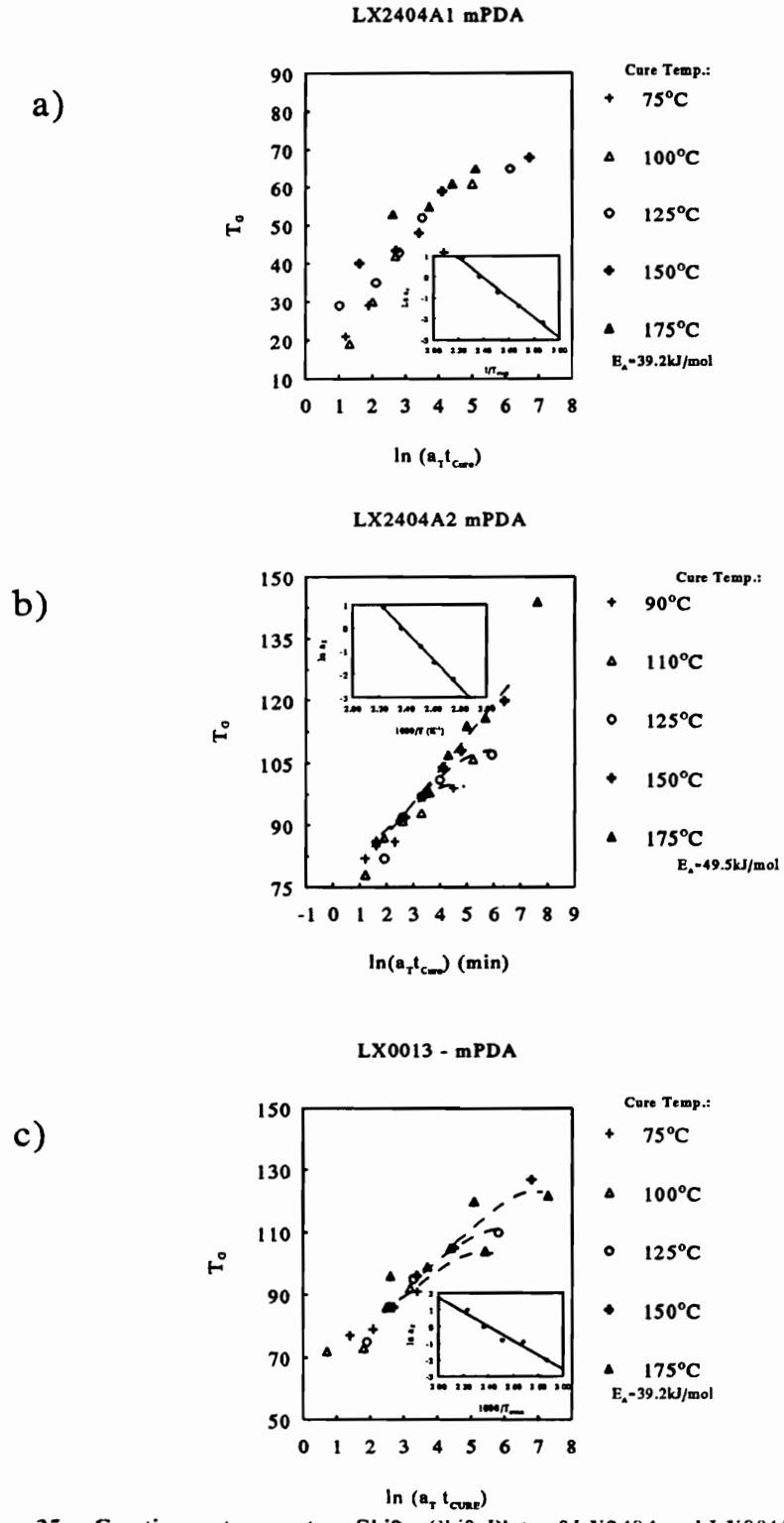

Figure 35. Curetime - temperature Shifts, Shift Plots of LX2404 and LX0013 Epoxy - Amine Resins

occurring well before the main glass transition temperature is reached. This assumption is supported by the fact that the transitions are very broad indicating a considerable degree of in-homogeneity. Also Plazek and Frund [63] found that a Epon828 resin cured isothermally with methylene dianiline (MDA) at 130°C did not show a leveling off of the fictive temperature, T_{fg} vs. log t_C curve before $T_{fg} = T_C$. The fictive temperature is the glass transition temperature of a polymer system which is a complete equilibrium glass. Since the fictive temperature is always lower than the measured T_g, the results of Plazek and Frund indicate that vitrification of this commercial system does not happen before $T_g > T_C$.

Cross-linking of star-like molecules having reactive functionalities situated at the terminus of the flexible chains, and rigid centers, depends mostly on the mobility of the arm. However, at higher conversions close to vitrification the rigid centers are interconnected and form a network with density fluctuations. This will impair the mobility of the reactants, even before the glass transition, defined as peak of the tanδ transition, reaches the level of the cure temperature. On the other hand, in well defined homogeneous systems, such as DGEBA resins, the entire gel experiences a homogeneous environment and, thus, overall mobility ceases once $T_g \geq T_C$. Such systems are also characterized by a relatively narrow tanδ transition while heterogeneous networks like those based on lignin have a very broad transition. Therefore, the diffusion of the reactants, which by themselves are mobile, is limited by denser inhomogeneities even before the network passes through the state of glass transition. Thus, the reaction will terminate "prematurely" before $T_g > T_C$.

3.3.2.2 Construction of Vitrification Curves

In order to estimate the influence of compositional parameters and molecular weight of the copolymer on the vitrification behavior of the cross-linking copolymers fractions, it is useful to compare their respective TTT-diagrams, especially the vitrification traces. If vitrification is defined as the event which takes place when the glass transition temperature becomes equal to the cure temperature during isothermal cure, and this stops the reaction due to diffusion limitation, then the

maximum glass transition temperature of the cured material is equal to the cure temperature. The times necessary to reach this point during the reaction as a function of cure temperature is t_{vit}, the vitrification time. t_{vit}, as function of T_C and t_C form part of the time-temperature-transformation (TTT) thermosetting cure diagram proposed by Gillham [25]. (see Figure 15). These vitrification time traces are typically S-shaped which reflects the fact that vitrification, unlike gelation is not an iso conversion event but depends on cure temperature and the difference $T_C - T_{g,0}$. Sandwiched between the glass transition temperature of the uncured resin, $T_{g,0}$, and the glass transition temperature of the fully cured material, $T_{g,\infty}$, the trace passes through a time maximum at low cure temperatures and a minimum at cure temperatures close to $T_{g,\infty}$. Beyond this point, vitrification times rapidly increase, reflecting the concentration dependent reduction of the reaction rate.

As demonstrated by Enns and Gillham [25] and shown in Ch. 3.1.3, it is possible to construct a major portion of the vitrification curve by measuring the times to reach the second damping maximum in isothermal dynamic mechanical experiments (TBA, DMTA, DMA). However, this approach was not possible, since for the lignin based epoxides the isothermal traces of tanδ during cure do not show the typical second transition as indication of vitrification. An alternative method to determine the vitrification times, is to measure the maximum attainable glass transition temperature for a sequence of materials cured at temperatures ranging from $T_{g,0}$ to $T_{g,\infty}$. Unfortunately, the early onset of diffusion control of the reaction makes it difficult to reach the necessary extents of conversion during isothermal cure, especially at low T_C. Additionally, the lower lignin content resins have a very low $T_{g,\infty}$, so that curing at temperatures below this levels is a long process due to the low T_C's.

Therefore, a third method was investigated, which takes advantage of the shiftability of T_g vs. ln(t) lines obtained from different cure temperatures, according to eq. 3.26. This method has been applied successfully by Wissanrakkit and Gillham [12] to develop a TTT diagram of a DGEBA resin cured with a blend of aromatic diamines. Having defined $T_g = T_C$ as vitrification, eq. 3.26 can be recast to calculate the vitrification time, t_{vit}, at any cure temperature T_C, based on the knowledge

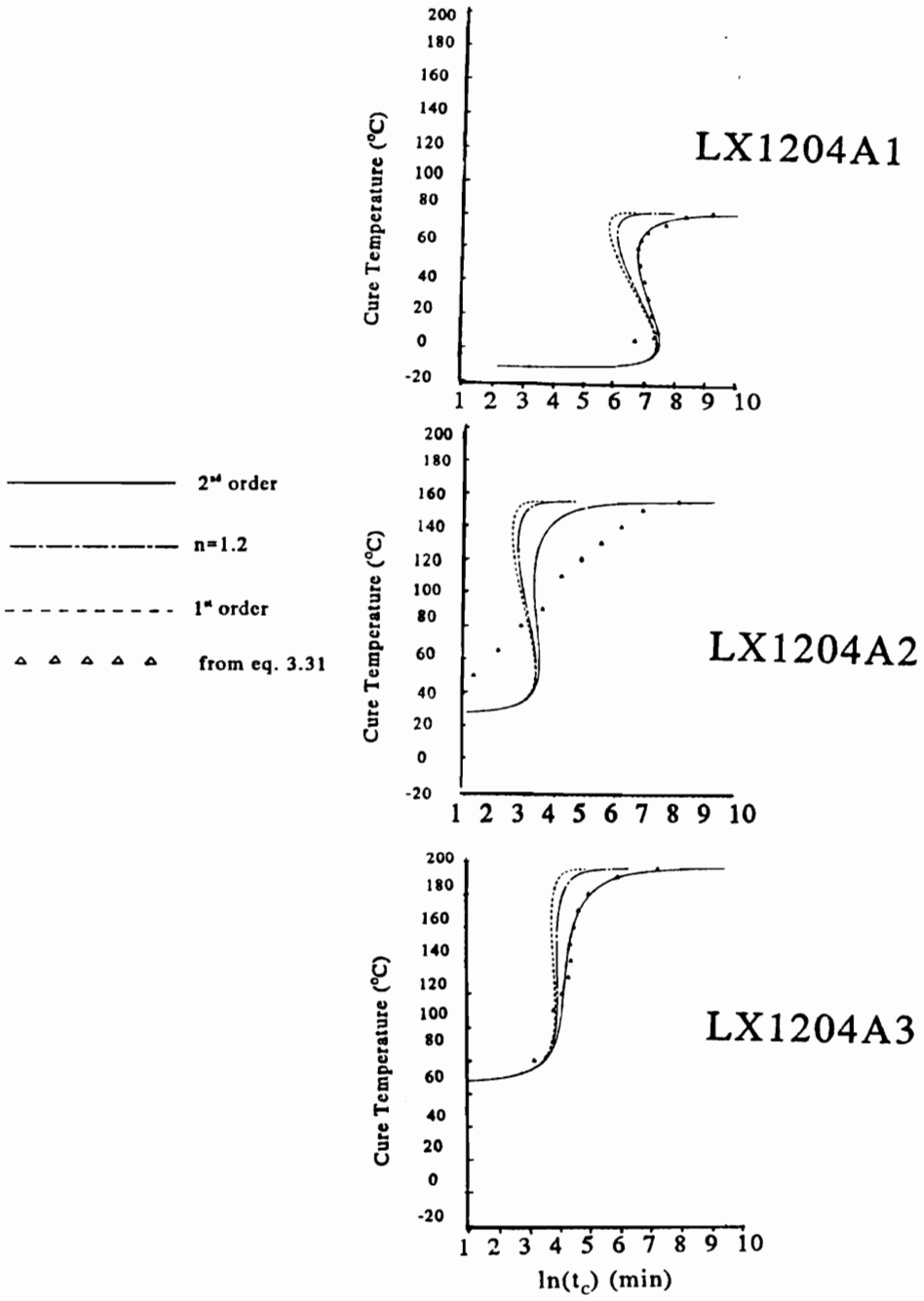

Figure 36. Vitrification Traces (TTT Diagram) of LX1204 Fractions Cure

of the time t_{ref}, necessary to reach the respective glass transition temperature, $T_{g,ref}$, at the reference cure temperature, $T_{C,ref}$

$$\ln(t_{vit}) = \ln(t_{ref}) + \frac{E_A}{R}\left(\frac{1}{T_C} - \frac{1}{T_{C,ref}}\right) \qquad [3.31]$$

Thus, by knowing the activation energy, E_A and the values of t_{ref}'s, the times to reach the glass transition temperature ($T_G = T_C$) at the reference temperature, it is possible to map the vitrification time versus $\ln(t_C)$ trace. The master curves of T_g vs. $\ln a_T t$ (Figure 34 and Figure 35) allow to determine the t_{ref}'s for a wide range of T_C's at $T_{ref} = 150$ °C. Values of the vitrification times have been calculated (eq. 3.31) for the three fractions of LX1204 at temperatures ranging from $T_{g,0}$ to close to $T_{g,\infty}$. Furthermore these semi-experimental vitrification data have been compared with calculated vitrification curves, whereby the segmental mobility ratio F has been kept constant at 1.0 (see eq. 3.21), and ε has been calculated by virtue of equation 3.22, whereby for $T_{g,\infty}$ the highest obtained glass transition temperature of the cross-linked fractional epoxy system was inserted. The activation energies were obtained from the $\ln a_T$ vs. T^{-1} shift plots. The pre-Arrhenius frequency factor has been used as adjustable parameter for the fitting of eq. 3.23. Three values of the reaction order n have been tried: 1, 2, and the value obtained from the DSC kinetic investigation (Figure 30). The reaction order is the single most important parameter determining the S-shape of the vitrification curve, while F, A, and E_A determine the position of the trace on the time axis.

The respective vitrification data and the calculated and fitted vitrification curves are compiled in Figure 36. The low lignin containing fraction LX1204A1 and to a lesser extent LX1204A3 exhibit the sigmoidal shape as it is known from the cure of DGEBA based epoxies with aromatic diamines, while the medium lignin content fraction, LX1204A2 does not exhibit any S-character in the range for which t_{vit}'s could be calculated.

The three vitrification plots of LX1204 fractional systems exhibit a distinct trend to shorter vitrification times with increasing lignin content. Since it has been found that the extent of the kinetically controlled reaction as a function of cure time does not change among the fractions (see

Figure 31), it is evident that higher lignin content and/or molecular weight of the copolymer leads to diffusion control of the reaction at lower extents of conversion. Furthermore, the vitrification data visualize that ΔT_g, the rise of the glass transition temperature during cross-linking is nearly constant for the three fractions. Thus, the $T_{g,\infty}$ differences among the fractions are a direct result of the respective $T_{g,0}$ variations. A more detailed discussion of the influence of cross-linking on ΔT_g can be found in section 4.3.4.1.

As has been shown by Kelley et al. [59] and will be discussed hereunder, the glass transitions of the lignin containing networks is much broader than those of homogeneous networks such as DGEBA based ones. This implies that the mobility of the reactant carrying flexible polyether chain is impaired even before the peak of the transition is reached. An additional evidence for the "premature" reduction of mobility is the fact that the reaction kinetics at or below vitrification changes from the fractional order close to one to a second order type. This can be seen from Figure 36 where only the calculated traces of the second order kinetics fit the shape of the vitrification data. This change in order indicates that the rate of the bimolecular ring opening step is now smaller than the unimolecular oxirane activation step. As long as the reaction is only kinetically controlled, these two steps have comparable rate constants. Since the ring opening step as a bimolecular reaction is mobility dependant, the change to second order is a strong indication of restrained oxirane mobility at higher stages of reaction. The explanation based on premature diffusion limitation is also supported by the fact that the superimposed T_g vs. $\ln(a_T t)$ traces of the higher lignin content systems (Figure 34 and Figure 35) start to branch off the master curve at a T_g below the respective cure temperature, especially for higher T_C's.

3.3.2.3 Summary of DMTA Cure Studies

Concluding, the following statements about the DMTA investigation of lignin epoxy - amine cure can be made:

- the cure of epoxy - amine systems was monitored from the uncured to the highly cured state by subjecting a resin impregnated glass fiber braid to oscillatory bending at isothermal temperatures, and by simultaneously recording the change of log E' and tanδ;
- the isothermal tanδ traces did not permit the identification of gelation and vitrification based on damping maxima, as it is possible for DGEBA based resins;
- master curves of T_g vs. reduced times for cure temperatures ranging from 90° to 200°C could be constructed, and the activation energies calculated from the shift plots a_T vs T^{-1};
- it was possible to construct semi experimental vitrification plots for each system, based on the knowledge of activation temperature and the cure times at a reference temperature to reach given glass transition temperatures, and to fit theoretical vitrification lines to these data;
- while lignin content did not influence the reaction kinetics at low extents of reaction, it clearly controls the reaction kinetics at higher extents of conversion, close to vitrification;
- the rate of reaction changed from a fractional order close to one to a second order type;
- increasing lignin content of the fractions shortened the time to vitrification, i.e. vitrification took place at lower extents of reaction.

3.4 Conclusion

In the foregoing chapter, an attempt was made to shed light on the cure and network formation of lignin-PPO copolymer based epoxy resins with an aromatic diamine. Based on dynamic DSC studies it has been established that the curing reaction follows n^{th} order kinetics with reaction orders ranging from 1.21 (low lignin content fraction) to 1.28 (high lignin content fraction), indicating that the rate determining step is not the bimolecular ring opening step, but both, the initial unimolecular activation step and the oxirane - amine reaction have similar rates of reaction. The n^{th} order type of reaction is a strong indication of relative high initial abundance of hydrogen donating species.

Although the activation energies determined from dynamic DSC experiments with multiple heating rates increase with lignin content, the difference of isothermal conversion is minuscule among the fractions. Lignin does not seem to have an effect on the overall time dependance of the rate and extent of the kinetically controlled conversion. However, as could be found by conducting DMTA studies of these resins, lignin content has a distinctive influence on the vitrification behavior. The onset of diffusion control is a function of the lignin content and typically happens at lower extents of conversion for higher lignin content fractions. Furthermore, the reaction changes close to vitrification to a second order type which indicates a general reduction in polyether chain mobility.

Thus, summarizing these observations, it can be concluded that at later stages of the curing reaction, the epoxy carrying polyether arms of the star-like lignin-PPO pre-polymer lose mobility. But while diffusion related reduction of reactant mobility is common for all thermosetting systems, the onset of this process seems to start earlier for these copolymer systems. Furthermore, the time to vitrification is reduced as a function of lignin content, thus the extent of conversion at vitrification is inversely related to lignin content. This suggests, together with the observation that individual T_g vs. reduced time traces deviate from the master curves, that, even before the glass transition temperature approaches the cure temperature, the interconnecting of the lignin centers with

polyether arms produces a network where the potential flexible reactant carrying polyether arms do not have the necessary free volume to react with others. The considerable breadth of the glass transition also supports the notion that well before the transition reaches its peak, many chemical features of the heterogeneous network experience mobility constraints. Nevertheless, further studies, such as viscoelastic, scattering, TEM, and NMR experiments are necessary to substantiate the assumptions about the morphological nature of the lignin containing networks.

The rise in glass transition temperature, ΔT_g, during cross-linking is constant for all fractions of one lignin copolymer. From a practical point of view this means that, since ΔT_g is in the order of 100°C or smaller, high final glass transition temperature can be achieved only by using high T_g copolymers. However, since such materials are solids they are difficult to handle and to mix with cross-linking agents.

3.5 References.

1. C. A. May, in: C. A. May, Ed., "Epoxy Resins, Chemistry and Technology", Marcel Dekker Inc., New York and Basel, 1988
2. R. B. Prime, in E. A. Turri, Ed., "Thermal Characterization of Polymeric Materials", Academic Press, New York, 1981
3. W. G. Potter, "Epoxide Resins", Springer Verlag, New York, 1982,
4. Dusek and Blecha, *J. Pol. Sci., Chem. Ed.*, 15, 1977
5. M. A. Acitelli and R. B. Prime, *Polymer*, 12, 1971, 333
6. K. Horie, H. Hiura, M. Sawada, I. Mita, and H. Kambe, *J. Pol. Sci.: A-1*, 8, 1970, 1357
7. G. L. Hagnauer, P. J. Pearce, B. R. LaLiberte, and M. E. Roylance, in C. A. May, Ed., "Chemorheology of Thermosetting Polymers", ACS Symp. Ser. 227, Washington, 1983, 25
8. M. A. Golub and N. R. Lerner, *J. Appl. Pol. Sci.*, 32, 1986, 5215
9. Y. Tanaka and R. S. Bauer, in: C. A. May, Ed., "Epoxy Resins, Chemistry and Technology", Marcel Dekker Inc., New York and Basel, 1988
10. I. T. Smith, *Polymer*, 2, 1961, p.95
11. S. Sourour and M. R. Kamal, *Thermochimica Acta*, 14, 1976, p. 41
12. G.Wissanrakkit and J. K. Gillham, *J. Appl. Pol. Sci.*, 41, 1990, 2885
13. M. R. Kamal, *Pol. Eng. Sci.*, 14, 1974, 231
14. G. Widman, *Thermochimica Acta*, 11, 1977, 331
15. T. Ozawa *J. Therm. Anal.*, 7, 1975, 601
16. T. Ozawa, *J. Thermal Anal.*, 2, 1970, 301
17. C. D. Doyle, *J. Appl. Pol. Sci.*, V(15), 1961, 285
18. R. B. Prime, *Pol. Eng. Sci.*, 13(5), 1973, 365
19. A. A. Duswalt, *Thermochimica Acta*, 8, 1974, 57
20. T. H. Hsieh and A. C. Su, *J. Appl. Pol. Sci.*, 41, 1990, 1271

21. H. E. Kissinger, *Anal. Chem.*, 29, 1957, 1702
22. H. Lee and K. Neville, "Handbook of Epoxy Resins", McGraw Hill, New York, 19??,
23. H. L. Friedman, *J. Pol. Sci.*, C6, 1965, 183
24. L. E. Nielsen, , *Macromol. Sci. - Revs. Macromol. Chem.*, C3(1), 1969, 69 - 103.
25. J. B. Enns and J. K. Gillham, *J. Appl. Pol. Sci.*, 28, 1983, 2567
26. G. Odian, "Principles of Polymerization", J. Wiley & Sons, New York, 1981
27. J. L. Stanford, R. F. T. Stepto, and R. H. Still, in S. S. Labana and R. A. Dickie, Eds., "Characterization of Highly Cross - linked Polymers", ACS Symp. Ser. 243, Washington, DC, 1984
28. M. Gordon and S. B. Ross-Murphy, in B. Sedlácek, Ed., "14th Prague Microsymposium on Macromolecules", Prague, 1974, 1
29. R. F. T. Stepto, in R. A. Dickie, S. S. Labana, and R. S. Bauer, Eds., "Cross - Linked Polymers", ACS Symp. Ser. 367, Washington DC, 1988.
30. K. Dusek and W. J. MacKnight, in R. A. Dickie, S. S. Labana, and R. S. Bauer, Eds., "Cross - Linked Polymer", ACS Symp. Ser. 367, Washington, DC, 1988
31. K. Dusek, in K. Dusek, Ed., "Epoxy Resins and Composites, III", Advances in Polymer Sciences, Vol. 78, Springer Verlag, Berlin, 1986,
32. C. W. Macosko and D. R. Miller, *Macromolecules*, 9, 1976, 199.
33. D. R. Miller and C. W. Macosko, *Macromolecules*, 11, 1978, 191
34. D. R. Miller and C. W. Macosko, *Macromolecules*, 9, 1976, 206
35. S. A. Bidstrup and C. W. Macosko, in J. L. Bauer and R. Dunaetz, Eds., "Materials Science for the Future", Proc. 31st Int. SAMPE Symp., 4, 1986, 551
36. D. R. Bauer, in *Proc. of PMSE Symposium*, 199th ACS Nat. Meeting., 1989, 257
37. D. R. Bauer, in: T. Provder, Ed., "Computer Applications in Polymer Science II", ACS Symp. Ser. 404, Washington DC, 1989
38. X. Peng and J. K. Gillham, *J. Appl. Pol. Sci.*, 30, 1985, 4685
39. L. C. Chan, H. N. Naé, and J. K. Gillham, *J. Appl. Pol. Sci.*, 29, 1984, 3307
40. A. T. DiBenedetto, *J. Pol. Sci., B: Pol. Phys.*, 25, 1987, 1949

41. J. K. Gillham, in A. J. Kinloch, Ed., "Structural Adhesives: Development in Resins and Primers", Elsevier Appl. Sci. Publ., London and New York, 1986,

42. K. Hofmann and W. G. Glasser, *Thermochimica Acta*, 169, 1990, 169

43. J. M. Barton, in: K. Dusek, Ed., "Epoxy Resins and Composites, I,", Adv. in Pol. Sci., 73, Springer Verlag, Berlin, 1985

44. W. W. Wendtlandt and P. K. Gallagher, in: E. A. Turri, Ed., "Thermal Characterization of Polymeric Materials", Academic Press, New York, 1981

45. S. Tai, M. Nagata, J. Nakano, and N. Migita, *Nihon Mokuzai Gakkai*, 13(6), 1967, 102

46. S. Tai, J. Nakano, and N. Migita, *Nihon Mokuzai Gakkai*, 13(6), 1967, 257

47. W. Nieh, in W. G. Glasser and S. Sarkanen, Eds., "Lignin, Properties and Materials", ASC Symp. Ser. 397, Washington, DC, 1989

48. G. F. D'Alelio, *US - Pat. #3,905,926*, 1975

49. R. L. Miller and M. A. Oebser, *Thermochimica Acta*, 36,121

50. M. R. Kamal, S. Sourour, and M. Ryan, SPE 31st

51. C. C. Foun, A. Moroni, E. M. Pearce, and J. Mijovic, *J. Pol. Mat. Sci. Eng.*, 51, 1984, 411

52. H. Stutz and J. Mertes, *J. Appl. Pol. Sci.*, 38, 1989, 781

53. G. Pannetier and P. Souchay, "Chemical Kinetics", Elsevier Publ. Co. Ltd., Amsterdam, 1967

54. J. P. Pascault and R. J. J. Williams, *J. Pol. Sci., B: Pol. Phys.*, 28, 1990, 85

55. H. E. Adabbo and R. J. J. Williams, *J. Appl. Pol. Sci.*, 27,1982, 1327

56. P. S. Gill and R. L. Blaine, in B. Miller, Ed., "Proc. &th Int. Conf. on Thermal Analysis", Vol. 2, Wiley, Chichester, 1982, 994

57. W. X. Zukas, J. MacKnight, and N. S. Schneider, in C. A. May, Ed. "Chemorheology of Thermosetting Polymers", ACS Symp. Ser. 227, Washington, 1983

58. P. W. Atkins, "Physical Chemistry", W. H. Freemann and Comp., New York, 3rd Ed., 1986

59. S. S. Kelley, "Lignin Copolymers in Polyurethane Materials", PhD Thesis, Virginia Tech, Blacksburg, 1987

60. R. A. Fava, *Polymer*, 9, 1968, 137

61. M. T. Aronhime and J. K. Gillham, in K. Dusek, Ed., "Epoxy Resins and Composites, III", Advances in Polymer Sciences, Vol. 78, Springer Verlag, Berlin, 1986,

62. R. E. Wetton, T. G. Croucher, and J. W. M. Fursdon, in C. D. Craver, Ed., "Polymer Characterization", Adv. in Chem. Ser. 203, Washington, 1983

63. D. J. Plazek and Z. N. Frund, Jr., *J. Pol. Sci., B: Pol. Phys.*, 28, 1990, 431

4.0 Properties of Lignin Based Epoxy Networks as Function of Copolymer Composition

4.1 Preface

The preceding chapters dealt with the aspects of synthesizing epoxidized lignin-poly(propylene oxide) copolymer of various compositions, and the kinetics of the curing reaction. The following section describes selected ultimate properties of the cross-linked materials with respect to compositional parameters such as lignin content, chain length, and copolymer molecular weight. The first part summarizes mechanical properties of two fractionated and one unfractionated networks in relation to compositional features. As reference material a DGEBA-*m*PDA system was chosen. The second part of this section deals with viscoelastic and morphological aspects of lignin containing networks based on the results of dynamic mechanical thermal analysis (DMTA) and transmission electron microscopy (TEM). And thirdly, ^{13}C cross polarized magic angle spinning nuclear magnetic resonance (CPMAS NMR) relaxation studies will be presented emphasizing the change of $T_{1,\rho}$ with change of copolymer composition.

4.2 Mechanical Properties

4.2.1 Introduction

One of the most important macroscopic aspects of selecting polymeric solids for engineering purposes is their performance under mechanical load. Since the range of possible applications pose ever changing requirements on a material's mechanical specifications, the ability of modifying a parent polymer to meet those needs is a valuable asset. Lignin, as a brittle and not very well defined biopolymer was long thought of not meeting these challenges. In recent years, however, great progress have been made to improve the picture and it is now certainly possible to tailor lignin to meet a variety of mechanical response requirements [70].

4.2.1.1 Stress - Strain Relations of Polymers

In a broad sense, a material's response to mechanical load can be described by its geometrical deformations. Of course, a detailed discussion of mechanical responses and properties must take into account the rate of applied load, viscoelastic properties of the material, fracture mechanics, linearity, environmental factors such as temperature and humidity, long term stability, etc. Nevertheless, for the purpose of basic comparison and initial screening of materials it is often sufficient to subject isotropic solid polymers to simple uniaxial tensile stress-strain (σ-ε) measurements. Thereby, parameters such as yield and breaking stress and strain, initial and maximum Young's modulus of elasticity, shape of and area under the σ-ε curve, etc. can be obtained. Linear elastic behavior can be described by the general Hooke's law

$$\sigma = E\varepsilon \qquad [4.1]$$

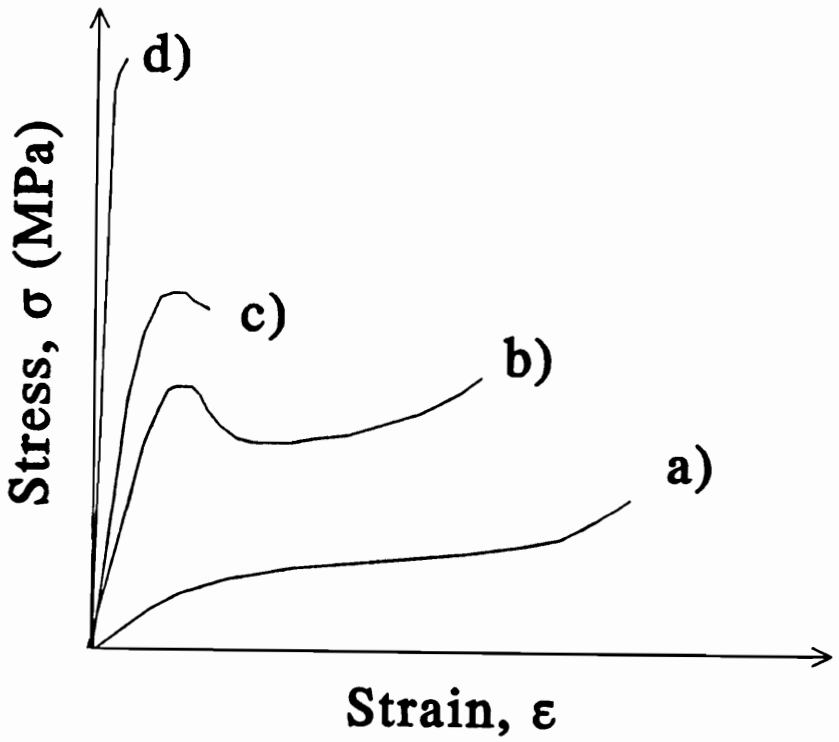

Figure 37. Examples of Possible Stress - Strain Relations of Polymeric Solids: rubber like (a), cold drawing (b), ductile failure (c), brittle failure (d); after [66]

where the modulus E is the proportionality factor between the applied stress and the strain response. In general, most polymers only obey eq. 4.1 in the limits of very small deformations. Beyond this point the strain response is very often non-linear, and at larger strains permanent deformations take place. In the most general sense stress-strain, or load-deformation curves of polymers can be classified as (Figure 37) [66]

a. rubber like
b. cold drawing
c. ductile failure
d. brittle failure

Rubber like behavior is characterized by small moduli, very large strains, the absence of a yield point, sudden increase of the modulus before failure, and by the recoverability of deformations up to high extensions. Cold drawing type $\sigma - \varepsilon$ response can be recognized by an initial linear elastic portion followed by a nonlinear response, giving way to a more or less intense yield point where geometric deformations (necking) become unrecoverable. The final flow region is terminated by a modulus increase due to strain hardening and failure. The ductile failure type is very similar to the foregoing one, however, without apparent flow. The material fails at the yield point or shortly thereafter. Brittle failure occurs in high modulus materials which do not undergo permanent deformation before failure. Polymers which exhibit this type of response can be excellent, high strength materials. However, very often it is desirable to reduce the initial modulus in order to increase ductility. The relative area under the stress-strain curve can be taken as a preliminary measure of a material's toughness, or its ability to absorb mechanical energy.

During tensile deformation the cross-sectional area reduces which gives rise to an underestimation of the true stress, σ_t, by the engineering stress σ_e which is calculated as the load divided by the initial cross-section A_0. For materials with a Poison's ratio, $\nu = 0.5$, i.e. iso-volume deformations, the true stress changes continuously with strain as

$$\sigma_t = \sigma_e(1 + \varepsilon) \qquad [4.2]$$

Whenever possible true stress values will be reported within this study.

4.2.1.2 Stress-Strain Relations of Lignin Containing Networks

The challenge of incorporating lignins into chemical networks is to find a balance between optimum mechanical performance and a maximum amount of lignin used. Lignin by itself is a very brittle material with moduli in the order of 2 MPa [72]. However, depending on the type and extent of modification, lignin based networks can assume all of the in Figure 37 outlined mechanical response types [8]. Replacing lignin's hydroxyl groups with one unit of propylene oxide (PO) and its subsequent cross-linking alleviates the extreme brittleness of pure lignin but still produces glassy, high modulus thermosets. Moduli ranging from 1.5 to 2.1 MPa have been reported by Saraf and Glasser [73] for MDI and HDI based lignin polyurethane films. The introduction of aromatic cross-links with TDI generally led to higher E values, but cross-link density did not seem to influence the modulus. Ultimate strain values ranged from 2 to 14% depending on the NCO : OH ratio. Surprisingly, a trend to higher elongations with increasing feed ratio was reported. Nieh [74] made DETA cross-linked hydroxy propyl lignin (HPL) epoxide networks which also exhibit a brittle fracture type of stress-strain response. However, the Young's modulus was with 191 MPa about ten times lower than that of the HPL PU networks. Ultimate strain and maximum stress were 9% and 14.6 MPa, respectively.

Lignin's brittleness is a major drawback for such applications as wood adhesives. However, modification of lignin very often improves mechanical performance. Tai et al. [75] for instance reported that the shearing strength of wood bonding lignin epoxides doubled once the lignin has been phenolated, rather than used unmodified. Ayla and Nimz [76] reported that blending lignin with carbohydrates improves significantly the shearing strengths of wood composites made from spent sulfite liquor lignin. Thus, lignin based networks need a certain addition of "soft" materials either

as blends, plasticizers, or copolymer segments. For example, Saraf and co-workers [77,78] co-reacted HPL's and glycols with isocyanates. Using poly(ethylene glycol) (PEG) of molecular weights ranging from 400 to 4 000 in amounts of 0 to 18% yielded uniform networks. Higher PEG 400 concentrations in HDI based PU films resulted in a reduction of modulus and σ_{max} by simultaneous increasing ε_{max}. The Young's modulus also dropped in general with increase of PEG's molecular weight. The same process carried out with poly(butadiene glycol) (PBDG) as soft segment yielded phase separated, "filled" thermosets. Modulus and maximum stress dropped continuously with increasing PBDG amounts from 1670 to 36 MPa, but σ_{max} increased at high glycol contents. Nieh [74] co-reacted amine terminated poly(butadiene-*co*-acrylonitrile) (ATBN) and HPL epoxides with DETA and was able to produce networks ranging from elastomeric (75% ATBN) to ductile (5-15% ATBN) performance. Unfortunately, the absolute values of σ_{max} were with 5-10 MPa rather low. Kelley et al. [79] reviewed the effect of soft segment content on the properties of lignin based polyurethanes. Chain extension of lignins with ethylene or propylene oxides produces copolymers which already have incorporated the soft segment so that potential pre-gel phase separation during cross-linking are not a problem. The general observation was that the modulus of elasticity decreased with extent of chain extension, although the type of isocyanate used as cross-linker plays also a very important role. Also ε_{max} increased and it was possible to produce elastomeric lignin containing thermosets without resorting to co-reactants or fillers. This approach in connection with copolymer fractionation were recognized as most potential route to produce tailored networks with relative high lignin contents to meet a variety of mechanical performance requirements.

4.2.2 Materials

Networks from chain extended and fractionated lignin epoxides with *m*PDA as cross-linking agent were prepared as described in Ch. 3.2.1.1. Two fractionated chain extended steam explosion lignins (LX1204, LX2404) and one hydroxyethylated unfractionated organosolv lignin (LX0013) were used

for the investigation of mechanical performances. Copolymerization of the steam explosion lignins with propylene and ethylene oxide, epoxidation, and fractionation are described in Ch. 2.2.1.1, Ch. 2.2.1.2, and Ch. 2.2.1.3, respectively. The analytical results are compiled in Table 2 and Table 3.

4.2.2.1 Sample Preparation

All systems listed in Table 3 with the exception of LX2404A1, were prepared as solution cast films for mechanical testing. Due to the necessary longer exposure of the resin-amine blends to room temperature during film drying partial reaction could not be avoided; it was even considered beneficial since it allowed to use the essential liquid resins, LX1204A1 and LX0013 to be handled as sticky but stable solid films. LX2404A1 was too fluid too be processed this way. The films were prepared by dissolving the pre-weighed epoxy in CH_2Cl_2 (~ 20% w/v). The tars were easily dissolved, but it needed 24hrs and slight warming of the solvent to dissolve the high molecular weight LX1204A3 (~ 5% w/v). The stoichiometric amount of *m*PDA was added as THF solution (1 *g/ml*) since methylene chloride is not a good solvent for it. On the other hand, CH_2Cl_2 was chosen as casting solvent over THF since it was found during test casting that it produced more uniform films. However, no survey of other solvents for the purpose of film casting was conducted. After thorough mixing the films were cast and the remainder of the solution was stored at -70°C. The casting molds were composed of a glass plate covered with a thin teflon film. A teflon ring of 10 *cm* diameter and a height of 0.5*cm* was clamped onto the plate and served as container for the casting liquid. 20*ml* of solution were filled into the molds which were subsequently covered with aluminum foil. Left in the hood until dry (for at least 24 hours) the films were transferred to a desiccator and dried under vacuum at room temperature for more 24 hrs and subsequently stored at -20°C. Five dogbone specimens were dye-cut with a Brockton Cutting dye (Model D-638-5) for each sample.

In addition to the film cast and dye cut samples, the two low molecular weight fractions LX1204A1 and LX2404A1, as well as LX0013 and the control EPON826 were prepared by casting the liquid resin without the aid of a solvent into dogbone shaped, silicon rubber molds.

The dogbone shaped samples, either as dye-cut or moldcast specimens were tested on a miniature stress-strain materials tester ("Minimat") manufactured by Polymer Laboratories. Measurements were carried out at room temperature and the rate of deformation was $0.25mm/$ min. Load and deformation data were transmitted to a personal computer and could be redrawn as stress vs. strain, load vs. deformation, or modulus vs. strain curves.

4.2.3 Tensile Properties

Results of the uniaxial tensile stress-strain are compiled in Table 9. Except for the extremely weak sample LX2404A1, the values of σ_{max} and E_{max} are in the order or even surpass the respective numbers of the high cross-link density DGEBA based network. A general trend to stronger and stiffer materials can be observed with increasing lignin content, while simultaneously the ultimate extensions do decrease. Thus, in terms of ultimate stress, the epoxide networks of lignin-PPO copolymers are in the same league as the respective fractionated polyurethane films [7]. However, the PU's were slightly stiffer and showed less extensibility. The stiffest specimens came from the network which was made from the unfractionated hydroxyethylated organosolv lignin, LX0013. With a strength of nearly $42MPa$ and an elongation of 6% this sample combines high stiffness with good strengths at a lignin content of 57%. Of practical importance is that the organosolv lignin (Allcell™) copolymer has low molecular weight ($M_n \sim 1\,200$) which makes it a liquid at room temperature. But unlike the liquid low lignin content fractions, this high lignin content material can be cross-linked to become a high T_g, glassy material.

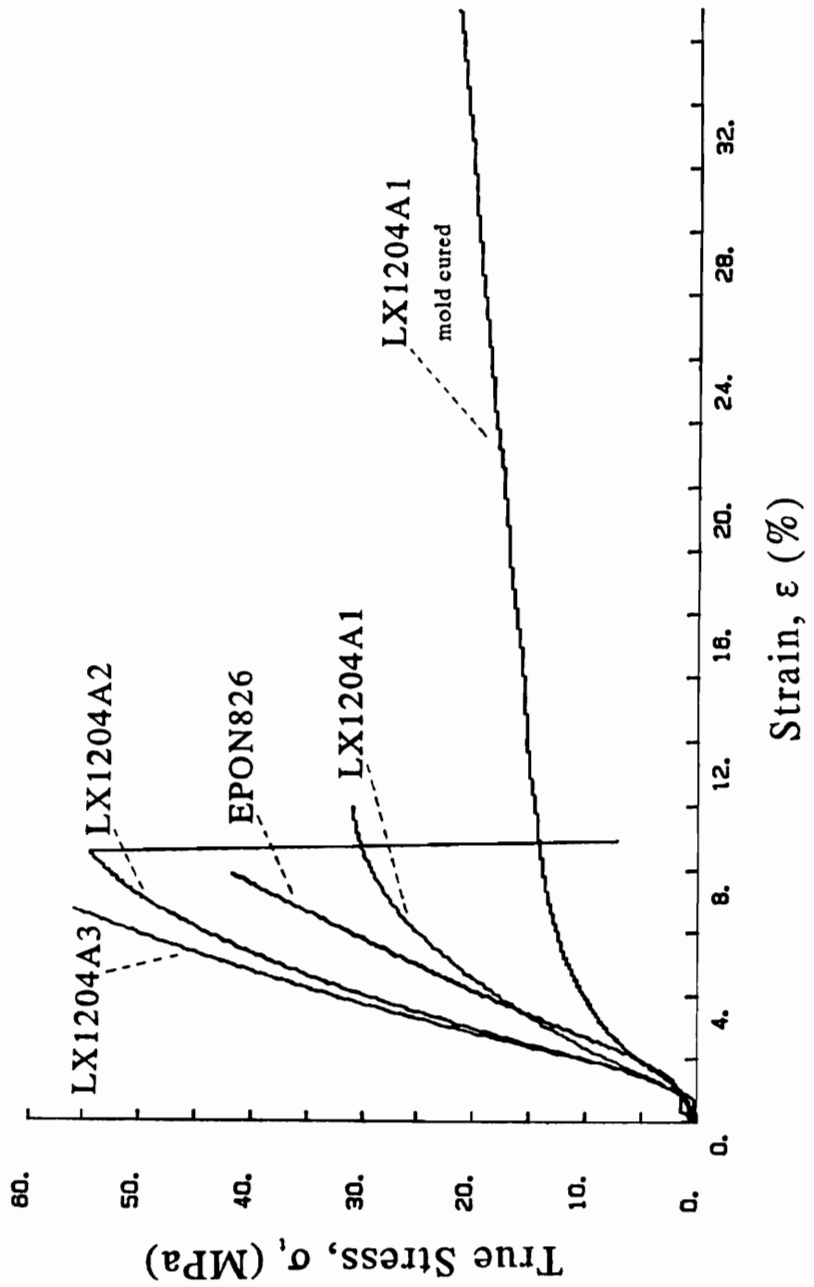

Figure 38. Tensile Stress Strain Plots of LX1204 Fractions and EPON 826, Cross-linked with mPDA

Table 9. Tensile Strength and Modulus of Lignin-Poly(propylene Oxide) Copolymer Based Networks

Sample	Prep.	σ_{max} (Mpa)	ε_{max} (%)	E_{max} (MPa)	M_n of copolymer ($\times 10^3$)	Lignin content (%)
LX1204A1	mold[1]	21.8	37	274	0.63	16
	film[2]	30.9	9.8	441		
LX1204A2	film	55.2	8.4	732	1.9	37
LX1204A3	film	56.9	6.1	917	93.8	42
LX2404A1	mold	4.5	16.2	77.8	0.8	21
LX2404A2	film	41.7	13.3	661	5.5	39
LX0013	mold	41.7	6.13	1012	1.2	57
DGEBA	mold	31.5	6.2	499		

[1]lignin copolymer epoxides and crosslinking agent (mPDA) were mixed in neat form and cured in dogbone shaped silicon rubber mold
[2]lignin copolymer epoxides and crosslinking agent (mPDA) were mixed in solution and film cast, test specimens were cut with a dog bone shaped Brokton Cutting Dye (Model D-638-5)
[3]EPON 826

Figure 38 gives examples of the stress-strain curves of the LX1204 film cured fractions. The high lignin content specimen LX1204A3 and the EPON826 networks could be described as brittle failure types, while both, the medium and the low lignin content film cured fractions exhibit ductile failure behavior. However, the mold cured sample LX1204A1 undergoes nearly cold drawing with a four times longer elongation than its solution cast and film cured counterpart. Both, the film and mold cured samples LX1204A1 were subjected to the same curing schedules, however the mold cast material was left in the silicon rubber mold during the entire cure cycle. Possible contamination by diffusion of small molecules from the mold into the epoxide could have caused the distinctly higher plasticity. On the other hand no such effect was observed for the mold cured LX0013 and EPON826 samples.

An attempt was made to correlate the so determined data to compositional parameters such as molecular weight and lignin content. Both, the maximum stresses and moduli are positively correlated with lignin content and molecular weight of the copolymer (Figure 39 and Figure 40), while a general trend to reduced elongations at break were observed. Except for the very weak sample LX2404A1, the moduli of all samples are a linear function of lignin content with an intercept of 0 and a slope of $1842 MPa$ (Figure 39, $R^2 = 0.904$). Extrapolated to 100% lignin the modulus is only slightly below the $2 MPa$ reported by Falkehag for pure lignin [72]. This also agrees to a certain extent with the results Kelley et al. [13] obtained from tensile testing of polyurethane networks prepared from fractionated lignin-PPO copolymers. However, he found that the logarithm of the moduli were a linear function of lignin content, i.e., the aromaticity of the networks. The apparent dependance of the mechanical data on molecular weight of the copolymers is believed to be coincidental since higher lignin containing fractions simultaneously have higher molecular weights.

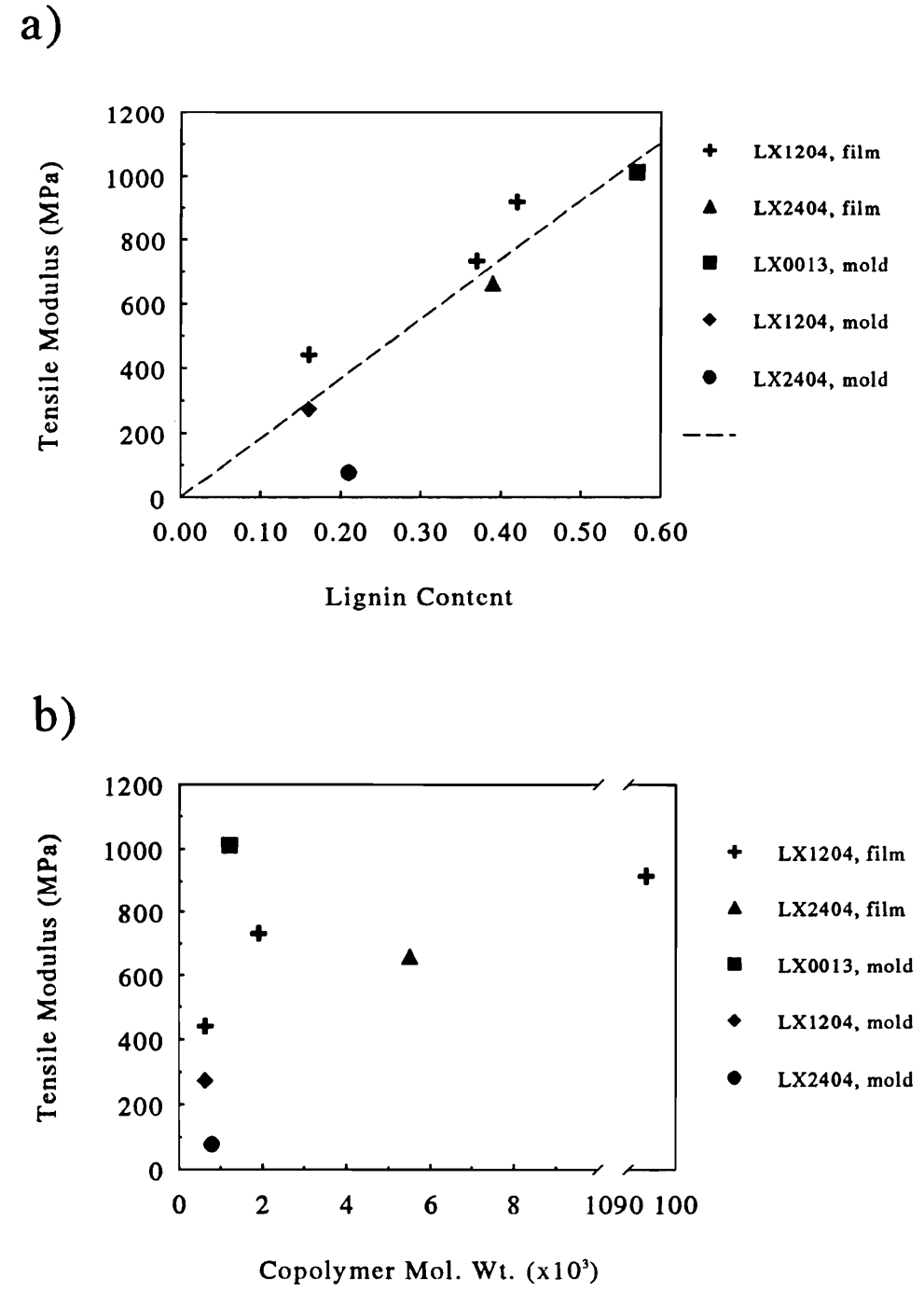

Figure 39. Tensile Modulus of LX1204 and LX2404 Based Networks: Function of lignin content (a), and copolymer molecular weight (b)

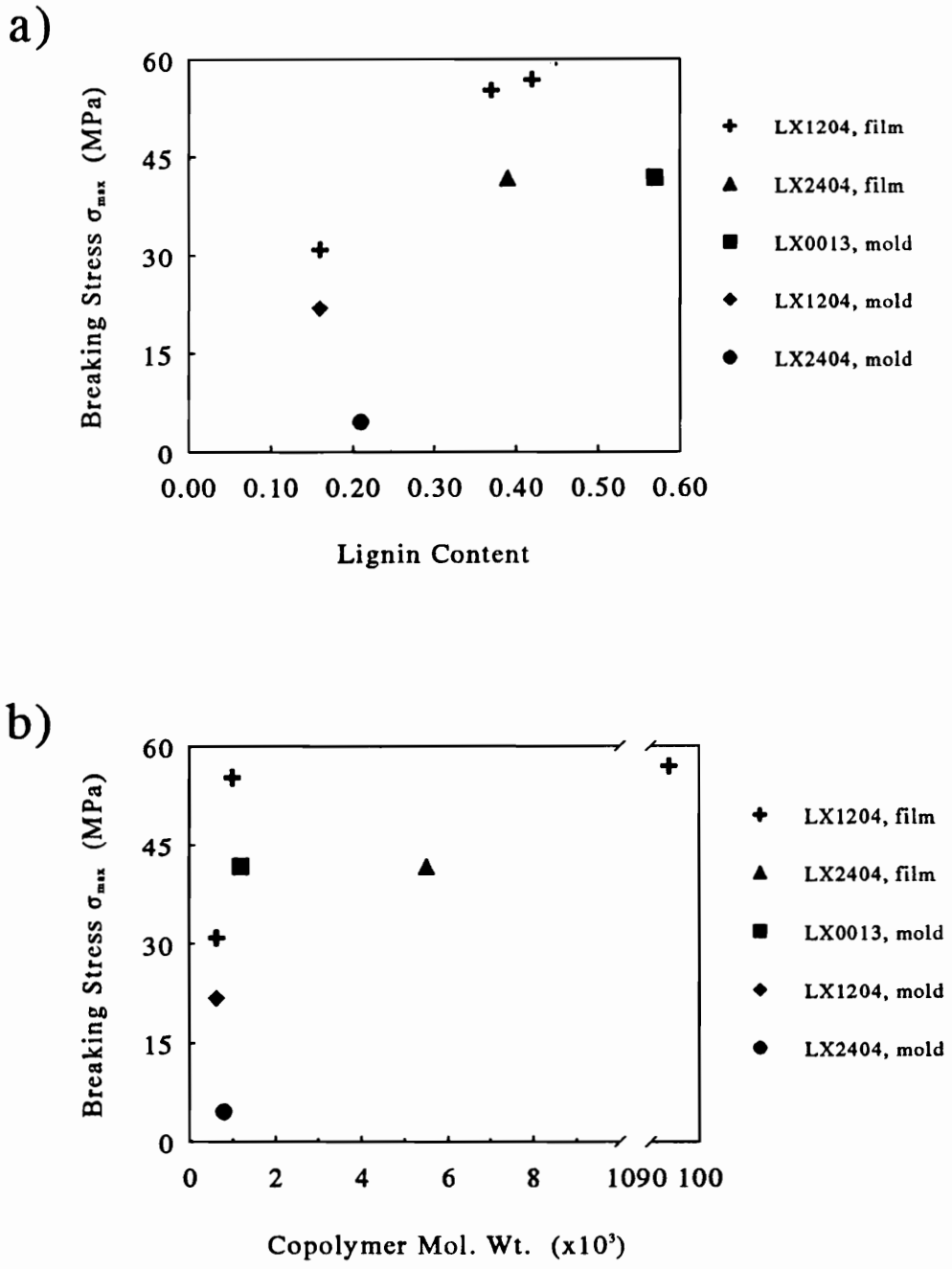

Figure 40. Maximum Stress of LX1204 and LX2404 Based Networks: Function of lignin content (a), and copolymer molecular weight (b)

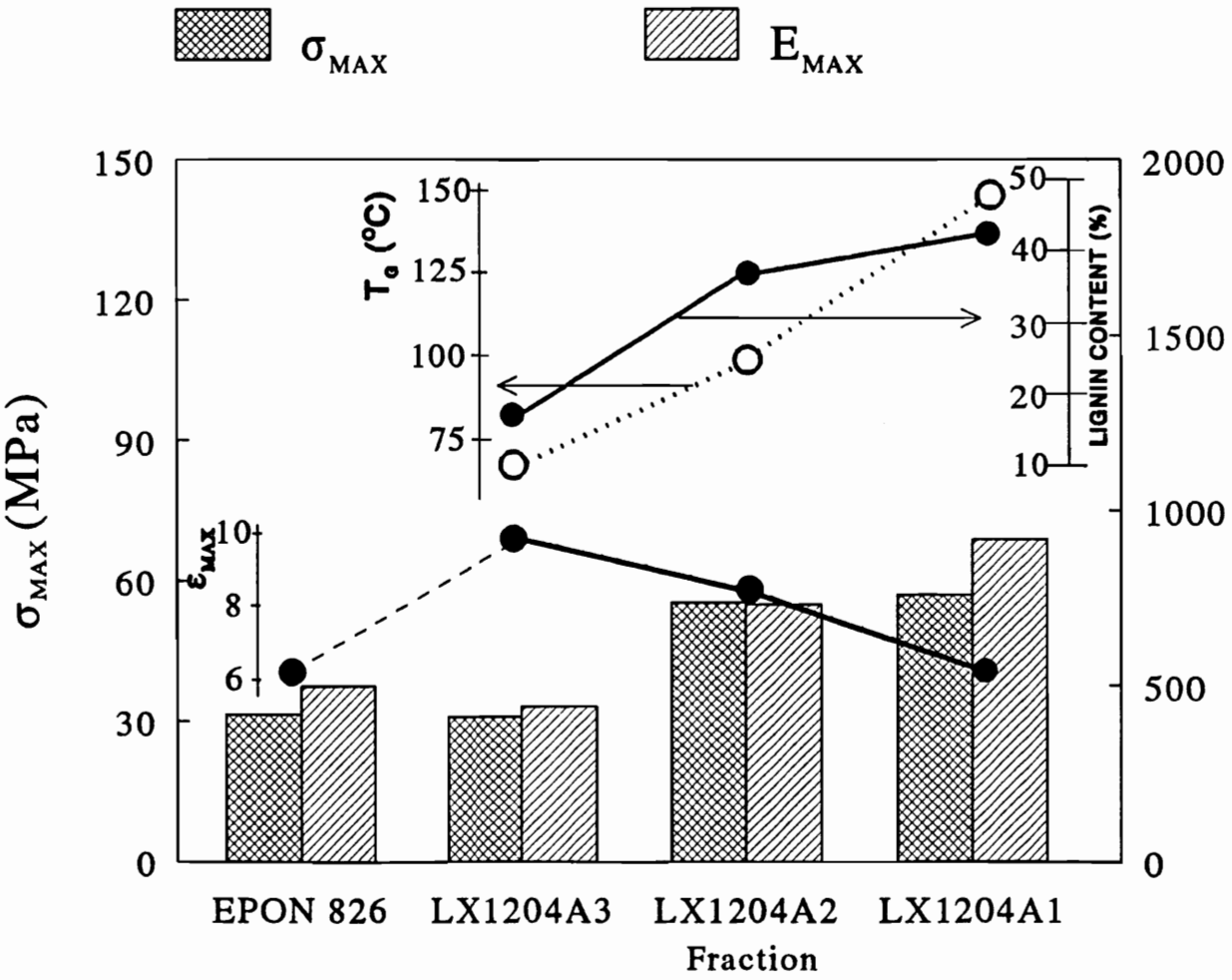

Figure 41. Comparison of LX1204 and DGEBA Networks with Respect to Tensile Strength, Modulus, and Glass Transition Temperature

4.2.4 Summary

Epoxy-amine networks which contain up to 57% lignin exhibit tensile strengths and moduli which are in the order of those of a commercial DGEBA-*m*PDA network. Independent of molecular weight of the prepolymers, a clear linear trend of modulus increase with lignin content was observed for all samples and fractions. This is a manifestation of the simultaneous increase of aromaticity of the network with lignin content. Furthermore, the maximum stresses show a positive trend with lignin content, while the elongation at break usually decline.

An illustration of these relationships as well as a comparison of the mechanical performance of the film cured LX1204 fractions can be seen in Figure 41. σ_{max} and E_{max} of the three fractions are contrasted in the bar chart with the respective numbers of the EPON826 network. Additionally, the change of ε_{max} is documented by the line graph above the bars. The inserted comparison of lignin content and glass transition temperature for the three fractions furthermore exemplifies the observed trend to stiffer and stronger materials having higher glass transition temperatures with increasing lignin content (see also Ch. 4.3.4.1).

The use of low molecular weight, high lignin content and unfractionated lignin epoxides has shown considerable promise since these materials can be handled as liquid prepolymers without the use of solvents, but on the other hand yield very stiff and strong thermosets of high glass transition temperatures. In fact the T_g gain of the low molecular weight and unfractionated hydroxyethyl organosolv lignin epoxides during cross-linking is higher than 130°C.

4.3 Viscoelastic Properties and Morphology of Lignin Based Epoxy Resins

4.3.1 Introduction

The analysis of cure kinetics of lignin epoxide - amine systems (see Ch. 3) raised questions about the morphology of the networks at conversions where the reaction becomes diffusion controlled. The extent of conversion where vitrification happens is a function of the lignin content of the fraction. Samples with higher lignin content experience a cessation at lower extents of conversion. Furthermore, it has been observed that the onset of diffusion control happens before the glass transition temperature rises due to the level of the cure temperature. Together with the finding that the range of the glass transition is unusually broad, these results indicate that the lignin containing networks have density heterogeneities. The interconnected rigid lignin centers form a dense network in which the flexible poly(propylene oxide) chains which carry the reactive functionalities, experience mobility constraints. Further clarification of the nature of the network heterogeneities was expected from the measurements of the energy dissipation properties at different frequencies, and from transmission electron microscopy.

4.3.2 Energy Dissipation and Damping Ability of Materials

A practical consequence of network heterogeneities and broad glass transitions is that such materials have good potential as damping materials. In the last years considerable interest has been shown for the use of polymers as damping materials for noise and mechanically transmitted vibrations [20]. Increasing awareness of the dangers of noise pollution and the destructive nature of unchecked vi-

brations has led to research on how materials absorb energy. Two streams of investigations have developed; one is concerned with the geometry and the structural application of damping materials while the other area deals with the assessment of the damping features of specific materials and its relation to chemistry, molecular architecture and morphology [1]. This section is partially concerned with the latter and describes the energy absorption properties of lignin based epoxy resins as a function of frequency and temperature, copolymer composition and molecular weight. Of special interest was the question whether lignin and poly(propylene oxide) form a homogeneous network or a certain amount of phase segregation occurs during the curing reaction.

Energy dissipation of materials is based on the ability to transform mechanical energy into heat due to resonance conditions between molecular features and the supplied energy. Since dissipation of energy is directly proportional to the value of the loss modulus E'' [67], polymers which have mechanical loss spectra exhibiting broad E'' maxima make good damping materials. Lignin has a multitude of molecular entities which can be excited by a range of vibrations, thereby broadening the frequency range over which resonance conditions can occur. However, the available free volume of pure lignin is too small to allow for sufficient molecular mobility at room temperature. Copolymerization with low T_g aliphatic polyethers increases lignin's available free volume by internal plasticization. But not only lignin's inherent molecular makeup could be beneficial for damping purposes, but also possible "interfacial heterogeneity" [1] might increase the frequency range over which the loss modulus is sufficiently high. As it was observed in Ch. 3, the premature slowing of the curing reaction prior to reaching the theoretical level of diffusion controlled kinetics where $T_g = T_C$ also suggests the formation of domain structures which immobilize the flexible reactant carrying polyether chains.

4.3.2.1 Time-Temperature-Superposition-Principle

The continuous measurement of a polymer's thermomechanical spectrum over a wider range of frequencies is often very difficult or impossible. Nevertheless, it is possible to make multiple

isothermal measurements of E'' and E' at a limited number of frequencies and to make use of the time-temperature-superposition-principle (TTSP) [2,16,25,66,67]. Although this treatment is only suitable for rheologically simple materials, i.e. for homopolymers or homogeneous copolymers in the absence of chemical or physical changes, an attempt was made to assess its applicability to lignin-PPO networks.

Amorphous polymers, cross-linked or thermoplastic, exhibit a temperature dependent energy absorption spectrum, which is more pronounced than that of non-polymeric materials. In general a maximum of absorption can be detected which resides in the glass transition zone of the polymer. This coincides with the onset of thermally induced cooperative motion of the polymer chains. At this temperature, usually termed glass transition temperature, T_g, the molecules are in resonance with the externally applied force field and therefore show a maximum energy absorption. The storage modulus, E', has dropped from its "glassy" to an intermediate value, and the loss modulus, E'', is at its maximum. Very often the glass transition temperature is referred to as the temperature where $\tan\delta$ passes through a maximum. Since $\tan\delta = \frac{E''}{E'}$ and E' is a continuously decreasing function of temperature, the $\tan\delta$ maximum is at a higher temperature than the E'' maximum. The application of a higher or lower frequency typically shifts the peak to lower or higher temperatures, respectively. It is therefore obvious that the use temperature has considerable influence on the frequency bands at which energy absorption is at its optimum. A practical consequence for instance, is that a sufficiently dampened machinery becomes loud once the temperature drops or increases beyond certain limits.

This relationship between frequency (or time) and temperature has been analytically described by Watts, Landel and Ferry (WLF) by the time-temperature-superposition principle (TTSP) [2]. Basically, this theory states that to a certain extent temperature changes can be compensated for by a change of the rate (frequency, time) of applied load. The WLF equation (eq. 4.3) describes how much one has to change the frequency (or time) in order to maintain the same value of time and temperature dependent properties (eg. E', E'', ..) once the temperature has changed. For rheologically simple materials, the logarithmic shift factor $\log a_T$ is the amount of the necessary

horizontal shift on the logarithmic frequency or time axis when the temperature changes from T_0 to T_1 and can be calculated as follows:

$$\log a_T = \frac{C_1(T_1 - T_0)}{C_2 + (T_1 - T_0)} \qquad [4.3]$$

where C_1 and C_2 are empirically determined constants which are conceptually linked to the free volume theory [2,66,67]. For amorphous homopolymers, and in the case of $T_0 = T_g$, C_1 and C_2 assume very often the values of 17.4 and 56.4, respectively. This equation also applies to other time and temperature dependent properties of polymers.

The practical importance of the TTSP is that it allows one, in certain cases, to make predictions about the change of time dependent parameters which lie beyond the possible measurement limits, either elapsed time or frequency ν. Data, such as $\log E'$ obtained over a range of temperature for a limited number of frequencies (Figure 42, a) can be re-plotted as isothermal functions of $\log \nu$ (Figure 42, b) and then shifted horizontally on the frequency axis so that they partially overlap. The so established "master curve" (Figure 42, c) of a polymer describes the desired properties at constant temperature over a wider range of "reduced frequency" ($\log a_T \nu$). The manually determined shift factors $\log a_T$ can be plotted against $T - T_0$ (Figure 42, d) from which C_1 and C_2 can be determined according to eq. 4.3.

Over a limited range of frequencies, the shift factor a_T obeys an Arrhenius relationship of the form

$$\ln a_T = \frac{\ln \nu_1}{\ln \nu_2} = \ln A + \frac{E_A}{RT} \qquad [4.4]$$

which is based on the theory that molecular segments have to overcome an energy barrier in order to change isomeric states [66]. Thus the frequency of change is a function of temperature and an activation energy which in turn controls the resonance conditions for externally applied vibrations. It is therefore possible to determine the activation energy of thermal transitions from the slope of a plot of the natural logarithm of the applied frequency versus the inverse peak temperature of the

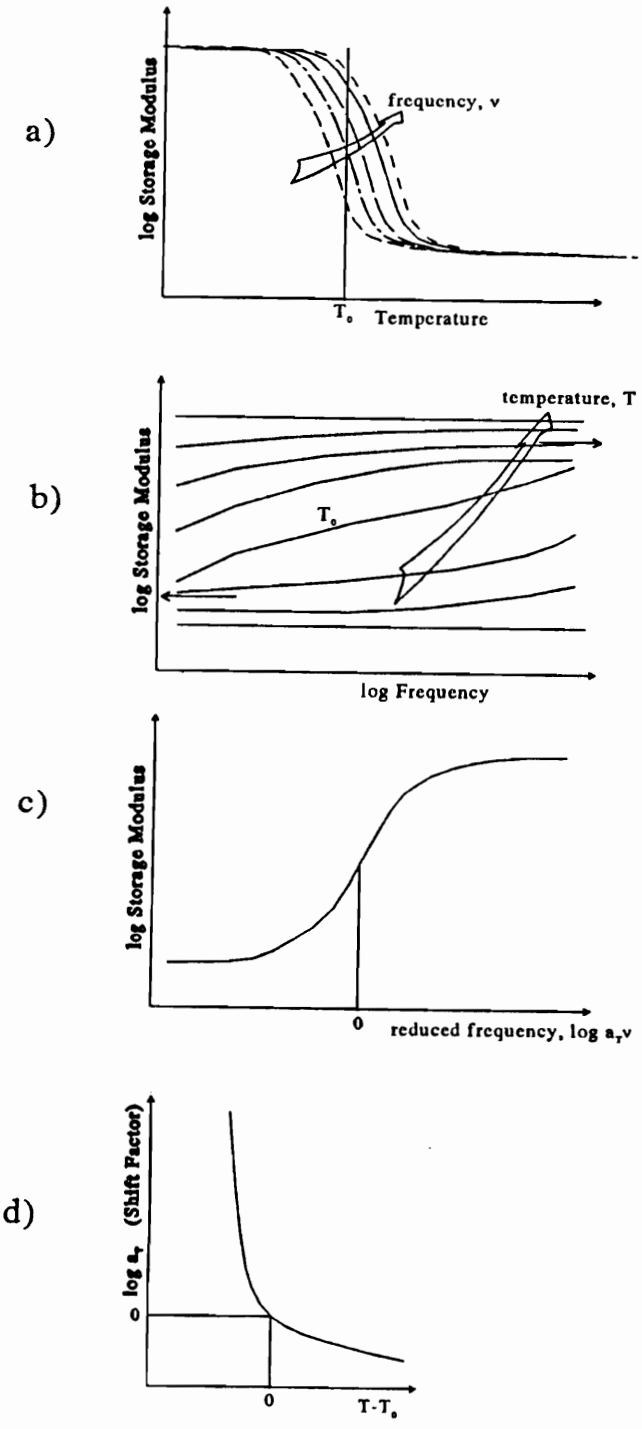

Figure 42. Schematic Construction Master Curves (log E′ vs. log reduced Frequency): a) isothermal moduli, b) iso frequency moduli, c) master curve, d) shiftplot

transition. Although the activation energy is not necessarily constant over a wider range of frequency, it can give a quick assessment of a polymer's or network's frequency dependence of their glass transition temperature. For instance, a high activation energy not only means that relatively small changes of temperature vastly change the resonance frequency at the glass transition, but is also a sign of a high energy barrier to segmental motion within a polymer or network. Furthermore, the area under the loss modulus peak which is a measure of the damping ability of the material is a function of the activation energy according to this semi-empirical expression of the damping ability [3,21]:

$$A_{E''} = \int_{T_g}^{T_r} E'' dT = (E'_g - E'_r) \frac{RT_g}{E_A} \qquad [4.5]$$

where E'_g and E'_r are the storage moduli in the glassy and rubbery region, respectively. Thus one criterion for a good damping material is a polymer having a low activation energy. Based on the principle of group contribution analysis [63] it has been shown that the damping area of a copolymer system is the sum of the individual homopolymer contributions [4,9].

4.3.2.2 Glass Transition Temperature of Cross-linked Star-like Copolymers

It has been shown that lignin-poly(propylene oxide) copolymers have a single glass transition which was described as an indication of miscibility of the copolymer segments, especially since the peak temperatures obeyed the Gordon-Taylor equation [7]. Also the polyurethane networks made from these copolymers show a single T_g indicating continuous miscibility through the curing reaction. Kelley et al. [13] showed also that for a range of polyurethane networks made from chain extended lignins the glass transition temperature is a linear function of the lignin content, i.e. of the aromaticity of the network. However, the PU networks were made from unfractionated copolymers and had sol fractions as high as 50%. Nevertheless, similar results were expected from the respective epoxy networks.

Glass transition temperature in multi-phasic networks is a multi-dependent variable [69]. Firstly, as for homogenous networks, the T_g is a function of the cross-link density, i.e. of the inverse average molecular weight between cross-links, $\overline{M}_c$. Nielsen [40] reported that a rough estimation of ΔT_g the difference between $T_{g,0}$ and $T_{g,x}$, the glass transition temperatures of the uncross-linked and cross-linked polymer, respectively, is possible by

$$\Delta T_g = T_{g,x} - T_{g,0} = \frac{3.9 \times 10^4}{\overline{M}_c} \qquad [4.6]$$

Shorter distances between cross-links reduce the mobility of the network constituents and therefore lead to an increase of T_g and of the equilibrium modulus. The DiBenedetto equation [52] (Eq. 3.2.1) which relates a network's glass transition to its extent of conversion is conceptually also based on the reduction of mobility due to the decrease in $\overline{M}_c$ during the curing reaction. In turn, the loss of mobility is related to the decline of free volume [2]. $\overline{M}_c$ can be determined by measurements of the equilibrium modulus [68] as it has been performed for a DGEBA/*m*PDA network in Ch. 3.1.3 or by application of the Flory-Rehner theory by measuring the swelling of homogeneous networks [14]. But $T_{g,x}$ is also effected by the introduction of cross-links by a third material. Especially if the cross-linking agents are relatively large this could amount to a significant secondary copolymer effect.

Secondly, the glass transition temperature $T_{g,0}$ of the copolymers is a function of the individual T_g contributions. In uncross-linked polymers this inter-relationship is expressed by the Gordon-Taylor [7,56] theory which manifests itself primarily in the value of $T_{g,0}$. Furthermore, $T_{g,0}$ is a function of copolymer molecular weight due to the influence of the relative amount of chain ends.

And thirdly, cross-linking of copolymers is often accompanied by a certain degree of phase separation and molecular regrouping. This can affect the level of internal plasticization which in turn will change $T_{g,0}$ during cross-linking and therefore alter ΔT_g. Combining these effects analytically by modifying a network model originally proposed by Chan et al. [65], yields the following expression

$$T_{g,x} - T_{g,0} = \Delta T_g = \Delta_x T_g + \Delta_c T_g + f(x) \qquad [4.7]$$

where $\Delta_x T_g$ is the rise of the glass transition temperature due to the decrease of $\overline{M}_c$ and $\Delta_c T_g$ is due to the secondary copolymer (i.e. the introduction of cross-linking agents) effect. The function $f(x)$ includes the influences of morphological changes during cross-linking on $T_{g,0}$, such as partial phase separation. In the case of the lignin-PPO copolymers, $f(x)$ would incorporate a possible demixing of lignin and PPO during cross-linking, which increases the potential glass transition temperature of the uncross-linked copolymer. However, physical aging of the cured material which is stored at temperatures below T_C has an effect on $T_{g,x}$ as has been shown by Plazek and Frund [83]. Samples stored at 37°C below the fictive temperature, T_{fg} of the thermosetting system (Epon828-MDA) showed spontaneous densification upon storage. Physical aging effects can be avoided by conditioning the samples above their T_g, which is not feasible for partially cured systems or by quenching the specimens after the predetermined cure time has elapsed and by immediate measurement of the T_g Nevertheless, aging effects during isothermal cure become important once the system has vitrified. This can be usually detected by a positive enthalpy peak upon heating.

In the case of lignin-PPO copolymer networks, whether as PU or epoxide, the aliphatic polyether arms are terminated by the functional group and, thus, connect the lignin cores with each other via the cross-links. Hence, these arms not only are major contributors to $\overline{M}_c$, but also lead to an increase of free volume within the lignin entities. Both effects work in the same direction, and thus, an increase of PPO content depresses $T_{g,0}$, the glass transition of the uncross-linked copolymer. Additionally, this conformational picture distinguishes networks, formed from lignin-PPO stars from those based on low molecular weight linear, bifunctional molecules with multifunctional cross-linkers. In the latter case, a large ΔT_g can be achieved with the ultimate $\overline{M}_c$ being close to the molecular weight of the precursor. The situation for copolymer stars is more complicated. Since lignin has a high T_g, and since the oxirane rings are attached to the flexible arms, a network would have two types of cross-links: one is the relative large lignin center and the other the smaller amine backbone. In this case, $\overline{M}_c$ would be a strong function of the polyether arm length. Thus, it was

expected that $T_{g,0}$ is a function of lignin content and molecular weight, $\Delta_x T_g$ a function of the arm length, and $f(x)$ depends on the degree of demixing during cross-linking which in turn might be a function of copolymer composition and molecular weight. Hence all factors influence $T_{g,x}$, the glass transition temperature of the cross-linked lignin-PPO copolymers.

4.3.2.3 Glass Transition and Morphology

In general the breadth of the transition region of homopolymers is rather small covering only about 30-50 degrees. Taking into account temperature changes during use it is evident that such materials are not very much suited for damping applications. Some methods are available to broaden the damping area of which the most important are co-polymerization and the formation of interpenetrating networks (IPNs) [22,23]. Both methods allow for the formation of materials with broad transition regions especially when a certain amount of "interfacial micro-phase separation" is possible. A domain size of 10 to 20*nm* has been found to be beneficial [1]. The energy dissipation range of certain micro-phase separated polyurethane networks consisting of soft and hard phases covers more than 10 decades of frequency [5,9]. IPNs have been formed from semicompatible epoxy-urethane blends achieving broad transition regions [6,17]. However, the trade-off was that in some cases the transition was shifted out of the desired temperature range and/or the material performed poorly under mechanical load. By selective application of "soft" and "hard" segments either as copolymer or as IPN, one can achieve the necessary phase separation and the desirable broad transition region. However, very often a necessary trade-off of increasing the frequency range of the glass transition is the reduction of the maximum tanδ value which is directly proportional to the acoustic damping as

$$\alpha\lambda = 8.686\pi \tan\delta \qquad [4.8]$$

where $\alpha\lambda$ is the absorption per wavelength in dB [2].

Lignin-poly(propylene oxide) copolymers can be regarded as star-like macromers [19] where the lignin constitutes the hard, rigid center and the poly(propylene oxide) chains are the soft, flexible arm segments. Kelley et al. have shown that polyurethane networks based on fractionated hydroxypropyl lignin exhibit an increase in temperature range of energy dissipation when lignins with higher molecular weights [7], and higher lignin content [13], were incorporated into the network. This phenomenon was contributed to the relative increase of chemical features such as functionality, inter unit bonds, and reactive sites on the lignin molecule which "increase the complexity of molecular events as the polymer passes through T_g" [8]. However, rather than purely the result of intra-phase heterogeneity it could be possible that lignin and its poly(propylene oxide) side chains partially disassociate. As has been pointed out by Sperling [1], micro-phase separated domain sizes in the order of 10 to 20*nm* do increase the breadth of the damping transition. He called this "interfacial phase separation" between the immiscible network components of an IPN, however, without specifying this assumption further. If lignin and poly(propylene oxide) were to phase separate it would be expected that this happens preferably in networks with higher molecular weight lignins. Nevertheless, no phase separation has been reported yet for this system [8].

4.3.2.4 Transmission Electron Microscopy of Lignin-Polyether Networks

It has been reasoned that the considerable width of the damping transition region might be due to micro scale phase separation in the order of 10-30*nm* [1]. However, this broadening can also be attributed to "molecular heterogeneity" [8] without exhibiting the characteristics of classical micro-phase separation. The theory of micro-phase separation of uncross-linked di- or tri-block copolymer predicts the formation of lamellar, tubular, and spherical domain structures depending on the molecular weight [10,27] and polydispersity [28]. No theory has been developed yet for starlike block copolymers. Styrene-isoprene starlike polymer have been prepared and show very distinct phase separation pattern [26]. However, the styrene arm molecular weight was with 71 000 Daltons not comparable with the star like lignin polyether copolymer structure [19] where the av-

erage arm length ranges from 200 to 300 Daltons. Besides incompatibility, certain phase separations in the form of microgels can take place in curing homogeneous thermosetting resins due to heterogeneous cross-linking dynamics [11]. In certain cases these microgel nodules can be detected by light scattering techniques [12]. The rate of micro-phase separation during cure is not necessarily effected by gelation as it is the case for macro-phase separation since the rate of inter-network diffusion is continuous prior and past the gelpoint. Transmission electron microscopy has been shown to also give insight into the domain structure of micro-phase separated copolymer systems [15]. Samples are normally prepared as either ultra thin film deposited onto a non solvent, or as ultra thin microtomed solids. If the electron density difference is sufficient, TEM can directly yield images of the domain configuration. In many cases however, preferential staining of one phase is required to achieve enough phase contrast. Vapor staining with osmium tetroxide or ruthenium tetroxide [28] have been proven to preferentially oxidize segments containing double bonds and aromatic structures. RuO_4 is more powerful than OsO_4 allowing for very brief staining times [58].

4.3.3 Materials and Methods

Four samples of lignin-poly(propylene oxide) copolymers were epoxidized for this study whereby two, LX1512 and LX4003 were fractionated and two samples, LX0513 and LX3010, were left unfractionated (see Table 10). In addition, also the LX1204 and LX2404 (see Table 3) fractions were subjected to multifrequency DMTA experiments, however no time-temperature-superposition shifts were performed. The sample designation reflects the propylene and ethylene oxide feed ratio whereby the first two digits represent the amount of PO used for chain extension in *mol* per *kg* of dry lignin, and the second two digits represent the respective EO amount used in succession of PO (see Ch. 2.2). Epoxidation and fractionation has been described in Ch.2.2.1 and the respective data are compiled in Table 2 on page 32. The molecular weight distributions of the lignin copolymers can be found Figure 8 and Figure 9.

Table 10. Compilation of Molecular Weight, Epoxy Equivalent Weight, and Lignin Content of LX0513, LX3010, LX1512, and LX4003

Sample Designation[1]	M_n [2] ($x10^3$)	M_w [2] ($x10^3$)	WPE[3] (g/eq)	Lignin Content[4] (%)	$T_{g,0}$ [5] °C
LX0513	11.3	129.0	532	55	78
LX3010	3.6	32.3	413	25	-22
LX1512A1	1.4	4.2	390	34	-43
LX1512A2	2.1	9.0	550	44	-32
LX1512A3	6.4	33.4	430	48	6
LX4003A1	5.2	24	385	34.9	3
LX4003A2	15.3	96.0	518	43.2	-4
LX4003A3	22.7	190.0	714	41.7	13

1) Sample designation reflects feed of propylene oxide (PO) and Ethylene oxide (EO) in mole/kg dry lignin
2) by GPC (see Ch. 2.2.2.2)
3) by HBr titration (see Ch. 2.2.2.1)
4) by UV (see Ch. 2.2.2.3)
5) Hydroxyethyl lignin PO = 0, EO = 13
6) by DSC

These eight samples, two unfractionated and the six fractions of the fractionated lignins were subsequently mixed with *m*PDA in stoichiometric amounts as described in section 3.4.1.1, cured at 100°C for *5hrs* and postcured at 200°C for *24hrs*. Depending on whether the prepolymer was solid or liquid the samples were cast from solution or in neat form (see Ch. 4.2.2). The cured samples were stored at room temperature.

4.3.3.1 Dynamic Mechanical Thermal Analysis

Measurements of viscoelastic energy dissipation characteristics of the cured lignin epoxides were carried out on a Dynamic Mechanical Thermal Analyzer (DMTA) of Polymer Lab [55]. This method has been recently compared with other viscoelastic techniques and found to give comparable and reliable results [64]. Samples were tested in double cantilever mode whereby the free length was *2mm*. The temperature scans were performed at a rate of $1°\ min^{-1}$ from -100 to 200°C while the sample was subjected to bending in five frequencies: 0.33, 1, 3, 10, and 30 Hz. The resulting E' and E'' vs temperature plots (Figure 50) were divided into a series of five degree intervals and plots of E' and E'' vs. frequency were produced for each temperature. Each curve was shifted manually to determine the shift factors. Thereby the construction of master curves was possible ranging about 30 decades of reduced frequency. Both, E' and E'', were shifted simultaneously with minor vertical adjustments necessary. Since the master curves cover a wide range of reduced frequency and in most of the cases two transitions, it was not possible to fit the entire shift plot to a single analytical form. Rather, the WLF constants C_1 and C_2 were only calculated for the main transitions by recasting eq. 4.3 as

$$\frac{(T - T_0)}{\log a_T} = \frac{C_2}{C_1} - \frac{1}{C_1}(T - T_0) \qquad [4.9]$$

Plotting $\frac{T - T_0}{|\log a_T|}$ versus $(T - T_0)$ for $\log a_T \neq 0$ the WLF constants were determined as slope (C_1^{-1}) and intercept (C_2/C_2).

For comparison of the damping behavior at room temperature all master curves have been shifted to $T_0 = 300K$ regardless of their glass transition temperature. The WLF constants, C_1 and C_2, however, were obtained by shifting the individual plots to their respective glass transition temperature ($T_0 = T_g$), determined as maximum of the main E'' transition at $1Hz$.

4.3.3.2 Transmission Electron Microscopy

TEM samples of the lignin-poly(propylene oxide) copolymer networks were prepared by microtoming small rectangular pieces of the solid glassy polymer. Flexible materials were cooled to about 10°C below their glass transition temperature. The thin cuts (~ 50nm) were floated onto methanol and collected with a ultra fine copper grid. Staining was carried out by exposing the thin cut specimens to RuO_4 vapors for 30 minutes in a small TLC container which contained a 2% aqueous solution of the staining agent. The transmission electron microscope used was a Philips STEM EM-420 instrument.

4.3.4 Results and Discussion

4.3.4.1 Glass Transition Temperature as Function of Copolymer Composition

Figure 43 and Figure 44 show the tanδ traces of the eight specimen as function of temperature. Besides the main transition, a small low temperature transition at -70°C can be observed which does not shift with compositional changes. It is therefore assumed that this is caused by residual and not incorporated poly(propylene oxide) homopolymer which phase separated during the curing reaction. The main glass transition however, is significantly influenced by changes of lignin content and copolymer molecular weight as will be shown later.

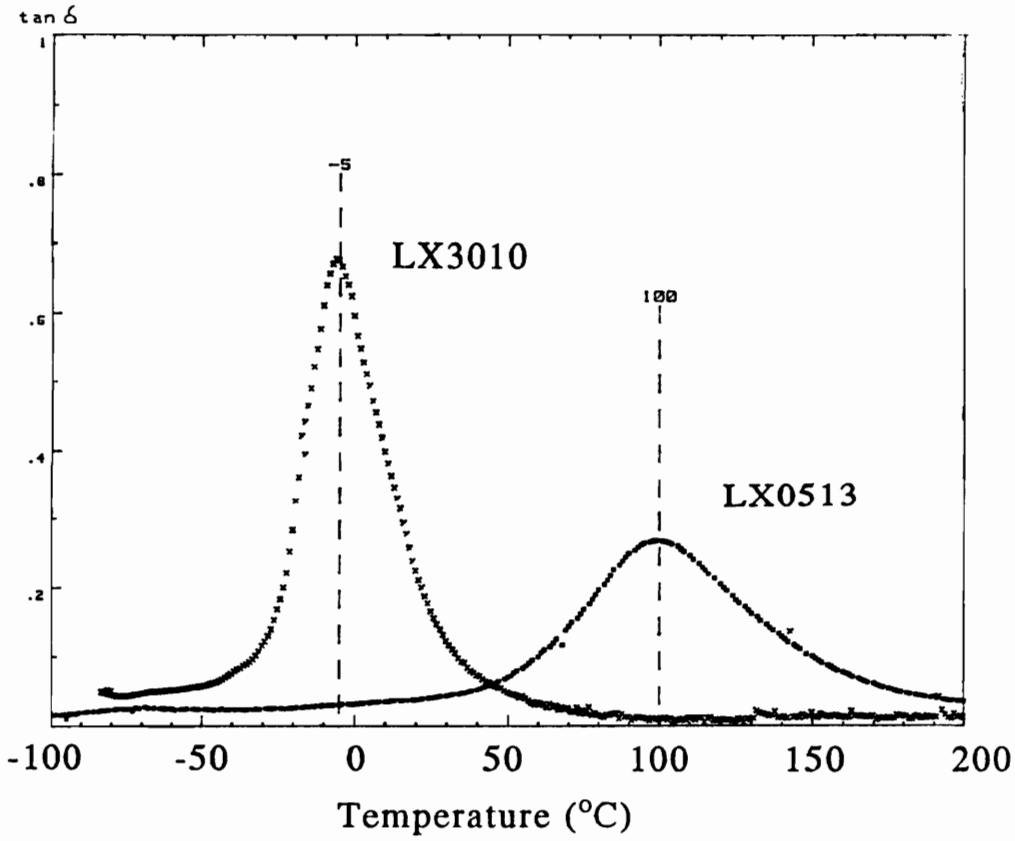

Figure 43. tanδ Traces of LX0513 and LX3010, Unfractionated: $\nu = 1$Hz, 1°/min

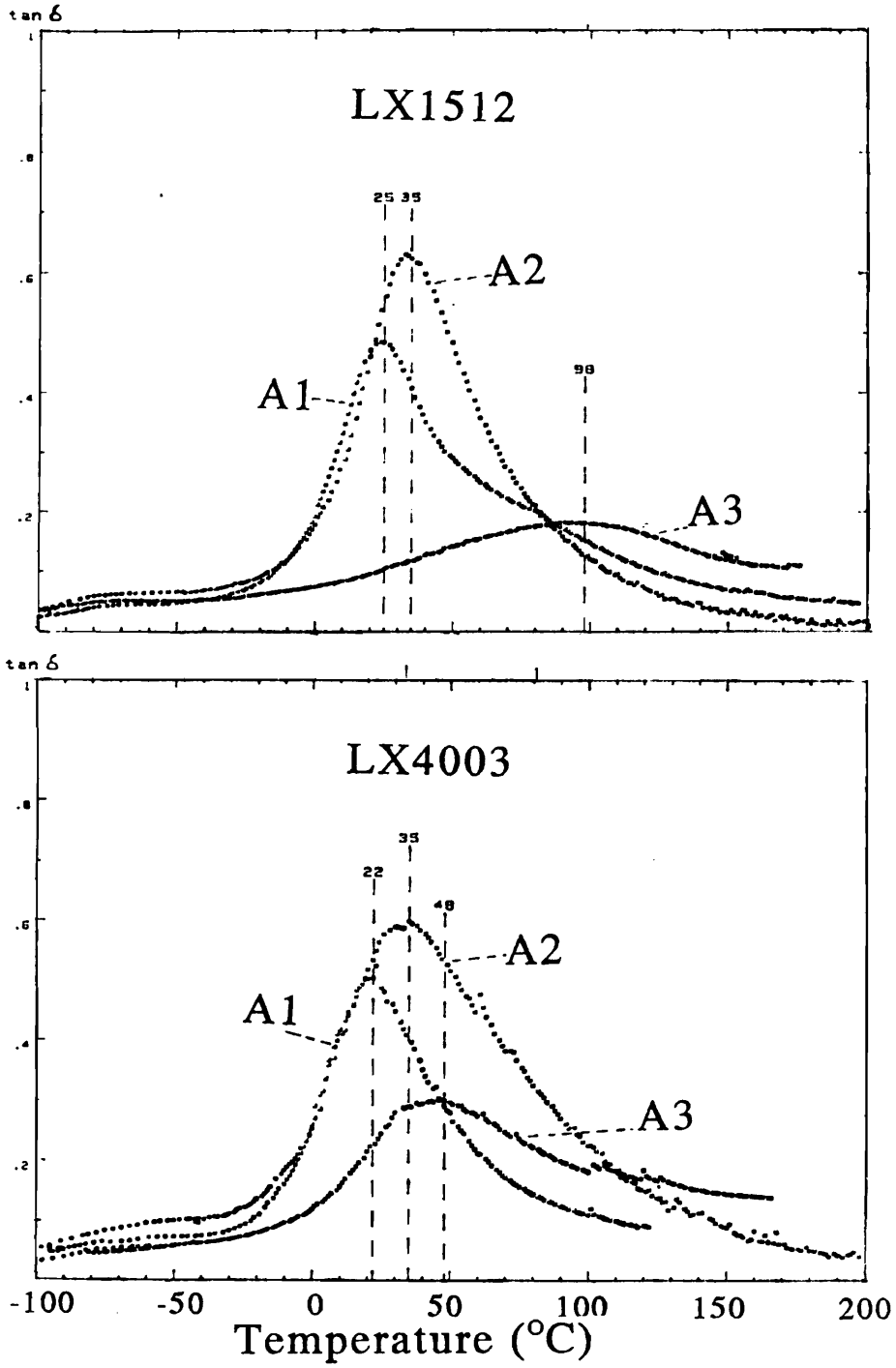

Figure 44. tanδ Traces of LX1512 and LX4003 Fractions: $\nu = 1$Hz, 1°/min

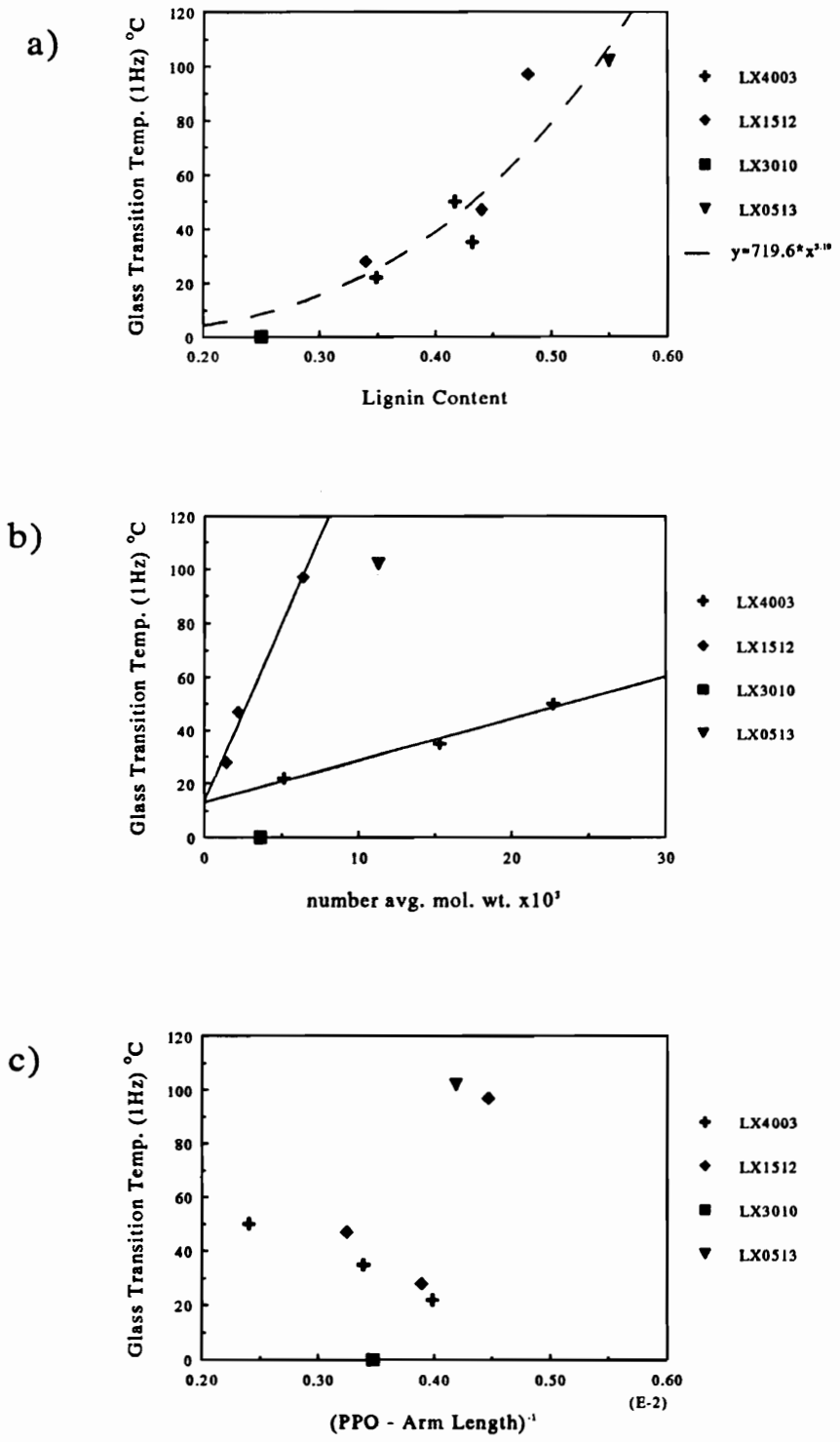

Figure 45. Glass Transition Temperature of Lignin-PPO Epoxy Networks: Function of a) Lignin Content, b) Copolymer Molecular Weight, and c) Inverse Arm Length

Comparing the T_g's of the unfractionated networks, LX0513 and LX3010 (Figure 43) it can be observed that the T_g of the high lignin content network LX0513 (55%[8]) is with 102°C substantially higher than that of LX3010, having a lignin content of 25% and a T_g of 0°C. This trend can also be observed for those networks prepared from the fractionated copolymers (Figure 44). Network glass transition temperatures of unfractionated samples (LX0413, LX3010) and of the fractions (LX1512, LX4003) were plotted against lignin content (Figure 45, a), whereby all values lie on the same upwardly curved trace. This agrees with observation of Kelley et al. [13], who, for polyurethanes based on unfractionated lignin-PPO copolymers reported a positive, though linear dependence of T_g on lignin content. However, the fractions do not only differ in lignin content, but also vary with respect to the molecular weight of the copolymer units (see Ch. 2.2.1.3). Although the respective fractions of the two copolymer sets, LX1512 and LX4004, have comparable lignin content, their molecular weight range is different (see Table 10 on page 150). Thus it is additionally of interest to relate the glass transition temperature to the respective molecular weights. T_g of the cross-linked fractions and unfractionated samples clearly increases almost linearly with copolymer size of the prepolymer fractions (Figure 45, b). Interestingly, the slope of the rise of T_g is almost 9 times smaller for the more modified lignin (LX4003) than for the medium chain extended LX1512.

The question remains whether the length of the polyether arms influences network T_g. Thus, an attempt was made to correlate the glass transition temperature to the inverse of the arm lengths, as they were calculated from lignin content and functionality (see Table 2 and Table 10). Results are compiled in Figure 45 c. While the behavior of the unfractionated networks, LX0513 and LX3010, would be consistent with the assumption that an increase in arm length results in lower glass transition temperature, the trends of the fractionated samples are inconclusive or point in the opposite direction. Within the relatively small range of arm lengths studied they do not seem to be an influential variable determining T_g.

---

[8] on account of the feed ratio

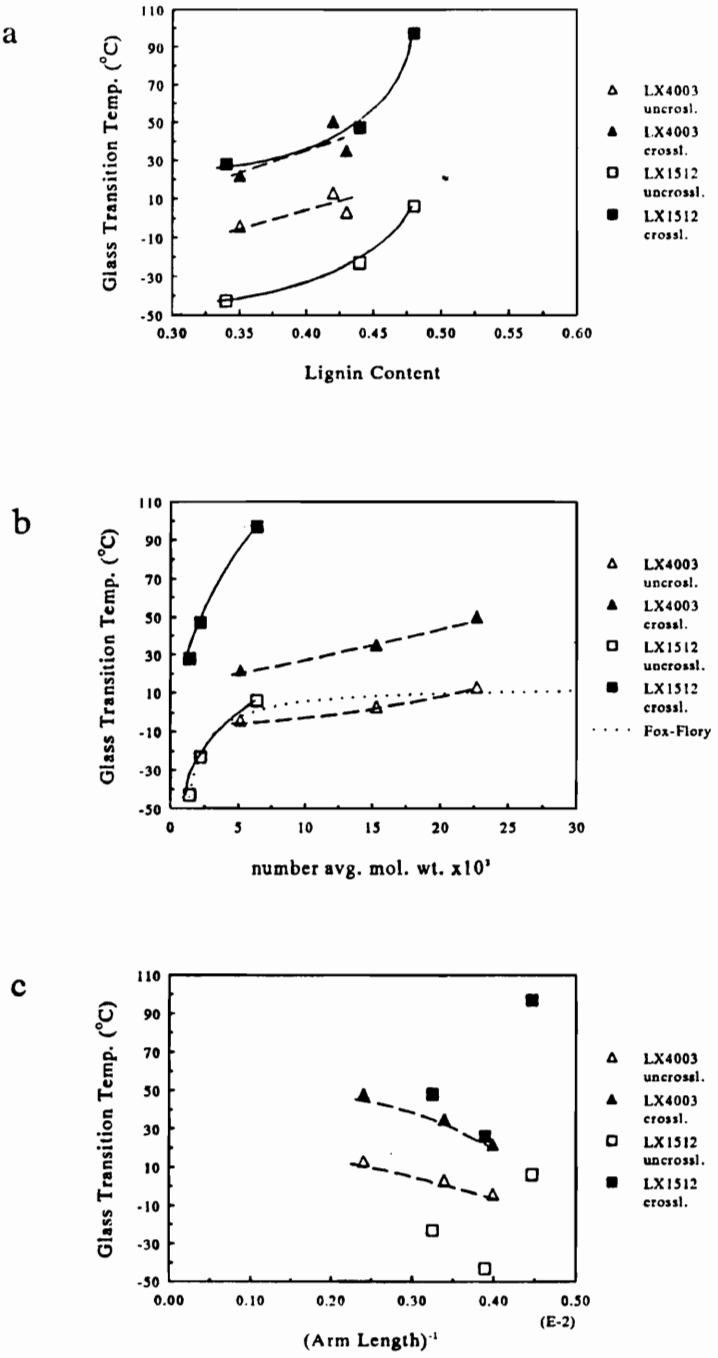

Figure 46. Glass Transition Temperatures of Uncross-linked and Cross-linked Copolymers (LX1512, LX4003): Function of lignin content (a), copolymer molecular weight (b), and inverse arm length (c)

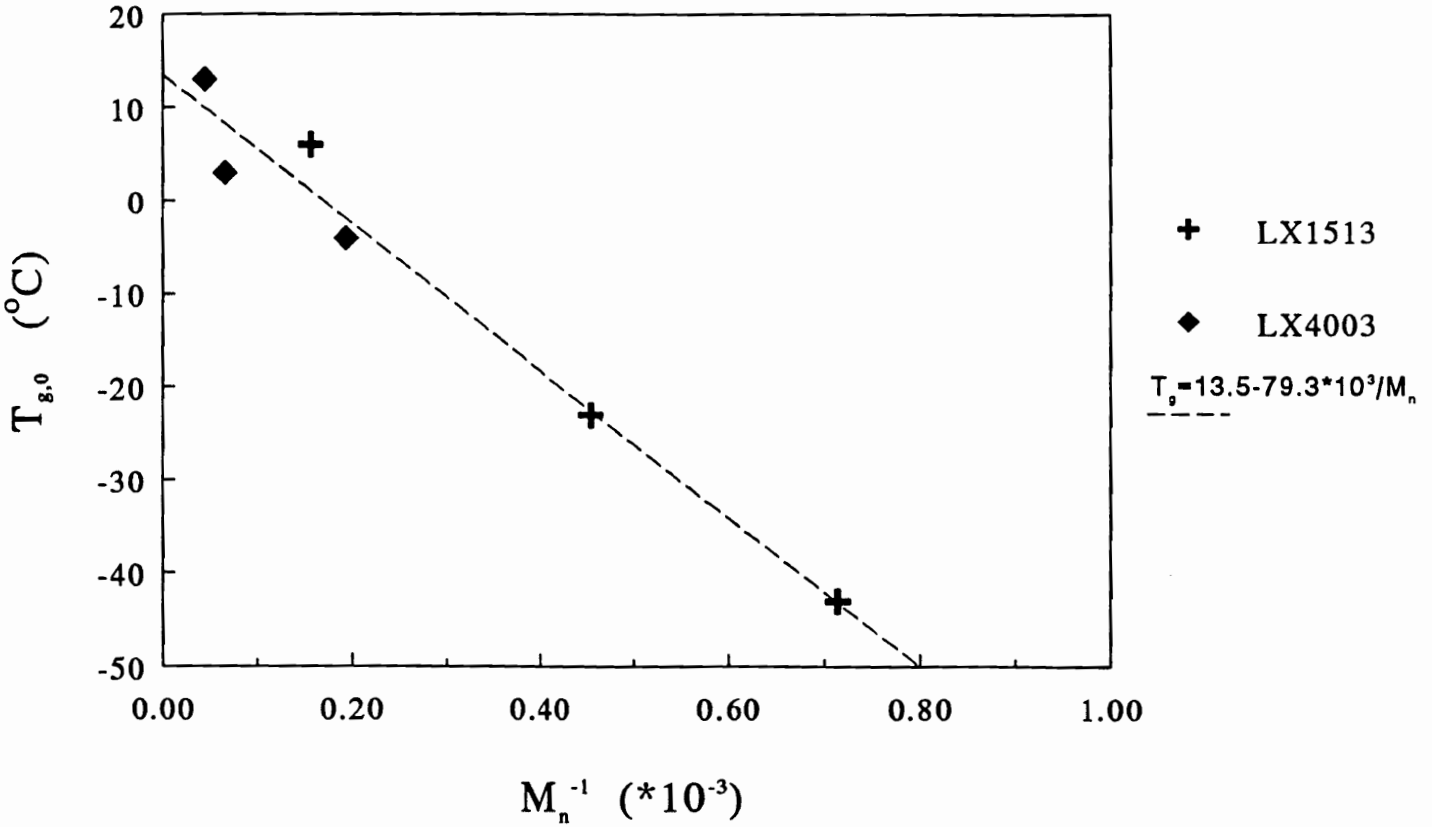

Figure 47. Fox-Flory Plot of LX1512 and LX4003 Fractions: $T_{g,0}$ vs M_n^{-1}

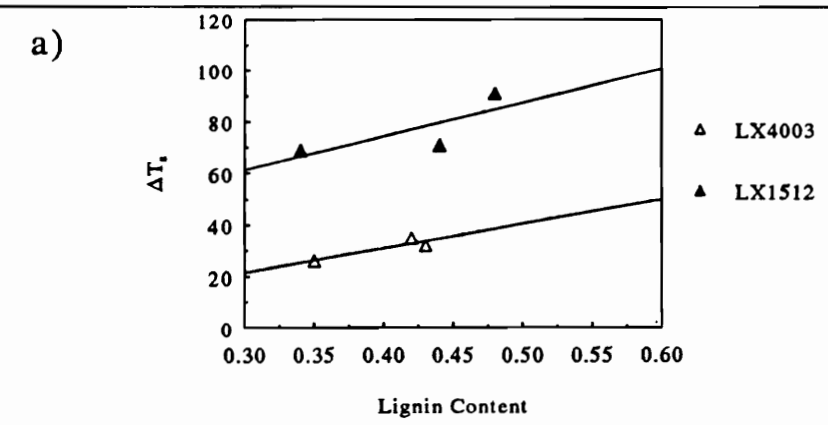

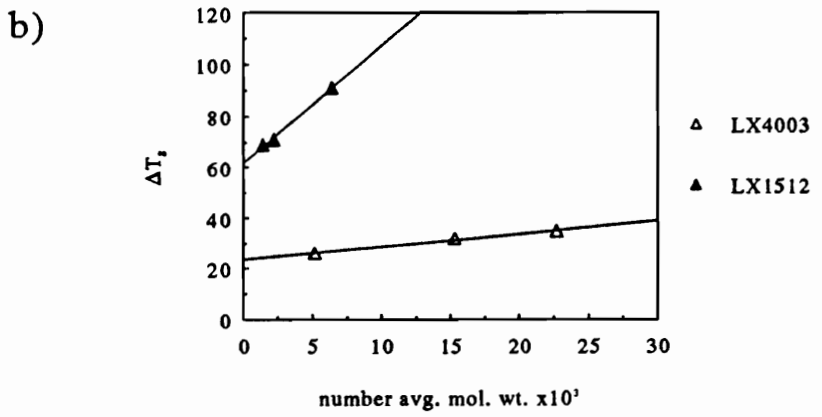

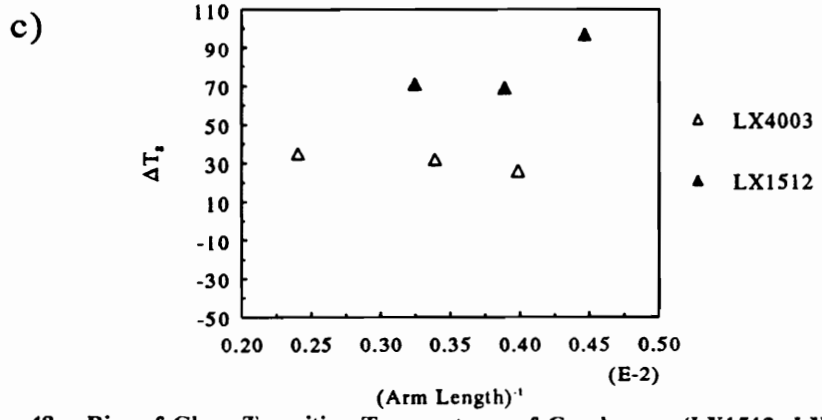

Figure 48. **Rise of Glass Transition Temperatures of Copolymers (LX1512, LX4003) During Cross-linking:** Function of lignin content (a), copolymer molecular weight (b), and inverse arm length (c)

As pointed out in section 4.3.2.2, cross-linking reactions are characterized by a rise in T_g from $T_{g,0}$ to $T_{g,x}$ (see eq. 4.7). To clarify the contribution of the compositional variables to $T_{g,0}$ and ΔT_g, the glass transitions of the uncross-linked copolymer fractions of LX1512 and LX4003 have been determined by DSC (see Table 10). Although T_g's determined by DSC and dynamic mechanical analysis techniques are not necessarily comparable, it is certainly possible to contrast $T_{g,0}$'s measured by DSC and $T_{g,x}$'s obtained from DMTA. Comparison of the $T_{g,0}$ and $T_{g,x}$ as function of lignin content, copolymer molecular weight, and inverse arm length (Figure 46) shows a remarkable symmetry of the respective traces. Independent of lignin content the $T_{g,0}$ of both copolymer sets obey the Fox-Flory relationship

$$T_g = T_g^{\infty} - \frac{k}{M_n} \qquad [4.10]$$

where T_g^{∞} is the maximum glass transition temperature. Plotting $T_{g,0}$ versus M_n^{-1} (Figure 47) of both sets yields a very good linear fit ($R^2 = 0.97$) with $T_g^{\infty} = 286.5K$ and $k = 79.3 \times 10^3$. Those values differ from those determined by Kelley et al. [7] who found a T_g^{∞} of 92°C and $k = 150 \times 10^3$ for fractions of hydroxypropylated kraft lignin. This reflects the lower level of plasticization in HPL's as opposed to the chain-extended lignin fractions of this study. On the other hand, the value of k which reflects the level of branching is only twice as high.

The respective values of ΔT_g (see eq. 4.7) rise nearly linearly with copolymer molecular weight (Figure 48, a) whereby the slopes are distinctly different for the two sets. In contrast, ΔT_g's of (Figure 48, b) both sets of copolymer fractions rise moderately with equal slopes as a function of lignin content. No conclusive dependence of ΔT_g on the arm length (Figure 48, c) can be observed. Summarizing these observations the following preliminary conclusions can be drawn:

- Independent of the degree of chain extension and the individual lignin content fractionated lignin-PPO copolymers obey the Fox-Flory relationship with $T_g^{\infty} = 286.5K$ and $k = 79.3 \times 10^3$;
- ΔT_g is a linear function of lignin content and copolymer molecular weight (Figure 47);

- the slope of ΔT_g vs. lignin content is independent of the level of chain extension (Figure 48 a);
- the slope of ΔT_g vs. copolymer molecular weight is a strong function of the level of chain extension (Figure 48 b);
- the same observations can be made for the $T_{g,x}$'s of the cross-linked copolymers: while $T_{g,x}$ vs. lignin content is independent of lignin modification and molecular weight, $T_{g,x}$ vs. copolymer molecular weight is a strong function of the level of modification;
- neither ΔT_g nor $T_{g,x}$ are dependent on arm length which implies that $\Delta_x T_g$ and $\Delta_c T_g$ are constants.

These conclusions and observations allow one to make predictions about the network model of equation 4.7. Both parameter, $\Delta_c T_g$ and $\Delta_x T_x$ are a function of the cross-link density which is a function of the polyether arm lengths of the connected stars. From Figure 48 c, it can be seen that ΔT_g is not a function of the arm length. Thus, for the limited range of polyether chain lengths, $\Delta_x T_g$ and $\Delta_c T_g$ can be regarded constant among the fractions of one copolymer set. However, ΔT_g is a function of lignin content and molecular weight which can be therefore only be explained by a change of $f(x)$, which incorporates the effect of morphological changes on $T_{g,0}$ during cross-linking. Nevertheless, those changes of $f(x)$ with lignin content are equal for both samples, the highly modified LX4003 and the medium modified LX1512. On the other hand, considerable differences in the changes of $f(x)$ with molecular weight are noticeable. The fractions of the medium modified LX1512 copolymer have smaller molecular weights at comparable lignin contents than LX4003. The glass transition temperature of these smaller size fractions increases nine times faster with molecular weight than the ΔT_g of the larger LX4003 fractions. Since these changes are a function of $f(x)$, they can be interpreted on a molecular level as an indication that copolymers with relatively lower degree of chain extensions (LX1512) to a larger extent undergo partial phase demixing as a function of copolymer size, while being cross-linked, which in turn leads to a reduction of internal plasticization of the lignin core with PPO and to a retroactive increase of $T_{g,0}$.

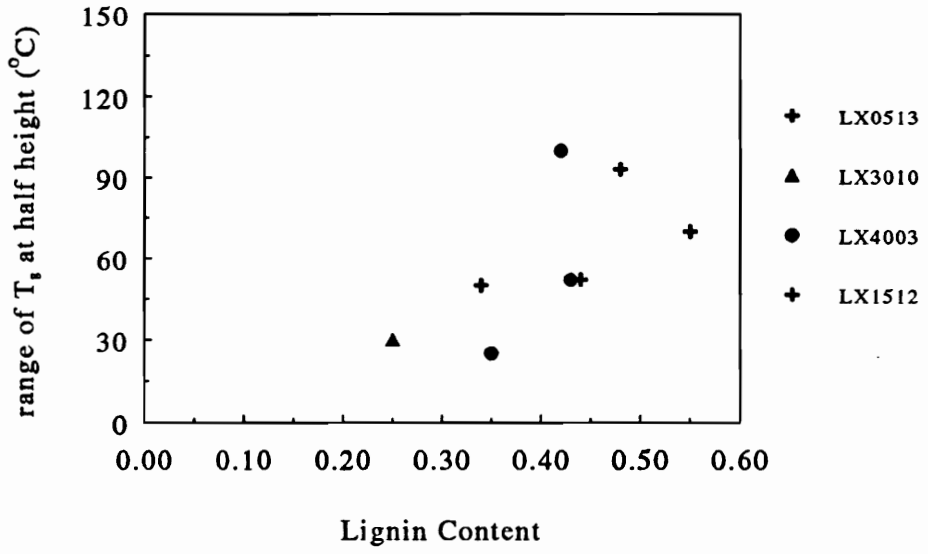

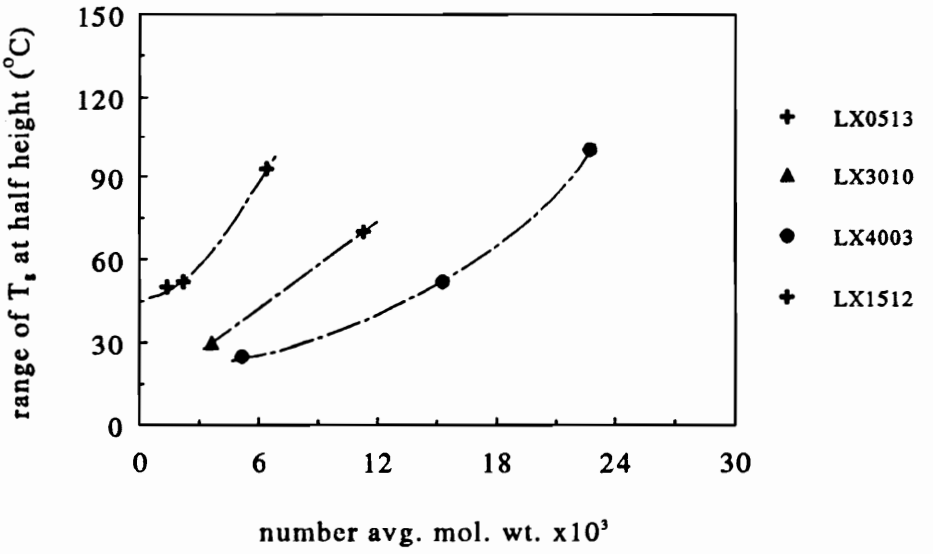

Figure 49. Range of Glass Transition at Half Height: function of lignin content (a), and copolymer molecular weight (b)

4.3.4.2 Range of the Glass Transition

The main transitions of all specimens with the exception of the low lignin content unfractionated sample LX3010 are very broad, ranging from 50°C to 100°C at half height, increasing with lignin content and molecular weight (see Figure 49). The same phenomenon has been reported by Kelley et al. [7,13] for uncross-linked and cross-linked lignin-PPO copolymers which can be the result of both, the large number of mechanically excitable molecular features within the lignin center, and interfacial heterogeneity [1]. But also plasticization is known to broaden loss peaks [66], especially if the solubility of the plasticizer in the polymer is poor. Nielsen [71] for instance reported that PVC plasticized with the well soluble diethyl phthalate (DEP) has a very narrow damping transition, which triples once DEP is replaced by n-dioctyl phthalate (DOP). Thus the apparent increase of the glass transition range of the lignin-PPO networks with copolymer size supports the observations, outlined above, that cross-linking induced demixing is emphasized by the molecular weight of the starting material especially for LX1512. Mechanistically, some demixing is necessary to connect the PPO chains via the epoxy groups to the tetra functional amine, thereby removing the chain ends from the lignin center. Certainly this is a complex process, but the trends are clearly recognizable.

The breadth of the transition as a result of internal friction must have implication on the energy dissipation performance of a material if it is to be employed for sound or vibration control [24]. If the transition region is narrow also the range of optimum use temperature is narrow and slight changes in the environmental temperature result in a loss of the good damping characteristics. By using materials with a broad transition range, it is possible to apply them over a wider range of temperatures without loosing the sound or vibration damping capability [1,20].

4.3.4.3 Activation Energies of the Glass Transition

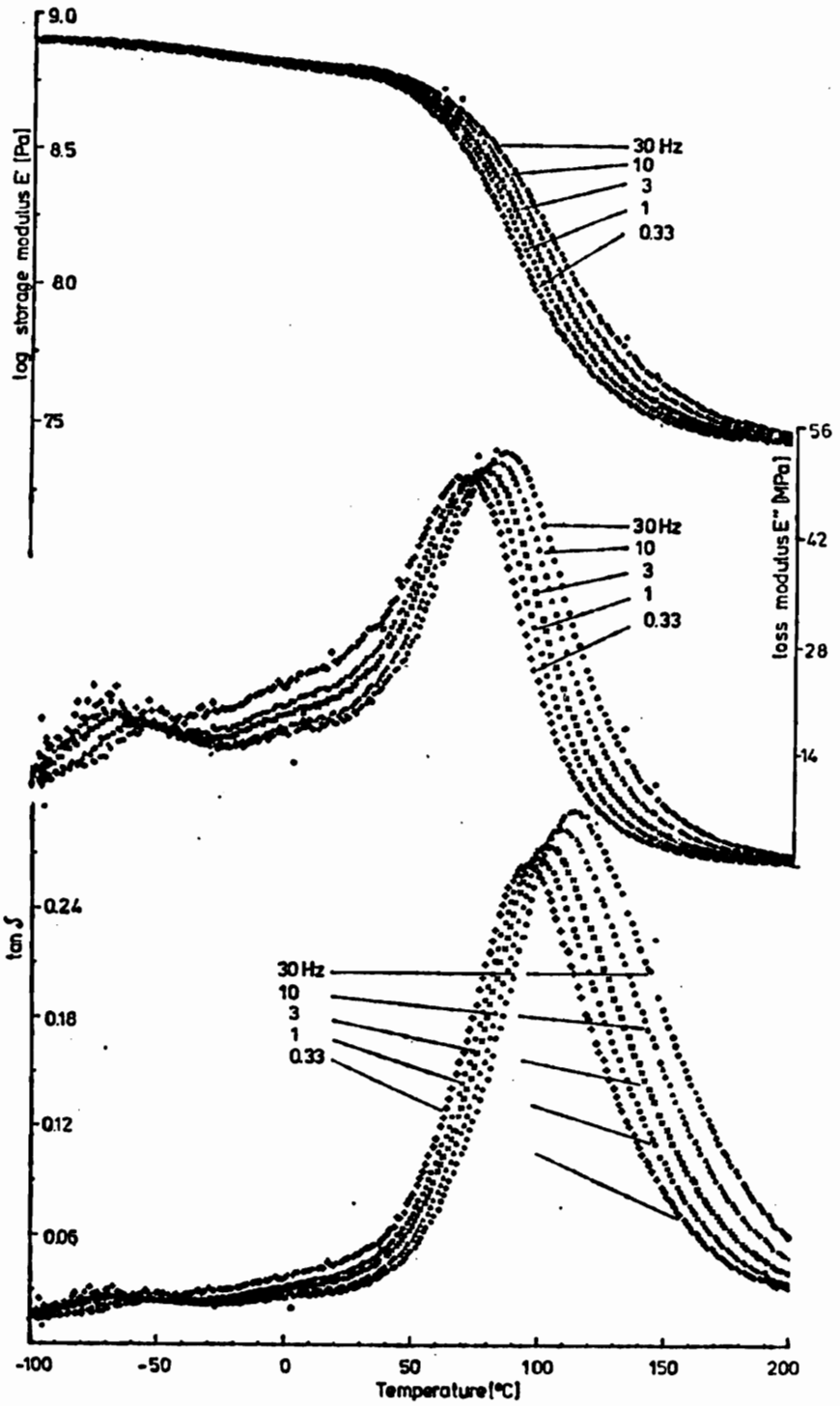

Figure 50. Multifrequency DMTA Analysis of LX1512, High Molecular Weight Fraction: log E′, E″, tanδ

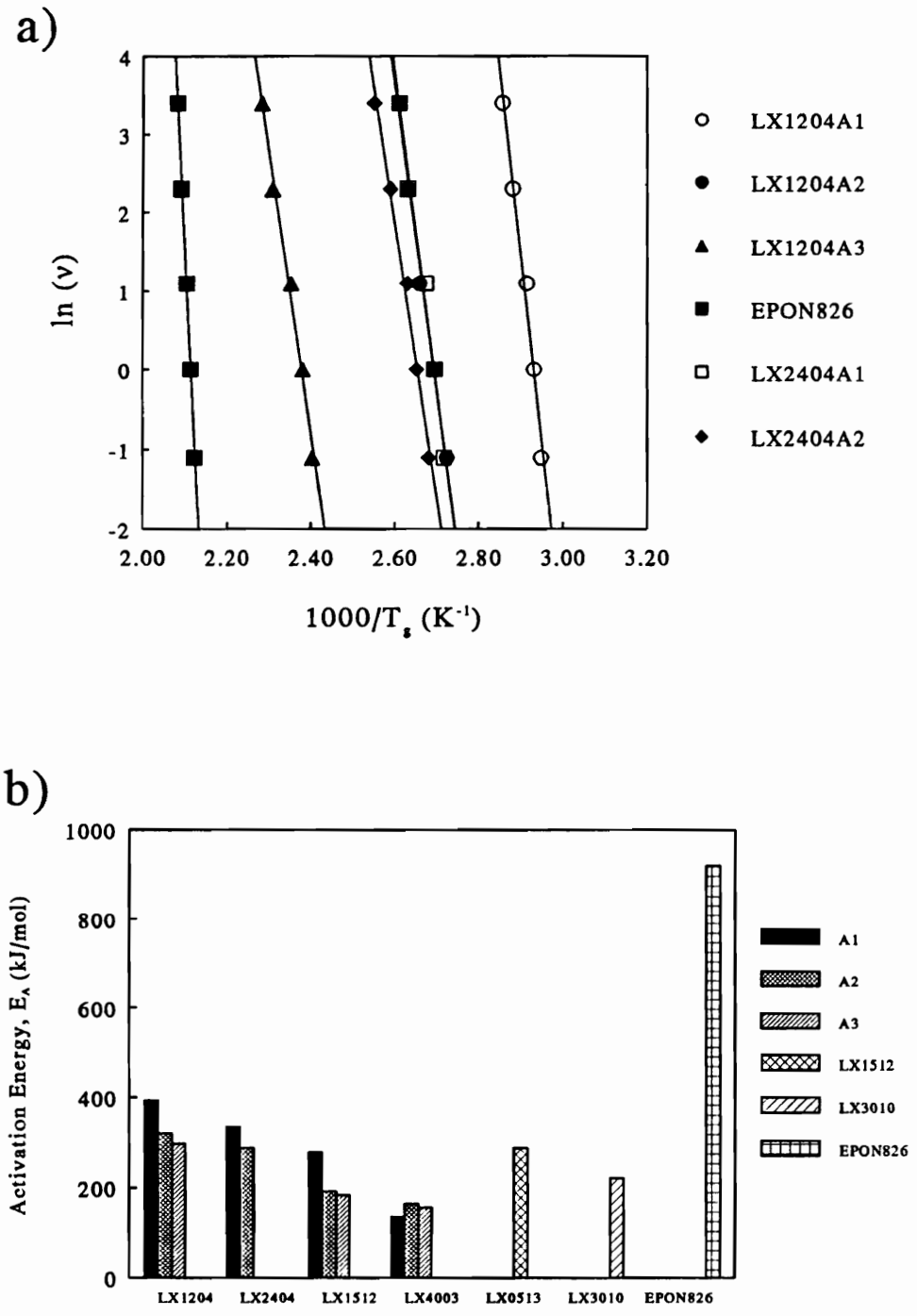

Figure 51. Arrhenius Plots of Measurement Frequency vs. Inverse tanδ Peak Temperature (a) and Histogram of Activation Energies (b)

Table 11. Activation Energies of DMTA Frequency Shifts

Sample	Fraction	E_A (kJ/mol)
LX0513	-	288.7
LX3010	-	221.6
LX1204		
	A1	392.3
	A2	320.4
	A3	297.9
LX1512		
	A1	279.1
	A2	191.6
	A3	183.9
LX2404		
	A1	325.5
	A2	288.4
LX4003		
	A1	136.0
	A2	165.0
	A3	157.1

a)

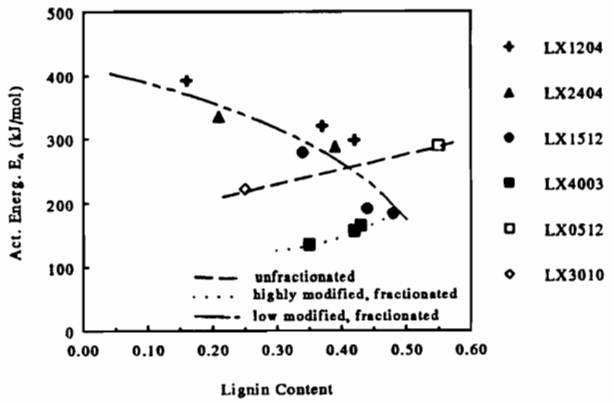

b)

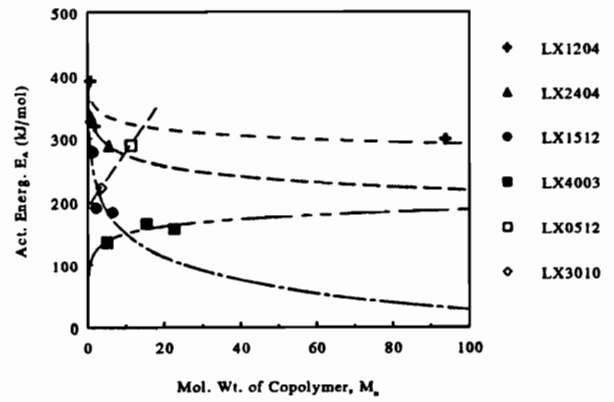

c)

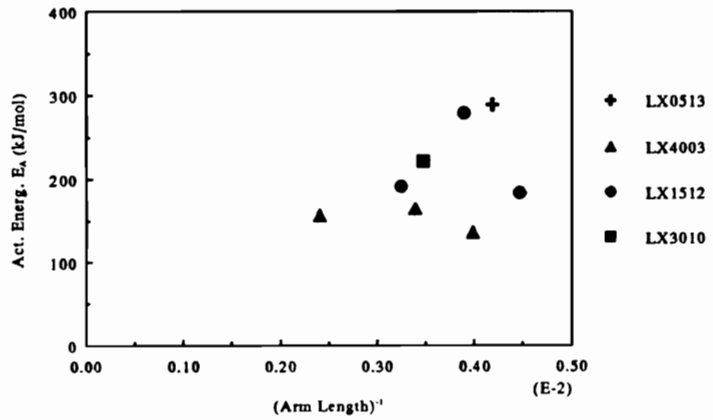

Figure 52. Activation Energy of DMTA Frequency Shifts: Function of lignin content (a), copolymer molecular weight (b), and inverse arm length (c)

To quantify the variation of the energy barriers to segmental motion in the amorphous network at or below the glass transition temperature the activation energies were determined from multifrequency dynamic mechanical analyses. Fixed frequency experiments at $\nu = 0.33$, 1, 3, 10, and 30 Hz were carried out on most fractionated and unfractionated copolymer networks, and on a DGEBA/*m*PDA system (EPON 826), and log E', E'', and tan δ were recorded (Figure 50). A shift of the transitions towards higher temperatures with increasing measurement frequency ν is observed. The activation energies (see eq. 4.4) have been obtained from a ln ν vs. T_g^{-1} plot (Figure 51, a) and are compiled in Table 11 and in Figure 51, b. Since the activation energy is a measure of the ease of segmental change of isomeric positions within the network, it is evident that all lignin-PPO epoxy networks do have larger motional freedom than the bisphenol-A network. No activation energies of unplasticized lignin are available, but the gradual reduction of the average E_A with increased PPO/EO : lignin feed ratio (Figure 51 b) suggests at first glance that an increase of the level of internal plasticization of the lignin center reduces mobility restrictions. However, except in the case of LX4003, activation energies are positively correlated with PPO content and molecular weight, i.e., the lignin richer and higher mol. wt. fractions have lower activation energies. This would mean that these specimens would have a lower energy barriers to segmental motions. From Figure 52, a) it can be clearly seen that all fractions of the low to medium modified lignins share a common and declining trace of E_A versus lignin content. LX4003, whose fractions do have a significantly higher molecular weight show a separate and opposite trend, as do the unfractionated networks. The same trend reversal is evident when E_A is correlated with copolymer size. It is certainly difficult to arrive at molecular interpretations of these observations. The decrease in activation energy with increasing lignin content for most of the fractions of low to medium modified lignins is bewildering, since it suggests that the barriers to segmental mobility become lower with higher lignin content. Conceptually, the mobility of segments is linked to the available free volume. Thus, attempts were made to relate the trends of activation energies to the respective trends in free volume and its thermal coefficient of expansion. This is discussed in section 4.3.4.5.

4.3.4.4 Time-Temperature-Superposition

Master plots of log E' and E'' were prepared by manually shifting the respective isothermal traces according to the procedure outlined in Figure 42 on page 143. All master curves were shifted to $T_0 = 300K$ (see Figure 53 to Figure 55). As it is expected, these plots mirror the observation deduced from the fixed frequency plots. Depending on the lignin content and molecular weight the glass transition frequency, ν_g, is at a slightly different position for each of the three fractions. Since the reference temperature was chosen to be $300K$ (i.e. room temperature), a log $a_T\nu > 0$ indicates a rubbery material.

It is evident that the transitions of the fractionated and unfractionated samples as function of reduced frequency follow the same trends as their iso-frequency, temperature dependent counterparts. The highly extended, unfractionated sample LX3010 has its glass transition clearly positioned in the rubbery region while the position of the transition of LX0513 at very low values of log $a_T\nu$ indicates a glassy material. Analogously, also the maxima of the LX1512 fractions are a more pronounced function of compositional variables, than those of the LX4003 fractions. Although no log $a_T\nu$ values of uncross-linked copolymers are available, it can be assumed by analogy that the same relationships are applicable to the decrease of log $a_T\nu$ which determine the rise of T_g as outlined in Figure 46 and Figure 48 during cross-linking.

The practical importance of the master plots lies in the visualization of the frequency band where the polymer efficiently dissipates energy. Of the unfractionated specimens, LX3010 exhibits a maximum at 10^4Hz and a transition ranging from about 10^3 to 10^6Hz. Thus, it covers the upper part of the acoustic spectrum. But the range of the transition is small compared with that of LX0513, which covers 9-10 decades of frequencies. And while the breadth of the transition is not important per se for acoustic damping, the advantage of broader transitions lies in the material's ability to experience considerable changes in temperature without loosing energy absorption effi-

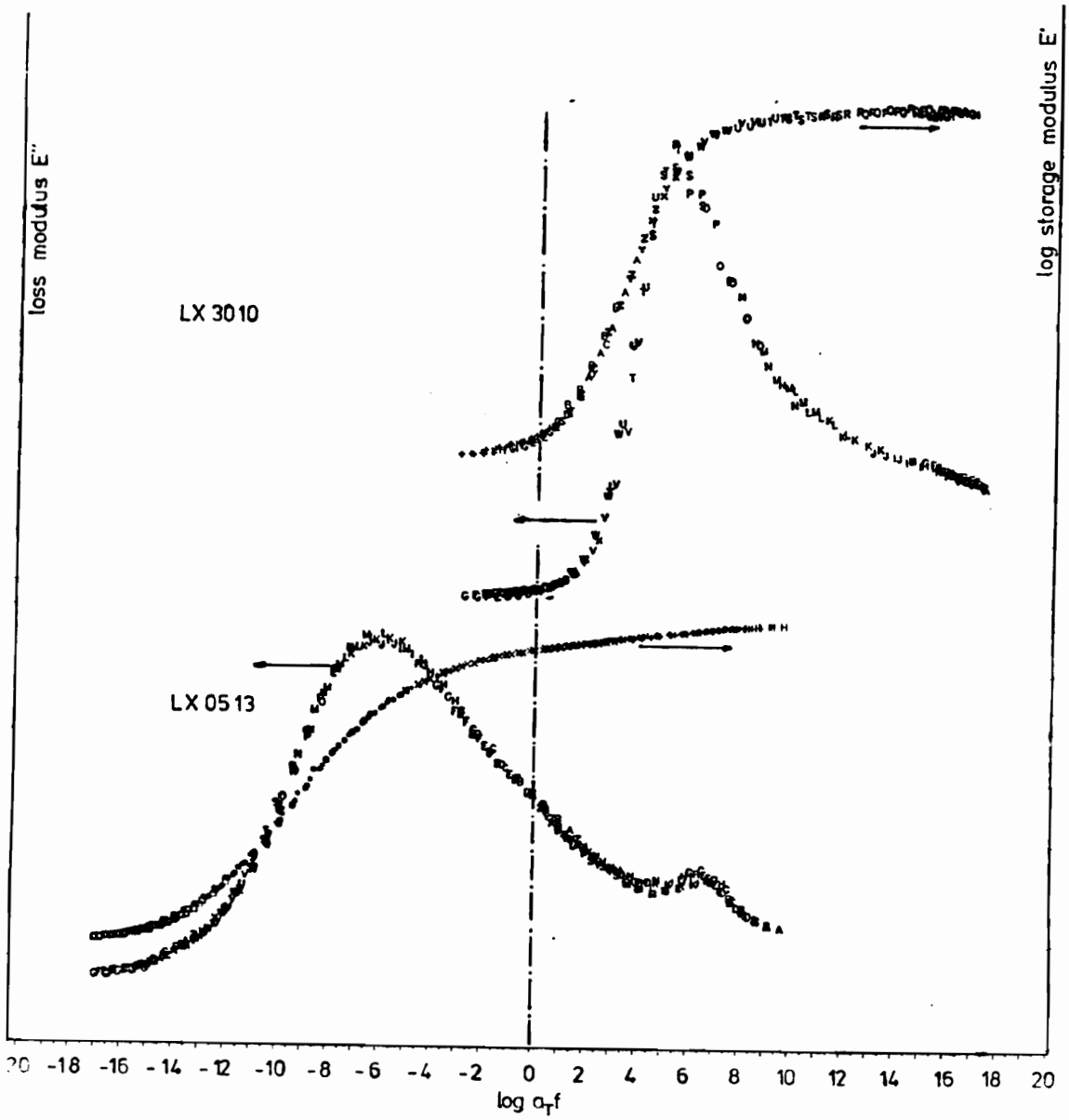

Figure 53. Master curves of log E′, and E″ for LX3010 and LX0513

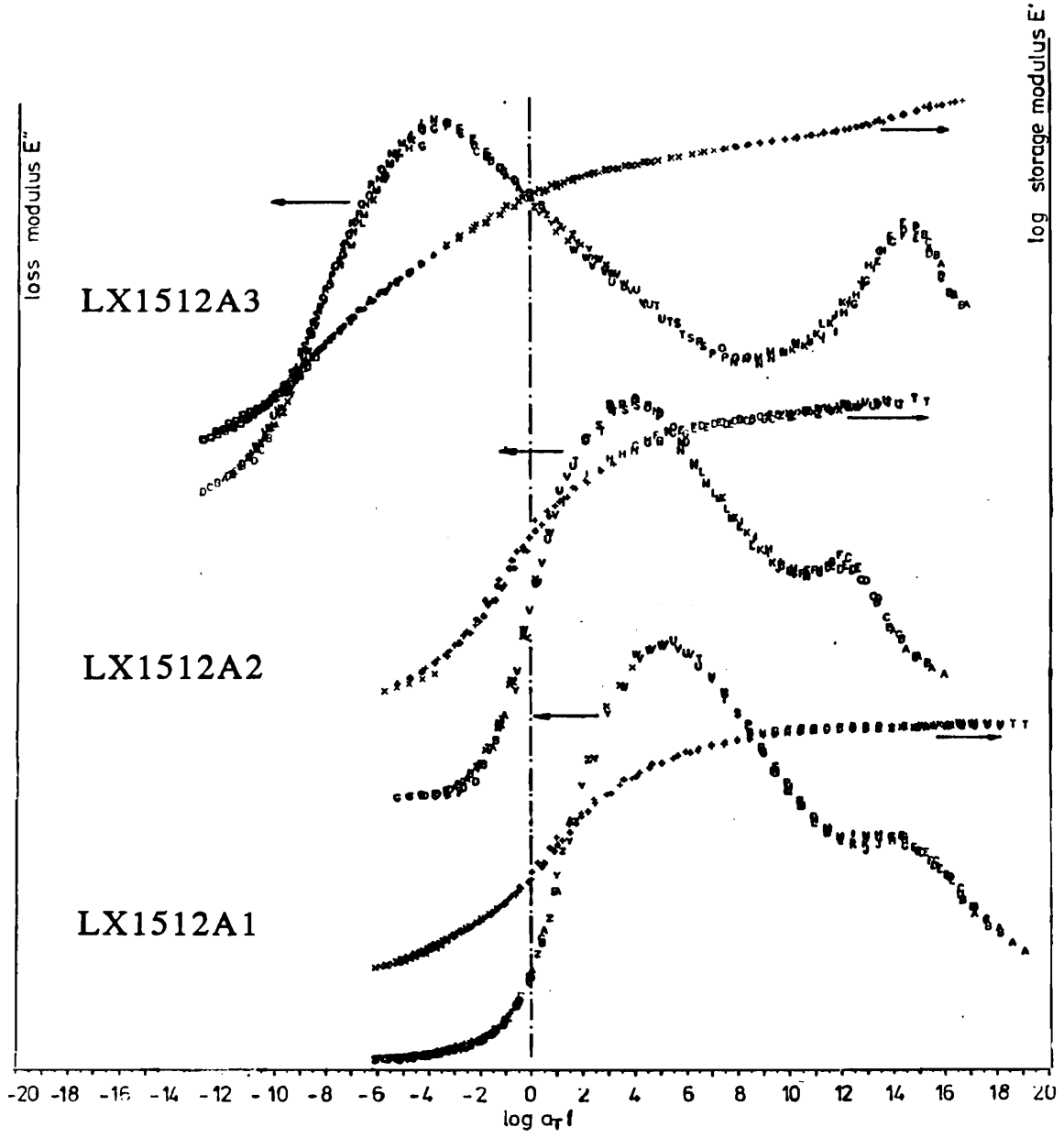

Figure 54. Master curves of log E′, and E″ for LX1512

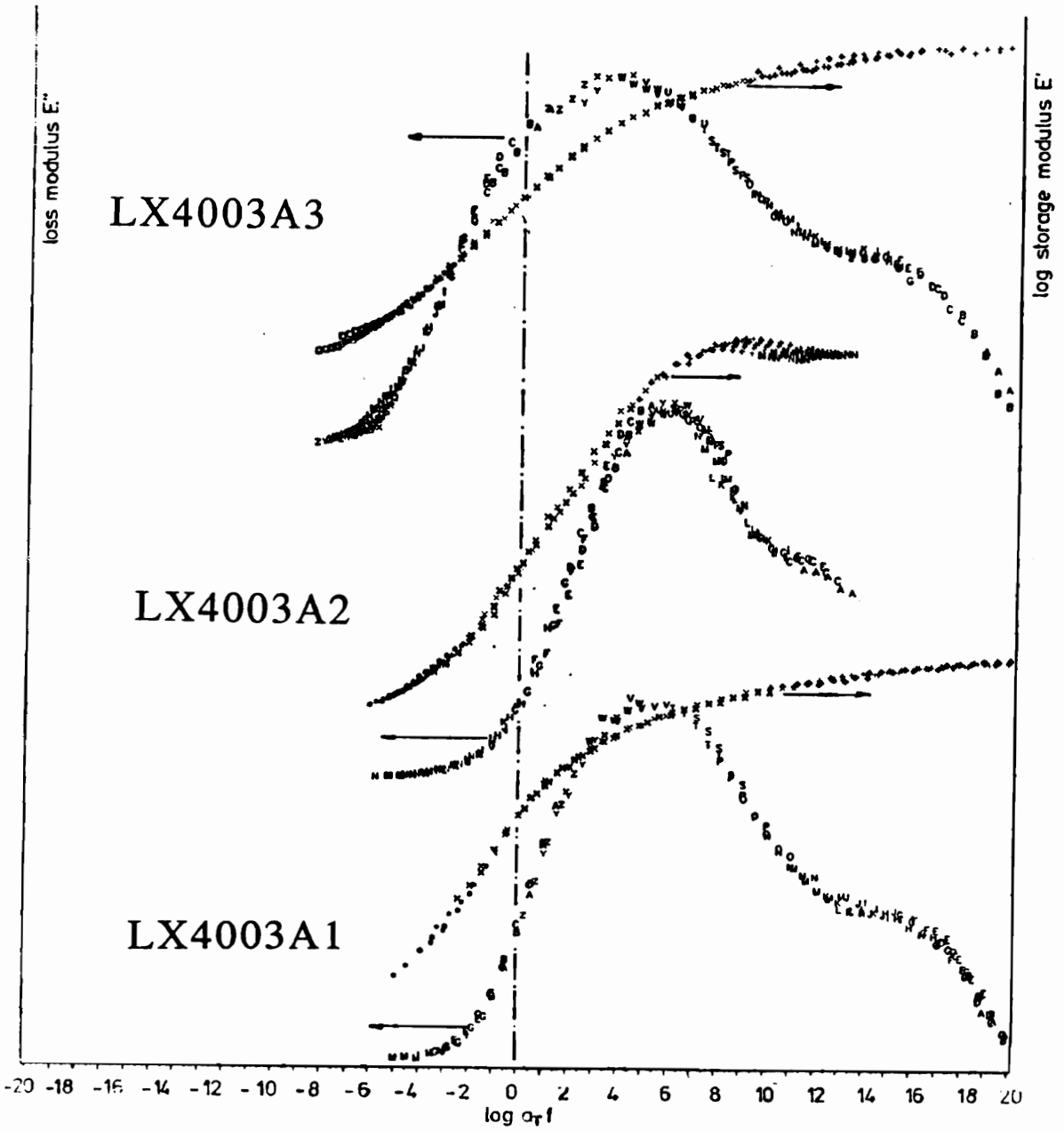

Figure 55. Master curves of log E′, and E″ for LX4003

ciency. All of the fractions of LX4003 and the two lower lignin containing fractions of LX1512 would be good candidates for acoustic damping polymers since they combine considerable breadth of transition with maxima in the acoustics or near acoustic frequencies.

4.3.4.5 WLF Equation and Free Volume

The shift factors C_1 and C_2 of the main transition were determined by plotting $T - T_g$ vs. $(T - T_g) / log\ a_T$ according to the procedure outline in Ch.4.3.1.1. By virtue of these constants, the WLF equations (eq. 4.3) of the individual specimens were determined and subsequently compared with the manual shift plots (see Figure 56 and Figure 57). The agreement is very good in all cases and deviation only starts at the onset of the low temperature transition. The coefficients C_1 and C_2 were recorded in Table 12. Since the concept of WLF equation is based on the free volume theory, it is possible to calculate f_g, the fractional free volume at the glass transition, and its coefficient of thermal expansion α_f. Below the glass transition temperature the fractional free volume is approximately constant but, changes at $T>T_g$ from the fractional free volume f_1 at temperature T_1 to the fractional free volume f_0 at T_0 [2] as

$$f_1 = f_0 + \alpha_f(T - T_0) \qquad [4.11]$$

α_f can be assumed to be essentially constant [2]. Combining eq. 4.9 with the empirical Doolittle Equation[9] yields

$$\log a_T = \frac{B}{2.303}\left(\frac{1}{f_1} - \frac{1}{f_0}\right) \qquad [4.12]$$

where B can be taken to be unity. Together with eq. 4.3, this equation allows to calculate the fractional free volume, f_g, and α_f,its thermal expansion coefficient as

---

[9] $\ln \eta_0 = \ln A + B(f - 1)$, where η_0 is the zero shear viscosity and A and B are adjustable parameters. f is the fractional free volume

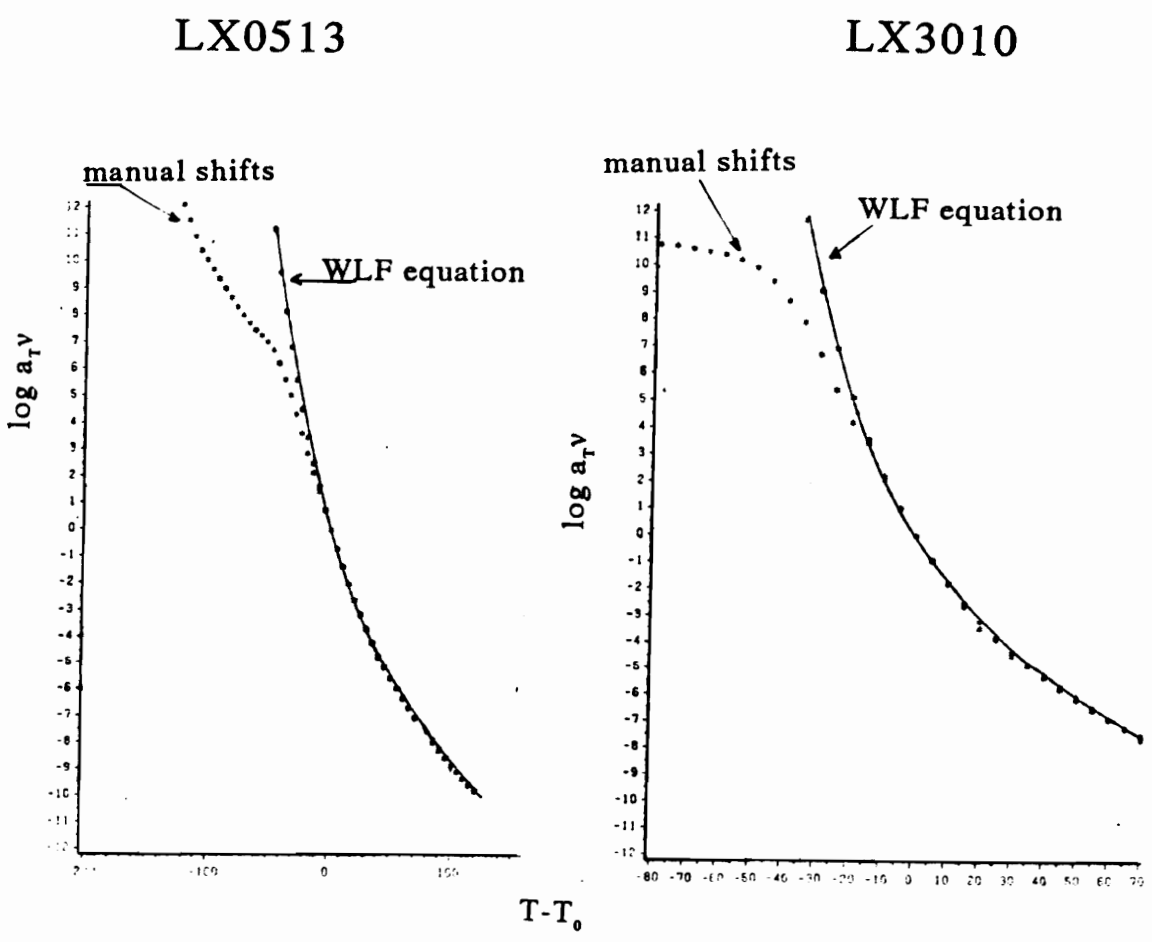

Figure 56. Manual and Calculated Shift Plots of LX0513 and LX3010

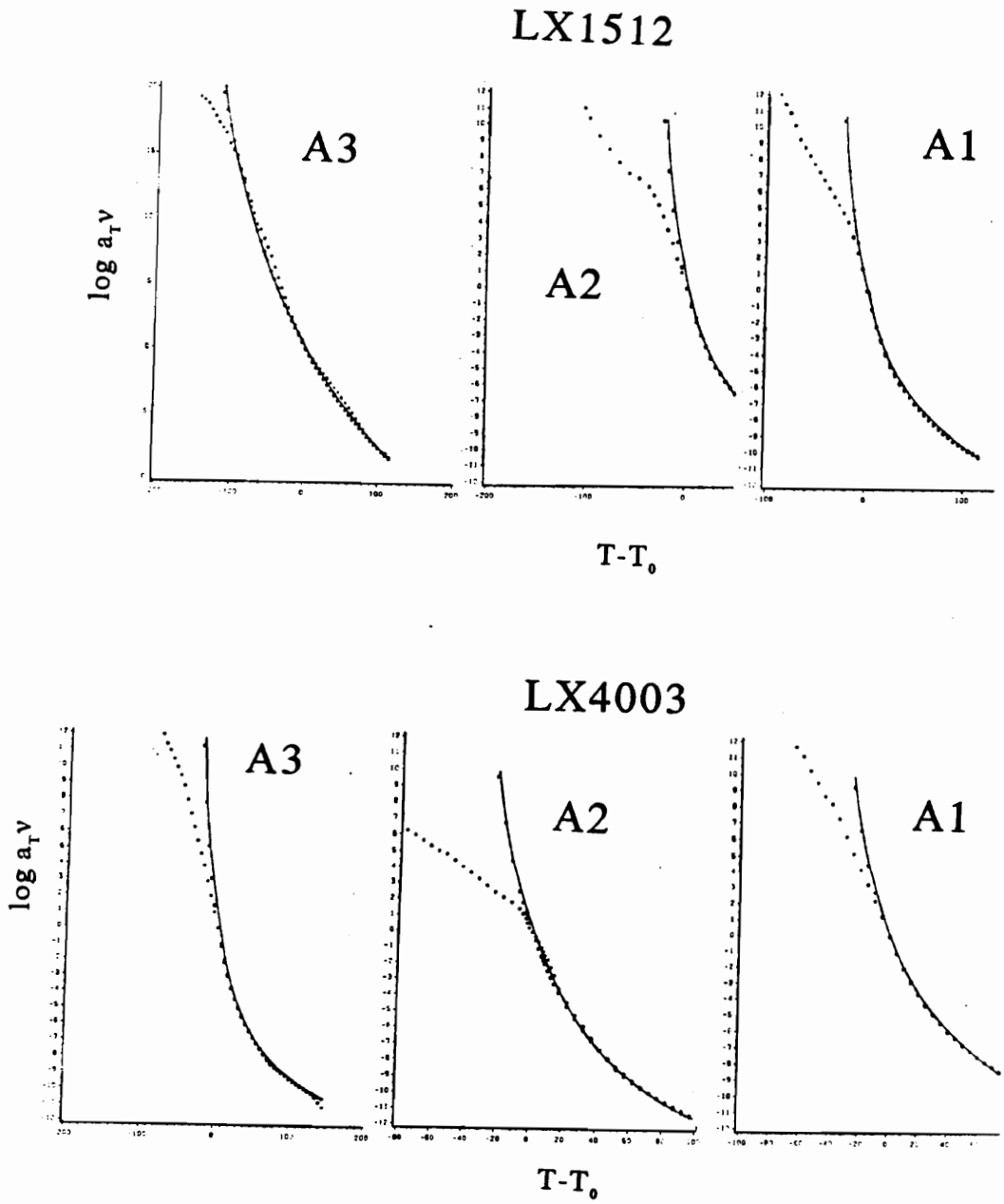

Figure 57. Manual and Calculated Shift Plots of LX1512 and LX4003 Fractions

Table 12. Compilation of Dynamic Mechanical Analysis Results

Sample[1]		T_g[2] (°C)	tanδ[3]	Transition[10] Range (°C)	Transition[11] Range (decad.)	E_A[4] (kJ/mol)	C_1	C_2[5]	f_g[6] (× 10⁻²)	α_f[7] (× 10⁻⁴)	M_n (× 10³)	Lignin Content[8] (%)
LX0513	-	102	0.27	70	10	-288.7	22.1	149.3	1.96	1.31	11.3	55.0[9]
LX3010	-	0	0.65	30	6	-221.6	16.5	84.5	2.63	3.11	3.63	25.0[9]
LX1512												
	A1	28	0.52	50	7	-279.1	15.6	62.5	2.78	4.45	1.4	34
	A2	47	0.64	52	8	-191.6	14.2	59.7	3.05	5.11	2.2	44
	A3	97	0.17	93	13	-183.9	31.0	310.0	1.4	0.45	6.4	48
LX4003												
	A1	22	0.69	25	8	-136.0	19.5	68.3	2.23	3.19	5.16	35
	A2	35	0.53	52	9	-165.0	16.0	69.7	2.72	3.98	15.3	43
	A3	48	0.3	100	12	-157.1	14.7	57.7	2.95	5.12	22.7	42
LX1204												
	A1	58				-383.7					0.63	16
	A2	97				-320.3					1.9	37
	A3	147				-297.9					93.8	42

[1]all samples from chainextended steam explosion yellow poplar lignin
[2]DMTA, $\tan\delta_{max}$, $\nu = 1Hz$, 1.5° min⁻¹
[3]DMTA, $\tan\delta_{max}$, $\nu = 1Hz$, 1.5° min⁻¹
[4]DMTA, $\tan\delta_{max}$, $\nu = 0.33, 1, 3, 10, 30Hz$, 1.5° min⁻¹
[5]WLF constants
[6]fractional free volume at glass transition
[7]thermal expansion coefficiant of f_g
[8]by UV_{280}; excpt. LX0513 and LX3010
[9]from propoxylation feed ratio
[10]tanδ transiton
[11]E'' transition, isothermal, from E'' vs. log $a_T\nu$

$$f_g = \frac{B}{2.303 C_1}$$
$$\alpha_f = \frac{B}{2.303 C_1 C_2} \qquad [4.13]$$

Usually f_g assumes an average of 0.025 for most polymers [2]. All f_g and α_f values were calculated by setting the reference temperature to the 1 Hz glass transition temperature (E''_{max}). The results are compiled in Table 12.

The free volume is a measure of molecular mobility [2] and can give information about the state of plasticization of a polymer. For instance, Duffy et al [5] reported that increasing the molecular weight of the soft segment in polyurethanes reduces the glass transition and increases both, α_f and ν_g, the isothermal glass transition frequency, thereby showing that the soft segments provide internal plasticization of the hard blocks. It was expected that in lignin-PPO copolymer networks the flexible polyether arms plasticize the rigid lignin centers. Indeed the free volume of the unfractionated low lignin content sample LX3010 is about twice as high as f_g of the higher lignin content LX0513, which indicates that the more chain extended LX3010 possesses higher segmental mobility. α_f is also higher, meaning that the free volume collapses faster once the temperature is lowered, which explains the considerably smaller glass transition range of LX3010. But overall the values of f_g's are not very much effected by lignin content. Only beyond a threshold of about 45% the free volume drops considerably (Figure 58 a). However, the simultaneous increase of copolymer size has opposing effects for the low and high modified samples (Figure 58 b). While an increase of the relatively smaller copolymer sizes of the LX1512 fractions lowers the free volume, the trend is reversed for LX4003. Comparison of these results with the activation energy versus copolymer size data of Figure 52 suggests the paradox situation that a reduction of free volume is accompanied by a decline of activation energy, and vice versa.

The free volumes of all specimens lie on the same f_g vs. inverse arm length trace (Figure 58, c) which supports the notion that reducing polyether chain lengths lowers free volume independent of lignin content and molecular weight of the copolymers. This is surprising, since within the limited

a)

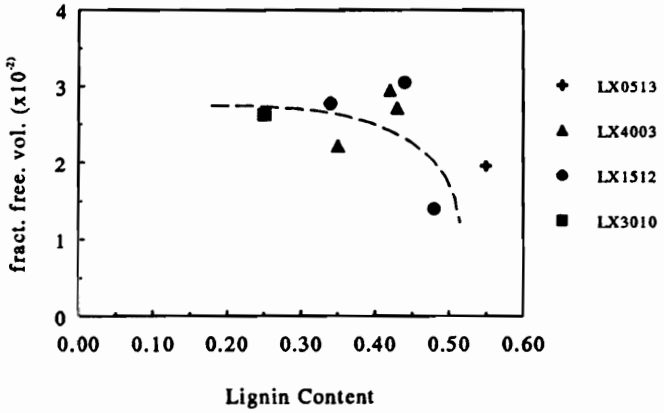

b)

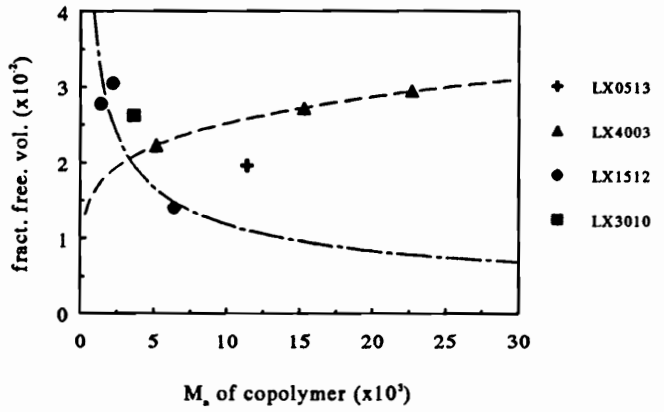

c)

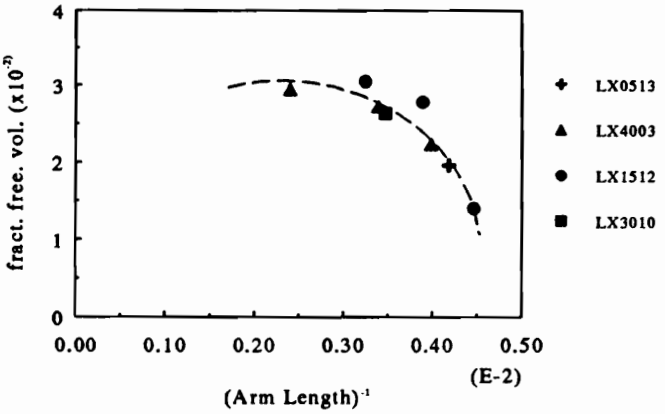

Figure 58. **Fractional Free Volume at Glass Transition:** Function of lignin content (a), copolymer molecular weight (b), and inverse arm length (c)

a)

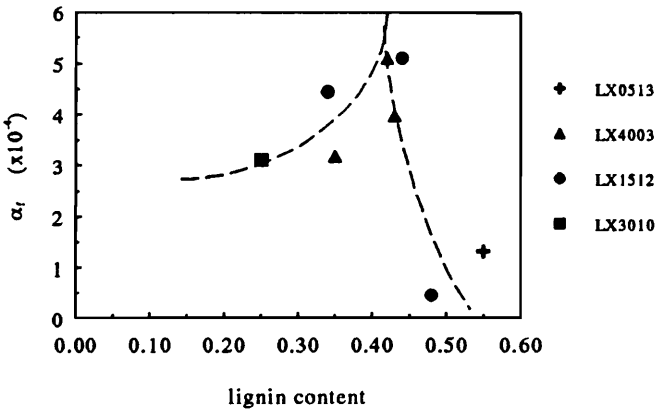

b)

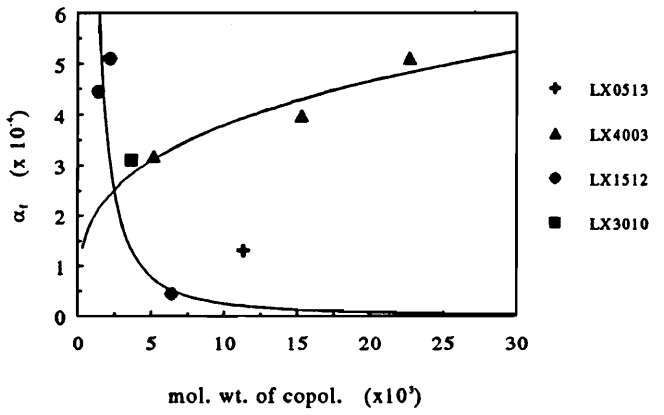

c)

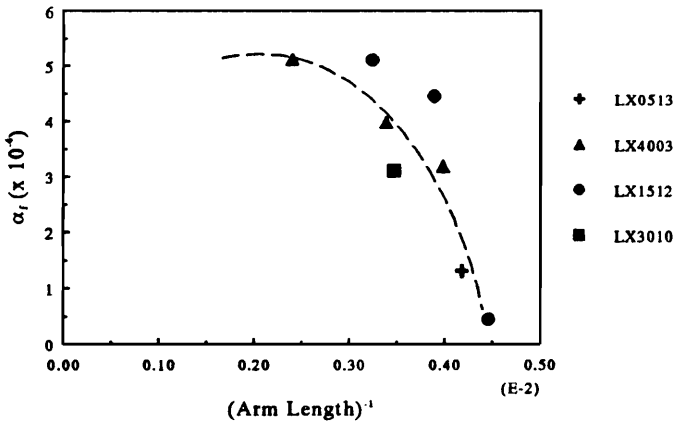

Figure 59. Coefficient of Thermal Expansion of Fractional Free Volume: Function of lignin content (a), copolymer molecular weight (b), and inverse arm length (c)

range of arm lengths, neither T_g, ΔT_g nor E_A are a function of PPO chain length. Thus, a primary conclusion can be drawn that, although the activation energy of the glass transition is a measure of the ease of segmental mobility it is not related to the fractional free volume.

However, it can be shown that the activation energies of the lignin-PPO networks, as a measure of the temperature-frequency shift of the glass transition temperature, are linked to α_f, the coefficient of thermal expansion of the free volume. The smaller α_f is, the less f_g changes with temperature (see eq. 4.11), which in turn means that also the glass transition maximum shifts less with changes in temperature. Subsequently, the shifting of T_g is a function of the activation energy (see eq. 4.4). Thus a lowering of α_f due to changes in copolymer composition should be paralleled by a reduction of the activation energy. Although not to the same extent both variables show a reduction with copolymer size (Figure 59 b, and Figure 52 b). Also, an overall trend to reduced thermal expansion with shorter PPO chains can be observed, however, without conclusive activation energy counterpart.

4.3.5 Transmission Electron Microscopy of Lignin Containing Networks

Ultra thin specimens were prepared by microtoming the cross-linked lignin-PPO epoxy copolymers and stained for observation by transmission electron microscopy. Figure 60 to Figure 62 contain the TEM micrographs of the LX1512 and LX4003 fractions as well as the unfractionated samples LX0513 and LX3010. The magnification is 135 000x. Since Ruthenium tetroxide preferentially stains the aromatic entities of lignin the variation in darkness is a measure of the lignin distribution in the network. The images show that most samples are to a certain degree heterogeneous with respect to lignin. However, this phase segregation does not resemble the clearly bordered structures of isoprene-styrene systems [26,27]. Rather, the dark lignin rich regions fade out at their borders into the lignin poor, not stained areas forming spherical to tubular connected structures. Almost like an interphase, broad and gradually changing, the lignin poor material builds something like a con-

tinuous phase. No trend among the fractions is observable so far although it seems that the high molecular weight fraction of LX1512 has a number of larger and denser particles while the background consists of smaller connected domains. The unfractionated, low lignin content sample, LX3010, appears as homogeneous image with no phase contrast, although it was prepared and stained the same way as the other samples. This observation of homogeneity in LX3010 correlates with the narrow damping range of this sample (see Figure 53) and supports the assumption that the range of the glass transition temperature is a function of network heterogeneity.

The characteristic feature diameters are in the order of $10nm$ which would be in the order of Sperling's [1] size requirement for broadening of the mechanical damping transition. Theoretical treatment of micro-phase separation states the requirement of a critical molecular weight below which no phase separation occurs which is about two to three times higher than the respective number for macro-phase separation in polymer blends [10]. In the case of SBS tri block copolymers whose segments are highly incompatible, phase separation begins between 6-$10x10^3 g/mol$ Although polydispersity significantly lowers the molecular weight requirement for the onset of micro-phase separation in block copolymers [28] it is questionable whether lignin-poly(propylene oxide) copolymers with a maximum arm length of 300 g/mol would ever phase separate. However, during cross-linking reaction the epoxy groups which are attached to the flexible polyether chains connect via the aromatic diamine. And it is conceivable that during this process, as it has been suspected from the cure kinetic investigation (Ch. 3), partial demixing and segregation of the poly(propylene oxide) and the lignin centers takes place.

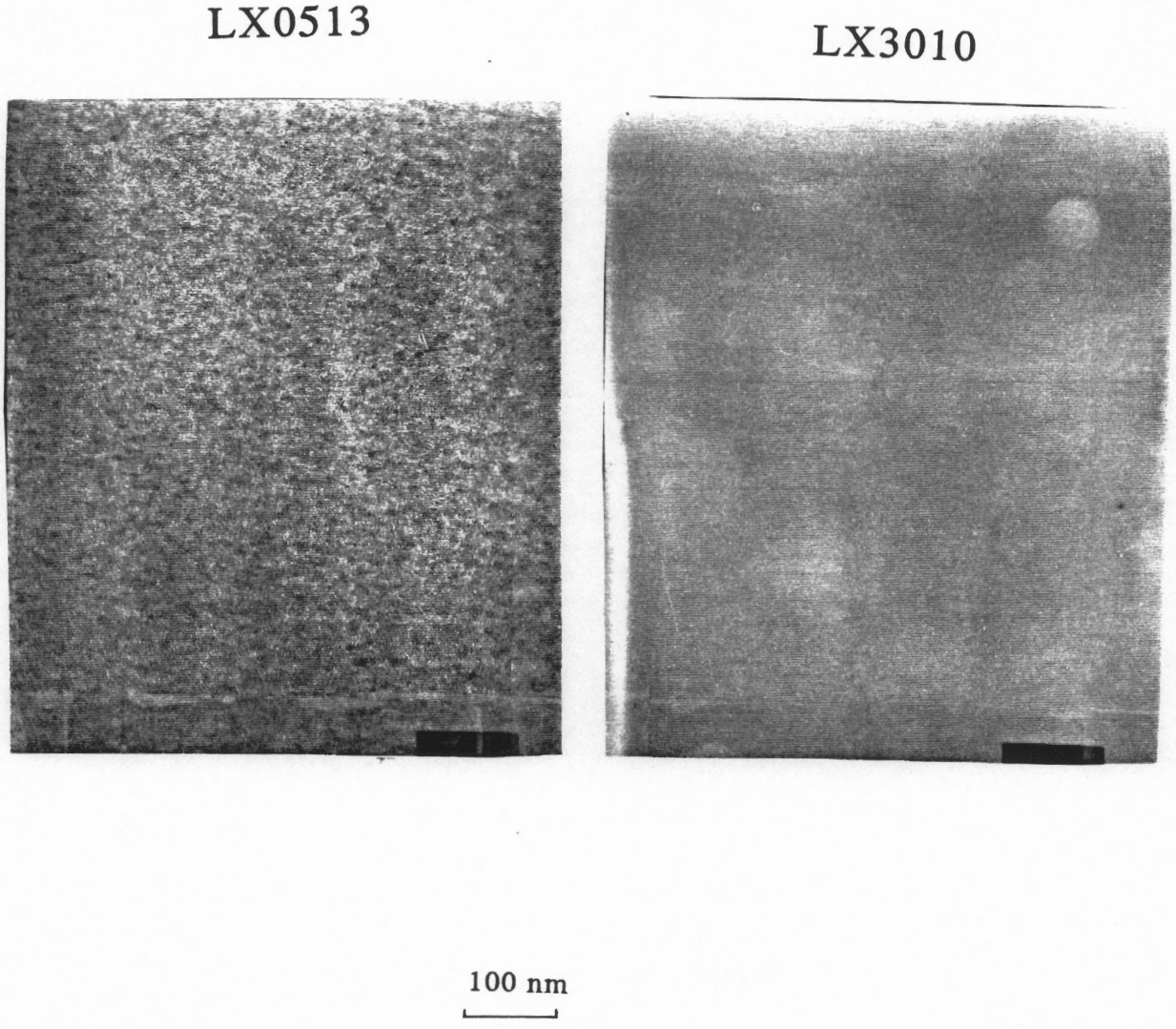

Figure 60. Transmission Electron Micrographs of LX0513 and LX3010: Stained with RuO_4 for 30 min, magnification = 135 000x

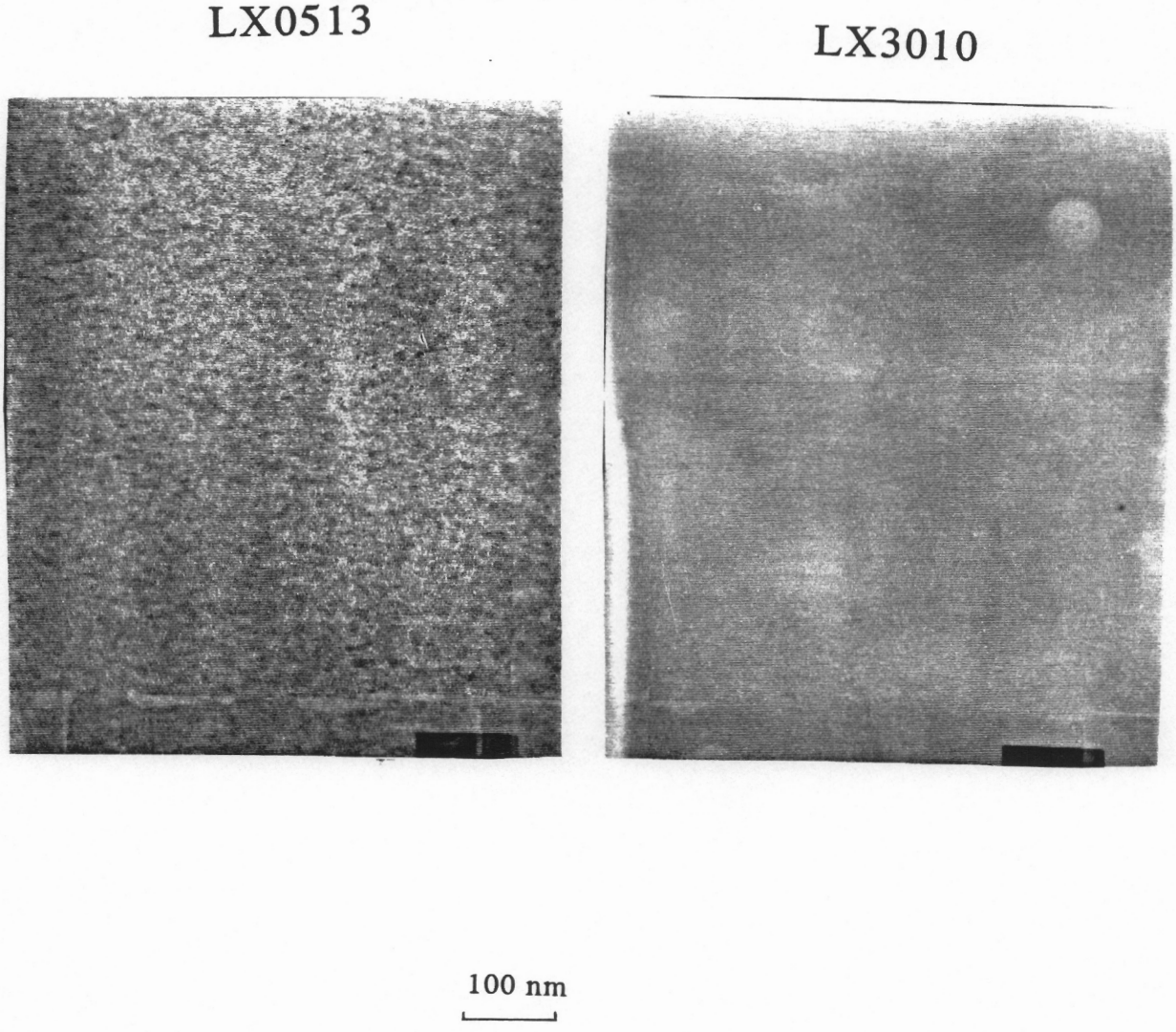

Figure 61. Transmission Electron Micrographs of LX1512 Fractions: Stained with RuO_4 for 30 min, magnification = 135 000x

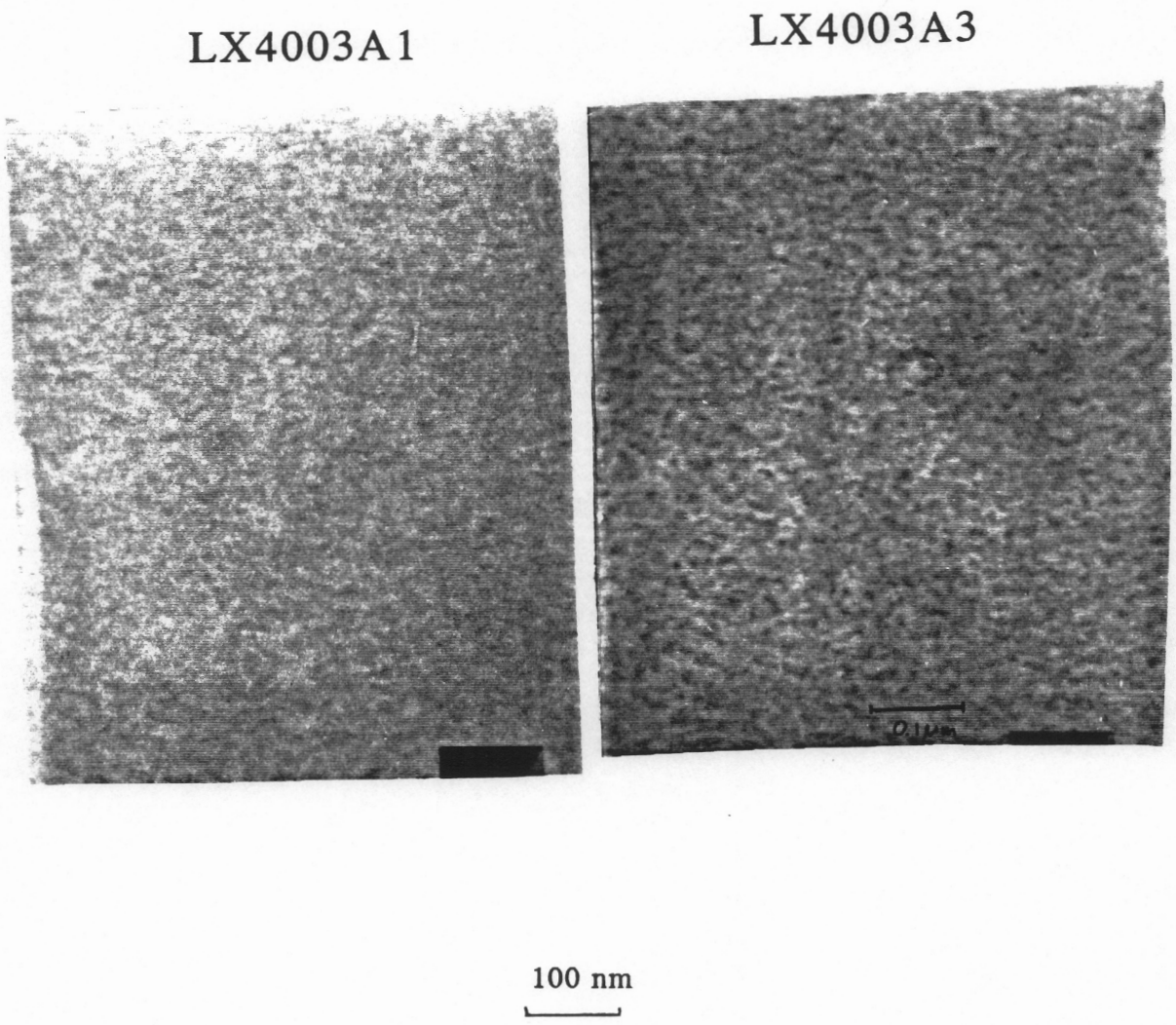

Figure 62. Transmission Electron Micrographs of LX4003 Fractions: Stained with RuO_4 for 30 min, magnification = 135 000x

4.4 Carbon-13 Solid State Nuclear Magnetic Resonance

4.4.1 Introduction

The molecular mobility of rigid components rises when their free volume increases due to plasticization by small molecules, chain ends, or flexible polymers. In the case of the cross-linked lignin-poly(propylene oxide) copolymers the carbon mobility of the lignin segment, and of the polyether should reflect the level of intermixing with PPO. If phase segregation were to occur the lignin carbon mobility would be lower than if intimate cohabitation takes place. Nuclear magnetic resonance relaxation times are closely linked to segmental or nuclei mobility. Lately, a host of ^{13}C cross polarized (CP) NMR studies of solid polymers involving magic angle spinning (MAS) have been reported which correlate molecular mobility with spin-lattice (T_1), spin-spin (T_2) relaxation times, and $T_{1,\rho}$, the T_1 in the rotating frame [29,30,74]. Also a great deal of work was and is being published about the applicability of solid state nuclear magnetic resonance (NMR) techniques to the study of heterogeneous polymeric materials. Whether in the case of semi-crystalline polymers [31], conformational structure determination of random co-polymers [32], or morphological investigations on polymer blends [33,34,35,36,37], block co-polymers [33,38,39,59], or interfacial properties of filled polymers [41], ^{13}C solid state NMR has been shown to yield qualitative and quantitative insights into polymer heterogeneity in bulk.

This section discusses the influence of copolymer composition on the relaxation times ($T_{1,\rho}$) of the lignin and PPO carbons. Additionally, also as a function of copolymer composition, the dependence of the carbon signal on the cross-polarization contact time will be analyzed.

4.4.1.1 Principles of Magic Angle Spinning, Cross-polarized Solid State C-13 NMR

The principle of many spectroscopic techniques lies in the establishment of resonance conditions between an applied outside field and the atomic or molecular oscillatory properties of interest. In the case of nuclear magnetic resonance one examines the resonance between an applied magnetic field and the magnetic moments of spin possessing nuclei (^{1}H, ^{13}C, ^{15}N, ^{19}F, ^{29}Si, ^{31}P, ...) [42].

High resolution solid state ^{13}C nuclear magnetic resonance spectra can show a high degree of fine structure allowing to clearly identify the various carbons. However, this is only possible by overcoming the severe line-broadening inherent to solid state NMR due to the restricted mobility of most molecular groups. Low abundance of the ^{13}C nuclei, $^{13}C - {}^{1}H$ dipolar coupling, and chemical shift anisotropy (CSA) are the three most important causes for the line broadening phenomenon [45,48]. Dipole interactions with the neighboring protons can be reduced by averaging their z-components whose fluctuations are experienced by the carbon nucleus. This is achieved by irradiating the sample with a strong field at the Larmor frequency of the protons so to force them to precess rapidly thereby destroying the carbon - proton coupling. To be efficient the decoupler field strength must be beyond 10 kG (40kHz). But even then some residual dipolar line broadening remains due to the chemical shifts of the proton Larmor frequency. Each nucleus has an electronic environment which partially shields it from the static field, B_0 to a certain extent and therefore changes its Larmor frequency. This effect is widely used to characterize molecular structure by nuclear magnetic resonance. However, the anisotropic nature of the shielding, and the low mobility, which prevents averaging the anisotropy causes excessive line broadening which confounds fine structure in solid state NMR. The three dimensional local field is a function of the anisotropic, shielding tensor σ. In solution or melts, rapid tumblings of the molecule averages all directional shielding and the isotropic chemical shift σ_{iso} becomes 1/3 σ. In solids however, spinning of the sample at rates above 2 kHz at an angle of 54.74° (magic angle) is necessary to time average the shielding tensor in order that it becomes identical with the isotropic shielding σ_{iso}. For effective line

narrowing, spin rates in excess of 2000 Hz are necessary. This is typically achieved with air driven cylindrical sample holders on air bearings [43].

Besides chemical shift anisotropy and dipolar coupling there remains another obstacle to the accumulation of high resolution "solution" like ^{13}C solid state NMR spectra, which is caused by the combination of low natural abundance of the ^{13}C isotopes and their long relaxation times, T_1, in the bulk. The delay time T_D between two subsequent rf-pulses in a FT-experiment is controlled by T_1 ($T_D > 5T_1$). This prevents the rapid accumulation of free induction decays (FID) which is necessary to offset the weak signals of the rare isotope. However, it is possible to establish resonance between the carbons and the abundant protons which due to their short communication distances have all the same short T_1's. This would allow the individual carbons to relax with the short T_1^H instead with the longer T_1^C. By a technique called cross-polarization (CP) [45,49] communication between the abundant protons and the rare nuclei is established. However, both systems are completely isolated from each other due to their different Larmor frequencies so that no mutual relaxation can take place unless the proton and carbon Larmor frequencies, ω_H and ω_C, can be matched so that the Hartmann-Hahn condition

$$\begin{aligned} \omega_H &= \omega_C \\ \gamma_H B_1^H &= \gamma_C B_1^C \end{aligned} \qquad [4.14]$$

is fulfilled. This condition, enables energy transfer from the carbons to the protons reservoir via T_{CH}, the cross relaxation time. The Hartmann-Hahn match is achieved by irradiating the carbon nuclei with a radio frequency field, B_1^C, forcing the carbon Larmor frequency to be equal to ω_H.

Figure 63 helps to visualize this mechanism in the rotating frame. First (a), both spin systems are equilibrate by B_0 along the z-axis. Secondly (b), the protons are tipped 90° by a rf-pulse, $B_{1,H}$ so to align them along the y-axis. To prevent them from immediately returning toward B_0 the protons must be spin-locked in the y-axis during the so called contact time, t_c. This is achieved by continuously applying the rf signal, but phase shifted by $\pi/2$ (c) which forces the protons to precess about the y-axis with the frequency $\nu_{1,H} = \gamma_H B_{1,H}/2\pi$. During the contact time a rf-pulse is turned on

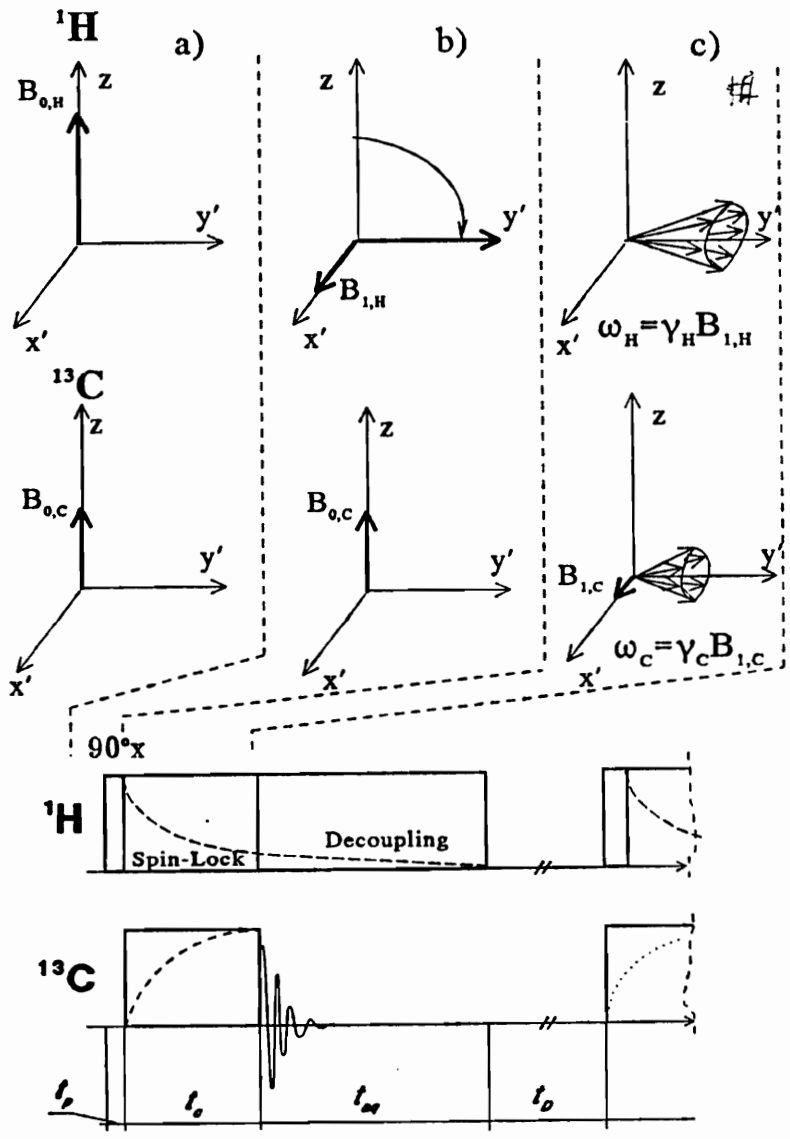

Figure 63. **Rotating Frame Vector Diagram and Pulse Sequence of a CP-Experiment:** a) Rotating frame diagram of the cross-polarization experiment b) pulse sequence of CP- experiment with spin locking

t_d	decouple time
t_c	contact time
t_{aq}	acquisition time
t_D	delay time
t_p	90° proton pulse time

which tips the carbons into the y-axis and gradually increases their magnetization. The carbons then precess with the frequency $\omega_{1,C} = \gamma_C B_{1,C}$ which is equivalent to $\omega_{1,H}$ once the Hartman-Hahn conditions is met at the end of the contact time. Now the carbons and the protons have identical z-components even though their rotating frames oscillate with their individual Larmor frequencies. This enable the polarization of the carbons by the abundant protons, and subsequently, after the carbon rf-pulse and the proton B_1 field is turned off, the carbons relax with the shorter $T_{1,H}$.

The signal gain due to cross-polarization is twofold. Firstly, the faster acquisition rate cross-polarization due to the short T_1^H improves the S/N ration. Secondly, the signal intensity theoretically increases four times since γ_H/γ_C is 3.977. This increase, however, is not uniform for all carbons, which prevents straightforward quantification of cross-polarization carbon spectra by integrating peak areas. Cross polarization is most efficient for protonated carbons in rigid environments because of sufficient static $^{13}C - {}^{1}H$ interaction. Mobile or non-protonated carbon signals do not undergo the same enhancement than their protonated, rigid counterparts [62].

4.4.1.2 Polymer Mobility and Carbon 13 Solid State NMR

The frequency of molecular reorientations in polymers range from 0.01-10^{12} Hz [45]. These main and side chain motions define to a great extent the mechanical and viscoelastic properties of macromolecular materials. Due to the partial dependence of NMR relaxations on molecular mobility, NMR can serve as a valuable tool to investigate these reorientations [46]. The study of relaxation time patterns provide information about the mobility of specific phase, segments or groups within the system and is used to complement viscoelastic techniques [44,47].

Very often it is beneficial to describe polymer motions by their correlation time, τ_c which is the time constant of the exponential decay of the autocorrelation function $G(\tau) = e^{-t/\tau_c}$, a segment's motional memory [48]. A short τ_c means rapid loss of a segment's positional memory. The Fourier inverse

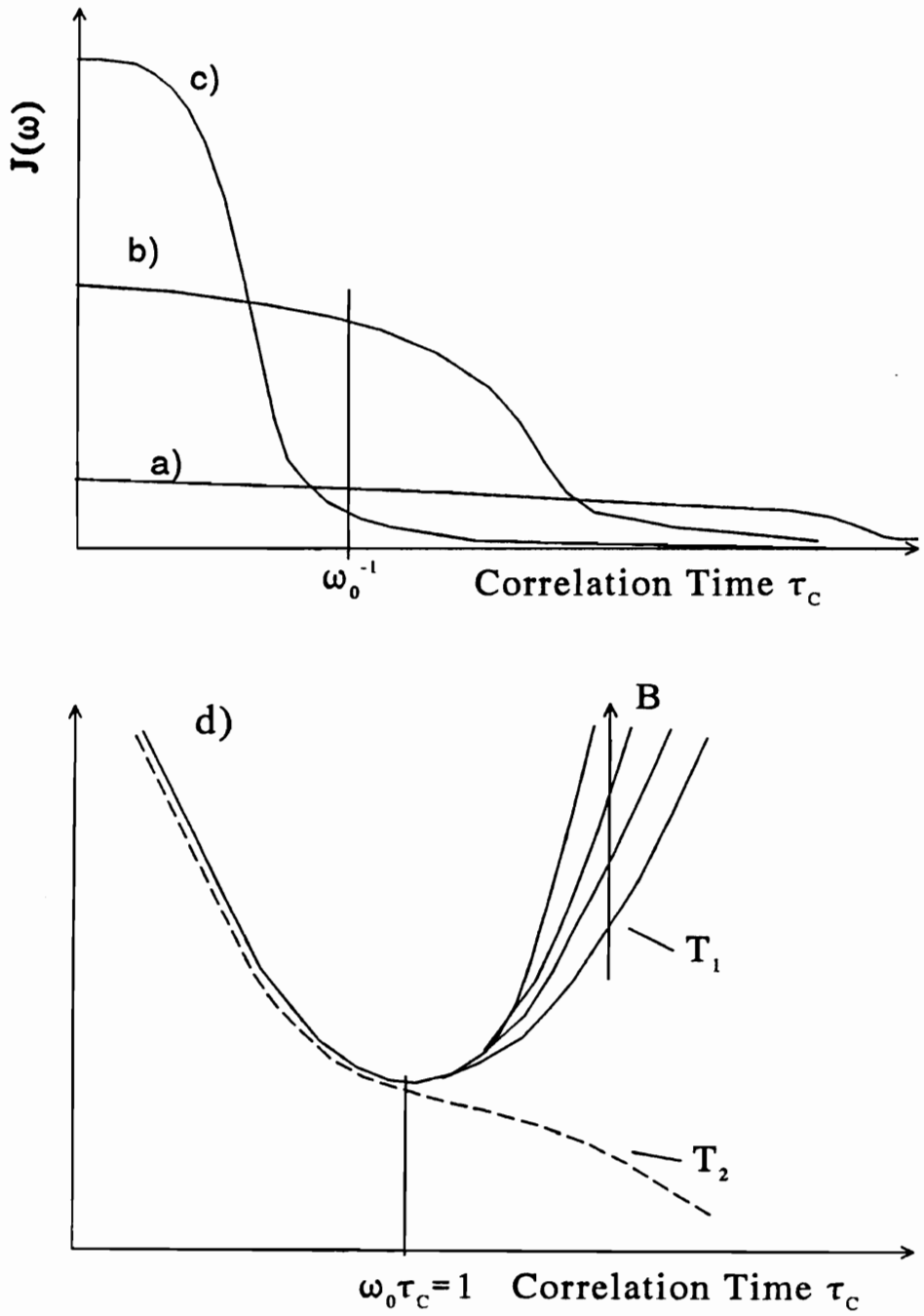

Figure 64. **Spectral Density Function and Magnetic Relaxations:**
a) slow motion ($\omega_0 > 1/\tau_c$)
b) intermediate motion ($\omega_0 = 1/\tau_c$)
c) fast motion ($\omega_0 < 1/\tau_c$)
d) T_1, T_2 vs. correlation time τ_c

of the autocorrelation function is the spectral density function $J(\omega)$, a distribution function of motional frequencies.

$$J(\omega) = \int_{-\infty}^{+\infty} G(\tau) e^{-i\omega\tau} d\tau = \frac{\tau_c}{1 + \omega_0^2 \tau_c^2} \qquad [4.15]$$

Examples of spectral density functions for slow, intermediate, and fast motions are displayed in Figure 64. The area under the curves are normalized. By comparing the correlation time of a particular chain or segment with the Larmor frequency, it is possible to characterize very stiff, slow chains or segments by $\tau_c\omega_0 > 1$, fast moving nuclei, on the other hand by $\tau_c\omega_0 < 1$. In both cases the components at ω_0 are relatively small. Only in the intermediate case where $\tau_c\omega_0 = 1$ the magnetic relaxation is considerably determined by the molecular motions.

4.4.1.3 Spin Lattice Relaxation Time

The longitudinal or spin-lattice relaxation is responsible for the exponential return of the magnetization vector to the equilibrium position along the static field B_0:

$$\frac{dM_z}{dt} = \frac{\Delta M}{t}$$
$$(\Delta M)_t = (\Delta M)_0 e^{-t/T_1} \qquad [4.16]$$

where $\Delta M = M_z - M_0$ This relaxation involves energy transfer from the spinning system to the random lattice. But this is only possible magnetically via temporary resonance between the precessing nucleus and the randomly tumbling lattice nuclei. Since the frequency range of the lattice is very broad only a small fraction of nuclei is effectively resonating and thus, the spin-lattice relaxation is relatively slow compared with the equilibrium relaxations of other spectroscopic techniques. Those segments or carbons for which the condition $\omega_0\tau_c = 1$ holds are in resonance with the precessing spins and contribute most to the spin-lattice relaxation, i.e., the spin-lattice or lon-

gitudinal relaxation time T_1 has its minimum for nuclei whose motional frequency is equal to the Larmor frequency. Thus, the spin-lattice relaxation is best suited to probe the mobility of fast moving nuclei whose reorientation frequencies are in the order of 10^6 to 10^{10} Hz [45]. T_1 has an inverse sixth power dependence on the the inter-atomic distance $r_{C\text{-}H}$ which renders the contribution of not directly attached proton to the spin-lattice relaxation virtually negligible. Therefore, the longitudinal relaxation time of quartenary carbons can be as long as hours.

4.4.1.4 Spin-Spin Relaxation Time

After removal of the rf-pulse which tips the magnetization M_0 into the y-axis the phase coherence of the precessing spins gradually declines. In a rotating frame this can be written as

$$\frac{dM_y}{dt} = -\frac{M_y}{T_2}$$
$$(M_y)_t = (M_y)_0 e^{-t/T_2} \qquad [4.17]$$

This process is usually called spin-spin relaxation which is theoretically an exponential decay with T_2 as time constant. In contrast to the longitudinal or spin-lattice relaxation, the spin-spin relaxation (T_2) process does not transfer energy but describes the dephasing of the precessing spins in the x-y-plane after the rf-pulse is extinguished, and contrary to T_1, the spin-spin relaxation time does not pass through a minimum at the Larmor frequency, but declines continuously with decreasing nuclei frequency (Figure 64 d). Spin-spin relaxation measurements are most sensitive to nuclear motions having frequencies in the order of 10^5 to $10^8 Hz$ [45].

4.4.1.5 Spin-Lattice Relaxation Time in the Rotating Frame

Longitudinal relaxation is an energy transfer process from the spin system to the random lattice. It is a function of the Larmor frequency, ω_0, which in turn is a function of B_0. This means that T_1 is

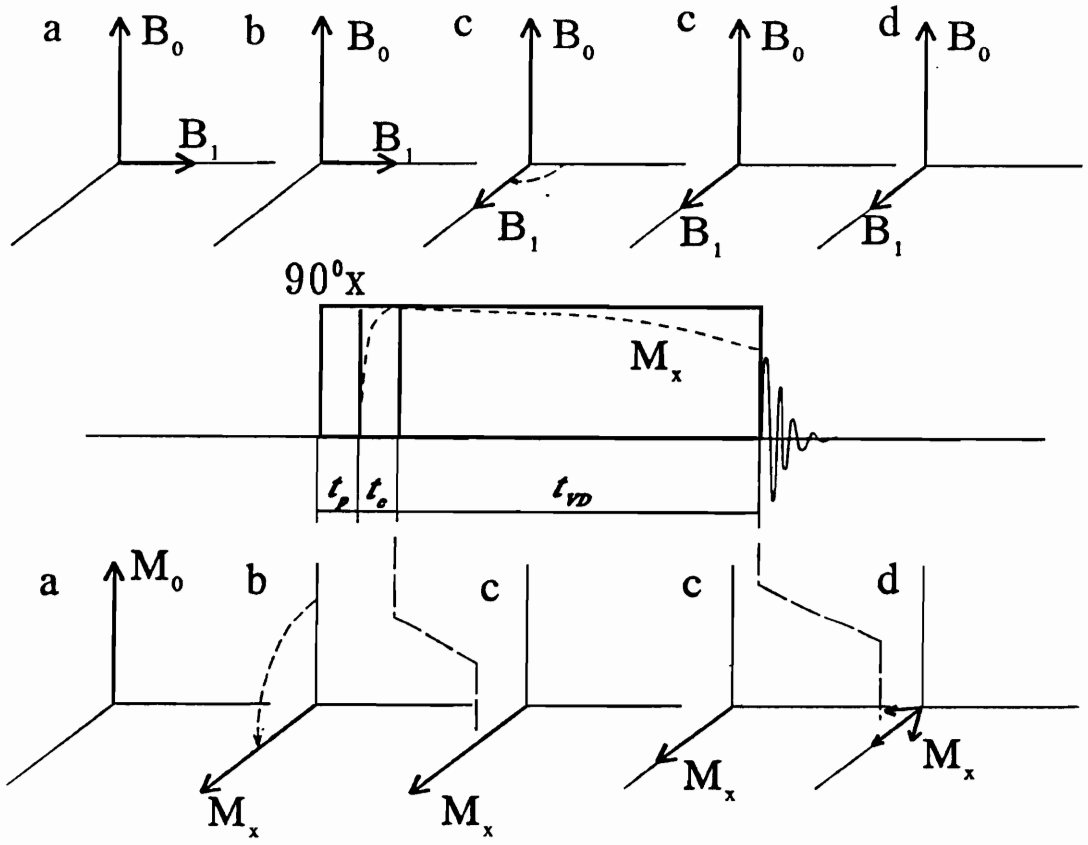

Figure 65. Pulse Sequence to Measure Spin -Lattice Relaxation Time in the Rotating Frame

a measure of high frequency motions. Very often, however, it is not the high frequency mobility but rather the intermediate and low speed reorientations which are of interest in solids. Reducing the static field would reduce ω_0, and shift resonance conditions towards higher correlation times (Figure 64 d). But aside from the fact that this is not an easy task from an engineering point of view, it also has detrimental effects on the sensitivity of the probe. One way to circumnavigate this obstacle is to place a small static field B_1 into the rotating frame and measure the longitudinal return of the magnetization in the rotating frame (Figure 65). The field B_1 locks the spins in the x-axis where they precess with the Larmor frequency ω_1 As long as spin-locking is active the magnetization M_x decays like [32]

$$M_x(t_p) = M_x(0)e^{-t_p/T_{1,\rho}} \qquad [4.18]$$

where t_p is the duration of the spin lock. After the spin lock is turned off the induction decay is controlled by T_2 [81]. Besides being a measure of polymer motions in the kHz region, the magnitude of $T_{1,\rho}$ may be also effected by the magnetic coupling of the ^{13}C spins with the protons during cross relaxation. As long as the coupling time constant, T_{CH} is much larger than the CP spin-lattice relaxation, $T_{1\rho}$ is a measure of carbon mobility. Schaeffer et *al* [50,51] established an elaborate procedure to accurately measure T_{CH} contributions to $T_{1,\rho}$ and could show that for polycarbonates, PET, various polystyrenes spin dynamic contributions to $T_{1,\rho}$ are negligible. However, the $T_{1,\rho}$'s of the methylene carbons in polymers such as polyethylene or poly(oxy methylene) are influenced by spin dynamics and are not unambiguous measures of molecular reorientation [53].

In analogy to T_1, $T_{1,\rho}$ also passes through a minimum at $\omega_1\tau_c = 1$. At the right side of the $T_{1,\rho}$ peak, towards higher τ_c and lower nuclei mobility the relaxation time is a function of B_1, while fast moving nuclei ($\omega_1\tau_c < 1$ relax independent of the magnetic field strength. Assuming the single correlation model with $J(\omega) = \tau_c/(1 + \omega^2\tau^2)$ and a B_1 field strength about 1000 to 2000 times smaller than that of B_0, $T_{1,\rho}$ becomes a measure of motions in the 10-100 kHz range [80].

Jelinsky [53] has shown that protonated ring carbons in poly(butylene terephtalate)-poly(tetramethylene-undecakis(oxytetramethylene) terephtalate) reduce their $T_{1,\rho}$ values from 2.5 ms to 0.7 ms by incorporating an increasing amount of soft segment In many cases carbon spin-lattice and spin-spin relaxations do not decay exponentially but rather show sometimes substantial dispersion (ratio of fastest to slowest time), which can be as high as 40 (protonated ring carbon of poly carbonate [54]). The initial slope is sometimes referred to as average relaxation time. In some cases relaxation times plots can be dissected into short, intermediate, and long T's.

4.4.1.6 CP Contact Time

Relaxation measurements in rigid polymers are normally carried out with cross-polarization and magic angle spinning as signal enhancing techniques. Cross-polarization is most successful for carbons of low mobility and close protons. Signal strength is a function of the CP contact time, t_c whereby non protonated carbons cross-polarize slower than protonated ones. On the other hand methyl carbons and flexible segments are in general not very effected by cross-polarization due to their high rotational mobility. Thus, by selectively decreasing the quality of the Hartmann-Hahn match it is possible to identify carbon signals coming from respective rigid or flexible segments. Depending on its local environment and mobility, each sufficiently slow carbon has an optimum contact time, whereby lengthening it beyond this point decreases signal strength. Furthermore, signals not effected by cross-polarization and by the change in contact time could be assigned to very fast moving, flexible carbons. This method has been used with good success to identify the soft and hard carbons in polystyrene-isoprene block copolymers and biphasic polyurethane networks [33], and to shape models about the involved phase separations.

4.4.2 Materials and Methods

The solid state ^{13}C experiments on the lignin containing epoxy networks were carried out on a Bruker MSL 300 solid state NMR instrument connected to an Aspects 3000 computer. The powdered samples were placed into a ceramic rotor which was driven by air pressure at the magic angle with spinning rates between 3900 and 4000 s^{-1}. Besides collecting the spectra of the various lignin copolymer fractions for the purpose of peak identification with CP MAS, two sets of experiments were carried out. The first one dealt with a series of spectra collected at changing spin contact times. The Hartmann-Hahn conditions were routinely adjusted by optimizing the spectrum of adamantane. The other set of experiments involved the measurements of the spin-lattice relaxation times of selected carbons in the lignin copolymer structure and their correlation with compositional parameters. A reduction of $T_{1,\rho}$'s of sufficiently rigid carbons could be taken, at least qualitatively as an increase in the mobility due to an increase of free volume. Absolute assignments of reorientation frequencies is in general not possible without applying elaborate correlation time distribution models [46].

The materials used in this studies were the three cross-linked fractions of LX1204, an unmodified lignin fragment, and an extracted and lignin free cross-linked poly(propylene oxide) epoxide. The lignin copolymer fractions were described in detail in Ch. 2 and their curing with *m*PDA in Ch. 3. The solid materials were powdered in a mortar under liquid nitrogen and subsequently filled into a ceramic rotor manufactured by Bruker Instruments. All Spectra were collected in cross polarization ($t_c = 2.5$ ms) and with magic angle spinning (MAS). The spin rate was 3900 s^{-1} and 3200 spectra were accumulated. Peak assignments were carried out following the work of Lüdemann and Nimz [60] and Glasser et al. [61]. The calculations of the relaxation times were carried out on the Aspects 3000 computer with the SIMFIT software supplied by Bruker Instruments.

4.4.3 Results and Discussion of NMR Experiments

The spectra of the three fractions, of the pure lignin, and the lignin free PPO network are compiled in Figure 66. The identifiable signals in lignin (see Figure 1) are two carbonyl peaks at 206 and 199 ppm, followed by a sequence of lignin ring carbons starting with C_4 at 156 ppm and C_3/C_5 at 147 ppm, followed by C_1 (135 ppm) and C_2/C_6 (106 ppm). The side chain carbons $C\beta$ and $C\gamma$ are found at 80 and 70 ppm, respectively, and $C\alpha$ at 35 ppm. The most prominent signal at 56 ppm stems from the methoxyl carbon. The methylene signals lie between 71 and 74 ppm. The spectrum of the homopolymer network basically contains two peaks: the methylene resonance at 74 ppm and the methyl peak at 17 ppm. No methine signal could be identified which is probably masked by the methylene peak. The three fractions incorporate the combined signals of pure lignin and of poly(propylene oxide). However, the carbonyl twins do not resolve and the C_3/C_5 peak almost disappears. The side chain signals of $C\gamma$ and $C\beta$ are masked by the CH_2 peak.

Despite the fact that cross polarization is a very inefficient method of probing polymers above their T_g, since the nuclei mobility is in general too high to allow for spin energy transfer from the carbons to the proton reservoir [62], the spectrum of the rubbery PPO homopolymer network has a very good signal-noise ratio.

4.4.3.1 Variable Contact Time

Since the variation of the CP contact time leads to an increasing mismatch of the Hartmann-Hahn condition, it was expected that it is possible to selectively change the signals of only these carbons stemming from the rigid carbons, if there is a separation between soft and hard micro-phases, Thereby it would be possible to assess whether the flexible segments of the copolymer are impaired in their mobility or freely moving as it would be the case in phase separated situations. However, due to the relative rigidity of the poly(propylene oxide) network this could not be achieved. As one

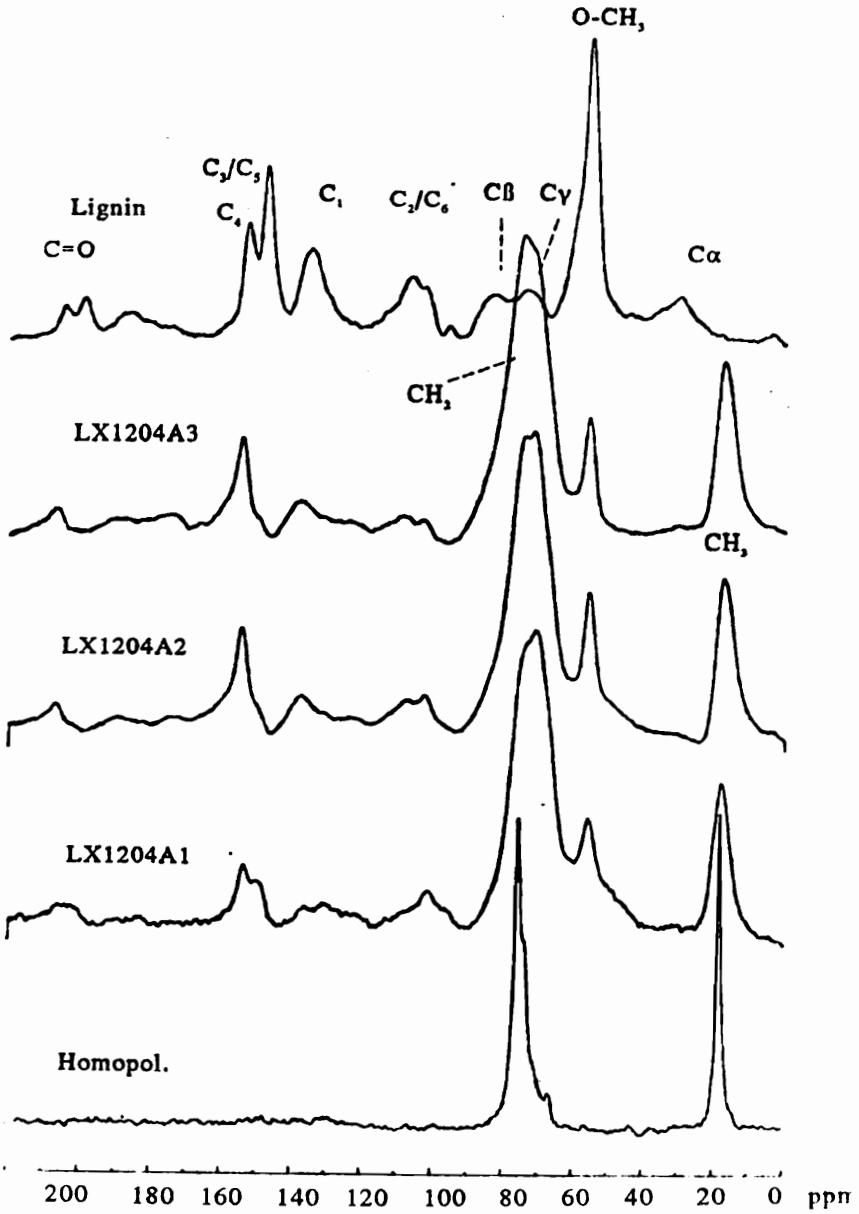

Figure 66. Spectra of Unmodified Lignin (a), LX1204A1 (b), LX1204A2 (c), LX1204A3 (d), and Lignin Free Homopolymer Network (e)

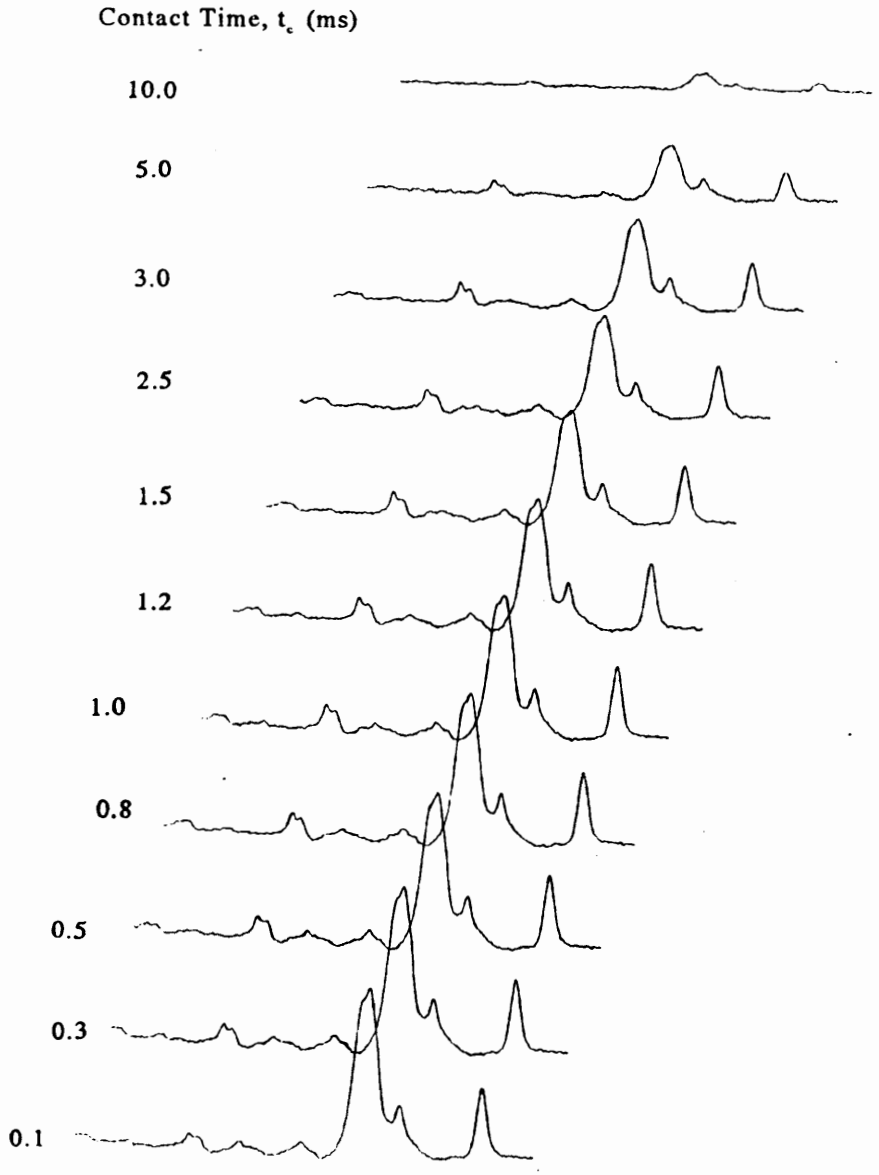

Figure 67. CPMAS Spectra of LX1204A1 Fraction at Variable Contact Times

can see from the sequence of spectra in Figure 67 both the lignin and the poly(propylene oxide) signals decay with about the same rate, while, if the PPO carbons were truly flexible their signals would decay much slower. Indeed, as can be seen from the signal strength versus contact time plot in Figure 68, where in the case of the methylene carbon the maximum is at less than $1ms$ while it has been reported [45,62] that for elastomeric carbons the maximum should be at about $5ms$. The optimum contact time for the lignin ring and the methoxy carbon has been found to be $2.5ms$. Nevertheless, a reduction of signal strength for each of the three individual carbons was observed with decreasing lignin content of the fractions. This is an indication that the level of segmental mobility increases with higher PPO content due to internal plasticization.

The findings of the variable contact time measurements support the conclusion that these networks do not experience a distinct micro-phase separation morphology with well defined domain borders, and that higher levels of PPO content increase the mobility of lignin and PPO carbons.

4.4.3.2 Spin Lattice Relaxation Times in the Rotating Frame

An attempt was made to measure and compare the variation of $T_{1,\rho}$, the spin-lattice relaxation time in the rotating frame, for all fractions of LX1204, pure lignin, and the lignin free poly(propylene oxide) network. The spin-lattice relaxation times in the rotating frame, $T_{1,\rho}$ of most carbons have been recorded by adjusting the variable delay time (see Figure 65) from $2\mu s$ to 500ms. The results are compiled in Table 13. No dispersion was detectable for the lignin ring carbons which relaxed essentially exponentially in all samples. The methyl, methylene, and methoxyl carbons relaxation data, however, were fitted to a two parameter decay with a fast and a slow $T_{1,\rho}$

The carbonyl carbons in lignin show the longest $T_{1,\rho}$ which can be explained by the lack of attached protons. While it is certainly not possible to forge conclusions about the absolute mode of individual carbon reorientations from these data it is interesting to follow their trend with changing copolymer composition. All relaxation times decline from their pure lignin value once the rigid

Table 13. Carbon Relaxation Times in the Rotating Frame of Lignin-poly(propylene Oxide) Copolymer Networks in ms

Peak (ppm)	Assignment	PPO	LX1204A1	LX1204A2	LX1204A3	Lignin
17	CH_3	21.6/5.0	33.2/3.7	35.8/2.7	43.2/2.6	-.-
56	OCH_3	-.-	36.7	54.4	70.8	52.7
71/74	CH_2	7.0/2.5	16.4/3.9	11.2/2.2	15.1/1.1	18.6
106	C_2/C_6	-.-	38.0	-.-	39.5	-.-
135	C_1	-.-	-.-	81.5	82.6	122.4
147	C_3/C_5	-.-	64.3	-.-	119.3	
154	C_4	-.-	79.1	73.9	73.3	123.4
206	C=O	-.-	25.4	76.3	128.2	205.0

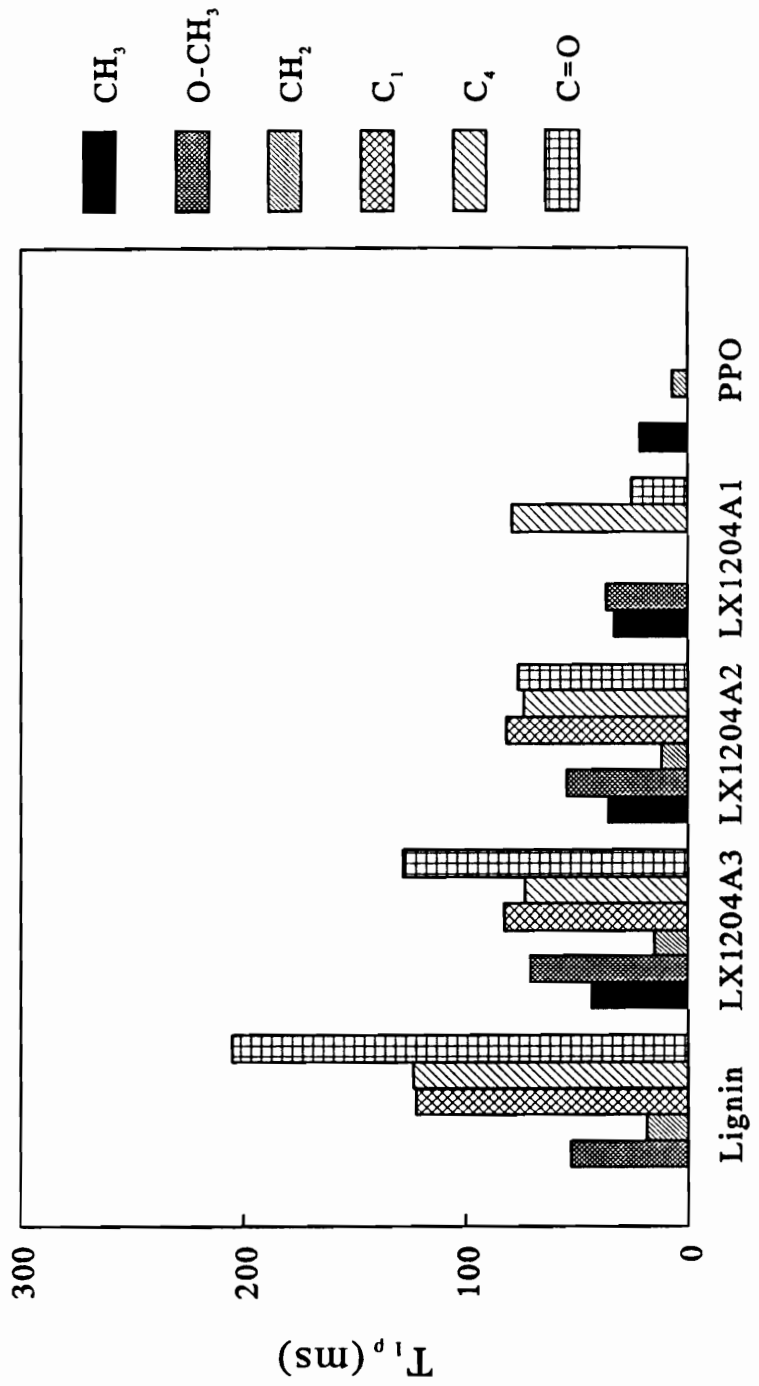

Figure 69. Relaxation Times of Selected Carbon: unmodified Lignin, LX1204A1, LX1204A2, LX1204A3, and Lignin Free Homopolymer Network

molecule becomes plasticized by poly(propylene oxide). However, the ring carbon relaxation times do not continuously decline, but remain constant, disregarding the copolymer composition after the initial drop (see Figure 69). The carbonyl carbon on the other hand, exhibits a continuously declining $T_{1,\rho}$. Since proton free carbonyls have a very unfavorable relaxation environment it could be possible that an increasing amount of PPO provides the necessary adjacent protons for better spin energy transfer. Probably, both the increase in mobility due to higher free volume and the better spin energy transfer via the protons of the adjacent polypropylene oxide segments aid to the decline in the relaxation time of the carbonyl carbons. Nevertheless, the constant level of the $T_{1,\rho}$'s of the aromatic lignin carbons might be due to the fact that only a certain amount of PPO is accommodated within the lignin structure. If one were to interpret the $T_{1,\rho}$ data as predominantly a function of mobility, it could be speculated that the aromatic lignin structure only allows a certain limited closeness of the interpenetrating PPO segments. This in turn could be interpreted as that the more flexible PPO chains are found closer to the rim of the lignin molecules forming a interphase with a declining lignin gradient which connects the neighboring lignin molecules. Also, all lignin connecting cross-links are formed via the poly(propylene oxide) segments. This agrees with the TEM observations and would confirm that the broadening of the mechanical loss maxima is due to "interfacial heterogeneity" [1]. However, further work involving variable temperature NMR with the use of changing B_1 field strength is necessary to clarify the mobility dependent portion of the $T_{1,\rho}$[54,75]. Furthermore, spin diffusion studies by measuring the proton free induction decay could help to not only ascertain whether there are composition gradients, but also enables to estimate the size of the denser domain [76,77].

4.4.4 Conclusions of NMR Studies

Despite their potentially flexible nature, the carbons of the poly(propylene - oxide) side chains have a low reorientation frequency which makes them susceptible to cross-polarization signal enhancements. This indicates that no micro-phase separated PPO domains are formed during cross-linking.

Rather, an increasing PPO content leads to higher levels of internal plasticization which lowers the CP signal strength.

The spin-lattice relaxation times in the rotating frame $T_{1,\rho}$ of the various copolymer carbons show different behavior upon increasing the PPO content of the network. While the methyl, methylene, methoxyl, and carbonyl relaxation times continuously decline with increasing PPO content, the $T_{1,\rho}$ of the ring carbons remain constant beyond the initial modification of lignin. This can be regarded as an indication that the mobility of the ring carbons in PPO modified networks is higher than in the pure lignin. But it would also mean that no differences in ring carbon mobility exist among the various fractions. However, the mobility of the PPO carbons increases with decreasing lignin content. Thus, cross-linked lignin-PPO copolymer fraction with increasing PPO content seem to have a higher percentage of partially demixed flexible arms.

These observations, together with the results of the network formation studies (Ch. 3.5.2), the multifrequency dynamic mechanical analysis (Ch. 4.3), and the transmission electron microscopy studies, may stand as further indication that these networks are heterogeneous. A model of such a network would look like a series of rigid lignin centers which are interconnected via semi flexible poly(propylene oxide) chains. These chains also provide internal plasticization of the lignin centers thereby controlling the glass transition temperature. The fact that the ring carbons of the modified lignin networks have constant relaxation times also suggests that only a certain amount of PPO is accommodated within the lignin centers.

4.5 References

1. L. H. Sperling, in R. D. Corsaro and L. H. Sperling, Eds., "Sound and Vibration Damping with Polymers", ACS Symp. Ser. 424, Washington, DC, 1989
2. J. D. Ferry, "Viscoelastic Properties of Polymers", J. Wiley & Sons, New York 1983
3. D. G. Fradkin, J. N. Foster and L. H. Sperling, *Rubber Chemistry and Technology*,59, 1986, 255
4. M.C.O. Chang, D. A. Thomas, and L. H. Sperling, *J. Pol. Sci.; B: Pol. Phys.*, 26, (1988), 1627
5. B. J. V. Duffy, G. F. Lee, J. D. Lee, and B. Hartmann, in R. D. Corsaro and L. H. Sperling, Eds., "Sound and Vibration Damping with Polymers", ACS Symp. Ser. 424, Washington, DC, 1989
6. R. Y. Ting, R. N. Capps, and D. Klempner, in R. D. Corsaro and L. H. Sperling, Eds., "Sound and Vibration Damping with Polymers", ACS Symp. Ser. 424, Washington, DC, 1989
7. S. S. Kelley, T. C. Ward, T. G. Rials, and W. G. Glasser, *J. Appl. Pol. Sci.*, 37, 1989, 2961
8. S. S. Kelley, "Lignin Copolymers in Polyurethane Networks", PhD Thesis, Virginia Tech, Blacksburg, 1987
9. B. Hartmann in R. D. Corsaro and L. H. Sperling, Eds., "Sound and Vibration Damping with Polymers", ACS Sym Ser. 424, Washington, DC, 1989
10. D. J. Meier, in N. R. Legge, G. Holden, H. E. Schroeder, Eds., "Thermoplastic Elastomers", Hanser Publishers, Munich, 1987
11. J. D. LeMay and F. N. Kelley, in K. Dusek, Ed., "Epoxy Resins and Composites III", Springer Verlag, Berlin, 1986
12. G. C. Stevens, in A. J. Kinloch, Ed., "Structural Adhesives, Development in Resins and Primers", Elsevier Applied Science, London, 1986
13. S. S. Kelley, W. G. Glasser, and T. C. Ward, *J. Appl. Pol. Sci.*, 36, 1988, 759

14. E. A. Collins, J. Bares, and F. W. Billmeyr, "Experiments in Polymer Science", Wiley-Interscience, New York, 1973
15. G. York, "TEM/EDXS Studies of Phase Separation in Block and Graft Polymers" MS Thesis, Virginia Tech, Blacksburg, 1987
16. P. T. Weissmann and R. P. Chartoff, in R. D. Corsaro and L. H. Sperling, Eds., "Sound and Vibration Damping with Polymers", ACS Sym Ser. 424, Washington, DC, 1989
17. R. B. Fox, J. J. Fay. U. Sorathia, and L. H. Sperling, in R. D. Corsaro and L. H. Sperling, Eds., "Sound and Vibration Damping with Polymers", ACS Sym Ser. 424, Washington, DC, 1989
18. J. S. Trent, J. I. Scheinbein, and P. R. Couchmann, *Macromolecules*, 16(4), 1983, 589.
19. W. de Oliveira and W. G. Glasser, *J. Appl. Pol. Sci.*, 37, 1989, 3119
20. E. E. Ungar, in L. L. Beranek, Ed., "Noise and Vibration Control", McGraw Hill, New York, 1971
21. T. Hur, *J. Pol. Sci.; B: Pol. Phys.*, 27, 1989, 225
22. M. C. O. Chang, D. A. Thomas and L. H. Sperling, *J. Appl. Pol. Sci.*,34, 1987, 409
23. J. A. Grates, D. A. Thomas, E. C. Hickey, and L. H. Sperling *J. Appl. Pol. Sci.*,19, 1975, 1731
24. J. N. Foster and L. H. Sperling, *J. Appl. Pol. Sci.*,33, 1987, 2637
25. Murrayama in "Encyclopedia of Polymer Science"
26. S. L. Aggarwal, in M. J. Folkes, Ed., "Processing, Structure, and Properties of Block Copolymers", Elsevier Apl. Sci. Publ., London, 1985
27. G. Holden and N. R. Legge in N. R. Legge, G. Holden, and H. E. Schroeder, Eds., "Thermoplastic Elastomers", Hanser Publishers, Munich, 1987
28. R. J. Spontak and M. C. Williams, *J. Pol. Sci.; B: Pol. Phys.*, 28, 1990, 1379
29. V. McBrierty and D. C. Douglas, *Phys. Reports*, 63(20, 1980, 61
30. D. J. O'Donnel, in J. C. Randall, Ed., "NMR and Macromolecules", ACS Symp. Ser. 247, Washington DC, 1984
31. D. E. Axelson, in R. A. Komoroski, Ed., "High Resolution NMR Spectroscopy of Synthetic Polymers in Bulk", VCH Publishers, Inc., Deerfield Beach, 1986

32. A. E. Tonelli, "NMR Spectroscopy and Polymer Microstructure: The Conformational Connection", VCH Publishers, New York, 1989

33. T.-S. Lin, "Applications of High Resolution Solid State Carbon-13 NMR to the Study of Multicomponent Polymer Systems", PhD Thesis, Virginia Polytechnic Institute and State University, Blacksburg, 1983

34. E. O. Stejskal, J. Schaefer, M. D. Sefcik, and R. A. McKay, *Macromolecules*, 14, 1981, 275

35. B. Albert, R. Jérôme, P. Teyssié, G. Smyth, N. G. Boyle, and V. J. McBrierty, *Macromolecules*, 18, 1985, 388

36. J. Schaefer, M. D. Sefcik, E. O. Stejskal, and R. A. McKay, *Macromolecules*, 14, 1981, 188

37. L. W. Jelinsky, F. C. Schilling, and F. A. Bovey, *Macromolecules*, 14, 1981, 581

38. L. W. Jelinsky, J. J. Dumais, and A. K. Engel, *Macromolecules*, 16, 1983, 403

39. L. W. Jelinski, *Macromolecules*, 14, 1981, 1341

40. L. E. Nielsen, *J. Macromol. Sci.-Revs. Macromol. Chem.*, C3(1), 1969, 69

41. T. P. Huigen, *Macromolecules*, 23, 1990, 3063* look for.

42. P. W. Atkins, "Physical Chemistry", W. H. Freeman and Co., New York, 1986

43. W.W. Flemming, C. A. Fyfe, R. D. Kendrick, J. R. Lyerla, H. Vanni, and C. S. Yannoni, in a. E. Woodward and F. A. Bovey, Eds., "Polymer Characterization by ESR and NMR", ACS Symp. Ser. 142, Washington, DC, 1980

44. A. N. Garroway, W. M. Ritchey, and W. B. Moniz, *Macromolecules*, 15, 1982, 105 *

45. R. A. Komoroski, in R. A. Komoroski, Ed., "High Resolution NMR Spectroscopy of Synthetic Polymers in Bulk", VCH Publishers, Inc., Deerfield Beach, 1986

46. V. D. Fedotov and H. Schneider, "Structure and Dynamics of Bulk Polymers by NMR-Methods", Springer Verlag, Berlin, 1989

47. J. Schaefer, M. D. Sefcik, E. O. Stejskal, R. A. McKay, W. T. Dixon, and R. E. Cais, *Macromolecules*, 17, 1984, 1108 *

48. F. A. Bovey, in Mark, Bikales, Overberger, and Menges, Eds., "Encyclopedia of Polymer Science and Technology", 2nd Ed., Vol. 10

49. C. S. Yannonni, *Acct. Chem. Res.*, 15, 1982, 201 *Macromolecules*, 16, 1983, 409

50. J. Schaefer, M. D. Sefcik, E. O. Stejskal, and R. A. McKay, *Macromolecules*, 17, 1984, 1118

51. J. Schaefer, *Macromolecules*, 6, 1973, 882

52. A. T. DiBenedetto, *J. Pol. Sci., B: Pol. Phys.*, 25, 1987, 1949

53. L. W. Jelinsky, J. J. Dumais, P. I. Watnick, A. K. Engel, and M. D. Sefcik, *Macromolecules*, 16, 1983, 409

54. A. Dekmezian, D. E. Axelson, J. J. Dechter, B Borah, and L. Mandelkern, *J. Pol. Sci.; Pol. Phys. Ed.*, 33, 1985, 367

55. R. E. Wetton, T. G. Croucher, and J. W. Fursdon, in C. D. Craver "Polymer Characterization", Advances in Chemistry Ser. 203, ACS, Washington, 1983

56. J. P. Queslel and J. E. Mark, in J. P. Kennedy, Ed., "Analysis / Reactions / Morphology", Springer-Verlag, Berlin, 1985

57. N. Patel, "Multicomponononent Network and Linear Polymer Systems; Thermal and Morphological Characterization", PhD Thesis, Virginia Tech, Blacksburg, 1990

58. J. S. Trent, J. J. Scheinbeim, and P. Couchman, "Macromolecules", 16(4), 1983, 594

59. D. W. Duff and G. E. Maciel, *Macromolecules*, 23, 1990, 3069

60. H.-D. Lüdemann and H. Nimz, *Makromol. Chemie*, 175, 1974, 2393

61. W. G. Glasser, D. Robert and J. Hyatt, unpubl. results

62. R. A. Komorosky, *Rubber Chem. Techn.*, 56, 1983, 959

63. Van Krevelen, "Properties of Polymers, Their Estimation and Correlation with Chemical Structure", 3rd. Ed., Elsevier, New York, 1990

64. J. J. Dlubac, G. F. Lee, J. V. Duffy, R. J. Deigan, and J. D. Lee, in R. D. Corsaro and L. H. Sperling, Eds., "Sound and Vibration Damping with Polymers", ACS Sym Ser. 424, Washington, DC, 1989

65. L. C. Chan, H. N. Naé, and J. K. Gillham, *J. Appl. Pol. Sci.*, 29, 1984, 3307

66. I. M. Ward, "Mechanical Properties of Solid Polymers", 2nd Edition, Wiley-Interscience, Chichester, 1983

67. J. J. Aklonis and W. J. MacKnight, "Introduction to Viscoelasticity", 2nd Edition, Wiley-Interscience, New York, 1983

68. J. D. Lemay, B. J. Swetlin, and F. N. Kelley, in S. S. Labana and R. A. Dickie, Eds., "Characterization of Highly Cross-linked Polymers", ACS Symp. Ser. 243, Washington, DC, 1983
69. H. Stutz, K.-H. Illers, and J. Mertes, *J. Pol. Sci., B: Pol. Phys.*, 28, 1990, 1483
70. W. G. Glasser, in R. W. Hemmingway and A. H. Conner, Eds., "Adhesives from Renewable Resources", ACS Symp. Ser. 385, Washington, 1989
71. L. E. Nielsen, Buchdahl, and Levreault, *J.Appl.Phys.*, 21, 1950, 607
72. S. I. Falkehag, *Appl. Pol. Symp.*, 28, 1975, 247
73. V. P. Saraf and W. G. Glasser, *J. Appl. Pol. Sci.*, 29, 1984, 1831
74. W. L.-S. Nieh, "Synthesis and Properties of Lignin Epoxide", MS-Thesis, Virginia Tech, Blacksburg, 1986
75. S. Tai, J. Nakano, and N. Migita, *J. Jap. Wood Res. Soc.*, 13, 1967, 257
76. C. Ayla and H. H. Nimz, *Holz Roh Werk.*, 42, 1984, 415
77. V. P. Saraf, W. G. Glasser, G. L. Wilkes, and J. E. McGrath, *J. Appl. Pol. Sci.*, 30, 1985, 2207
78. V. P. Saraf, W. G. Glasser, and G. L. Wilkes, *J. Appl. Pol. Sci.*, 30, 1985, 3809
79. S. S. Kelley and W. G. Glasser, in W. G. Glasser and S. Sarkanen, Eds., "Lignin, Properties and Materials", ACS Symp. Ser. 397, Washington DC, 1989
80. F. A. Bovey and L. W. Jelinsky, *J. Phys. Chem.*, 89, 1985, 571
81. D. A. Torchia, *J. Magnet. Reson.*, 30, 1978, 613
82. V. J. McBrierty and D. C. Douglas, *J. Pol. Sci., Macromol. Rev.*, 16, 1981, 295
83. D. J. Plazek and Z. N. Frund, Jr., *J. Pol. Sci., B: Pol. Phys.*, 28, 1990, 431

5.0 Conclusions

The results of this study show that lignins can be, if properly modified, epoxidized and made part of chemical networks. Modification in the form of replacing lignin's hydroxyls with poly(propylene oxide) resulted in the formation of soluble star-like copolymers. Both segments, the rigid, high T_g lignin center, and the flexible polyether arms are miscible, which is indicated by a single T_g. Capping the polyether arms with ethylene oxide, and reacting the primary hydroxyl groups with epichlorohydrin yielded multi-functional star-like copolymer epoxides. However, these resins contained considerable amounts of poly(propylene oxide) homopolymer and had a high polydispersity. Removing the homopolymer was efficiently carried out by precipitation in hexane. Thereafter, polydispersity was reduced by acetone/hexane fractionation of the copolymer epoxide. By virtue of this technique fractions with lignin contents ranging from 16 - 48% and molecular weights of 0.63 to 93 *kg/mol* were obtained.

The epoxides were cross-linked with meta phenylene diamine (*m*PDA). Contrary to many commercial resins, the curing reactions followed distinct n^{th} order kinetics with reaction orders ranging from 1.21 to 1.28. However, during the course of reaction this changed to a second order type, which indicates diffusion related reduction of mobility of the reactant carrying polyether arms. Since this happened at higher extents of conversion for fractions having lower lignin content, it is believed that the partially interconnected lignin centers are mostly responsible for the diffusion control of the

mobility. Vitrification, which is the cessation of the reaction due to the immobilization of the reactants, happened at conversions where the glass transition temperature had not reached yet the level of the cure temperature. Together with the width of the tanδ and E'' transition, this premature slowing of the reaction was seen as indication of partial demixing of the lignin core and the flexible polyether arms.

This notion of partial demixing was furthermore supported by the fact that results of ΔT_g, the rise of the glass transition temperature during cross-linking, as a function of lignin content and molecular weight of the fractions, were only explicable by a de-plasticization of the lignin during cross-linking, since other factors, such as $\overline{M}_e$, and the effect of introducing the cross-linking agent remain constant. The effect of de-plasticization was more pronounced for the fractions having smaller molecular weights. Mechanistically, a certain amount of demixing is necessary in order to connect the copolymer molecules via the epoxy terminated poly(propylene oxide) chains.

The broad range of the glass transition of the cross-linked copolymers has potential implication on their use as energy absorbing damping materials. Frequency-temperature shift procedures were carried out on multi-frequency thermo-mechanical spectra which allowed to predict the frequency bands where damping is most efficient at isothermal conditions. It was found that those bands span 6-10 decades of frequency, whereby the maximum of the transition is a function of lignin content.

The frequency-temperature shift principle also yielded information about the fractional free volume of the networks at glass transition and its thermal expansion coefficient. The respective values of the free volume were correlated with the activation energies of the glass transition temperature shifts, which is a measure of segmental mobility. It was found that both variables followed opposite trends with lignin content and molecular weight of the fractions. While the activation energy clearly fell with increasing level of propoxylation, it increased among the fractions of one set with declining lignin content. The free volume on the other hand remained constant with respect to lignin content up to 40%, after which it declined sharply. Thus, no or only weak correlation between these mobility related variables seem to exist in these networks. However, the coefficient of thermal expan-

sion of the free volume and the activation energies exhibit the same declining slope as a function of increasing lignin content. These results, and the fact that higher lignin content favors broadening of the transition region, indicates that increasing amounts of lignin within the network lead to an increase of heterogeneity.

Further substantiation of the assumption of lignin concentration dependent network heterogeneity came from transmission electron microscopy. Except in the case of a low lignin content unfractionated sample, the TEM micrographs exhibit an array of circular lignin richer structures in the order of $10nm$ imbedded in a lignin poor matrix, however without the well defined and sharply bordered domain morphology of classical micro-phase separated block copolymers. That the morphology of the lignin containing networks is not that of a micro-phase separated system is also based on the results of solid state ^{13}C cross polarized magic angle spinning NMR with contact times varying from 0.5 to 200 *ms*. It was found thereby that both, the carbons from the flexible polyether arms and those from the rigid lignin center were affected by cross polarization and had about the same optimum t_c between 1 and $2.5ms$, and both types experienced the same rate of signal strength decline at longer t_c's. This is a good indication that the polyether chains are not micro- phase separated in the classical sense with an ordered, well defined domain structure. $T_{1,\rho}$, the spin-lattice relaxation times in the rotating frame of the lignin ring carbons and the polyether carbons show different trends with lignin contents of the fractions. While the relaxation time of the latter continuously increases with lignin content, those of the ring carbons remain constant but rise considerably from the lignin rich fraction to pure lignin. As a measure of segmental mobility, this could be interpreted as a sign of non-homogeneous distribution of the plasticizing poly(propylene oxide) chains which additionally adds to the assumption that these networks are heterogeneous.

Depending on the lignin content, the thermosets were either low modulus elastomers, very ductile, or high modulus brittle solids. The modulus of elasticity was found to be a strong and linear function of lignin content whereby the highest value of 1 100 *MPa* was achieved by an unfractionated, 57% lignin containing, resin. The moduli and strengths of high lignin resins sur-

passed the respective values of a commercial DGEBA-*m*PDA system which was prepared under the same conditions.

This study could decisively show that epoxidation of hydroxyalkylated lignins with epichlorohydrin yields soluble and cross-linkable resins. The resulting thermosets can range from being rubbery, elastomeric to high modulus solids with good ductility. Nevertheless, most samples suffered from a low ΔT_g, i.e., they were either easy to handle liquids in the uncured state who became low T_g, low modulus thermosets, or, if high T_g's were achieved they were also solids in their non cross-linked state which made the difficult to process. The best results in this respect were obtained from a high lignin (57%) low molecular weight and unfractionated copolymer, which was liquid at room temperature but formed a high strength modulus solid with a glass transition temperature beyond 130°C

Summarizing, it can be concluded that lignins, once they are modified, become polymers which can be characterized like other polymers and can be reacted in solution with epichlorohydrin, and that epoxidation of propoxylated lignins could be a potential use of a vastly abundant bio-based raw material source to produce thermosets for a range of applications. Furthermore, crosslinking of these lignin containing epoxides yield tough thermosets in which lignin, on a molecular level is heterogenously distributed.

Klaus Hofmann was born on March 29, 1958, in Salzburg, Austria, where he earned a bachelor's degree in electrical engineering. In 1977, he went to Vienna, Austria to study Forest Products at the University of Agriculture. After completion of the Austrian mandatory citizen service, Klaus attended Virginia Tech from 1985 to 1986 and obtained an MS in Wood Science and Forest Products. After having returned for six months to Austria, he enrolled at Virginia Tech in the Wood Science and Forest Products Department where, in May 1991, he earned his doctoral degree in the Materials Engineering and Science program under Prof. Wolfgang Glasser.

In June 1991, Klaus will commence his post-doctoral work in Tsukuba, Japan at the Industrial Products Research Institute under Prof. H. Hatakeyama.